FINITE ELEMENT ANALYSIS AND EXPERIMENTAL INVESTIGATION OF TYRE CHARACTERISTICS FOR DEVELOPING STRAIN-BASED INTELLIGENT TYRE SYSTEM

BY

XIAOGUANG YANG

A thesis submitted to the College of Engineering and Physical Sciences

of the University of Birmingham for the degree of

DOCTOR OF PHILOSOPHY

School of Mechanical Engineering

College of Engineering and Physical Sciences

The University of Birmingham

September 2011

ABSTRACT

This thesis reports an investigation into the relationships between the tyre strain feature and tyre operating conditions based on finite element analysis and experiments for the development of a strain-based intelligent tyre system, which could estimate the tyre operating characteristics for optimising vehicle dynamics control and improving vehicle safety.

A 175/505R13 tyre is adopted as the subject of this study. An efficient and effective material property determination procedure is developed for investigating the rubber and reinforcement material properties by experiment. Considering the possibility of the absence of tyre composite profile due to proprietary protection by tyre manufacturer, a novel image-based method is developed to capture the tyre geometry feature from the tyre product cut cross-section. Both the 2D and 3D finite element tyre models are created in the commercial finite element code ABAQUS.

The generated finite element tyre models are validated with experimental data and then adopted to construct the comprehensive relationship between tyre strain feature and tyre operating characteristics. Experimental validation of these estimation models are implemented based on a custom designed test system. Finally, some recommendations are presented for improving the capability of the finite element tyre model and the strain-based intelligent tyre test system.

In Memory of My Grandfather

In Memory of My Friend, Long Lv

To Strive, To Seek, To Find and Not To Yield

ACKNOWLEDGEMENTS

I would like to express my appreciation to my supervisor, Dr. O. A. Olatunbosun for his unbounded encouragement, guidance, support and help during my PhD course. It has no doubt that it is his solicitude and professional experience inspiring me to go to the end of my PhD with confidence.

I also would like to give my thanks to my colleague Dr. E.O. Bolanrinwa and Mr. M. H. Behroozi for their help and discussion on tyre technology and finite element method. The thanks also extend to our technicians including Carl Hingley, Lee Gauntlett and Peter Thornton for their help during my experiment.

Thanks are also delivered to Dr. Daniel Garcia Pozueluo from Universidad Carols III de Madrid for his contribution to the tyre test. The gratitude is also extended to all the other friends and colleagues giving help, encouragement and concerns to me during my PhD study.

I would like to acknowledge the financial support from the School of Mechanical Engineering, University of Birmingham, and the Overseas Research Students Awards Scheme (ORSAS), UK.

Finally, I would like to give my appreciation to my parent and my fiancée for their support, encouragement, and understanding and love as always.

TABLE OF CONTENTS

PAGE NUMBER

LIST OF FIGURES

FIGURE **PAGE NUMBER**

LIST OF TABLES

TABLE **PAGE NUMBER**

LIST OF SYMBOLS

K_x	:	Tyre Longitudinal Stiffness
K_y	:	Tyre Lateral Stiffness
K_z	:	Tyre Vertical Stiffness
F_x	:	Tyre Longitudinal Force
F_y	:	Tyre Lateral Force
F_z	:	Tyre Vertical Force
M_x	:	Tyre Overturning Moment
M_y	:	Tyre Rolling Resistance Moment
M_z	:	Tyre Aligning Moment
s	:	Pneumatic Trail
l	:	Sample Length along Tyre Circumferential Direction
ε	:	Circumferential Strain
α	:	Slip Angle
γ	:	Camber Angle
r	:	Tyre Effective Rolling Radius
ω	:	Tyre Angular Velocity
V	:	Tyre Travelling Velocity
κ	:	Tyre Longitudinal Slip
C_α	:	Tyre Cornering Stiffness

F_γ	:	Tyre Camber Thrust
C_γ	:	Tyre Camber Stiffness
B	:	Stiffness Factor of Magic Formula
C	:	Shape Factor of Magic Formula
D	:	Peak Value of Magic Formula
E	:	Curvature Factor of Magic Formula
U	:	Strain Energy Per Unit of Reference Volume
$\overline{I}_1, \overline{I}_2$	:	1st and 2nd Deviatoric Strain Invariant
J	:	Total Volume Ratio
$\overline{\lambda}_i \, (i = 1,2,3)$	:	Deviatoric Stretch
$\lambda_i \, (i = 1,2,3)$	:	Principal Stretch
$\varepsilon_i \, (i = 1,2,3)$	:	Principal Strain
C_{01}, C_{10}	:	Mooney-Rivlin Rubber Hyperelastic Material Property Model Constant: Describe Material Shear Behaviour
$C_{i0} \, (i = 1,2,3)$	:	Yeoh Rubber Hyperelastic Material Property Model Constant: Describe Material Shear Behaviour
$D_i \, (i = 1,2,3)$	:	Rubber Hyperelastic Material Property Model Constant: Introduce Material Compressibility
J^{el}	:	Elastic Volume Ratio
L	:	Final Length of Rubber Sample
L_0	:	Original Length of Rubber Sample

P	:	Tension Force
σ_i	:	Tension Stress
A_0	:	Original Rubber Sample Cross-section Area
N	:	Material Constants of Prony Series Expansion
$\overline{g}_i^p$	:	Material Constants of Prony Series Expansion
τ_i^G	:	Material Constants of Prony Series Expansion
$g_R(\infty)$	:	Long-term Normalized Shear Compliance
$g_R(t)$	:	Normalized Shear Relaxation Modulus
$U1$	:	Displacement of Tyre Tread along Tyre Radial Direction
$U2$	:	Displacement of Tyre Sidewall along Tyre Lateral Direction
$\varepsilon_0, \varepsilon_{45}, \varepsilon_{90}$	:	Strains of Rectangular Rosette Strain Gauges
ε_x	:	Strain along X Axis Direction
ε_y	:	Strain along Y Axis Direction
ε_{xy}	:	Shear Strain in XY Plane
$\varepsilon_{1,2}$	:	Maximum Principal Strain
$\varepsilon_{x'y'}$	:	Maximum In-plane Shear Strain
θ_c	:	Rotational Angle Corresponding to Contact Length
θ_d	:	Rotational Angle Corresponding to Deformed Length
M	:	Symmetric Mass Matrix

K	:	Symmetric Stiffness Matrix
$t_i\,(i=n,n+1)$	:	Time of Step i
$F_i\,(i=n,n+1)$	:	Time Dependent External Force Vector at Step i
$\overline{\alpha}$	:	Numerical Damping Factor
$X_i\,(i=n,n+1)$	:	Position Vector at Step i
$\dot{X}_i\,(i=n-1/2,n,n+1/2,n+1)$	:	Velocity Vector at Step i
$\ddot{X}_i\,(i=n,n+1)$	:	Acceleration Vector at Step i
Δt	:	Step Size
β	:	Assumed Parameters
$\overline{\gamma}$	:	Assumed Parameters
I_n	:	Internal Force Vector
ε_{nom}	:	Nominal Strain
σ_{nom}	:	Nominal Stress
ε_{true}	:	True Strain
σ_{true}	:	True Stress
μ	:	Friction Coefficient
ε_f	:	Front Tensile Strain Peak
ε_r	:	Rear Tensile Strain Peak
r_ε	:	Tensile Strain Peak Ratio

CHAPTER 1

INTRODUCTION

1.1. OVERVIEW

Globally, about 60% of people and cargo are transported by vehicles that move on rubber tyres [1]. The pneumatic tyre plays an increasingly important role in the human being's life. However, this status is achieved because of more than one hundred years' tyre evolution since the initial invention of the pneumatic tyre by John Boyd Dunlop around 1888. The inflated rubber structure provides comfortable ride for transportation. With the growing demand for the pneumatic tyre, many improvements have been made based on the initial conception, such as the reinforcement cords, the beads, the vulcanization, the materials and the introduction of the tubeless tyre, etc. The tyre is required to perform multiple functions, not only support the weight and cushion the irregularities of road, but also provide the desired braking/traction and lateral force for vehicle control system. Furthermore, the concerns on the relationship between tyre and humans and surrounding environment raise a higher requirement for the development of tyre technology. These concerns include traffic accidents caused by tyre failure, the waste of energy due to bad tyre conditions, the pollution through the emission of harmful compounds by tyres, and the degradation of road surfaces related to tyre performance, etc.

In spite of the effects of tyres on the environment, the vehicle safety issue has always been of great concern to the public. It depends on the driver-vehicle-road system where the tyre is the only link between the road and vehicle, and the vehicle dynamics control system links the driver, vehicle and tyres. Incorporation of intelligent technology into the tyre could contribute greatly to its potential in accident prediction and prevention and thus enhance the tyre's important role in improving vehicle safety, The requirement is for an "intelligent tyre" that incorporates a system that is able to sense its health, working conditions and road conditions, and then cooperate with the vehicle dynamics control system to optimise the vehicle performance as well as provide warning information to the driver. These multiple functions of an intelligent tyre can be realized by integrating the sensor technology, wireless communication technology, energy harvesting technology and estimation/diagnosis scheme, etc. into tyre technology.

These benefits from the so called "intelligent tyre" have drawn much attention not only from the tyre industry but the government. However, the realization of intelligent tyre technology is a gradual process. In 2002, the USA government issued the Tread Act [2] to require the installation of Tyre Pressure Monitoring System (TPMS) in tyres in order to provide warning for driver if the tyre is significantly under-inflated. In 2012, TPMS will become mandatory in the European Union to improve vehicle safety and reduce CO_2 emissions. Therefore, tyre is being used as a sensor for the vehicle active safety system. Nevertheless, the development of intelligent tyre technology is still in an immature stage as only the TPMS has been commercialized so far. The huge potential market of intelligent

tyre technology has drawn considerable amounts of investment from different tyre companies.

As one of the core technologies for developing the intelligent tyre, the relationship between the parameters measured by the sensors, such as strain and the tyre mechanical properties such as inflation pressure and forces need to be constructed as a predefined estimation model in the vehicle electronic control unit (ECU). At present, the available estimation methods in literatures [3-5] are mainly obtained from physical tests. A large number of tests need to be done in order to achieve a comprehensive relationship for different tyre working conditions, which is inefficient in time and cost. A few of the existing researches [6-9] mention the adoption of the model-based approach such as finite element tyre model to simulate tyre behaviour and generate the estimation model. These model-based methods, however, mainly focus on one aspect of tyre performance such as steady straight line rolling and are poorly supported by experimental data.

As one of the most popular modelling methods used in the tyre industry, the finite element method has been used in tyre design and investigation of tyre behaviour. The significant advantage of finite element method with the availability of high performance computers has also been widely recognized in vehicle design and vehicle dynamics analysis. Good prediction of tyre global behaviour such as deflection and forces from finite element tyre model has been achieved at the Automotive Engineering Centre (AEC) in the University of Birmingham by using different commercial FE software such as MSC/NASTRAN and ABAQUS [10, 11]. The corresponding experiments including deflection, modal analysis,

and steady state straight line rolling and cornering have been carried out on the AEC tri-axial tyre test rig.

As a further development of the existing model for the study of intelligent tyre, accurate prediction of tyre global and local behaviour is necessary to be provided by the new finite element tyre model. Thus, the output can be utilized to construct the relationship between the sensor measurement and tyre mechanical property after necessary validation. In this study, a suitable finite element tyre model is developed for the study of strain-based intelligent tyre. As the fundamental requirement for a successful finite element tyre model, sufficiently accurate representation of the tyre composite geometry and nonlinear material properties is necessary. A new efficient and effective approach of extracting tyre composite profile and sophisticated material properties is proposed considering the non-availability of this information from tyre manufacturers for reasons of proprietary protection. The finite element tyre model was validated by static and dynamic physical tests in order to assess its suitability as an alternative of real tests for the investigation of strain-based intelligent tyre. A comprehensive estimation procedure was carried out for constructing the relationship between tyre strain sensor output and tyre variables during typical manoeuvres including tyre steady state rolling, braking/traction and cornering. It is expected in this study that these estimated relationships can be helpful for the optimisation of vehicle dynamics control systems such as anti-lock braking system (ABS), traction control system (TCS) and electronic stability control system (ESCS). An advanced intelligent tyre system is under development featuring a high performance, small size, light weight, self-powered, data acquisition system with wireless communication. Of particular interest is the integration of

different sensors for measuring various working parameters of the tyre, such as inflation pressure, temperature, acceleration, forces and road conditions, etc. Finally, the development of an intelligent tyre system is proposed to be validated in field vehicle tests for commercialisation to replace the existing TPMS and integrated into the vehicle active safety system in the future.

1.2. THESIS OUTLINE

This chapter presented the motivation of developing intelligent tyre technology and emphasised the significance of finite element method application in the process of establishing an estimation model for the intelligent tyre system.

In Chapter 2, a review of the literature on tyres, relevant to this study, is presented. The tyre mechanical properties including tyre deformation, force and friction are introduced firstly. Three different tyre modelling methods are addressed, particularly the finite element tyre modelling method. A comprehensive review of the existing intelligent tyre technology is carried out to give a deep insight into the pros and cons from literature.

In Chapter 3, the complex material properties of rubber and reinforcement cords are investigated. A feasible and efficient testing procedure for determining the rubber's hyperelastic and viscoelastic material property and reinforcement's linear elastic material property are developed in this Chapter. Then, the material properties from test are converted into material property model for use in ABAQUS.

In Chapter 4, an image-based tyre composite profile detection method is introduced when the tyre CAD profile is not provided by the tyre manufacturer. The tyre, wheel and road finite element modelling methods are also introduced for different analysis requirements.

Chapter 5 presents the static experimental validation of finite element tyre model by 2D inflation analysis, 3D radial stiffness analysis, footprint analysis and local sidewall strain analysis to demonstrate the tyre model's suitability for investigating tyre global and local behaviour.

In Chapter 6, the development of the estimation model for the strain-based intelligent tyre based on the foregoing finite element tyre model as well as experiment is described. The relationship between the tyre strain feature and the tyre mechanical properties are established for the tyre under steady state straight line rolling, braking/traction and cornering.

The deficiencies found in the present research work and the future works for developing an advanced intelligent tyre system are highlighted in Chapter 7.

The following Appendix lists some of the author's publications during his PhD course.

CHAPTER 2

LITERATURE SURVEY

2.1. INTRODUCTION

A number of different perspectives about tyre characteristics have been studied by experiments and simulations in the past decades. As an efficient approach, tyre modelling is adopted to provide accurate prediction on the tyre mechanical behaviours in terms of its reaction to various inputs associated with wheel motions and road conditions [12, 13]. Models, such as the in-plane and out-of-plane tyre models, are considered for the investigation of tyre longitudinal force and lateral force, respectively. Modelling tyre dynamic behaviour can provide a better understanding of tyre performance for optimising tyre design and improving vehicle dynamics.

Recently, with the increasing concerns on the vehicle safety issue, precise estimation and control of tyre behaviour are required for designing and developing vehicle active safety systems. Intelligent tyre technology provides a feasible and potential solution to the requirement. As the main expressions of tyre behaviour, tyre force and tyre/road friction are difficult to measure but possible to estimate by resulting variations of other tyre mechanical properties, such as tyre deformation. Intelligent tyre technology is still in the early stages of development and no mature products have been reported in the market. Consequently, there exists tremendous potential for intelligent tyre technology products in the market and a thorough study of the relationship between the tyre force and the resulting variations of

other tyre mechanical properties by experiments and modelling is essential for the development of intelligent tyre technology as well as vehicle active safety system [14].

In this chapter, the primary mechanical properties of pneumatic tyre, which were investigated in this study, are presented firstly. They include the tyre deformation, generated forces and moments and tyre/road friction. This chapter also reviews the mainstream of tyre modelling methods especially finite element modelling method which is utilized for developing intelligent tyre technology. Furthermore, the current methodologies, challenges and perspectives of intelligent tyre technology are documented. This review presents an overview of all the relevant background of this study and reveals the current limitation in developing intelligent tyre technology.

2.2. MECHANICAL PROPERTY OF TYRE

The vehicle tyre has such an intricate structure and behaviour that to cover all the mechanical properties of the tyre is impossible in this section. In order to provide background information for the further chapters about developing intelligent tyre technology, the relevant and predominant tyre mechanical properties are reviewed herein.

2.2.1 TYRE DEFORMATION

Tyres carry different loads in service including inflation pressure, externally applied mechanical loads and thermal loads [15]. Due to the effect of these loads and the contact

with the wheel rim and road, the tyre geometric shape changes, noted as deformation. This deformation can be represented by measuring the displacement of selected locations on the tyre. Specific relationship between mechanical load and tyre displacement is defined to represent the tyre flexibility, namely stiffness, which is composed of the effect generated by tyre structure rigidity and the effect of inflation pressure [15]. As the result of deformation, the surface and internal strains and stresses are developed in the tyre. The study of tyre responses to loads can be used to describe the tyre's behaviour, performance, and durability [16].

2.2.1.1 Tyre Vertical Stiffness

The tyre vertical stiffness is defined as the ratio of tyre vertical force and vertical deflection, which influences the vehicle vertical vibration characteristics and ride behaviour [17]. The tyre vertical stiffness can be measured using different approaches as described in [13].

Static stiffness of a non-rolling tyre can be measured by applying selected value of the vertical force slowly and measuring the deflection, or vice versa. Dynamic stiffness of both non-rolling and rolling tyre can be obtained by applying small amplitude sinusoidal excitation on tyre axle sweeping a range of frequency. Both the vertical tyre static and dynamic stiffness are unavoidably affected by tyre type, preload, inflation pressure and rim width, etc.

2.2.1.2 Tyre Longitudinal Stiffness

The tyre longitudinal stiffness is usually defined as the ratio of tyre longitudinal force and longitudinal deflection. It is important for the investigation of longitudinal cushioning of road irregularities which will cause tyre shimmy [15]. The longitudinal stiffness is only measured for non-rolling tyre by applying a longitudinal displacement or a rotational angle on the rim. The value of displacement or angle is relatively small before complete sliding of tyre occurs. In the rotation case, the longitudinal stiffness is the longitudinal force due to rim rotation angle. The longitudinal stiffness obtained by the aforementioned two methods could be different according to [13, 15].

2.2.1.3 Tyre Lateral Stiffness

The tyre lateral stiffness is defined as the ratio of tyre lateral force and lateral deflection. The lateral stiffness is measured for non-rolling tyre by applying a lateral displacement on the rim, and can be utilized for the investigation of relaxation properties of rolling tyre [15]. The lateral relaxation length can be obtained by dividing the cornering stiffness by the tyre lateral stiffness [13, 18]. The lateral tyre stiffness is relevant to the oscillation of tyre in lateral and yaw directions.

Generally, a tyre is most stiff in the longitudinal direction and least stiff laterally [19], namely $K_x > K_z > K_y$ as shown in Figure 2.1.

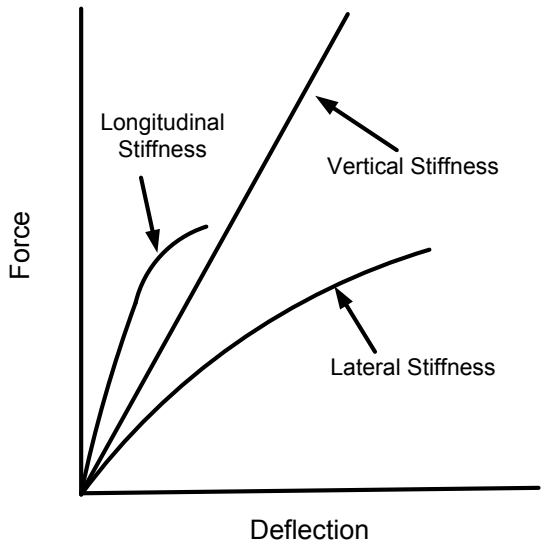

Figure 2.1 Tyre Stiffness [19]

2.2.1.4 Strain and Stress

Due to the complexity of tyre structure and material property, the strain and stress states of the tyre in service can provide significant information about the tyre's operational behaviour especially when it experiences extreme operating conditions. The knowledge of stress and strain distribution and magnitude, developed in critical regions of tyre such as the regions of the breaker edges and the carcass turn-up edges, is important and capable of providing a good understanding of premature tyre design failures [20]. S. L. Sokolov introduced a finite element tyre model using bulk isotropic elements to investigate the tyre stress concentrations and predict the failure regions [21]. Wang, et al. [22] suggested that the stress and strain concentration, especially in the critical transition areas between the tread and casing, could potentially lead to early fatigue-related tyre failures. They studied

the stress and strain along the bond line between new tread and casing for a retreaded tyre by both experiment and finite element analysis.

Apart from the fatigue-related tyre strain and stress study, the strain and stress state also can be considered as an alternative reflection of tyre global behaviour. Namely, the tyre strain and stress state has certain relationship with tyre operational conditions. However, the strain and stress, especially the internal strain and stress is very difficult to model and validate in order to get reasonable results.

Moreover, the proper method and tool to measure large strain of tyre rubber has been a critical issue in the past decades. Clip gauge [23], rubber-wire gauge [24], liquid-metal gauge [25], photoelastic measurement [20], and digital imaging correlation techniques [26], have been developed to measure the large strain. Although the application of these strain gauges has been demonstrated, they are more difficult to manufacture or operate than the traditional metal foil strain gauge. With the development of metal foil strain gauge technology, some of them can not only measure large deformation but minimize the local stiffening effect with suitable adhesive.

2.2.2 TYRE FORCE AND MOMENT

In this study, the tyre force and moment characteristics are introduced in the coordinate system given by the Society of Automotive Engineers (SAE) shown in Figure 2.2 [27]. The axis x, y, z represents the tyre longitudinal direction, lateral direction and vertical direction,

respectively. They are perpendicular to each other and the z axis is perpendicular to the ground. The translational forces F_x, F_y and F_z along the three axes are tyre longitudinal force, lateral force and vertical force, respectively. The rotational forces (moments) M_x, M_y and M_z about the three axes are tyre overturning moment, rolling resistance moment and aligning moment, respectively. Slip angle alpha α is defined as the angle between tyre velocity direction and the intersection line of tyre plane and ground. Camber angle beta γ is defined as the angle between x-z plane and tyre plane.

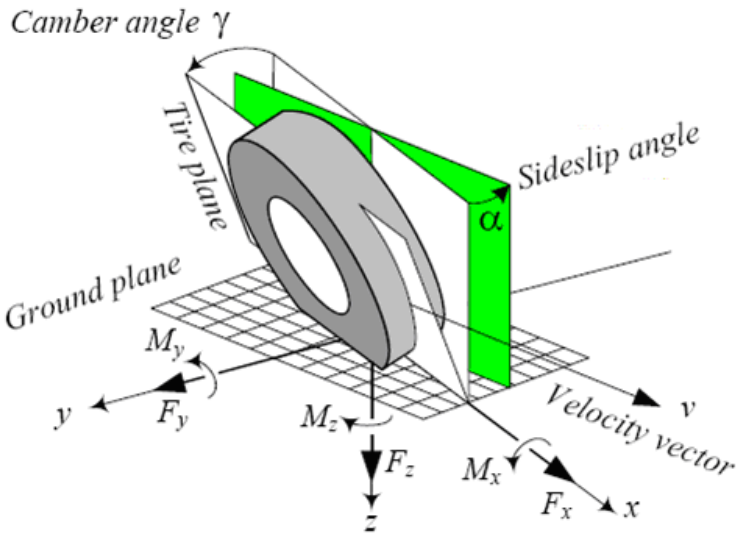

Figure 2.2 SAE Tyre Coordinate System [27]

The tyre force is the resultant from normal and shear stresses distributed in the contact patch. The non-uniform distribution of normal and shear stresses leads to the generation of tyre moments. The shear stress is responsible for the generation of longitudinal and lateral forces due to the friction coupling effect between tyre tread and road. The friction coupling effect is caused by two primary mechanisms: surface adhesion and hysteresis [28].

The tyre forces and moments not only are the response to driver input at the tyre/road contact patch but also provide the means to change vehicle direction and keep the vehicle travelling in the expected lane. The control of tyre vertical force can improve the vehicle vertical vibration characteristics and ride behaviour. The control of tyre lateral force usually benefits the vehicle stability and cornering, and an optimised tyre longitudinal force control can improve vehicle braking/traction performance and reduce fuel consumption. There is a large body of literature presented about modelling tyre force and moment. Sharp and Pacejka present a comprehensive review covering this subject [29].

2.2.2.1 Traction and Braking

The traction and braking properties of a tyre are related to the tyre longitudinal deflection and the tyre/road friction. For the rolling tyre in traction, the tread element compressed before entering the contact patch is bent forward due to the longitudinal shear stress. For the rolling tyre in braking, due to the longitudinal shear stress in opposite direction, the tread element is stretched and bent backward before entering the contact patch The traction and braking states of a tyre can be illustrated by Figure 2.3 and Figure 2.4, respectively [30].

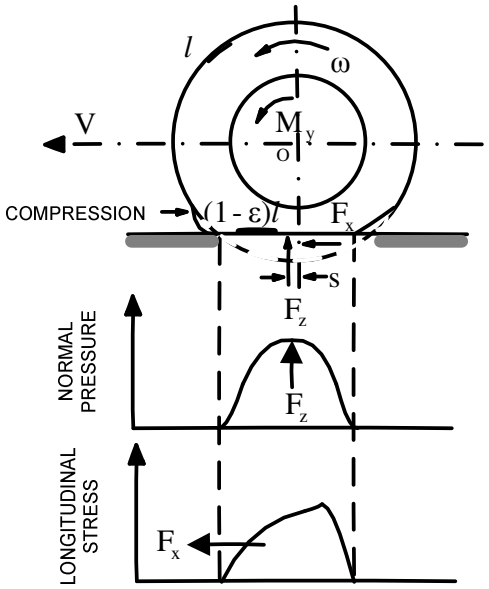

Figure 2.3 Behaviour of A Tyre under Traction [30]

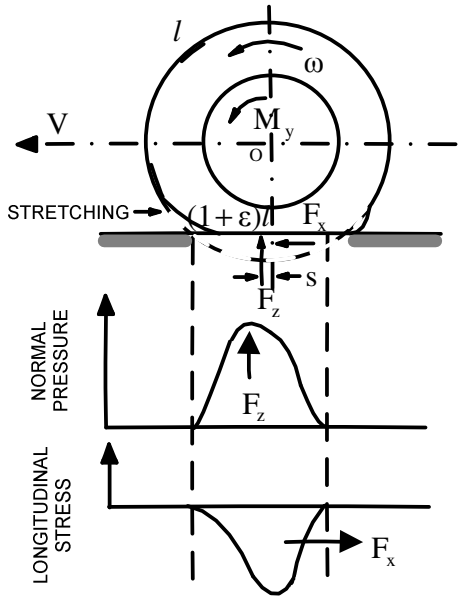

Figure 2.4 Behaviour of A Tyre under Braking [30]

When the tyre moves with a linear speed higher than its circumferential speed about the *y* axis, braking occurs in the contact patch where the tyre tread deflects to develop and sustain the friction force, viz. braking force. Likewise, traction force is generated when the tyre moves slower than its circumferential speed about the *y* axis. In one word, the traction and braking forces are generated due to the difference between tyre travelling speed and tyre rolling speed. The difference is defined as longitudinal slip, as

$$\kappa(\%) = \left(\frac{r\omega}{V} - 1 \right) \times 100 \tag{2.1}$$

where:

$r =$ Tyre effective rolling radius.

$\omega =$ Wheel angular velocity.

$V =$ Tyre travelling speed.

When the longitudinal slip is equal to zero viz. tyre rolling speed multiplied by effective radius is equal to tyre travelling speed, the tyre is under steady state rolling. When the longitudinal slip is negative, viz. tyre rolling speed multiplied by effective radius is smaller than tyre travelling speed, the tyre is under braking. When the longitudinal slip is positive, viz. tyre rolling speed multiplied by effective radius is bigger than tyre travelling speed, the tyre is under traction. The braking and traction force can be written as the function of longitudinal slip shown in Figure 2.5 and Figure 2.6 [31].

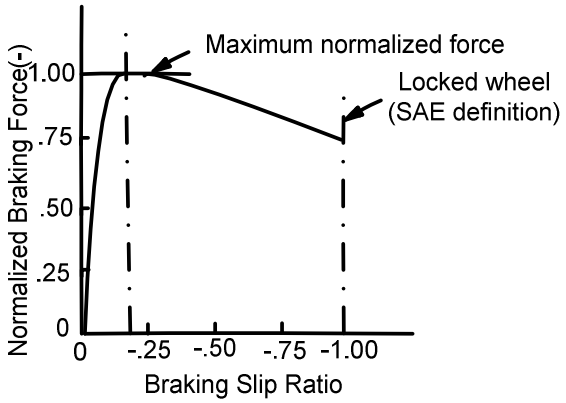

Figure 2.5 Typical Braking Slip Ratio Curve; Slip Angle= 0° [31]

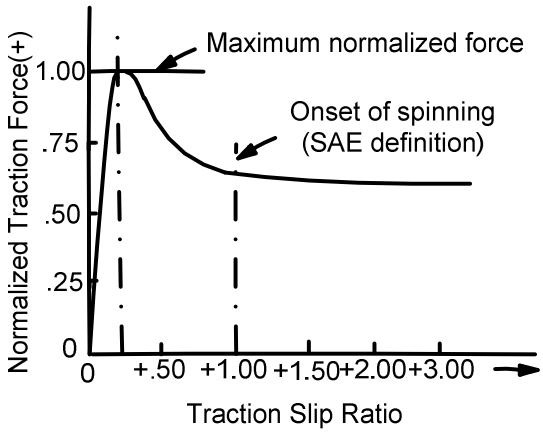

Figure 2.6 Typical Traction Slip Ratio Curve; Slip Angle= 0° [31]

It can be found that the longitudinal force increases with the longitudinal slip until the slip ratio reaches around 0.2. Then it reduces rapidly and the wheel will be locked or onset of spinning when the longitudinal slip ratio is equal to -1.0 or 1.0. In order to prevent the wheel lock occurring, anti-lock braking system (ABS) was developed to provide safer braking. At the onset of wheel lock, the ABS will release the brakes momentarily on the

locked wheels, and reapply them when the wheel spins up again [28]. This repeated operation can keep the braking force around the peak value thus optimising the braking efficiency.

As aforementioned in [28], the tyre traction and braking properties are dependent on a variety of factors such as vertical load, tyre inflation pressure and surface friction, etc. Intelligent Tyre System seeks to provide a platform that can enable this information to be acquired in real time and assist the vehicle dynamics control system to optimise tyre traction and braking properties.

2.2.2.2 Cornering Characteristics

When a vehicle is given a steering input to execute a lane change operation, a lateral force will be generated at the tyre/road contact patch. This cornering property of the tyre is mainly related to the change of tyre slip angle and camber angle during cornering.

Slip angle

The tyre contact patch experiences a distortion, as well as the tyre sidewall, when lateral slip occurs. In this case, the deformation of tyre contact patch is usually used to illustrate the generation process of lateral force by slip angle shown in Figure 2.7 [28].

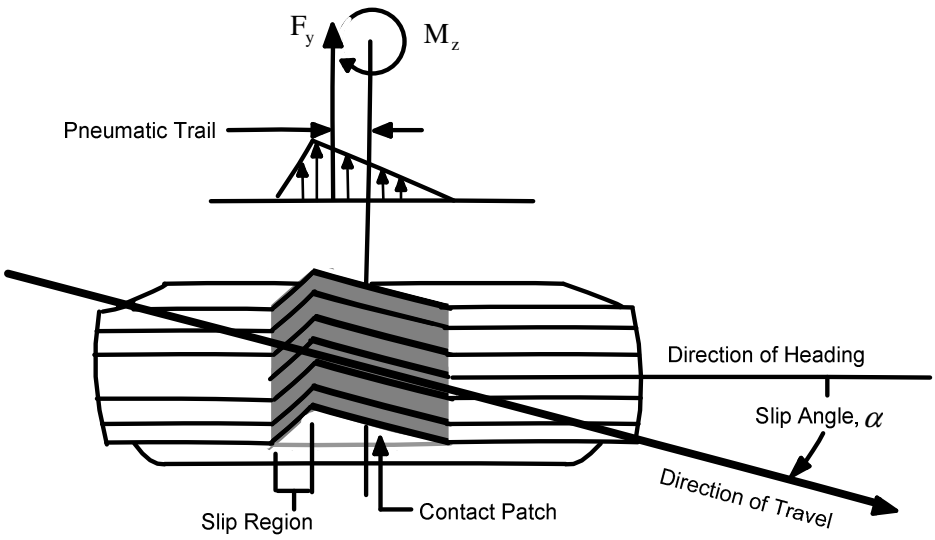

Figure 2.7 Rolling Tyre Deformation under Cornering [28]

Under the lateral force, the tread element of a rolling tyre experiences two states: lateral deflection and lateral slide. Firstly, with the tread element moving into the contact patch, the lateral deflection of tread element increases to generate more lateral shear stress. During this process, the resultant of lateral shear stress is still smaller than the lateral friction force which sustains the state balance force and keeps the tread element in the position of their original contact with the road. However, when the resultant of lateral shear stress overcomes the friction available, the tread element will slip to the side. It is found that the critical point between lateral deflection and lateral slide is located at the rear part of tyre contact patch. This asymmetry of force build-up process induces the resultant lateral force located in some position at the rear part of contact patch rather than the centre of it. It can be converted equally to the centre of the contact patch as a lateral force and an aligning moment. The distance between the real position of lateral force and the contact patch centre

is defined as the pneumatic trail. The variation of lateral force for slip angle is illustrated in Figure 2.8 [28].

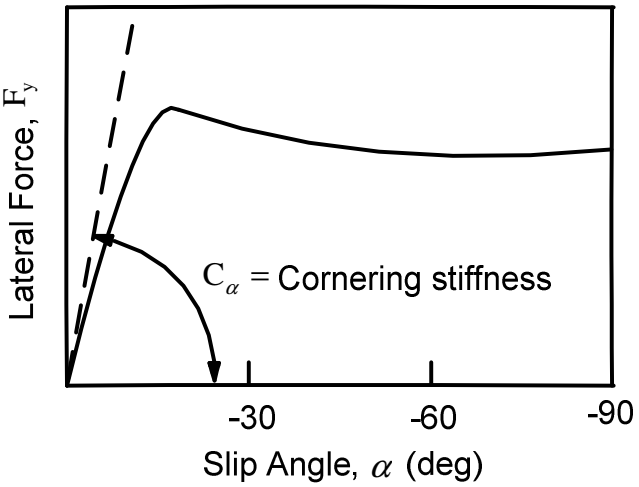

Figure 2.8 Variation of Lateral Force for Slip Angle [28]

The cornering stiffness C_α is defined as the negative slope at zero slip angle. The tangent of the slip angle is denoted as lateral slip. There exists a transfer process between current steady-state tyre and former steady-state tyre during cornering. The tyre needs between half and one revolution to build up lateral tyre deflection and generate the lateral force to reach the steady-state force condition.

Camber angle

Camber angle is another factor that can cause tyre to generate cornering force. A rolling tyre with camber angle will lead to the deformation in the tyre tread and carcass to generate the camber thrust (lateral force). The rolling tyre will follow an elliptical path forced by

camber thrust. The camber thrust is always oriented in the direction the tyre is inclined as shown in Figure 2.9 [28].

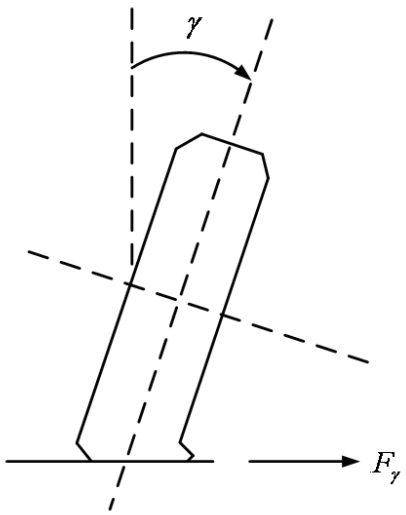

Figure 2.9 Tyre Camber Properties [28]

The ratio between camber thrust and camber angle is defined as camber stiffness

$$C_\gamma = \frac{\partial F_\gamma}{\partial \gamma}\Big|_{\gamma=0} \tag{2.2}$$

Where γ is the camber angle and F_γ is the camber thrust.

Generally, the camber angle range is smaller than the value range slip angle can reach. It is known that the contribution by camber angle to tyre cornering force is less than that of the slip angle.

Furthermore, the cornering characteristics of tyre depend on many variables, such as tyre size and type, number of plies, cord angles, wheel width and tread design, etc. The real-time information about the tyre cornering force is useful for vehicle stability control, which is one of the reasons for developing intelligent tyre technology.

2.2.3 TYRE/ROAD FRICTION

Tyre/road friction actually is one of the main factors considered in tyre traction, braking and cornering. The reason to list the tyre/road friction as an individual section is that the estimation of tyre/road friction becomes significant for the development of tyre active safety system as well as vehicle dynamics control system.

The traction/braking force and lateral force can only increase to the limit of the friction coupling between the tyre and road, respectively. As aforementioned, the surface adhesion and rubber hysteresis mechanism are responsible for the generation of friction. It is found that the surface adhesion contributes more to the friction force rather than the hysteresis mechanism. However, the surface adhesion effect is mainly dependent on the road conditions such as dry road giving more friction than wet road.

The friction circle gives the diagram of lateral force vs. longitudinal force for a series of slip angles and slip ratios [31]. Figure 2.10 shows one quarter of the diagram, which illustrates the trends going of lateral force for different slip angles when braking is applied [28].

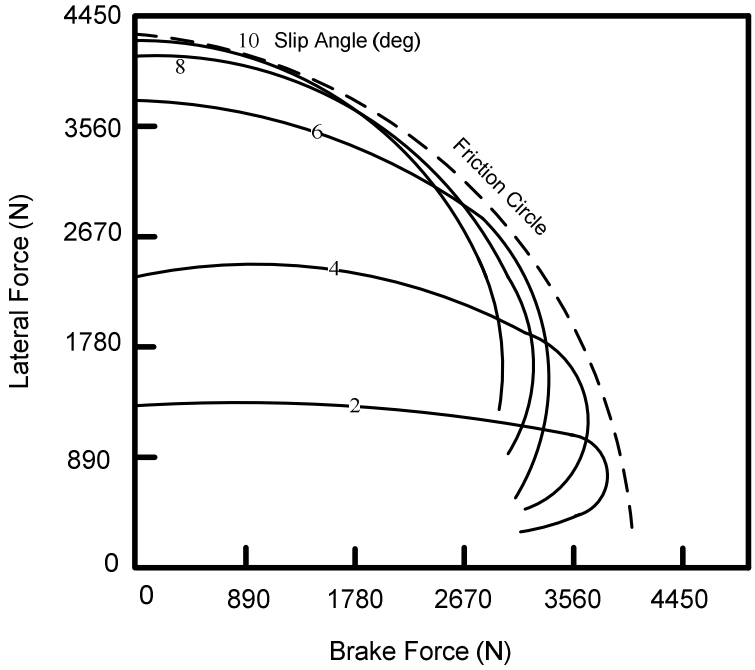

Figure 2.10 Lateral Force Variation for Different Slip Angle under Braking [28]

The whole curves region is enveloped by the friction circle. Any point located on the curve represents a combination situation of traction/braking and cornering. In order to achieve the maximum performance of the vehicle, the tyre working condition should be continuously staying close to the friction circle limit. Therefore, the profound understanding of the friction condition such as the potential friction and used friction is very vital for achieving reasonable and efficient driving operation, which leads to the development of tyre/road friction estimation technology.

The tyre/road friction estimation methods have been developed for decades from both simulations and experiments. According to [32], the research on tyre-road friction estimation can be classified into “cause-based” approaches and “effect-based” approaches.

The cause-based approaches are based on measuring the factors which contribute to the generation and changes of friction. The effect-based approaches are based on measuring the effect that friction induced on tyre or vehicle during driving. The tyre/road friction estimation approaches may be classified as shown in Figure 2.11.

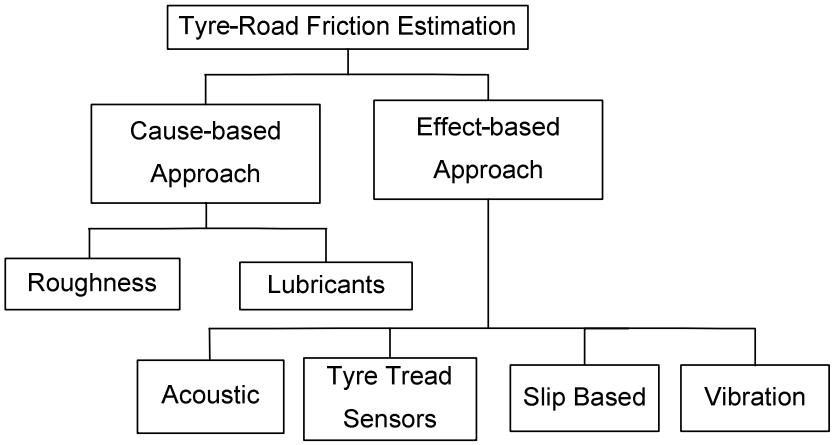

Figure 2.11 The Classification of Tyre/Road Friction Estimation Approaches [32]

In this section, a brief and up to date literature survey about tyre-road friction estimation method is presented based on [32, 33].

For cause-based approach, it mainly includes two branches, roughness and lubricants. The roughness usually refers to the road type such as soil, sand, asphalt, etc. The road surface considering pavement types and pavement surface macrotexture and microtexture, must ensure an adequate level of friction to provide safe operation of vehicles [34]. The lubricant refers to the road conditions such as water film, ice, snow, etc., which plays a lubricant role

between tyre and road. In this case, the friction will be reduced and the tyre grip force falls, which may lead to the vehicle losing control.

In order to detect the road type and condition viz. roughness and lubricant, different types of sensor have been adopted such as optical sensors [35, 36], microwave spectrometers, doppler sensors [37].

For effect-based approach, it mainly consists of the branches of acoustic, tyre tread sensors, slip based and vibration.

For acoustic approach, the tyre/road noise level has certain relationship with tyre/road friction. By analyzing the noise and identifying the different features for different friction conditions, the friction coefficient can be estimated [38].

For vibration approach, the torsional resonance characteristic of wheel is considered to vary with the tyre-road friction, especially the strength of the resonance [39].

For the approach based on tyre tread sensors, the sensors are embedded into the tyre tread to measure the tyre tread deformation. These deformations contain the information about the total longitudinal, lateral and vertical forces as well as the road condition [32].

For the slip-based approach, it utilizes the tyre longitudinal slip to classify road friction levels, which may not need additional equipped sensors since the ABS provides the wheel

speed sensor, such as [40]. Numerous studies have been carried out based on slip-based approach. It is found that many of the friction estimation methods are based on tyre brush model such as [41-43]. However, as a simplified model, brush model cannot deal with the complex tyre behaviour and the estimator is sensitive to the inaccuracy of the model [44].

With the development of high performance computing, the finite element method is also used to estimate the tyre/road friction. Gurkan Erdogan, et al. developed a finite element tyre model to generate acceleration profiles including lateral, tangential and radial accelerations. The simulated acceleration profiles were validated by experimental data and used for the estimation of slip angle and tyre/road friction coefficient [45]. However, considering the simplification of the finite element tyre model and the sensitivity of accelerometers to noise, there is still space for improvement such as the utilization of complex finite element tyre model which is capable of providing accurate simulation results, and the use of strain sensor which is able to provide stable test data with less noise. Moreover, the strain sensor is cheaper than the MEMS accelerometer.

2.3. TYRE MODELLING METHOD

In the past decades, many tyre modelling methods have been developed to investigate the tyre mechanical properties and improve tyre performance. The choice of tyre model generally depends on the aim of the research, such as static and dynamic behaviours, NVH (Noise, Vibration and Harshness), reliability and durability, and thermal effect, etc.

Although some tyre modelling methods have become matured and adopted in commercial software, such as FTire, RMOD-K and SWIFT, more work still needs to be carried out towards realistic simulation for the dynamics responses of a rolling tyres [46].

In this section, a brief review about analytical tyre model and empirical tyre model is given firstly. Then, an extensive literature survey is presented about finite element tyre model which is the main tool used in this thesis to study tyre characteristics and develop intelligent tyre technology.

2.3.1 ANALYTICAL TYRE MODEL

In order to explore the behaviour of the pneumatic tyre under various conditions, particularly for being regarded as a significant component of vehicle dynamics system, the analytical models of tyre were developed.

Research on analytical modelling of tyre/road contact developed in the following order before the 1980's: point contact model, rigid tread band model, fixed footprint model and adaptive footprint model. In spite of the simplicity and inaccuracy of these initial analytical models, they provided fundamental knowledge of the principal characteristics of the tyre and contributed to the analytical parts of terrain-vehicle model for dynamic vehicle simulation [47].

Meanwhile, for vehicle handling analysis, corresponding simple models were also developed. The principal models were: the string model, the beam model and the ring model with/without elastic or viscoelastic foundation. The common feature of the aforementioned analytical models is that the tread is regarded as a prestressed string or a ring (with bending stiffness), and the sidewalls as elastic (or viscoelastic) foundations supporting the tread structure [16]. Some of the analytical tyre models are illustrated in Figure 2.12.

With the progress in tyre research, the analytical model has become more suitable to be integrated into the vehicle system for vehicle dynamics study. However, the choice of how to represent the nonlinear properties in tyre model still affects the accuracy and practical application of tyre analytical models.

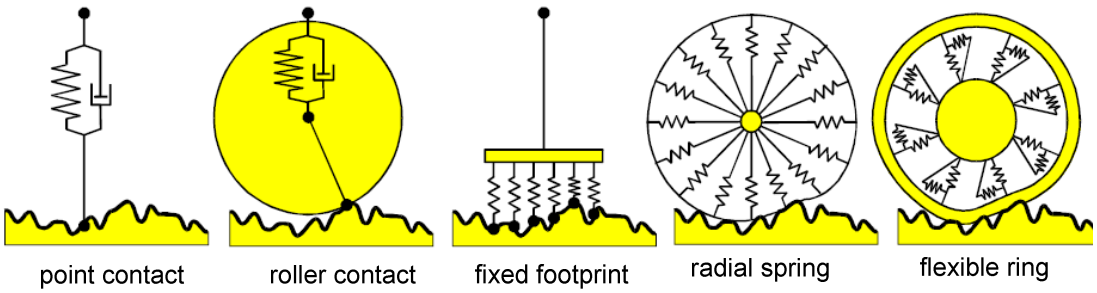

Figure 2.12 Examples of Analytical Tyre Models [13]

In one word, analytical tyre models are setup from the physical point of view based on the knowledge of force generation at tyre/road contact patch. Due to the simplification for physical phenomenon, analytical tyre models are not capable to explain various situations

encountered in reality. However, the parameters of analytical tyre models have their own physical explanation such as brush model.

2.3.2 EMPIRICAL TYRE MODEL

In order to get over the inaccuracy caused by simplification in analytical model, semi-empirical/empirical models were developed considering the validation from experimental data. To some extent, this formulation compensates the margin of error brought by theoretical assumption in analytical model. Several classical empirical models have been developed and used in the tyre dynamics analysis such as "Magic Formula" tyre model [48, 49].

The Magic Formula tyre model presented by Pacejka is one of the most famous empirical models. Its original goal was to achieve accurate description of measured steady-state tyre behaviour. Then it was developed to different derivatives according to the tyre conditions such as transient tyre dynamics. The core part of Magic Formula tyre model is based on tyre pure slip condition for predicting tyre force and moment. The coefficients of Magic Formula can be identified by experiments.

The general form of Magic Formula for pure slip or pure longitudinal slip is expressed as:

$$y(x) = D\sin\left[C\arctan\{Bx - E(Bx - \arctan Bx)\}\right] \tag{2.3}$$

The formula is capable of describing the curves for the side force F_y, the aligning torque M_z and the longitudinal force F_x as functions of their respective slip quantities: the slip angle α and the longitudinal slip κ.

where the output variable y represents either F_y, M_z or F_x and the input x represents α or κ.

The coefficients are:

B: stiffness factor

C: shape factor

D: peak value

E: curvature factor

It can be seen from the Magic Formula tyre model that empirical tyre models usually need a lot of test data, which try to adjust functions to measured data without giving a physical explanation. In this case, it is difficult to get a physical understanding of the derivation of empirical tyre models.

2.3.3 FINITE ELEMENT TYRE MODEL

Over the past twenty years, numerical analysis, especially the Finite Element Analysis (FEA), has been increasingly applied during the whole tyre design process. Because the basis of the finite element method is to divide the whole structure into finite elements and calculate the structure's mechanical properties by integrating the corresponding variables

on the nodes of elements, it is potentially more accurate and applicable for tyre realistic simulation. At present, the FEA is taking the place of some tyre tests.

At the University of Birmingham, various finite element models were developed to simulate the tyre behaviour. Andrew Burke [50, 51] investigated the tyre/road interaction and the characteristics of tyre dynamic response by the finite element code MSC/NASTRAN using a model made up of shell elements. Different inflation pressures and hub loads were adopted in the simulation of tyre/road interaction modelled by the gap element formulation, which gave accurate results compared with experiments. Furthermore, in Burke's work [52], a cleat test was carried out to obtain an insight into the response of a rolling tyre to road inputs as well as the enveloping characteristics in the time domain. However, only hub loads and inflation pressures were considered at zero slip and camber angle.

Recently, E.O. Bolarinwa and O. A. Olatunbosun [53-55] reported on the research of tyre characteristics using finite element code ABAQUS in the University of Birmingham. The finite element tyre model was built using 3D solid elements by revolving the 2D cross-section tyre profile. The simulation of tyre steady-state behaviour during cornering was addressed and compared with experiments which were carried out on the AEC tri-axial tyre test rig. Particularly, the relaxation length effect is investigated for the tyre transient behaviour under the impact of preload. However, Bolarinwa's tyre model suffered from lack of accurate information of tyre composite geometry and viscoelastic material property.

With the development of commercial finite element software, the amount of papers published about tyre dynamics analysis based on FEA has increased dramatically. Kazuyuki Kabe and Masataka Koishi [56] analyzed the typical tyre cornering property using ABAQUS implicit and explicit. They investigated the relationship between driving force and angular velocity of steady-state rolling tyre by ABAQUS/Standard, whilst transient response including cornering force and self aligning moment considering different parameters effects are also described by ABAQUS/Explicit.

In the series of publications by M. H. R Ghoreishy, several facets of tyre simulations were investigated [57-61]. In [58], M. H. R Ghoreishy carried out a parametric study for steady-state rolling tyre considering type of cords, belt angle and tyre/road friction coefficient, etc. As to the tyre static analysis considering tread pattern, M. H. R Ghoreishy tied the two meshed sections together to achieve the model of tyre with tread pattern [59]. He carried out finite element analysis of tyre cornering considering the effect of belt angle [60]. It is concluded that maybe the belt angle of 20 degree gives the best performance for the designated tyre by analyzing the distribution of frictional shear stress and contact pressure at different slip angles and belt angles. It was shown in this study that the interlayer shear stress at belt edge zones and total strain energy can be used to predict the separation of belts and large deformation of the tyre.

Many other researches have focused on the effect of belt angle on tyre behaviour or durability with a view to optimise tyre design. Guan Yanjin, et al [62] took the belt cord angle of a radial tyre into account for different rolling conditions using MSC.MARC. By

investigating the influences of belt cord angles of 64°, 68°, 72°, 76° and 80° under free rolling, full traction and full braking, the normal stress distribution, friction stress distribution and cord equivalent stress distribution were studied in the contact patch. It was concluded that the cord stress was concentrated in the tyre shoulder and decreases with the increase of the belt cord angle. The simulation predicted that the optimum belt cord angle of the 195/60R14 radial tyre was $\pm 72^{\circ}$.

Obviously, the finite element tyre model can provide useful information for tyre designers, to some extent, more than the physical testing. Jani K. Ojala reported that the development process of tyre can be reduced by using modern simulation tools, such as ABAQUS which involves less cost and time and provides more trial data utilizing its expandability and flexibility before carrying out any physical testing. An example about optimising shear stress concentration in the belt edge was used to demonstrate the significance of using ABAQUS for design in the tyre industry [63]. Similarly, finite element tyre model was developed for tyre design with respect to tyre constructional changes, such as variable belt angle, tread material, apex height and ply turn-up height in [64]. P. Ghosh [64] used continuum 3 dimensional, 8 nodes with hybrid formulation element in generating a 3D tyre model. Nonlinear FEA was carried out iteratively for single and interactive effects of individual parameters considering design matrix. The simulation results, including inflation and load defection, lateral, tangential and cornering stiffnesses correlate well with the experimental data. However, the complex effect of tyre parameters such as the combination

of slip angle and camber angle were not taken into consideration while the geometry details of the tread were also ignored.

The combination of optimisation algorithm and finite element tyre model is also one of the prospective and applicable approaches to tyre design. Generally, the geometry of tyre cross-section and the construction of tyre reinforcement are the two main areas for design optimisation. In the research carried out by Abe, et al. [65] the topological tyre structure was explored with respect to optimising the Young's modulus of each tyre material in order to improve the tyre performance, particularly the rolling resistance. Furthermore, the genetic algorithm (GA) [66] was introduced to optimise the belt structure including the belt angle and belt width. The optimisation process was validated by physical testing revealed that it can increase the cornering stiffness by 15%. Cho, et al. [67] presented a multi-objective optimisation method to optimise the tyre carcass contour. By using non-equilibrium tyre contour theory, an optimum tyre carcass contour was achieved using satisfying trade-off methods (STOM) by satisfying the conditions of increasing the carcass tension in the bead-side to improve tyre maneuverability and minimizing the carcass tension in the belt-edge region and strain-energy density to improve the tyre durability using a 2D FE tyre model under inflation. The inner nodal radii of carcass element were chosen as design variables.

In addition, J. R. Cho [68] developed a 3-D patterned tyre model to investigate the standing wave phenomenon using transient dynamic rolling analysis. Two belt layers, one carcass layer and an inner-liner are modelled using composite shells, whilst the solid element is

chosen for modelling the steel cord and bead region considering the analysis accuracy and CPU time. Since the standing wave phenomenon generally appears at a high speed in reality due to the damping effect, a damped frictional dynamic rolling analysis is carried out by the total Lagrange method together with the penalty method to enforce the dynamic contact. As a result, the maximum relative error of critical speed between simulation and experiment is limited within 5%. J.R.Cho also performed the parametric investigation for the tyre critical speed which was influenced by the inflation pressure and vertical load. For example, the critical speed increases with the square of the tyre inflation pressure, but decreases with the vertical load.

As a significant part of tyre characteristics, the tyre NVH also attracts many attentions from tyre researchers. Sandberg, U. and Ejsmont, J.A. [38], divided tyre/road noise generation mechanisms into two main aspects: vibrational mechanisms and aerodynamical mechanisms. At lower frequency range of investigation, the tyre vibration plays a dominant role for the production of tyre/road noise. Meanwhile it is also the main contributor to occupant feeling. In [69], in order to carry out the study of tyre and vehicle NVH, Zhang, Y. et al developed a complete finite element tyre model which can serve for full vehicle finite element model real time proving ground simulations. Several non-conventional analyses including 3D free vibration and harmonic/randomly forced vibrations with ground contact were run using the explicit nonlinear dynamic finite element code LS/DYNA3D. All the vibration analyses were carried out in time domain and the result data were decomposed using Fast Fourier Transformation (FFT). This study provided a possibility for more reasonable tyre and vehicle NVH study. Similar full finite element vehicle model can

be found in [70]. However, at present stage, the study did not consider the vibration simulation for rolling tyre in [69]. Moreover, there are also disadvantages for explicit analysis in time domain such as CPU time requirements as well as the FFT resolution depending on the total simulation time. In [71], a wave number concept based on the circumferential and meridional motions of the tread/belt was introduced to categorize tyre modes, which can simplify and improve identification and physical understanding of tyre vibration modes. The tyre modal analysis based on finite element tyre model was implemented and the modes obtained were distinguished by the above approach. The effect of loads, design considerations, wheel property and enclosed air on mode identification was revealed. It provides a method for studying the tyre vibration modes systematically. In [72], the natural frequency and mode shape of a non-rotating tyre was studied by using finite element tyre model. The predicted results agreed well with the experimental data. In [73], Gabriel Anghelache and Raluca Moisescu investigated the effects of rubber elastic material properties on the tyre modal properties by finite element analysis. The C10 coefficient of hyperelastic material property model of tyre tread rubber was varied successively within the value range from literature and its influence on tyre natural frequency was observed. It was found that the C10 coefficient has a pronounced effect on the high order tyre resonant frequency.

It is obvious that the finite element tyre model has many advantages and is useful for the tyre designer, manufacturers and even customers. In order to improve the efficiency of product development during design, testing and manufacturing processes, an integrated system which can seamlessly combine the tyre CAD design system and tyre FEA system

together is required [74]. It is even expected that this integrated system can have seamless interface with vehicle dynamics simulation software such as SIMPACK and CarSim. However, there is still a long way to go even for developing an integrated approach for tyre FEA efficiently. An integrated approach for transient rolling of tyres is presented by ABAQUS technicians [75], which show a prospective streamlined total analysis approach for tyre from ABAQUS/standard steady-state analysis to ABAQUS/explicit transient analysis using import function shown in Figure 2.13. At the same time, ABAQUS also provides co-simulation function to perform FEA from ABAQUS/Standard to ABAQUS/Explicit in parallel. One of the important benefits ABAQUS provides is that the definition of tyre reinforcing cords makes the meshing of the cords independent of the meshing of the rubber matrix [75].

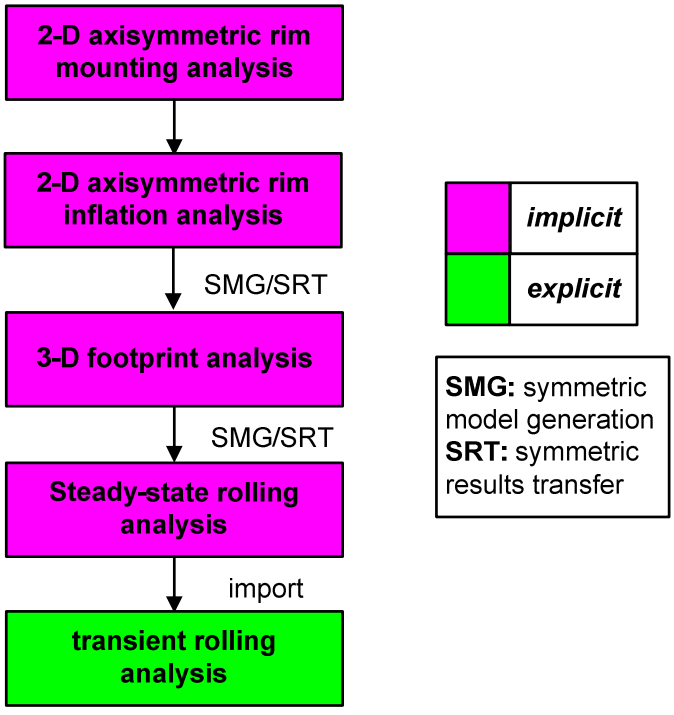

Figure 2.13 Tyre Finite Element Analysis Diagram [75]

Yamanishi, T. and Matsuda, K. [76] reported that the Ohtsu Tire & Rubber Co. Ltd in Japan is developing an integrated tyre analysis and simulation tool based on MSC.Acumen. The difference for a new tyre design process before and after adopting integration method is shown in Figure 2.14 and Figure 2.15. As outlined below, with the virtual analysis and simulation tools, designers can carry out virtual test rather than physical test by themselves to accelerate the iterative processes. It is expected that this integrated system will have 8 months cycle time reduction for a typical passenger tyre design process after 3 years from introduction.

As to the application of finite element tyre model on developing intelligent tyre technology, Matsuzaki, R. and Todoroki, A. [7] employed FEA to construct the relationship between tyre strain on the inner surface and tyre mechanical parameters including contact patch length, effective radius, wheel load and braking torque, which was expected to contribute to the development of optimising vehicle braking control and road condition warning systems. Although their research provides a perspective view of finite element tyre model in developing intelligent tyre, necessary experiments are still required for the validation and complement. Moreover, many issues such as the selection of sensor location, sensor output and the effect of tyre cornering on the correlation need further profound study.

Based on the aforementioned literature survey, the finite element code—ABAQUS is employed for this study. It can be seen that ABAQUS provides the feasibility to simulate the tyre behaviour accurately considering the tyre complex structure and material property.

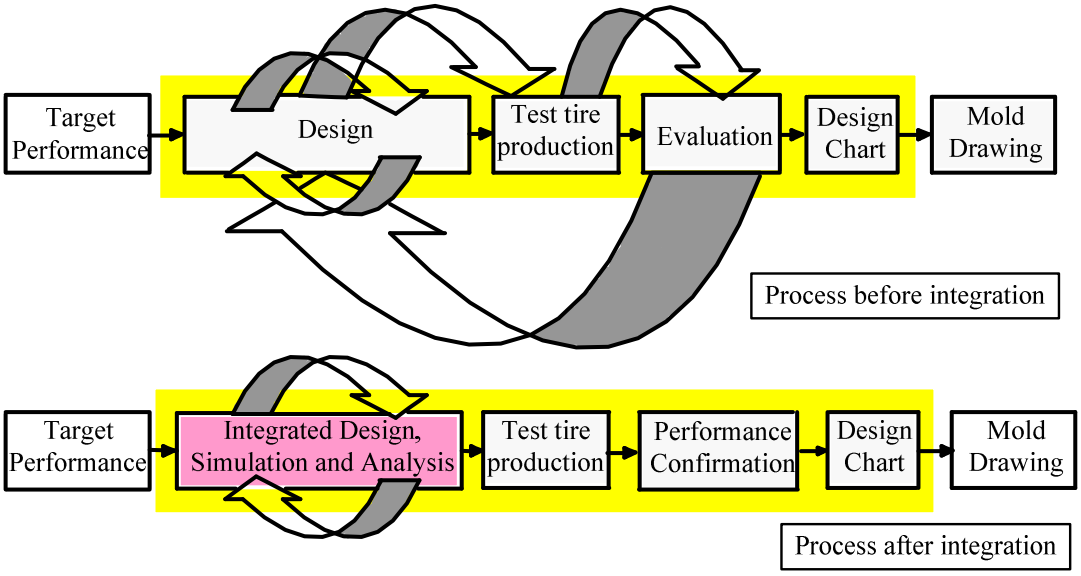

Figure 2.14 Iterative Process in New Tyre Development before and after Integration: Part I [76]

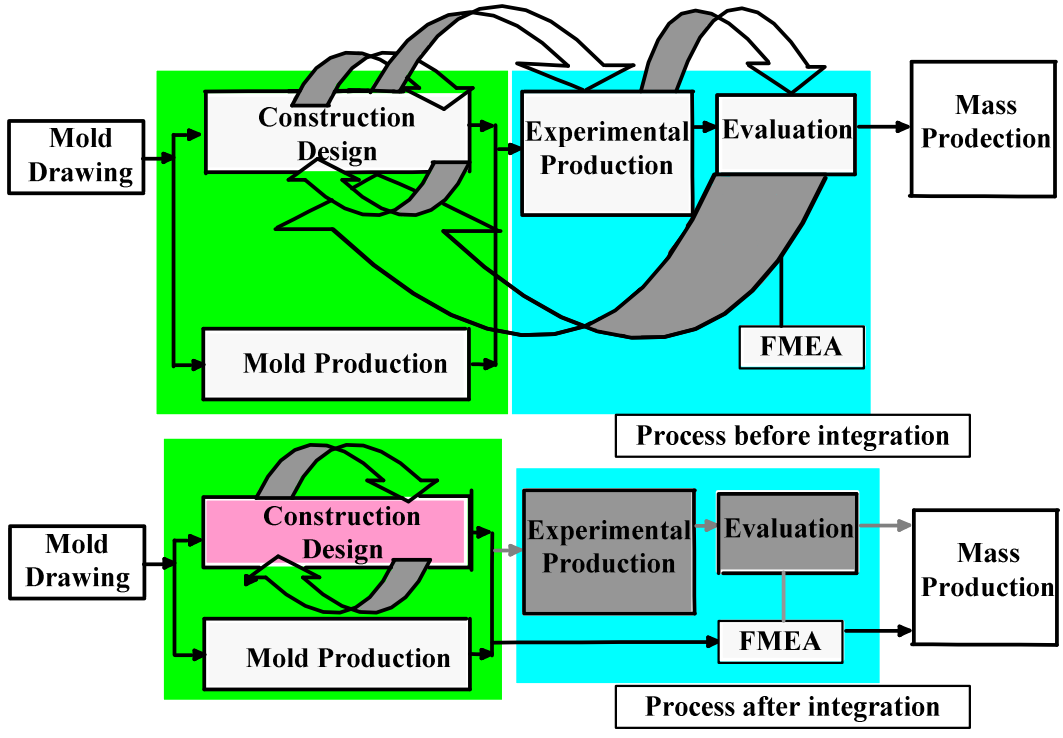

Figure 2.15 Iterative Process in New Tyre Development before and after Integration: Part II [76]

2.4. INTELLIGENT TYRE TECHNOLOGY

Because of the dependence of vehicle safety on tyre performance, in recent years a large amount of research has been focused on tyre monitoring technology which was then developed into intelligent tyre technology. The intelligent tyre technology can improve the vehicle safety by monitoring tyre status and cooperating with vehicle dynamics control systems. In addition, it can contribute to reducing the fuel cost and environmental effects by ensuring that the tyre is at the required inflation pressure.

The development of intelligent tyre technology can be divided into three stages. The first one is the tyre pressure monitoring system. At present, it is the only applicable intelligent tyre technology in the market, which can provide direct information about tyre inflation pressure.

The second stage is the multi-facets monitoring system. The tyres equipped with different sensors exhibit a positive impact on the traffic safety because of the possibility of early detection of tyre failures and working status. According to the investigation by Li Li, et al, the second stage can be defined as follows [77]:

(1) Tyre pressure monitoring, since an under-inflated tyre may cause a serious accident especially when steering or braking;

(2) Tyre temperature monitoring, since too high temperature may lead to tyre explosion and severe tyre wear;

(3) Tyre force and deformation monitoring, which can be used for tyre design, tyre dynamics modelling and vehicle dynamics control system optimisation;
(4) Tyre/road friction monitoring, which is directly related to vehicle motion control.

The last stage can be referred to as “smart tyre” or “conscious tyre”, with ability to change the tyre’s structure or material characteristics to fit different road conditions. It can provide the driver information when to replace the tyres. As to this aspect, the smart material plays a very important role, with ability to change its stiffness, shape and natural frequency, if it is stimulated by the changes of current or temperature. The tyre made of this smart material is expected to perceive the road condition variation and response automatically, such as changing the tread pattern. At present, some smart materials are available including piezoelectric ceramic, magnetostrictive material, optical waveguide fibre and shape memory alloys, etc [78].

Recently, in order to improve the driving safety and operation efficiency, as well as solve the relevant problems generated by the transportation system, the Intelligent Transportation System (ITS) is addressed based on the utilization of computing and information technologies. The ITS may include Intelligent Vehicle System, Intelligent Track System and even Intelligent Space System [77].

Most works which have been developed about ITS focused on the Intelligent Vehicle System. To achieve the above goal needs many advanced technologies including sensory, decision and control, etc. All the information from different components of the vehicle is

expected to be collected and processed by the central unit in order to assist or complement the driver's operation.

As a major subsystem of Intelligent Vehicle System, the Intelligent Tyre System can provide the important information for the realization of safer driving. As shown in Figure 2.16 [6], apart from the driver's misjudgement, the tyre/road contact condition is a significant factor in vehicle accidents.

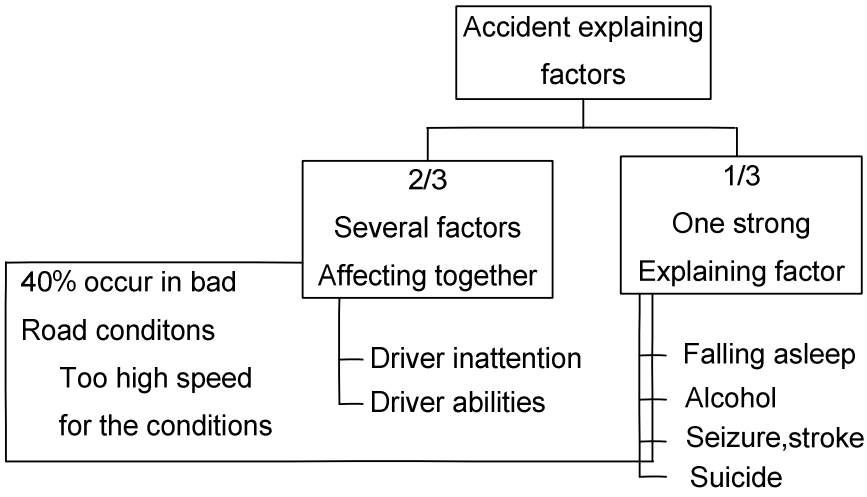

Figure 2.16 Causative Factors in Severe Road Conditions [6]

Since the tyre is the only interface between vehicle and road, the tyre response caused by road condition and driver operation presents abundant information for vehicle control system and can be measured directly or indirectly. It is expected that great benefits can be achieved from the application of Intelligent Tyre System, such as optimising the anti-lock brake system and vehicle stability control, identifying the friction coefficient and road

condition [3]. All the above benefits which are expected to be achieved are related to the knowledge of the mechanical properties of rolling tyre such as tyre force, moment and contact patch information.

A macroscopic perspective of the role of Intelligent Tyre System was discussed as shown in Figure 2.17 [79].

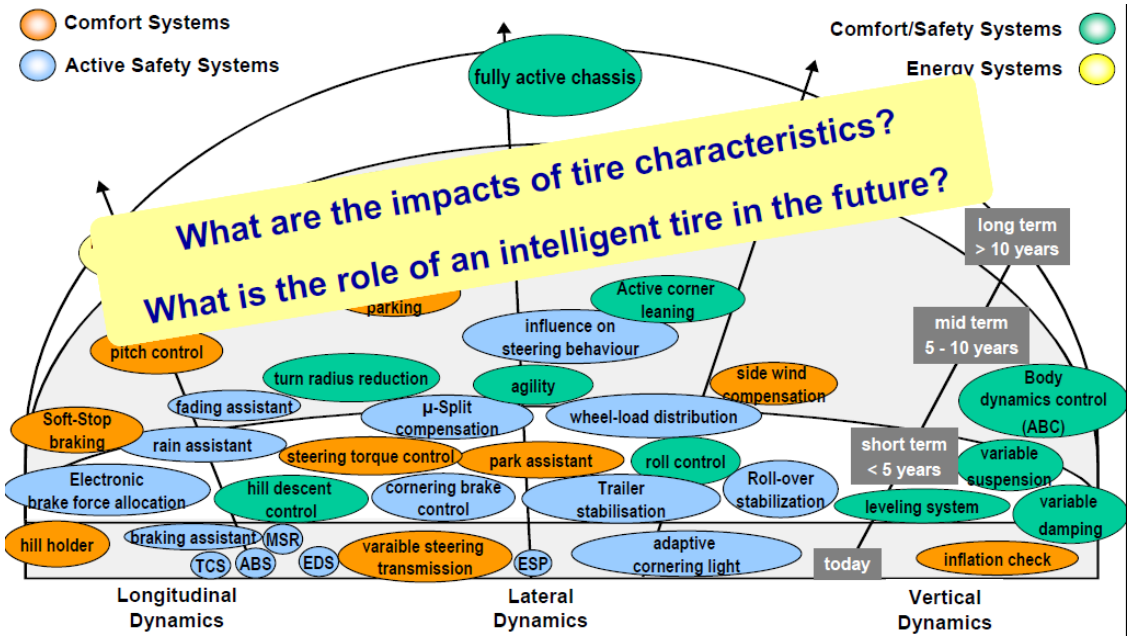

Figure 2.17 The Role of An Intelligent Tyre in the Future [79]

It can be seen that the impact of an intelligent tyre is various. From the point of view of providing the information of forces and friction at the tyre/road contact patch for improving driving safety, predicting the tyre damage and avoiding accident, the application of Intelligent Tyre System will greatly change the situation of present transportation. In [80],

the capability of a vehicle to change the driving state to avoid a dangerous driving situation is discussed. The maximum friction available was considered as one of the main factors for achieving safer driving and Advanced Driver Assistance Systems (ADAS). It is expected that apart from the drivers, external users (such as occupants in other vehicles) can also share these information on the internet in future.

Although many different devices have been invented and it was announced that they can achieve some of the goals of intelligent tyre, most of them are still laboratory bound and not mature enough to be converted into mass product in the market.

The Apollo project [6] is an example utilizing on-line tyre monitoring system, which was engaged in an ambitious perspective in creating an Intelligent Tyre System for accident free traffic using tyre-related information for vehicle control and driver operation as shown in Figure 2.18.

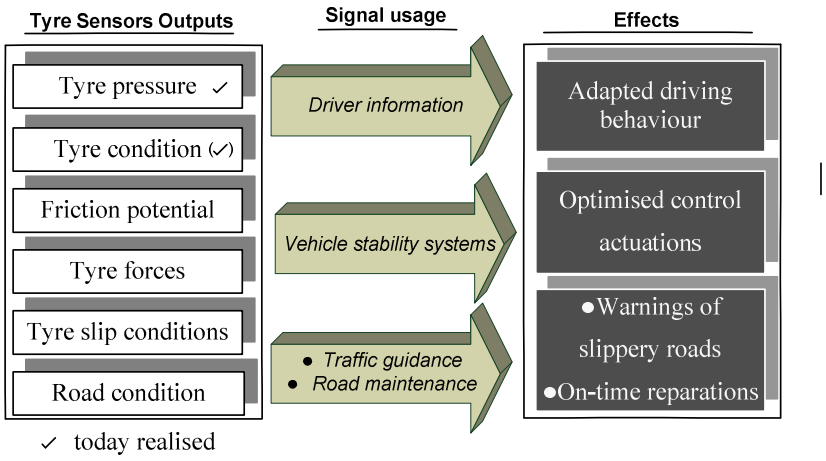

Figure 2.18 State of the Art in the Used of Tyre-related Information for Vehicle Control and Driver Information [6]

At present, many related works are ongoing in order to realize Intelligent Tyre System. In this study, a wide literature review of the Intelligent Tyre System is carried out in order to get a comprehensive understanding about the development of Intelligent Tyre System in recent years. Usually, the construction of an Intelligent Tyre System does not only need the sensor technology but also the communication and power technology.

2.4.1 TYRE PRESSURE MONITORING SYSTEMS (TPMS)

An abnormal tyre inflation pressure will cause big issue for the vehicle safety so that it is necessary for driver to know tyre inflation pressure in time in order to avoid irreparable accident. Tyre Pressure Monitor System is the first product which has been commercialized and put into market. In 2002, the USA passed the Tread Act [2] to require an installation of a TPMS to warn the driver if the tyre is significantly under-inflated. This legislation could be considered as the first strong step for the intelligent tyre development. In 2012, TPMS will become mandatory in the European Union. This measure is intended to not only improve vehicle safety, but also reduce CO_2 emissions.

There are two approaches to get the tyre inflation pressure information: indirect measurement and direct measurement. The indirect measurement is usually utilizing the already existing sensor installed in the vehicle such as the wheel speed sensor from ABS to estimate the tyre pressure based on certain algorithm. In such case, the pressure measurement is prone to be disturbed by other variables. Direct measurement usually

adopts sensors on the rim inside tyre or over the valve measuring the pressure directly. Many different types of TPMS sensors can be found in the market, such as [81].

It is obvious that the direct measurement provides much more accurate data than that by indirect measurement. As the core technology of TPMS, pressure sensors technology has experienced significant development from metal diaphragm sensors with bonded silicon strain gauges to present surface-micro machined, optical, resonant, and smart pressure sensors [82]. At present, some TPMS systems have integrated the measurement of tyre inflation pressure and temperature. Also it requires the integration of not only pressure sensor technologies but also measurement principle, power supply, data transmission and data handling, etc.

2.4.2 SENSOR TECHNOLOGY IN DEVELOPMENT

The Intelligent Tyre System providing the tyre status information have already been developed and tested in lab, such as Darmstadt sensor [35] and the SideWall Torsion(SWT) [83]. Darmstadt sensor can detect three-dimensional movements of a tread embedded magnet. The SideWall Torsion (SWT) sensor provides an estimate of the longitudinal and lateral forces in the contact patch by monitoring the magnetic field generated by alternate north-south poles embedded in the tyre. However, there is still a long way ahead to go for the maturing of Intelligent Tyre System. A number of sensor technologies suitable for use in intelligent tyre technology are described below.

2.4.2.1 Surface Acoustic Wave Sensor

Surface Acoustic Wave (SAW) sensor was developed based on the radio sensor technology in the last two decades. The SAW filters can screen out harsh environment frequencies from the signal received by the device. It is an ideal device for remote measurement. For a SAW sensor, the input request signal is transformed into a surface acoustic wave. This wave is reflected on the sensor. Then the sensor responds with a radio signal which will be detected by a receiver. The SAW sensory system employs the sensitivity of special crystal cuts of different substrate materials to strain, temperature and mechanical stress, or their stability against such environment effects. The value of the associated physical parameter could be converted and measured by the change of sensor's surface length or surface acoustic wave's velocity, respectively [77]. It means that the SAW sensor [84] [85] can not only be used for tyre inflation pressure and temperature measurement but also many other mechanical properties such as deformation.

Many other literatures can be found about using SAW sensor in tyre inflation pressure measurement in [86].

The SAW sensor can also be directly vulcanized into the tread elements of tyres, and used to measure the road friction which can provide valuable information for future driver-assistance systems and for optimizing slip-control and vehicle-stability systems, even more accurate than ABS [87]. Since the SAW transponders are small, robust, inexpensive, and can withstand extreme conditions, its application has been investigated broadly for

developing Intelligent Tyre System.

2.4.2.2 Ultrasonic Sensor

An ultrasonic sensor was mounted on the base of the wheel rim inside the tyre, and it can evaluate the tyre vertical load and deformation, even tyre temperature and tyre-road contact parameters by measuring the varying distance to the opposite tyre inner wall online [88].

According to the variation of measuring distance, the varying deflection of tyre can be derived as a function of the rotational angle of the wheel. This technology can give a warning to the driver or automatically bring the vehicle to a safe status when the evaluated effective tyre radius changes over the predetermined threshold.

2.4.2.3 Optical Sensor

An optical position detection sensor was developed by the EU-funded Apollo [89] and FRICTI@N project [90]. Ari Tuononen carried out a series of studies on measuring tyre carcass deflections for vehicle state estimation using the optical sensor shown in Figure 2.19. By measuring the variation of relative position, it can capture the characteristics generated by tyre behaviour. Although this optical tyre sensor is not designed for commercial market, it provides the basis for studying tyre behaviour in details in order to develop algorithm for estimating tyre forces based on the optical tyre sensor.

Although the calibrated tyre sensor is suitable for estimating force in completely different frictional conditions, it needs to repeat the calibration when the tyre's carcass property and inflation pressure change. It is one of the reasons that the optical sensor is not for commercial production. Furthermore, the problematic measurement of light intensity will also influence the accuracy of measured data [91] [92].

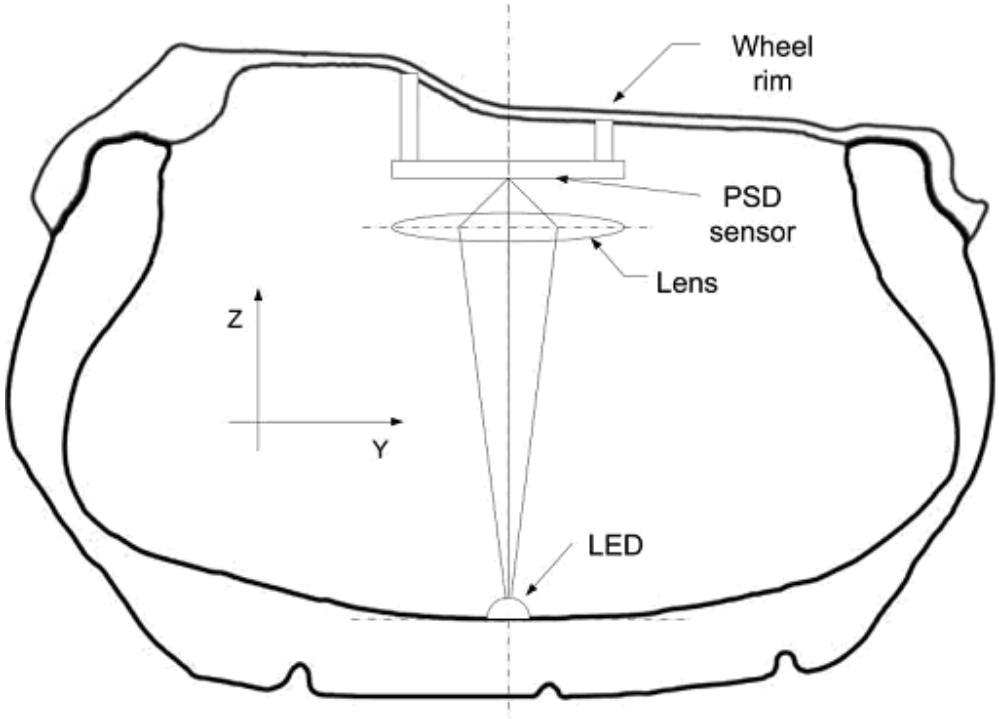

Figure 2.19 Optical Sensor for Tyre Tread Deformation Measurement [91]

Some preliminary results on the displacement signals and estimated forces are given such as measured vertical, longitudinal and lateral displacements, and estimated vertical and lateral forces. However, these data were obtained with the tyre rolling at low speed (30km/hr). Furthermore, the disturbance brings some possibilities of errors because of the

decay of intensity of LED and the vertical force is difficult to estimate during heavy braking manoeuvres [93].

Based on the measured tyre forces, the vehicle lateral state (vehicle yaw rate and lateral velocity) can be estimated using Kalman filter estimator [94]. This optical sensor technology is also used for measuring the carcass deflection when the tyre experiences partial and/or full aquaplaning. It gave a deep insight into the influence of road condition on the tyre mechanical properties, as well as a useful validation method for tyre behaviour simulation, such as the aquaplaning using finite element tyre model [95]. Different levels of aquaplaning were estimated in real time by this proposed method [96].

To the author's knowledge, some patents [97, 98] based on brainstorming or laboratory research also utilize the optical sensors to measure tyre characteristics. They seem to have been developed specifically for research purposes rather than as commercial products or at least have not been converted into commercial products.

2.4.2.4 Piezo Sensor

Piezo sensor also has a large market and has been developed for many years. It usually can be divided into two types: one is suitable for application on tyre, the other one is not. The piezo polymer and Polyvinylidene fluoride (PVDF) can be integrated into tyre and can measure the tyre strain effectively. But the piezo ceramic is not suitable for measuring tyre strain due to its brittle characteristics. A PVDF-based sensor has been designed and

fabricated to embed in the tyre inner tread surface to measure the tyre rubber tread deformation. It can provide the wheel/ground contact information and friction characteristics for the control system of mobile robots and vehicles [99]. A skid-steered mobile robot was used to carry out the experiment for evaluating the sensor.

In [100], tyre lateral tread deflection and sidewall deflections were measured by PVDF. The tyre slip angle was estimated based on tyre lateral sidewall deflection, which is very consistent for both the camera measurement and piezoelectric sensor. The piezoelectric sensors used for tread deflection and sidewall deflection can be found in Figure 2.20 and igure 2.21 [101].

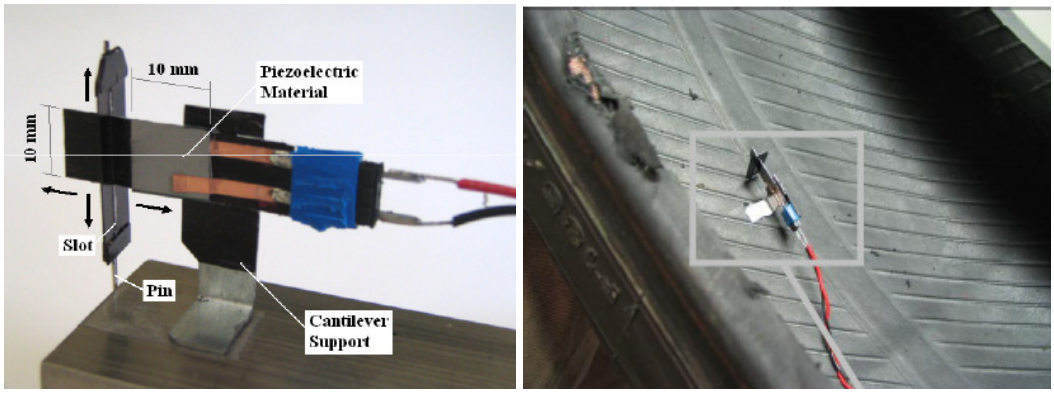

Figure 2.20 Piezoelectric Sensor for Tyre Tread Deflection Measurement [101]

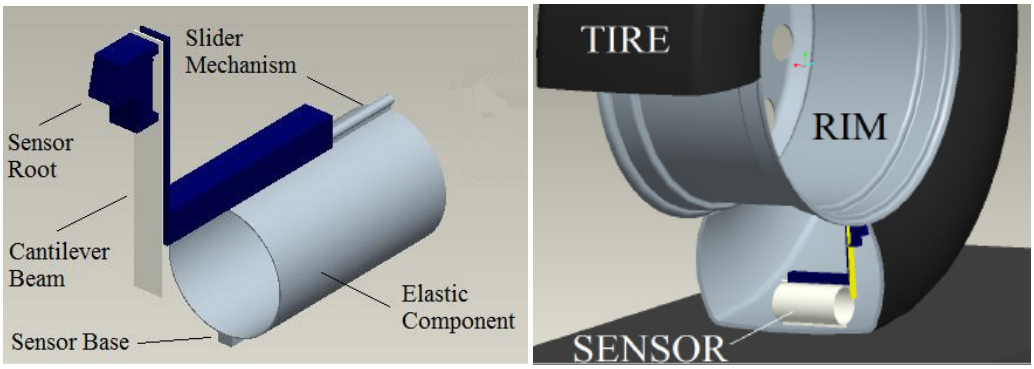

Figure 2.21 Piezoelectric Sensor for Tyre Sidewall Deflection Measurement [101]

2.4.2.5 Capacitive Sensor

The capacitive sensor has been used broadly in studying tyre behaviour by measuring the variation of capacitance. Cullen, J.D. [102] used the segmented capacitance rings to measure the tyre pressure. In the field trials, some validated results were obtained successfully.

More available applications of capacitive sensor are focusing on the deformation or strain measurement of tyre. The strain monitoring of a tyre in service is a significant topic for improving the reliability and safety of tyre. Akira Todoroki, et al [103-105] employed the tyre itself as a sensor by adopting the steel wire of the tyre as electrodes. A small oscillating circuit was embedded in the tyre to monitor the capacitance change of the tyre comprising steel wire and rubber. A rectangular specimen cut from commercial tyre was experimentally investigated. Different methods of capturing the strain features precisely are addressed such as multiple spectral features of the sensor output [106]. A capacitive-resistive sensor also was used to monitor strain in [107]. It was embedded in tyre tread and

used to measure the change of impedance caused by the variation of spacing between the steel wires due to the tyre deformation. A large amount of information can be measured in real road condition. Moreover, a novel flexible patch-type strain sensor utilizing electric capacitance change was proposed in [108]. It is low in stiffness and high in elongation and suitable for tyre strain measurement. This novel capacitive sensor is demonstrated by experiment that it is suitable for tyre strain measurement, but needs improvements when the temperature changes due to increase in the capacitance of the sensor with increasing temperature.

2.4.2.6 Other Sensors

There exist other sensors developed for Intelligent Tyre System. In order to generate a deformation following the deformation of the tyre, the sensor is preferably not stiffer than the stiffness of measured tyre portion. A magnetometric sensor is presented to monitor an analog output corresponding to the variation of the flux or the strain. Types of sensor are introduced in Figure 2.22 [109].

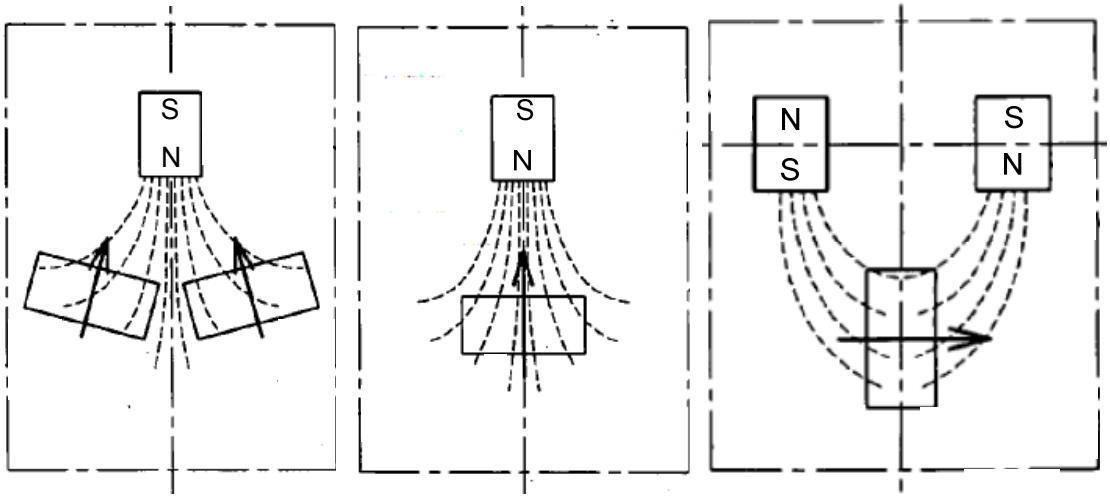

Figure 2.22 Magnetic Strain Sensors [109]

The magnetic sensor can measure different types of strain such as longitudinal strain, radial strain and shear strain on the tyre surface. Then, these strain data are correlated with the tyre forces.

In [110], a three-axis micro electro mechanical systems (MEMS) accelerometer was proposed to measure the acceleration inside the tyre tread. Both finite element analysis and indoor experiment shows its feasibility and potential application.

Apart from the above sensors, there are acoustic sensor, vibrating string sensor and utra wide band technology, etc. [81] which could also be applicable.

2.4.2.7 Summary of Sensor Technologies

From the literature review about the sensor technologies for Intelligent Tyre System, it can be concluded that most of the sensors are designed to measure the deformation of tyre, including acceleration, distance and especially strain (surface or inner). Since the measurement data of strain can reveal much more tyre characteristics in service and cost less, the strain-based sensor has become the major candidate to be the second product in the market after TPMS for intelligent tyre development. However, in order to obtain reliable and accurate information of tyre mechanical properties based on strain measurement, many issues still need to be explored. A detailed survey on strain-based Intelligent Tyre System is given in the following section.

2.4.3 STRAIN-BASED INTELLIGENT TYRE SYSTEM

An Intelligent Tyre System should be not only suitable for measuring and estimating desired variables accurately and quickly but also cheap and durable. In [92], Tuononen suggested that perhaps the algorithms for friction estimation can be developed with simple strain or movement sensors in research tyres. An evaluation of past researches (see Figure 2.23) indicates that a strain-based sensor system satisfies the requirements of an Intelligent Tyre System as follows [81].

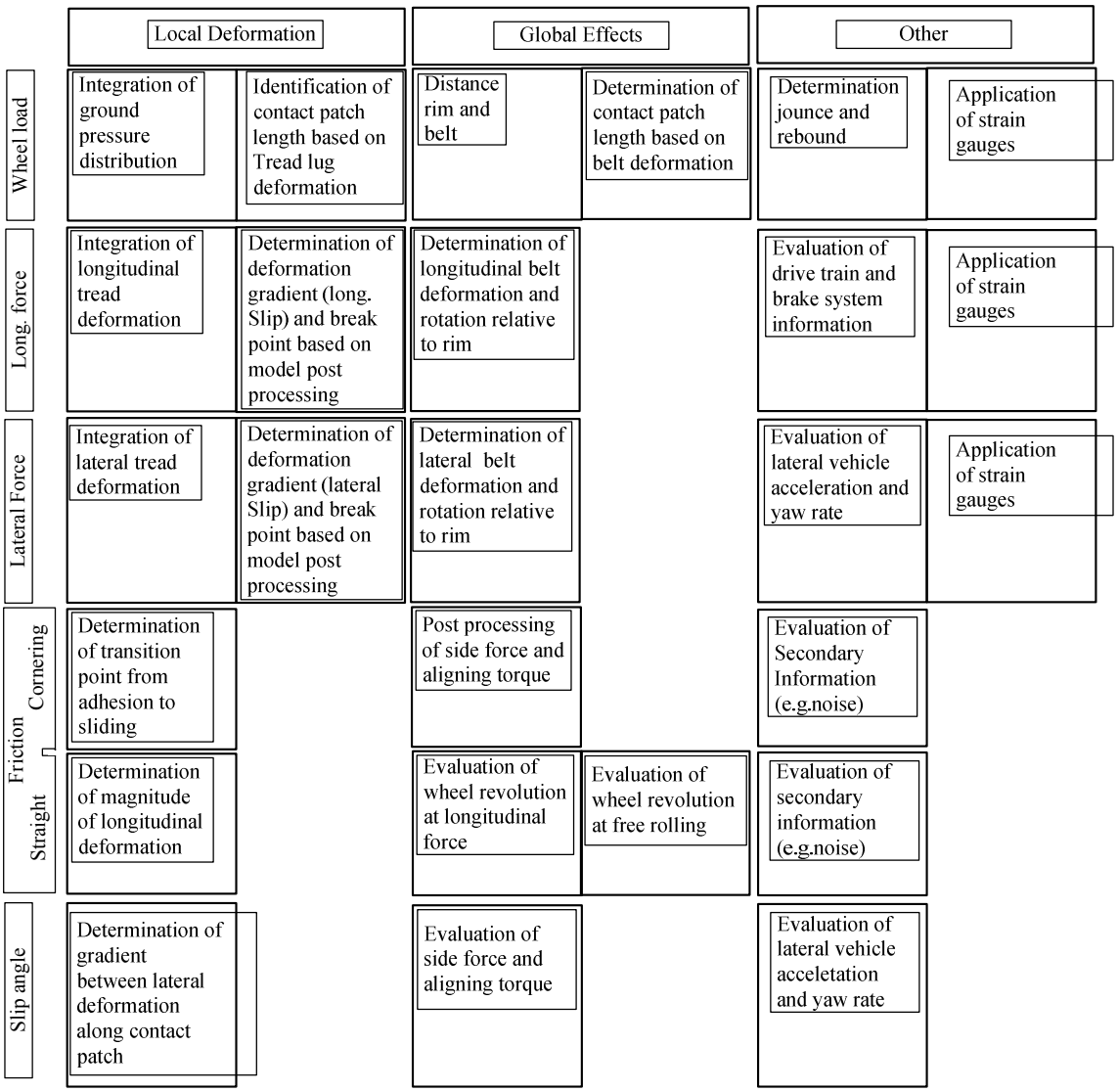

Figure 2.23 Overview of Potential Evaluation Strategies to Obtain Information from A Rolling Tyre [6]

- Which physical phenomena of the tyre/wheel system and the tyre-road contact contain relevant information needed for specified vehicle applications?
- Which measurement tasks for a sensor in a tyre/wheel system can be specified to detect the relevant information and which sensor type is the best solution?

- Which models and algorithms are needed to provide the relevant data for vehicle applications?
- Which is an appropriate design for an integrated electronics including all components of the total system and for a mechatronical integration into the tyre/wheel system?

For a strain-based Intelligent Tyre System, the tyre working conditions can be efficiently related to the tyre surface/inner strain and the strain sensor is also easy to integrate into the tyre such as during the vulcanization process.

Based on [110], a strain-based Intelligent Tyre System should have the following characteristics.

1. A simple and effective strain measurement to collect information of tyre deformation
2. Reliable and robust information collection
3. Batteryless and self power generation from the tyre deformation
4. Wireless transmission (without cable), small size equipment, good communication networks (designed protocol)
5. Ability to be integrated into tyre/wheel system or modular as an aftermarket product to fit different types of tyre
6. Durable and ability to last for the life of the tyre
7. Compatibility and non-interference with the operations of other intelligent systems in vehicle

For a more detailed literature survey on strain-based tyre monitoring system, reference can be made to the Table 2.1.

Given the foregoing discussion, it is expected that a novel prototype of a strain-based Intelligent Tyre System can be achieved. It should include an integrated sensor system, a wireless communication interface [79],[81], [100, 106], a power generator system [81] and a corresponding software system for post signal processing. The development of a strain-based Intelligent Tyre System is therefore selected as a major objective of this research. A major aspect of the work would be the development of the algorithms to relate the measured strain data to the mechanical properties of the tyre such as the forces generated at the tyre/pavement interface which could provide vital information for the vehicle chassis control systems.

From the literature review, the models and algorithms for the application of the Intelligent Tyre System are still under development. As emphasized in the Apollo project, the Intelligent Tyre System should be qualified in four different aspects: goal, sensor system, decision and commercialization [6]. As a potential application on the next generation of tyres, the decision system of intelligent tyre can utilize the data acquired to decide/estimate the useful variables for the vehicle system based on relation mapping, lookup table, etc. In the Apollo project, three sensors viz. optical sensor, acceleration sensor and piezo-strain sensor were installed in the tyre/wheel system to measure tyre behaviour. The output data from the three sensors provide complementary information to each other to identify the relationship between tyre forces and measured data. However, in the Apollo project, since

just two strain gauges (one longitudinal and one lateral) were used inside the tread, it is not feasible for estimating complex tyre behaviour such as tyre cornering.

Generally, the decision/estimation model of Intelligent Tyre System is based on the quantity and quality of acquired data. Finite element tyre model was thought to be an appropriate approach to provide predictive information for developing the estimation model.

In [6], a tyre model for steady-state rolling was developed using ABAQUS/Standard to identify the sensor position and to improve the comprehension of relationship between accelerations and the dynamic mechanical behaviour of the tyre under different operating conditions (i.e. speed, vertical load, camber angle, slip angle....) shown in Figure 2.24.

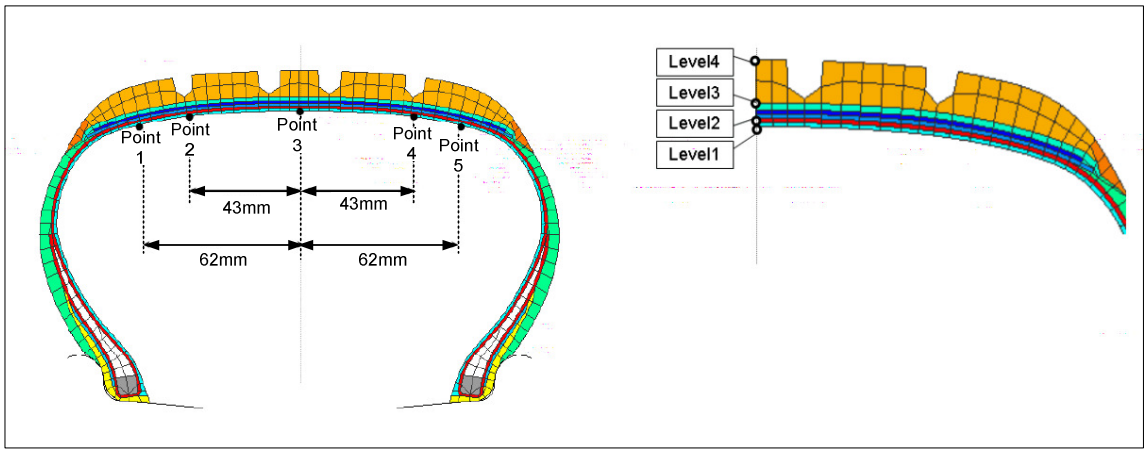

Figure 2.24 Investigated Sensor Positions in FE Tyre Model [6]

Table 2.1 Detailed Literature Survey of Strain-based Intelligent Tyre System

Year	Variables measured	Mechanical properties of tyre estimated	Sensor/Technology	Aim	Reference
1998	tyre tread deformation	force, moment and friction	Darmstadt tyre sensor	provide car systems with information about friction potential as well as friction demand, tyre forces and actual driving state.	[111]
1999	tyre tread deformation	friction coefficient	passive radio requestable SAW sensors	make contact monitoring for modern car control systems	[112]
2003	strain		strain monitor measuring electrical capacitance change of steel wires	improve the reliability of tyres and design tools	[103, 104]
2005-8	strain	braking torque, effective radius and contact patch length	a patch-type sensor and a self-sensing method utilizing the tire structure itself as the sensor	optimised braking control and road condition warning systems	[105, 106, 108, 113, 114]
2005-9	tyre sidewall outer surface strain	tyre forces	magnetic strain gages		[109, 115]

2006	strain		rubber sensor	aircraft/automobile tyre structural health monitoring	[116]
2006	strain		capacitive–resistive sensor	developing intelligent tyre	[107]
2006	tyre tread inner surface strain	lateral and vertical forces, camber angle, and slip angle	strain sensor	improve vehicle safety system	[3]
2006	strain on wheel spoke	Six force components	three mental foil strain gages on each spoke,	improve performance and reliability of control systems for vehicle dynamics	[117]
2008	inner tread surface deformation	wheel/ground contact information and friction characteristics	Polyvinylidene fluoride (PVDF)-based sensors	the feasibility and estimation of wheel/ground friction characteristics using the developed sensing system.	[99]
2008-9	Inner tread carcass deflection	tyre forces	optical position sensor	estimate the lateral state of a car and estimate partial and aquaplaning in real time	[91-96]
2010	tyre sidewall deformation	slip angle, tyre forces, slip ratio and tire–road friction coefficient	piezoelectric tyre sensor	significant improvements in traction control, skid control, lane departure avoidance and rollover prevention systems	[100]

Similar works on investigating the sensor positions and their effect on tyre mechanical property measurement have been carried out in [118]. In [91], it was announced that considering the complexity of the tyre structure and its nonlinear material properties, the proposed simple and mostly linear models with only a few compensation terms are not able to adequately describe the relation between carcass displacements and tyre forces. Although the linear relationship provides a convenient approach to generate the desired key parameters of the tyre, it is noticed that the linear algorithm is prone to be inflation pressure-dependent. Furthermore, it is not robust enough to cover different behaviours as they are so complex. Nonlinear or intelligent algorithms such as fuzzy logic and neural network have better potential for an accurate and feasible prediction of tyre mechanical properties.

From [3] and [6], it can be concluded that at least one strain gauge should be bonded to the inside of the tread. Meanwhile, the tyre sidewall deflection also contains interesting information. In [100], it is said that the sidewall deflection sensors are more advantageous than tread deflection sensors in terms of deflection decoupling, sensor sensitivity and measurement verification issues.

The tread strain and sidewall strain could be compensated for each other in order to get a precise estimation. Apart from the aforementioned discussion, many factors would influence the tyre strain measurement results such as the type and structure of the tyre, wear of the tread, etc.

The estimated output of Intelligent Tyre System should be capable of being applied to vehicle dynamics control [99, 110], which can be evaluated by the vehicle model.

2.5. SUMMARY

In the literature survey, three main parts including mechanical property of tyre, tyre modelling method and intelligent tyre technology are reviewed and discussed in detail. The mechanical property of tyre discussed in this Chapter is associated with the following study described in the rest of the thesis and provides a fundamental basis for better understanding of the following chapters. The section on tyre modelling methods introduced the main modelling methods used in tyre research field, especially the finite element tyre model which has become an increasingly used tool amongst tyre researchers and engineers. Due to its capability of providing realistic prediction of tyre behaviour, finite element tyre model created in software ABAQUS is utilized for this study. The last part gives a wide ranging review of the development of intelligent tyre technology in the past decades. It is found that the approach combining experiments and finite element tyre model on developing intelligent tyre estimation model has not been widely used and it has great potential advantages for developing the intelligent tyre system. Based on the literature survey, the improvements in both finite element tyre modelling and intelligent tyre technology will be utilised in the rest of this thesis for developing tyre models for accurately estimating the relationship between tyre behaviour such as tyre force and tyre strain data. The strain state in a rolling tyre is acquired experimentally and compared to simulation results for the purpose of

validating the tyre FE models. It is a novel and detailed approach in the development of intelligent tyre technology with assistance from both experiment and FEA.

CHAPTER 3

TYRE MATERIAL PROPERTIES

3.1. INTRODUCTION

As a product of composite material, the tyre has complex characteristics due to its diverse material properties and complex structure. Generally, the tyre is constructed using high modulus cord and low modulus rubber. The cord is made by twisting threads of cotton, rayon, nylon, polyester or steel wire, etc. Several layers of cord spaced in the rubber act as the reinforcing frame of the tyre as shown in Figure 3.1.

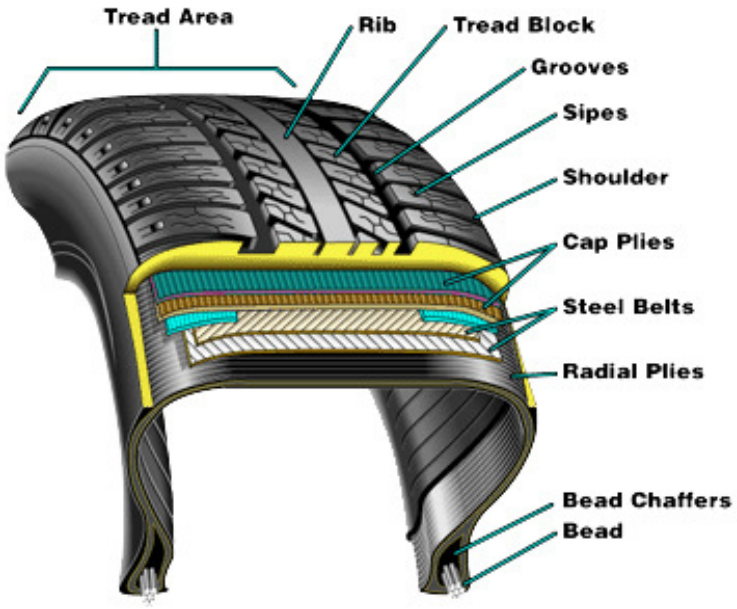

Figure 3.1 Structure of A Radial Tyre

The number of reinforcement layers is dependent on tyre type, size and tyre inflation pressure, etc., For example, the aircraft tyre has more reinforcement layers than that of passenger car or truck tyre due to the higher load capacity. The reinforcement layers are enveloped by the rubber which exhibits highly nonlinear stress-strain behaviour. The composite structure of the tyre is designed according to the service requirement in order to achieve the desired balanced of tyre mechanical properties, such as performance and durability. In the past, the constituent materials of the tyre were selected by experience and the construction details of tyre were established largely by trial and error method [119]. With the increasing understanding of tyre material physics, several classical formulas were created for the study of cord-rubber composite material property including Hermans formula, Halpin-Tsai formula, Gough-Tangorra formula and Tabaddor formula, etc. The parameters in a cord-rubber composite material formula can be obtained from tests and the formula is of great benefit to the tyre modelling.

In this study, a Dunlop slick radial tyre 175/505 R13 for SAE Formula Student (FS), shown in Figure 3.2, was selected as the subject.

Nowadays, around one hundred FS racing teams are using different makes of tyre, such as Dunlop, Goodyear and Hoosier. These tyres usually work under low pressure and load. The growing popularity of FS makes the competition more keen and forces the FS team to design a car with higher quality. As a cornerstone of FS racing car design, the tyre's characteristics are being paid more attention in order to take two seconds off the lap time during competition [120].

Figure 3.2 Formula Student Car with Dunlop Slick Tyre

The 175/505 R13 radial tyre is tubeless viz. without a separate and removable inner tube. It consists of different material components which can be observed and tested by cutting one of the tyre products. The 175/505 R13 tyre cut cross-section is shown in Figure 3.3.

Figure 3.3 shows that the tyre consists of different rubber components with embedded reinforcements. The dominant component of the tyre is rubber including tread, undertread, sidewall, apex, and the inner-liner. The reinforcement of the tyre includes belts, carcass, bead, cap ply, and bead reinforcement. The rubber material properties for different components such as tread and sidewall are not identical due to the different mixed proportions of rubber and carbon black [75]. The function of tread rubber is to keep the balance of tyre performance and durability, while the sidewall rubber is designed mainly for fatigue resistance.

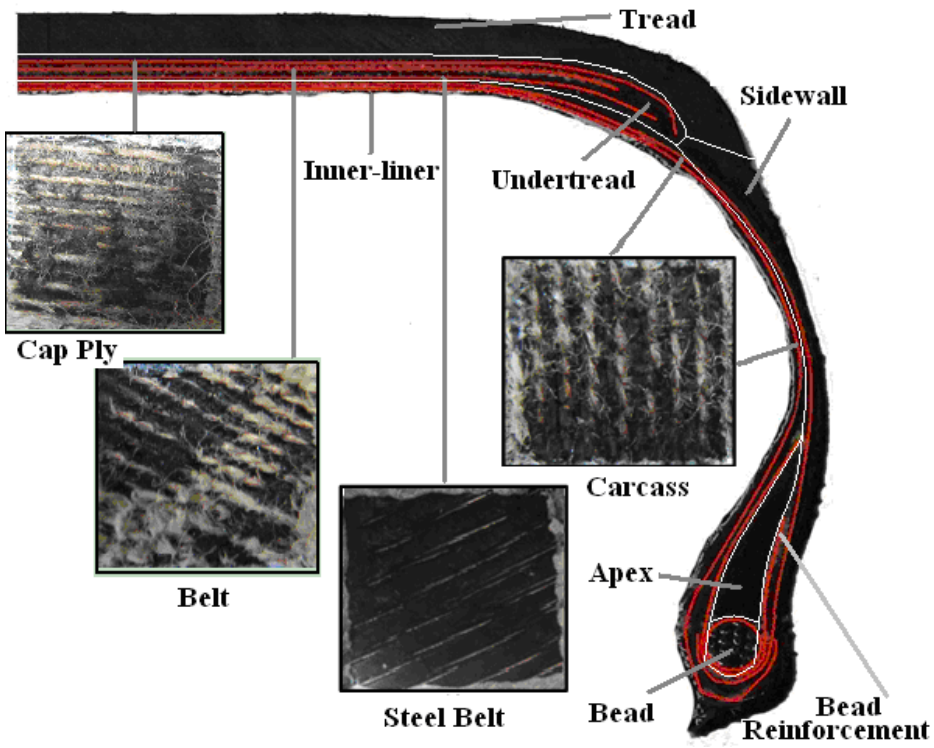

Figure 3.3 Cut Cross-section of Dunlop 175/505 R13 Radial Tyre

With the rapid development of high performance computing technology, the design of tyre steps into the computer-aided engineering era. The numerical simulation such as Finite Element Analysis was introduced into the tyre design process as well as the tyre performance prediction.

Meanwhile, availability of accurate knowledge of the structural lay-up of the tyre and properties of its constituent materials is vital for constructing a FE model capable of representing the behaviour of the tyre accurately. However, tyre material properties are usually not available to most researchers due to the proprietary protection from the tyre

manufacturers. To meet the challenge, extensive researches have been carried out on the investigation of rubber and reinforcement material properties [121, 122].

In the University of Birmingham, Andrew Burke [10] presented good prediction of tyre dynamic overall response using finite element tyre model developed in MSC.Nastran as described in Chapter 2. In order to create a reasonable model, Burke divided the 2D tyre profile into a number of zones with composite material and determined different zone's material properties experimentally, including two Young's modulus and one major Poisson's ratio. Then the minor Poisson's ratio and the shear modulus were calculated by equations. The composite material properties obtained were matched to the corresponding composite shell elements used in the tyre model. It avoids the complex procedure of determining properties of individual constituent materials making up the composite shell structure and it is effective and accurate for investigating the tyre macroscopic behaviour. However, the increased number of divided sections for accurate material property representation is time-consuming in Burke's case.. Moreover, it cannot provide details of stress and strain in the rubber and reinforcement materials from the FEA. Using a different approach from Andrew Burke's method, E. O. Bolarinwa [11] investigated the rubber hyperelastic material properties and considered the cord as linear elastic material in order to build finite element tyre model in ABAQUS. The approach involving determining tyre material properties for tyre modelling in Bolarinwa's work provided feasibility for a deep insight into the response of individual tyre reinforcement layers during tyre service. The Mooney-Rivlin model was used for rubber material property and its constants were obtained by fitting the test data. The linear elastic modulus of reinforcement cords was

determined by the combination of experimental testing and computational analysis using ABAQUS, where the cut section of composite structure was tested and the finite element model of the section was created to achieve the same strain-stress relationship by tuning the linear elastic modulus of the reinforcement cords in ABAQUS. This new technique avoids the direct test of reinforcement cord. A good prediction was obtained on tyre cornering behaviour by the aforementioned finite element tyre model. E. O. Bolarinwa assigns only one rubber material property to the whole tyre model, which may be suitable for studying tyre global behaviour but not for local behaviour because of the different rubber composition in different parts of the tyre.

As a result of the above review about the tyre material properties, it is apparent that a better understanding of tyre material property and its mechanism in tyre service can contribute significantly to precise tyre modelling and the optimisation of tyre design. As the aim of the research is investigating not only tyre overall response but the local behaviours, it is necessary to obtain the material properties of different components of the tyre in order to represent tyre behaviours accurately, especially strain and stress. To get over the constrains and satisfy the requirements, an appropriate and effective tyre material property test procedure is proposed in this chapter when the tyre modellers and researchers have to face the limited availability of tyre material specimen and test facilities.

Taking the advantage of the use of commercial finite element software—ABAQUS, the reinforcement cord can be represented by rebar elements and the rubber can be represented by solid elements. The material properties for different finite element tyre components are

derived from a series of tests using the extracted specimen from tyre product. A practical test procedure has been developed with basic requirements based on limited availability of material specimens. Techniques for the determination of required material properties for rubber are provided in ABAQUS, which gives a sound basis for the following FE tyre modelling and analysis. The FE tyre model is expected to provide a virtual tyre modelling and analysis platform for researchers.

3.2. RUBBER MATERIAL PROPERTY

Rubber is a complex material, the properties of which change with time and are affected by the environment. The properties of rubber deteriorate on contact with heat, oils, chemicals, sunlight, and the weather [123].

As an incompressible or nearly incompressible material, the rubber shows nonlinear elasticity under large strain which makes it necessary to account for the rubber nonlinear behaviour in the finite element tyre modelling. During the finite element tyre modelling process, the relevant material properties of rubber usually are the hyperelasticity, viscoelasticity and thermodynamics. However, because the information about compounding, mixing, processing, assembly and vulcanization are confidential, the rubber material properties are difficult to obtain from the rubber manufacturers. Furthermore, the material properties obtained from rubber specimens provided by tyre manufacturers could be different from those from tyre product due to the vulcanization process undergone during tyre manufacture. In order to have a suitable and practical tyre material property for

finite element tyre modelling, an overview of the material properties used in previous tyre FEA modelling studies is detailed in Table 3.1. Based on this extensive literature survey about rubber material properties, the hyperelastic and viscoelastic material property are investigated herein.

Table 3.1 Tyre Material Properties Adopted by Past Researches

Year	Software	Rubber Material Properties	Reinforcement Material Properties	Research Purpose	Ref.
1993	MSC.MARC	hyperelastic	linear elastic	contact pressure/load displacement	[124]
1997	LS-DYNA	hyperelastic viscoelastic	orthotropic	impact of cleat	[125]
2000	ABAQUS	hyperelastic	linear elastic	cornering	[56]
2001	MSC.MARC	hyperelastic.	linear elastic	cornering	[126]
2002,6,7	ABAQUS	hyperelastic	linear elastic	steady state rolling	[57, 58, 60]
2004	ANSYS/LS-DYNA ANSYS/MECHANICAL	hyperelastic hysteresis	linear elastic	rolling and thermal	[121]
2006,7	MSC.MARC	hyperelastic	linear elastic	static camber angle effect	[62, 127]
2006,7	ABAQUS	hyperelastic viscoelastic	linear elastic	optimization of tyre design	[64, 122]
2002,7	MSC.MARC	hyperelastic	linear elastic	deformation and stress	[128, 129]

3.2.1 HYPERELASTIC MATERIAL PROPERTY

The hyperelastic material property of rubber provides highly nonlinear and incompressible material behaviour. There are two methods: statistical thermodynamics and phenomenological approach for characterizing the hyperelastic material properties of rubber. From the point of view of material property modelling for tyre, the phenomenological method is usually adopted based on continuum mechanics [122]. The strain energy approach is derived from the phenomenological theory, which defines that the strain energy per unit volume stored in a material is a function of the general components of strain at any point.

In the FEA of elastomer, material models are characterized by different forms of their strain energy functions. The commonly available strain energy functions are represented in terms of the strain invariants which are functions of the stretch ratios. In ABAQUS, for isotropic, compressible materials the strain energy U is a function of $\overline{I}_1$, $\overline{I}_2$, and J:

$$U = U(\overline{I}_1, \overline{I}_2, J) \tag{3.1}$$

where U is the strain energy per unit of reference volume; J is the total volume ratio. $\overline{I}_1$ and $\overline{I}_2$ are the first and second deviatoric strain invariants defined as

$$\overline{I}_1 = \overline{\lambda}_1^2 + \overline{\lambda}_2^2 + \overline{\lambda}_3^2 \tag{3.2}$$

$$\overline{I}_2 = \overline{\lambda}_1^{(-2)} + \overline{\lambda}_2^{(-2)} + \overline{\lambda}_3^{(-2)} \tag{3.3}$$

The deviatoric stretches is

$$\overline{\lambda}_i = J^{-\frac{1}{3}} \lambda_i \quad (i = 1, 2, 3) \tag{3.4}$$

Where the principal stretches λ_i is

$$\lambda_i = 1 + \varepsilon_i \quad (i = 1,2,3) \tag{3.5}$$

The ε_i are the principal strains. For incompressible and isothermal material, $J = 1$ and $\lambda_1 \lambda_2 \lambda_3 = 1$.

Probably, the most popular tyre rubber material property model based on strain energy potential is the Mooney-Rivlin formulation. The strain energy potential of Mooney-Rivlin formulation with the first and second deviatoric strain invariants considering rubber incompressibility can be expressed as follows

$$U = C_{10}\left(\bar{I}_1 - 3\right) + C_{01}\left(\bar{I}_2 - 3\right) + \frac{1}{D_1}\left(J^{el} - 1\right)^2 \tag{3.6}$$

Where C_{10} , C_{01} and D_1 are temperature-dependent material parameters. J^{el} is the elastic volume ratio.

Considering the incompressible property of rubber, the above equation can be rewritten as

$$U = C_{10}\left(\bar{I}_1 - 3\right) + C_{01}\left(\bar{I}_2 - 3\right) \tag{3.7}$$

It was reported [122] that Mooney-Rivlin formulation is not capable of predicting large strain behaviour of rubber material. The Mooney-Rivlin and Neo-Hookean model also show a limitation that the determination of the coefficients from one deformation mode has limited value to predict behaviour in other deformation modes. For Ogden model, it works best when multiaxial test data is available. These limitations are crucial for tyre analysis and the Yeoh model is suggested for better interpretation of rubber uni-axial tension test. The advantages of Yeoh strain energy function as hyperelastic material model are listed as follows:

1. It can cover a much wider range of deformation than other models.

2. It can predict the stress-strain behaviour in different deformation modes from data gained in one simple deformation mode like uni-axial tension.

3. It can predict the shear modulus varying with increasing deformation.

Considering the test accuracy and cost, the Yeoh model is adopted for modelling hyperelastic property of tyre rubber. Yeoh strain energy function in terms of the first deviatoric strain invariant $\overline{I}_1$ is described as follows

$$\begin{aligned} U = & C_{10}\left(\overline{I}_1 - 3\right) + C_{20}\left(\overline{I}_1 - 3\right)^2 + C_{30}\left(\overline{I}_1 - 3\right)^3 \\ & + \frac{1}{D_1}\left(J^{el} - 1\right)^2 + \frac{1}{D_2}\left(J^{el} - 1\right)^4 + \frac{1}{D_3}\left(J^{el} - 1\right)^6 \end{aligned} \tag{3.8}$$

where $C_{i0}\ \ (i = 1, 2, 3)$ and $D_i\ \ (i = 1, 2, 3)$ are temperature-dependent material parameters.

3.2.1.1 Hyperelastic Material Property Test

The rubber of tread, sidewall, inner-liner, apex and toeguard were cut from tyre product and prepared for test specimen. Three samples were used in tests for identifying material properties of each rubber component.

The material specimens available were limited, since they were extracted from a manufactured product. The sections of rubber were manually cut from the product and sliced into small sheets with irregular contours. Therefore, the types of experiments and the attainable strain states that could be experimentally achieved were restricted.

The experimental requirements are different from those of standardized test methods. Because the experiment is not intended to fail the specimen, there is no need to use a dumbbell shaped specimen that is commonly used to prevent specimen failure in the clamps. For the requirement on specimen size in this case refer to [130].

The Lloyd test machine shown in Figure 3.4, under remote computer control was used for the test of hyperelastic material property. The load cell is 1kN. All the tests were carried out at room temperature condition.

Figure 3.4 Lloyd Test Machine and Its Remote Controller

In the uni-axial tension test, the dimension requirement of the specimen is that the length of the specimen is at least 10 times longer than the width or thickness. According to [130], if the sample length in elongation is more than 10 times of width, the strip sample can perform the same reliable test data as the dumbbell sample. The boundary condition is no lateral constraint, and the specimen is tensioned in direction 2 as shown in Figure 3.5.

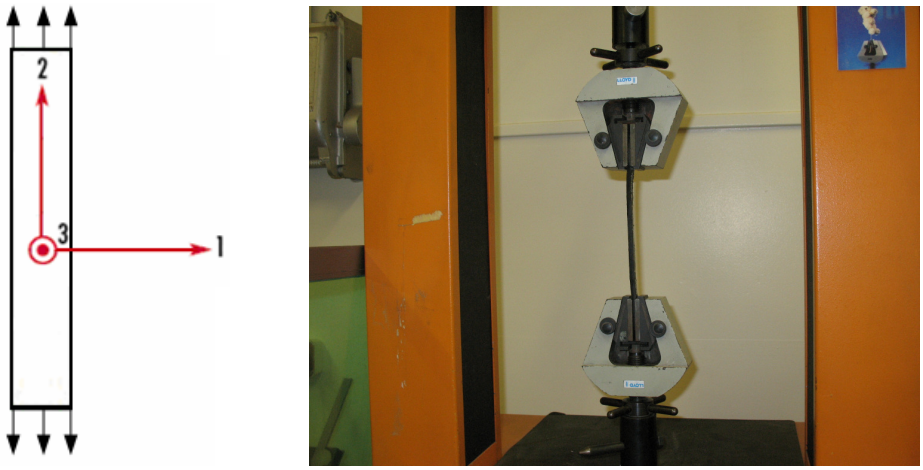

(a) (b)

Figure 3.5 (a) Sketch Figure of Uni-axial Test and (b) Uni-axial Test by Lloyd Test Rig

The test data can be converted into stress and strain according to the following formula [131].

a. Deformation state

$$\lambda_2 = \lambda = L / L_0 \tag{3.9}$$

$$\lambda_1 = \lambda_3 = 1/\sqrt{\lambda} \tag{3.10}$$

Where L_0 is the original length of sample in direction 2, L is the final length of sample in direction 2 after tension, A_0 is the original cross-section area of sample, and A is the final length of sample after tension.

b. Stress state

$$\sigma_2 = \sigma = P/A_0 \tag{3.11}$$

$$\sigma_1 = \sigma_3 = 0 \tag{3.12}$$

Where the P is the extension force, the σ_1, σ_2 and σ_3 are the stress in direction 1, 2 and 3, respectively.

In order to give a detailed description about the rubber uni-axial test procedure, the tread rubber test is taken as an example. In the uni-axial test of tread rubber, the samples were pre-conditioned at the speed of 50 mm/min up to 100% strain for ten cycles. During the pre-conditioning, 5 minutes relaxation was given between unloading and reloading of the sample. The effect of pre-conditioning is to eliminate the stress-softening effect. At the end of the pre-conditioning cycles, samples were removed from the clamp and given one hour relaxation time before the formal test. During the formal test, the samples were stretched to 100% strain at a speed of 50 mm/min. This procedure was repeated at least three times in order to obtain a realistic average test data [122].

The pre-conditioning state is shown in Figure 3.6. With the increasing of pre-condition cycles, the stress-strain relationship is approaching stability.

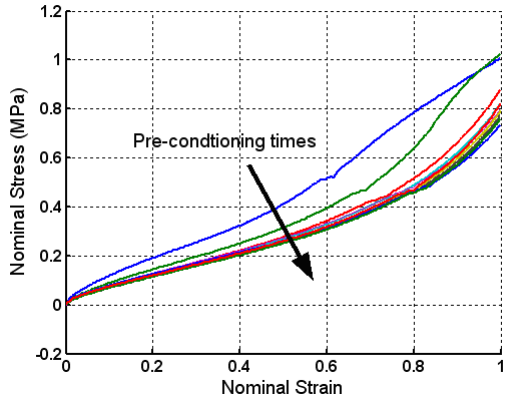

Figure 3.6 Pre-conditioning State in Rubber Uni-axial Test

The stabilized curves for three tread rubber samples are shown in Figure 3.7 together with the final average uni-axial test curve.

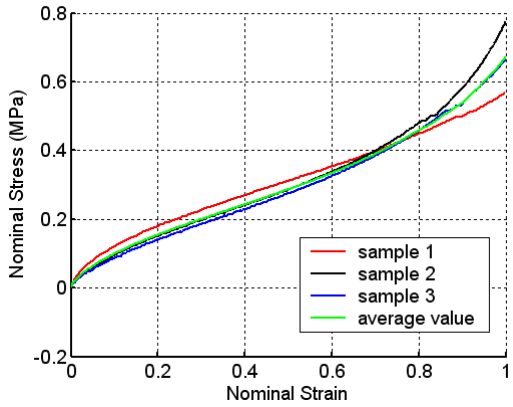

Figure 3.7 Uni-axial Test Curves for Tread Rubber of Tyre

3.2.1.2 Determination of Hyperelastic Model Constants

ABAQUS provides evaluation function to determine the material model constants. Different strain energy functions were used for the evaluation process, and the evaluation procedure for tread rubber is shown in Figure 3.8.

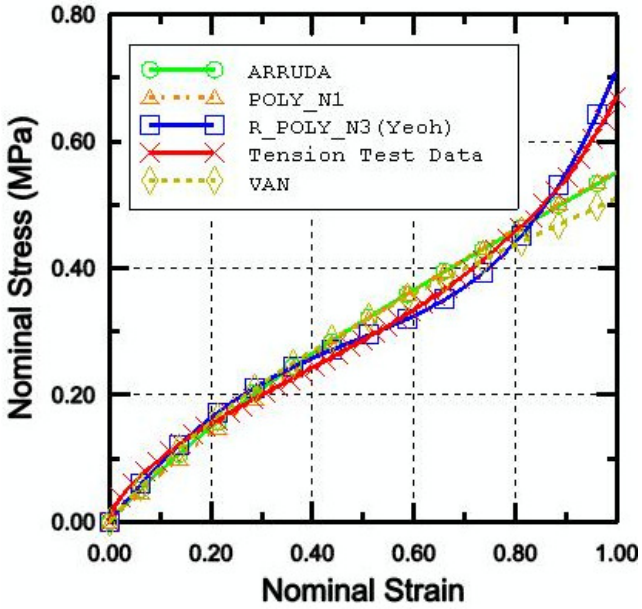

(a)

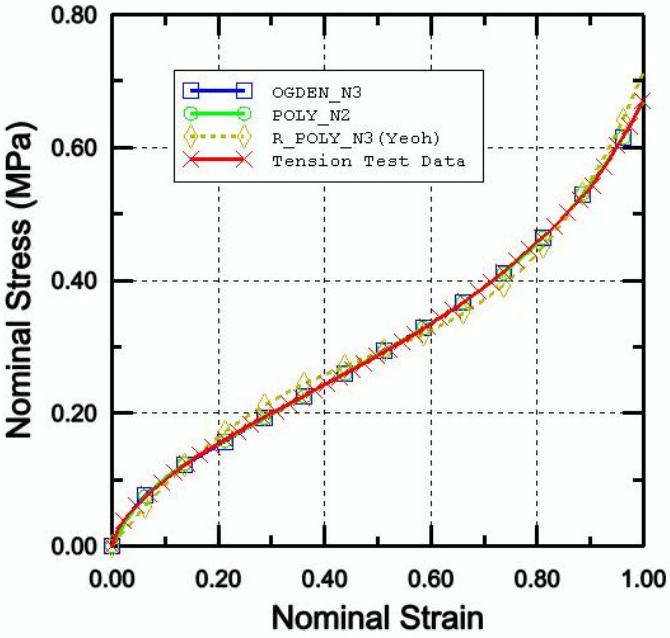

(b)

Figure 3.8 (a) The Comparison of ARRUDA, VAN, Polynomial N=1 (Mooney-Rivlin), Reduced Polynomial N=3 (Yeoh) and Uni-axial Test Data (b) The Comparison of OGDEN N=3, Polynomial N=2, Reduced Polynomial N=3 (Yeoh) and Uni-axial Test Data

The ABAQUS material property evaluation process for different rubber components using Yeoh model is illustrated in Figure 3.9.

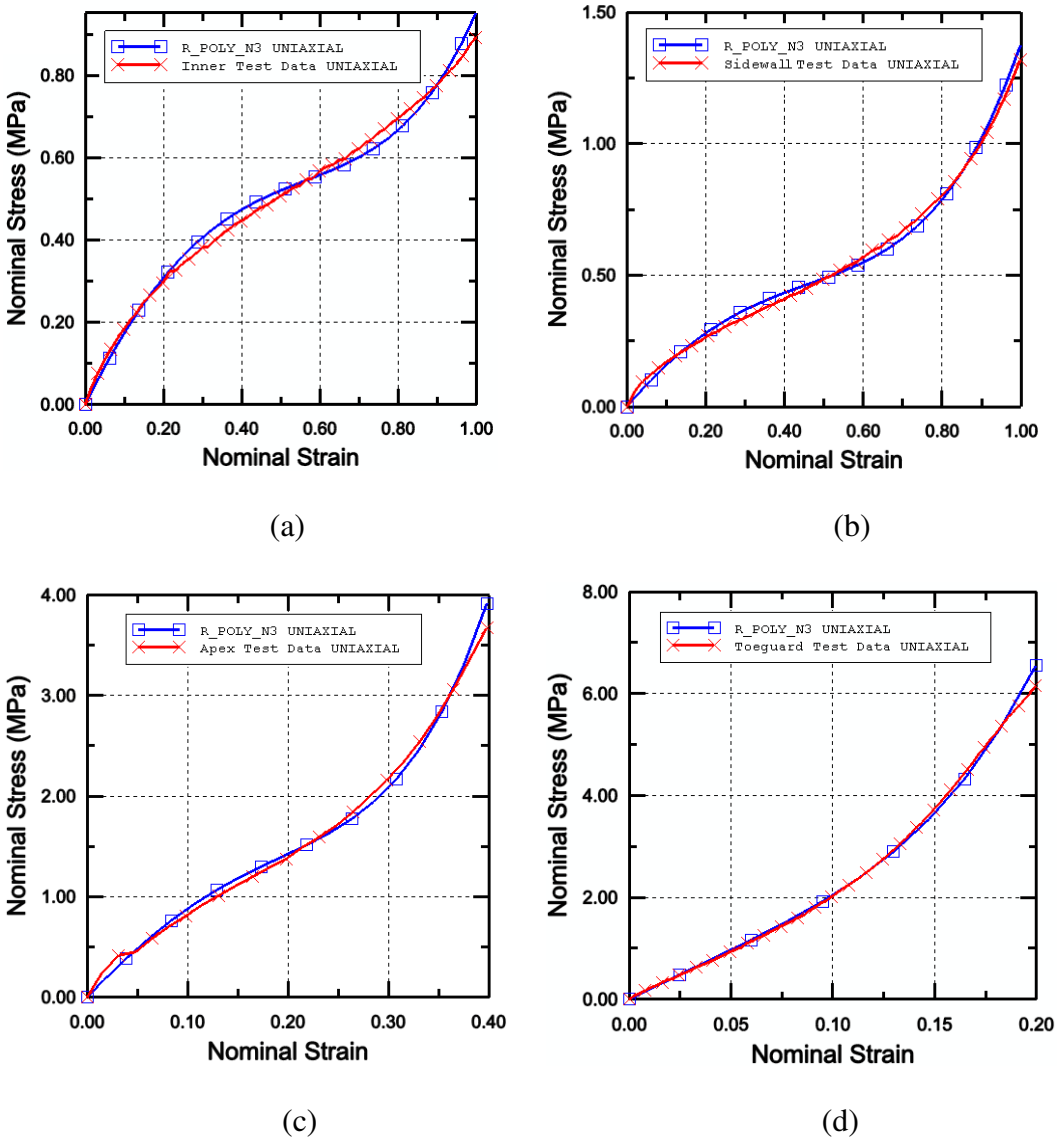

Figure 3.9 (a) Material Property Evaluation for Inner Rubber (b) Material Property Evaluation for Sidewall Rubber (c) Material Property Evaluation for Apex Rubber and (d) Material Property Evaluation for Toeguard Rubber

Based on a series of uni-axial tests and evaluations using ABAQUS, the Yeoh hyperelastic model constants for different rubber components were obtained and listed in Table 3.2.

Table 3.2 Hyperelastic Material Constants

Rubber Material	Yeoh strain energy potentials constants		
Component	C10(N/mm^2)	C20(N/mm^2)	C30(N/mm^2)
Tread	0.1714	-4.4041E-02	1.7383E-2
Sidewall	0.2933	-8.6149E-02	3.7144E-02
Apex	1.7245	-2.2922	5.0544
Inner-liner	0.3223	-8.6751E-02	2.4762E-02
Toeguard	3.3175	4.7823	63.5242

3.2.2 VISCOELASTIC MATERIAL PROPERTY

The rolling resistance, internal damping and thermal characteristics of tyre are related to the viscoelasticity of rubber. P.Ghosh [122] points out that it has a significant influence on the traction (wet and dry), steering response and rolling resistance (fuel efficiency) properties. E. O. Bolarinwa [11] emphasized that the incorporation of viscoelastic and hyperelastic property is very important for adequate simulation of tyre transient response. In this study, the viscoelastic material property was also investigated in order to get a realistic finite element tyre model.

The viscoelastic properties such as stress relaxation and creep are time and temperature dependent, as well as the dynamic properties being frequency dependent. Therefore, the viscoelasticity of rubber is usually divided into time dependent and frequency dependent material behaviour. Namely, the viscoelastic response can be identified either in time domain or frequency domain, depending upon the type of analysis. The viscoelastic material response in the time domain is adopted here, which is defined by a Prony series expansion of the dimensionless relaxation modulus [132]:

$$g_R(t) = 1 - \sum_{i=1}^{N} \bar{g}_i^P \left(1 - e^{-t/\tau_i^G}\right) \tag{3.12}$$

Where N, $\bar{g}_i^P$, and $\tau_i^G, i = 1, 2 \cdots N$, are material constants.

In ABAQUS, the viscoelastic material property should be considered together with the hyperelastic model to define large-deformation, nonlinear, viscoelastic behaviour for the transient static analysis, transient implicit dynamics analysis, explicit dynamic analysis and steady-state transport analysis, etc. Likewise, the viscoelastic material model must be combined with the isotropic linear elasticity model to define classical, linear, small-strain, viscoelastic behaviour.

3.2.2.1 Viscoelastic Material Property Test

The test methods adopted for the viscoelastic material property model are stress relaxation test and strain creep test in time domain and the dynamic mechanical analysis (DMA) in frequency domain. These test procedures also should conform to certain standards such as ISO 6914 describing the test of stress relaxation in tension. However,

due to the same reason as the hyperelastic material properties test, the types of experiments and the attainable strain states that could be experimentally achieved were restricted. The specimen samples and the test procedures were selected based on the related literatures and available conditions.

In the viscoelastic material property test, the same samples were used as those in the hyperelastic material property test. The instron test machine shown in Figure 3.10, under remote computer control was used for the test of stress relaxation instead of Lloyd machine.

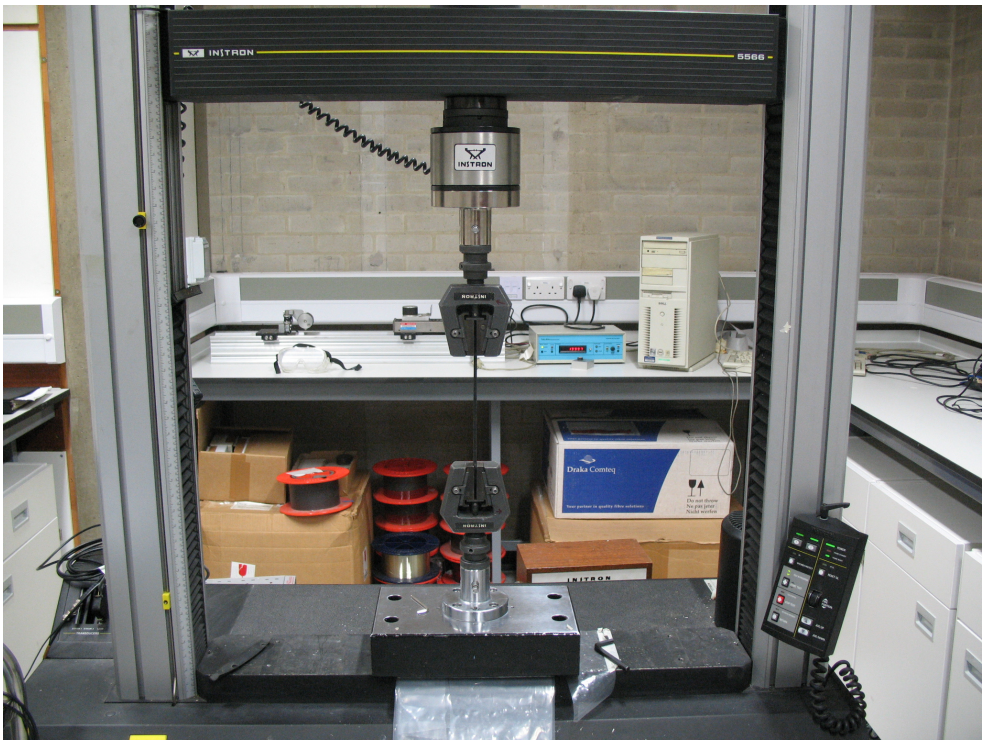

Figure 3.10 Instron Test Rig for Rubber Stress Relaxation Test

The rubber stress relaxation test is to measure the decreasing force which maintains the constant strain applied on the rubber sample.

For example, the tread material stress relaxation tests were carried out in tension mode using instron test rig. Pre-conditioning of the test samples was the same as the hyperelastic material property test apart from the load speed being 100mm/min. After pre-conditioning and one hour relaxation time, the samples were stretched to 10%, 20%, 50% strain level respectively and kept for 960 seconds at each level. Stress values at different time intervals were recorded.

3.2.2.2 Determination of Viscoelastic Model Constants

Before the stress relaxation data are imported into ABAQUS, it is necessary to normalize the test data as shown in Figure 3.11.

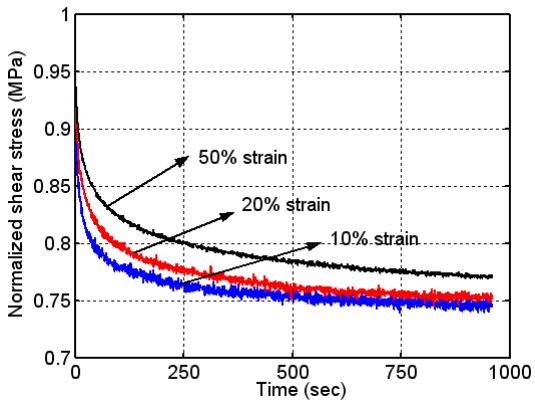

Figure 3.11 Normalized Stress Relaxation of Tread Rubber

Then, the Prony series parameters for viscoelastic materials were evaluated in ABAQUS. During the evaluation process, the long-term normalized shear compliance or modulus was fulfilled with $g_R(\infty)$. And the normalized shear relaxation modulus $g_R(t)$ ($0 \le g_R(t) \le 1$) for relaxation test data and the time t (t>0) were imported into the

table. It should be noted that the evaluation process includes time domain viscoelastic material data defined in conjunction with hyperelastic. The material model constants obtained from evaluation are listed in Table 3.3. The evaluation process in ABAQUS for viscoelastic material property for different rubber is illustrated in Figure 3.12. Since the undertread rubber specimen is difficult to extract from tyre product and its material property is similar to tread rubber, its hyperelasticity and viscoelasticity are assumed to be the same as tread rubber.

Table 3.3 Viscoelastic Material Constants

Rubber Material	Relaxation Modulus (g)		Relaxation Time (τ), sec.	
Component	g_1	g_2	τ_1	τ_2
Tread	0.1433	0.0852	7.6125	235.62
Sidewall	0.1613	0.0773	6.2257	224.29
Inner-liner	0.1017	0.0839	19.6480	363.70
Apex	0.1815	0.1197	3.5618E-02	206.28
Toeguard	0.1171	0.0891	21.2580	350.13

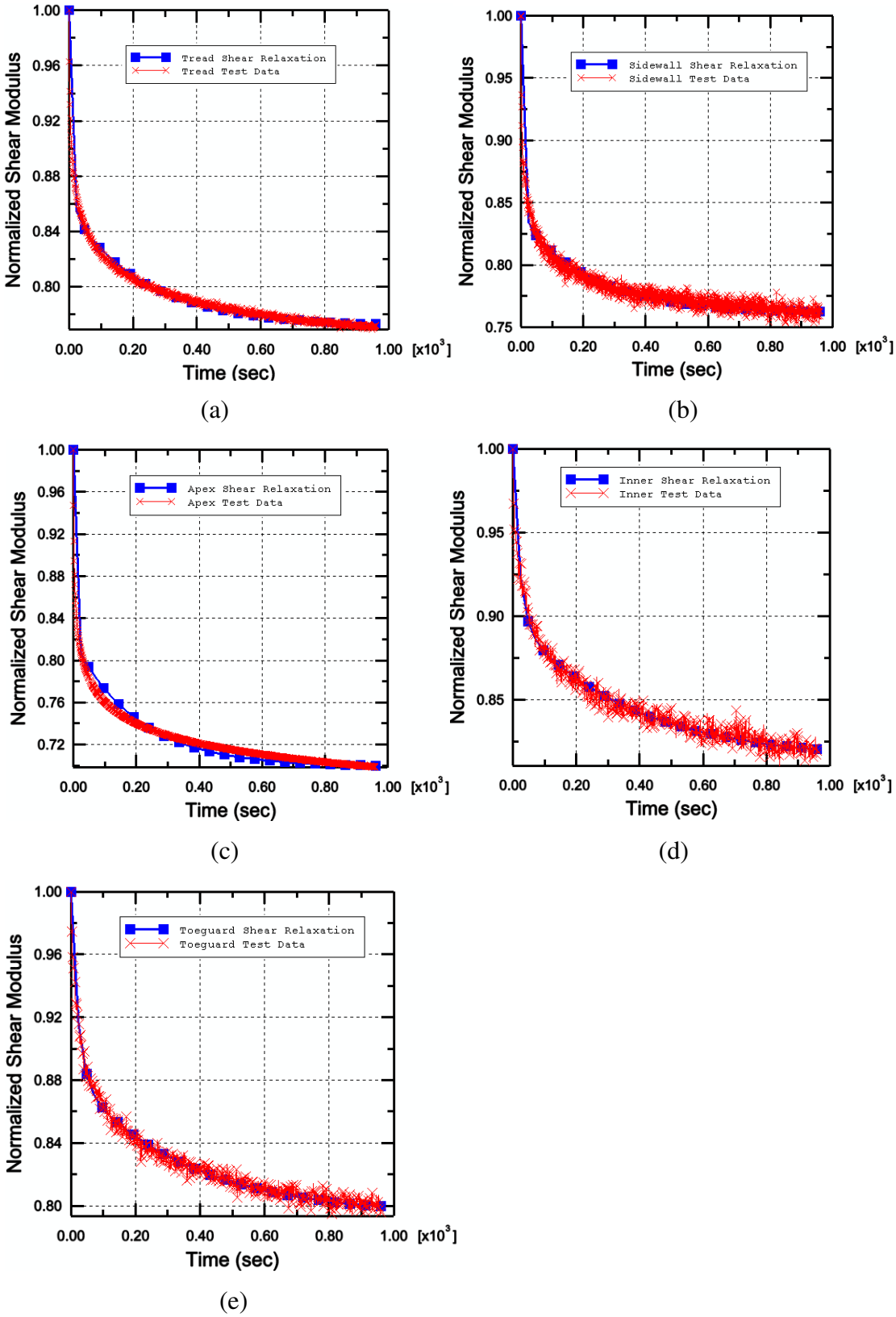

Figure 3.12 Viscoelasticity Evaluation (a) Tread (b) Sidewall (c) Apex (d) Inner (e) Toeguard

3.3. REINFORCEMENT MATERIAL PROPERTY

For the reinforcement component in tyre, the property of the anisotropic cord-rubber composite mainly controls the overall performance of pneumatic tyres. The material properties of cords, high modulus and low elongation, construct the support frame for rubber and carry most of the external loads. The cord-rubber composite material shows its adaptability to different tyre service conditions.

With the occurrence of large strains of cord-rubber composites, the strains in the cord vary only slightly, which is the reason most of the past studies adopt linear elasticity for tyre reinforcement (see Table 3.1).

In ABAQUS, the reinforcements are modelled using rebar element embedded into the rubber matrix. In this way, the reinforcement component and the host component (rubber) are described in different constitutive models. The material properties can be assigned to their corresponding component, separately. Before identifying the rebar material property, the area per rebar, orientation angle of rebar and position of rebar in rebar layer card in ABAQUS were measured by microscope.

The reinforcement details measured by microscope are listed in the Table 3.4.

Table 3.4 Reinforcement Detail

Component	Area per Bar (mm^2)	Spacing (mm)	Orientation Angle ($^\circ$)	Position (mm)
Cap ply	0.1385	0.75	90.0	0.0
Belt	0.3847	0.95	110.0	0.0
Steel belt	0.1994	1.28	70.0	0.0
Carcass	0.3630	1.34	0.0	0.0

Since the deformation of cords/steel wire during tyre inflation and deflection produces significantly small strains compared to rubbers, the material properties of cords remain well within their linear elastic limits hence their non-linear material properties are not required. Thus, the Young's modulus E and the Poisson's ratio ν were used to define the material property of reinforcement cords. For further study, the cord-rubber composite model considering the nonlinear material property can be programmed using Subroutine or Python in ABAQUS for realistic simulation [133].

3.3.1 REINFORCEMENT MATERIAL PROPERTY TEST AND DETERMINATION

For the present research, the cords' properties are characterized as linear elastic. The cords specimens are extracted from a tyre product. Although the experimental procedure for determination of cord properties can be based on some standards, such as ASTM standard D885/D885M, the Dynamic Mechanical Analysis (DMA) test was adopted as

a possible alternative of simple tensile test considering the restricted size of cords specimen extracted from the tyre product and the limited availability of facility in the laboratory. The DMA test clamp and rig are shown in Figure 3.13.

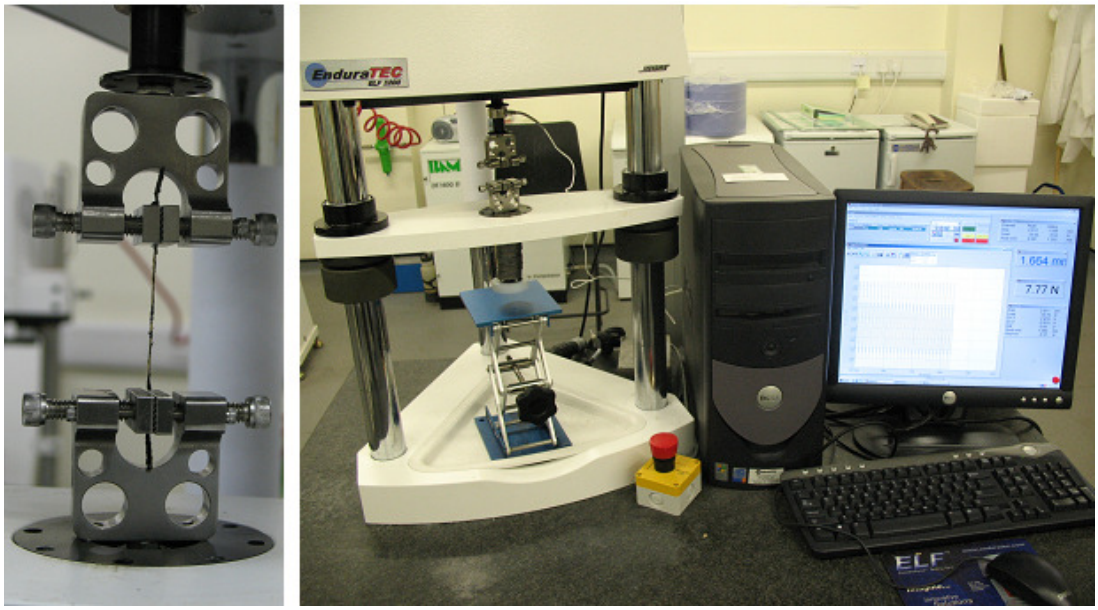

Figure 3.13 Test Rig for Cords DMA

DMA is an approach to investigate material property by applying small deformation to a sample in a cyclic manner, and can be used to determine the storage modulus (elastic modulus), loss modulus (viscous modulus) and Tan Delta (damping coefficient) as a function of temperature, frequency or time. The storage modulus is the measurement of the stored energy in viscoelastic material, representing the elastic portion. The loss modulus is a damping term describing the dissipation of energy into heat under deformation. The Tan Delta is the ratio of loss modulus to storage modulus, which indicates how efficiently a material loses energy due to molecular rearrangements and internal friction. The storage modulus was considered as the linear elastic modulus approximately in the low frequency range. The test was carried out in the low frequency

range from 1Hz to 10Hz. The specimen was pre-cycled before the test. When the equilibrium state is reached, the formal test is carried out. The test data are shown in Figure 3.14 and Table 3.5

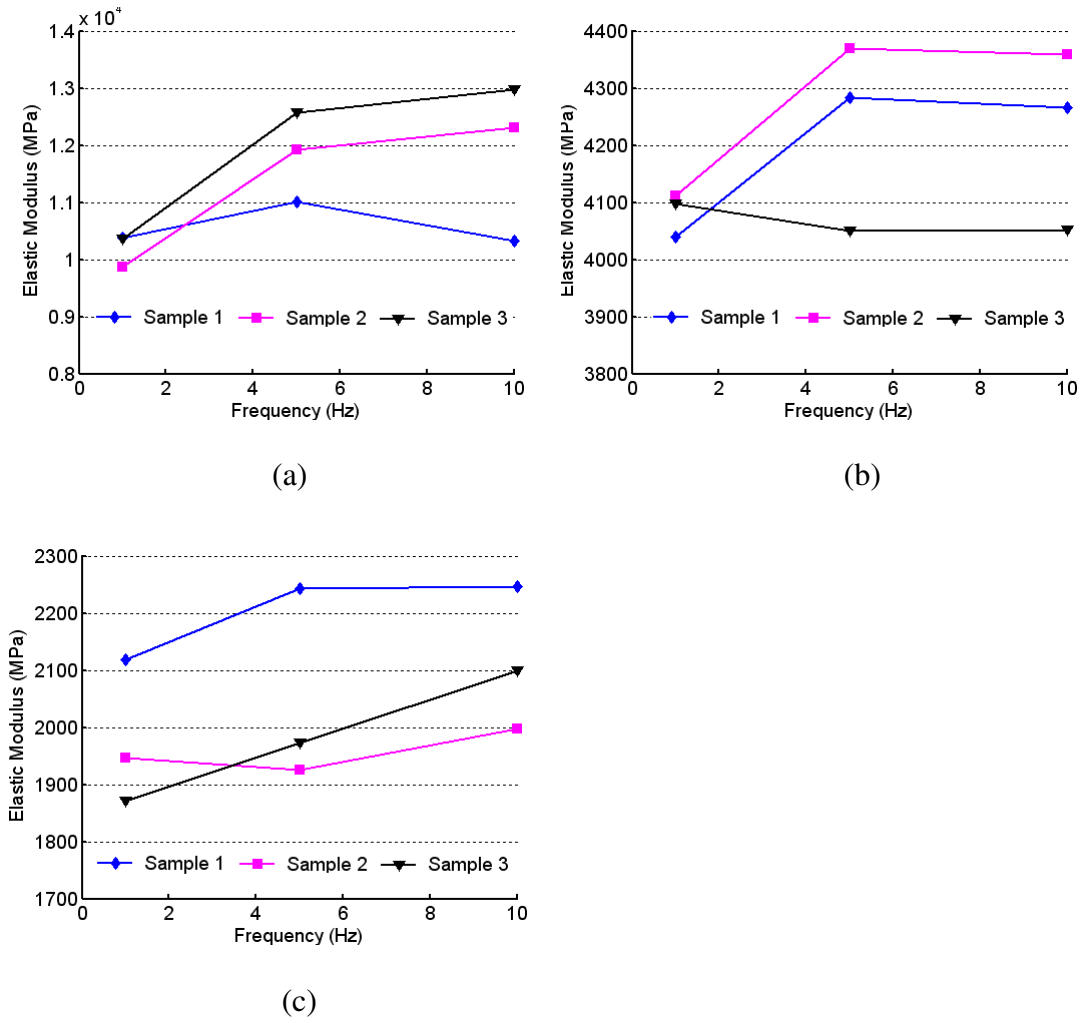

Figure 3.14 (a) Test Elastic Modulus of Belt (b) Test Elastic Modulus of Cap Ply (c) Test Elastic Modulus of Carcass

Table 3.5 Cord DMA Test Results

Cords Name	Sample number	Storage Modulus in 1Hz (MPa)	Storage Modulus in 5Hz (MPa)	Storage Modulus in 10Hz (MPa)	Average (MPa)
Belt	1	10380	11010	10330	10580
	2	9870	11930	12310	11370
	3	10360	12580	12980	11970
	Ave.	10200	11840	11870	**11300**
Cap ply	1	4040	4280	4270	4200
	2	4110	4370	4360	4280
	3	4100	4050	4050	4070
	Ave.	4080	4230	4230	**4180**
Carcass	1	2120	2240	2250	2200
	2	1950	1930	2000	1960
	3	1870	1970	2100	1980
	Ave.	1980	2050	2110	**2050**

The average results are taken as the Young's modulus of corresponding cords for the rebar element material property definition in ABAQUS. Namely, the Young's modulus of belt, cap ply and carcass are approximately 11.30GPa, 4.18GPa and 2.05GPa, respectively. The Young's modulus of steel belt and steel bead is 200GPa. The bead reinforcement property is assumed the same as the belt and the Possion ratio is taken as 0.3 approximately according to related literature [11].

3.4. MEASUREMENT OF DENSITY

Different component rubber specimens were tested using Density Measuring Device. All the test results were very close to 1200kg/m^3.Therefore, 1200kg/m3 was established for all the rubber components' density.

For the reinforcement, a nonzero density was also specified for the material in rebar layer. According to the density database of different types of cord in [134], the density of cords in this tyre was assumed as 1300kg/m^3, which has very little effect on the tyre inertia during dynamics simulation since the volume of reinforcement material is very small compared with the tyre rubber volume,. In addition, the density of steel wire is 7800kg/m^3.

3.5. SUMMARY

In this chapter, in order to model the tyre realistically, the tyre material properties were investigated by experiment. A feasible and practical material test procedure was developed considering limited specimen source with the support from tyre manufacturer. The specimens of rubber and reinforcement were obtained by cutting a tyre product. Uni-axial test was carried out to obtain the rubber hyperelastic material properties. Meanwhile, the viscoelastic material properties of rubber were identified by stress relaxation test. The constants of rubber material model were determined using the evaluation function in ABAQUS. The reinforcement cord material property was considered as linear elastic due to its small strain during normal tyre service. The linear elastic modulus of different reinforcement cords in this study was identified by DMA

test. The last but not the least, the density of rubber components and reinforcement components was established for future study. The accurate material properties achieved in this chapter provides a sound basis to investigate the tyre local behaviour by FEA. Moreover, it is useful for sensitivity study of tyre material components during tyre design process.

CHAPTER 4

FINITE ELEMENT TYRE MODEL

4.1. INTRODUCTION

The finite element tyre model plays an increasingly significant role in tyre behaviour investigation for tyre manufacturers and researchers. In order to achieve successful prediction of tyre characteristics using FEA, an accurate 3D tyre model is crucial. The fundamental requirement for the tyre modelling process is precise and adequate information about tyre material properties and tyre geometry. Apart from the material properties obtained from the last chapter, the tyre geometry information is the other important factor which needs to be explored.

In this chapter, a novel approach measuring tyre cross-section geometry based on image processing was developed. A two-dimensional (2D) cross-section finite element tyre model was built firstly considering the proper mesh density and element type. The cord embedded in rubber element was expressed using rebar layer card in ABAQUS. Then the three-dimensional (3D) finite element tyre model was generated based on the 2D model. In addition, the proper wheel and road models for different types of analysis are discussed.

4.2. TYRE GEOMETRY SPECIFICATION

4.2.1 OVERVIEW

Although many papers have been published in the past decades on the investigation of tyre FEA using 3D tyre model, the procedure to obtain geometric information of tyre cross-section is usually ignored. Most of the tyre manufacturers considered the structural details of their tyre products to be confidential.

However, several methods have been developed for acquiring tyre geometric information by researchers for related studies in the absence of any computer aided design (CAD) tyre data. Bolarinwa [11] obtained the geometric information of a tyre cross-section by measurement using coordinate measuring apparatus, such as trial-axial Coordinate Measuring Machine (CMM). Based on this measurement, a satisfactory 3D model was created by revolving the cross-section in ABAQUS, and the subsequent FEA gave accurate results [11]. However, this manual procedure can produce inaccuracies and can not measure the tyre bead region.

With the development of inspection technology for use during the tyre manufacture process, more and more image acquisition apparatuses are being applied including the CCD camera, X-ray tomography device and laser holography equipment [135, 136]. Some of the above devices have been used to validate finite element tyre model. For example, the CCD camera was used to investigate the vibration modes of a tyre [137], and the Digital Imaging Correlation (DIC) technique was used to obtain the tyre experimental data of displacements and strains [26, 138]. Moreover, some of these

techniques have been used to investigate the microstructure and behaviour of tyre materials in a micro scale, such as the X-ray tomography technology used to image the internal structure of tyre material before and after use-to-failure for predicting early failure of tyre [139, 140].

On the other hand, the image processing technology can be used to model the tyre. On the micro scale, it can distinguish the diameter and orientation of fibres, which contributes to locating the cords [141]. It is capable of detecting most of the structure and material details for tyre modelling. On the macro scale, Sophie Voisin, et al [142] introduced an approach to restructure 3D tyre CAD model using image-based reverse engineering (RE). Multiple views of the tyre surface are scanned, and then the view registration in RE is adopted to generate high fidelity models in preparation for manufacturing the prototype.

An alternative tyre modelling method is suggested by Danielson, et al [143] using the powerful functions of commercial software PV-Wave. Based on scanned images an accurate description of the perimeter of the tyre cross-section and the locations of plylines and cord-ends were identified. Then the geometric information of tyre cross section was converted into a computer aided drawing for creating different types of finite element tyre models.

One of the most important applications using image processing technology is biomedicine, which takes advantage of the generated data from CT images, MRI images and other images based on tomography technology [144]. It encouraged the tyre

researcher to adopt similar technology for tyre modelling. Subhendra N. Sarkar and Richard A. Komoroski [145] adopt multiple-slice, three-dimensional nuclear magnetic resonance imaging (NMRI) at micrometer level to study the elastomeric components of different tyre sections. The NMRI images accurately characterized the small features of different components in the tyre including rubber layers and cords.

Recently, with the appearance of advanced interface software such as the commercial software Simpleware, the 3D images can be transferred into FE simulation directly [146].

4.2.2 IMAGING-BASED TYRE GEOMETRY MEASUREMENT

From the literature review, it is found that the study of Danielson, et al [143] unfolded a simple and effective semi-automated procedure for distinguishing tyre geometric characteristics for tyre modelling. Based on the study of Danielson, this chapter introduces an alternative method for finite element tyre modelling by extracting accurate tyre cross-section data from a FS tyre using image processing technology. Some tests and comparisons are carried out to validate the accuracy of the tyre model created using this method which can be found in the Appendix.

The whole procedure from image acquisition to cross-section finite element modelling is illustrated in Figure 4.1.

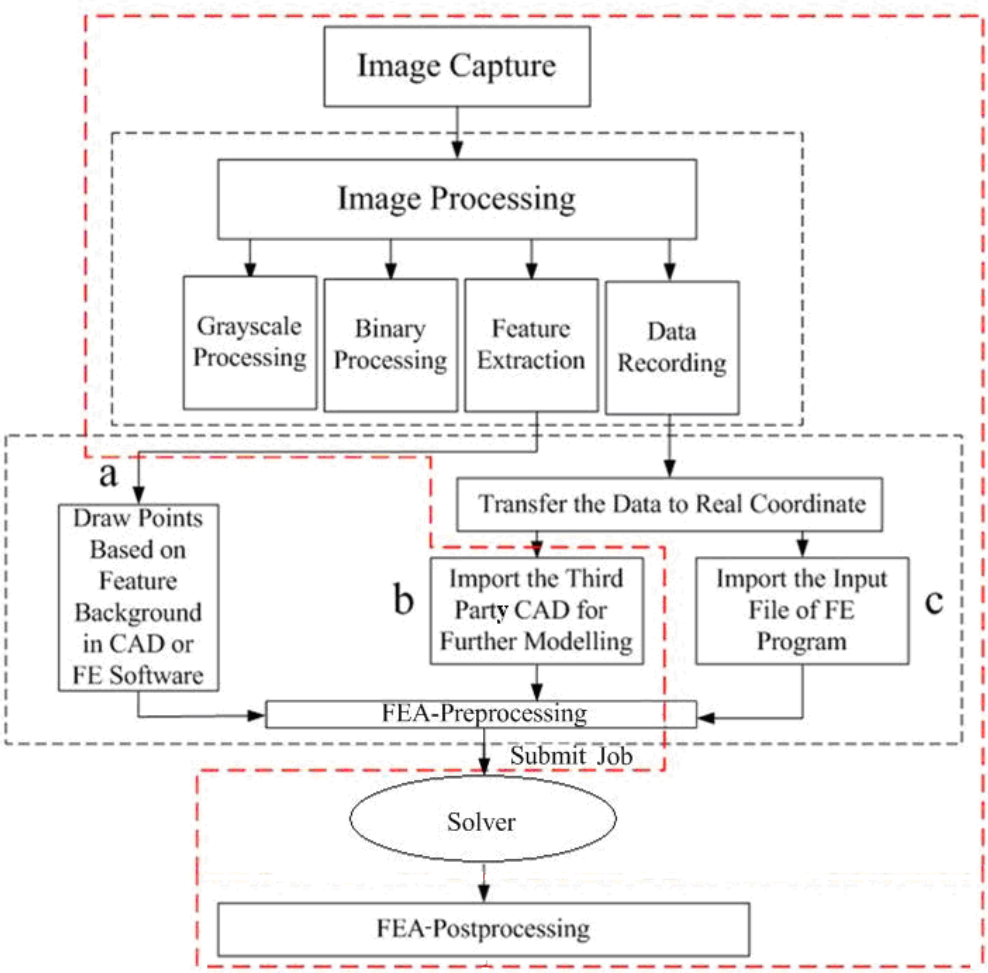

Figure 4.1 The Whole Procedure of Tyre Cross-section Modelling Based on Image

The methods a, b and c shown in Figure 4.1 possess different accuracy, respectively. The precision of method a is equivalent to traditional measuring method and besides, it can provide adequate points in less time. The methods b and c can provide adequate and accurate geometric information depending on the resolution of image capture pixels and the feature extraction approach used (such as edge detecting algorithm). Although the approaches introduced in this report involve some manual effort, the procedures within the red boundary in Figure 4.1 can be integrated into an automated FEA procedure depending on a proper strategy and algorithm. The relevant idea has been proposed in reference [74].

In order to demonstrate the universality of the proposed method, the tyre cross-section 2D image is taken by a common digital camera--Cannon Powershot A630 shown in Figure 4.2. Actually, a scanner can provide a higher resolution image than a digital camera for optical reasons.

Figure 4.2 Raw Image of Tyre Cross-section

The five push pins are used to constrain the tyre boundary in order to achieve the same dimensions as the rimmed-tyre at cold inflation pressure 0 kPa. The boundary conditions are measured including rim width, tyre section width and tyre section height. The Dunlop 175/505 R13 tyre cross-section image is captured by digital camera at a resolution 1600×1200 pixels. In a similar application in industry, the cross-section image can be obtained from a device of the tyre inspection system using tomography technology, which can divide the object into multiple slice images. To ensure high performance of image processing, a mouse click modification is carried out to diminish the disturbance, as well as repair the features in the cross-section. The following image

processing is accomplished using Matlab. The images after enhanced processing are shown in Figure 4.3.

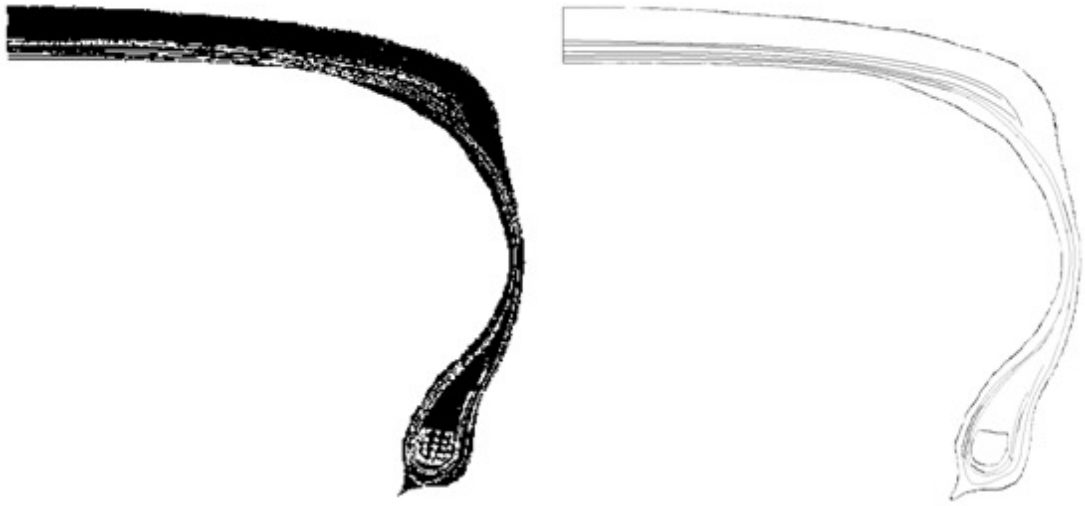

Figure 4.3 Tyre Cross-section Image after Enhanced Processing

From the left image of Figure 4.3, it can be seen that the locations of plylines, cord-ends and the bead are expressed by a cluster and several arrays of white points, which are used to determine their positions. However, due to some ambiguous feature points and some missing feature points, manual manipulation is adopted to delete inaccurate points and add accurate and necessary points. By this way, the corresponding points' coordinates for different plies and bead can be obtained. From the right image, the feature points of this tyre cross-section were finally identified.

Then, the feature pixel coordinates were recorded and transformed to real coordinates by scaling, thus expressing the real dimensions of the cross-section geometry shown in Figure 4.4. The scale is obtained by comparison of image dimensions with the real dimensions of tyre section width and section height. The approximate relative

coordinates are calculated from the pixel coordinates, which translate to the real geometric distance. The scale ratio in this case is 0.127mm/pixel.

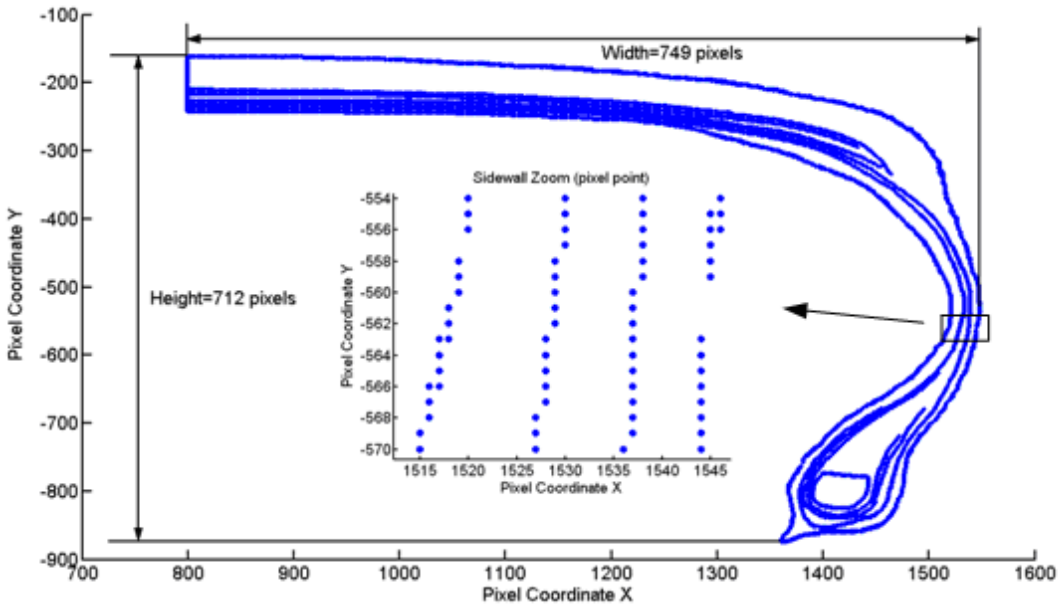

Figure 4.4 Tyre Cross-section Geometry by Pixel Points

The new coordinates are stored in a proper format and imported into CAD software for further FEA modelling. Obviously, Figure 4.4 provides adequate information about the tyre cross-section geometry, such as the belt location and cords spacing. With these information, the finite element tyre modelling process can commence.

Fortunately, with the support of Dunlop, the tyre CAD was made available shown in Figure 4.5. It can be seen that the cross-section of the tyre product has some differences from the design, which may be caused by the manufacturing process and variation from one individual tyre to another. The crown region from the product cross-section is curved, while it is almost flat for the design. The shape of the region around the bead area is different between the image of the product and design CAD. The spacing

between neighbouring reinforcement plies is nearly the same for design CAD drawing, while the distance between belt ply and steel belt ply is larger than the spacing between other neighbouring plies in the image of the tyre product. In the rest of this thesis, the finite element tyre model based on the geometry gained from image processing is named model I. The one based on CAD drawing is named model II.

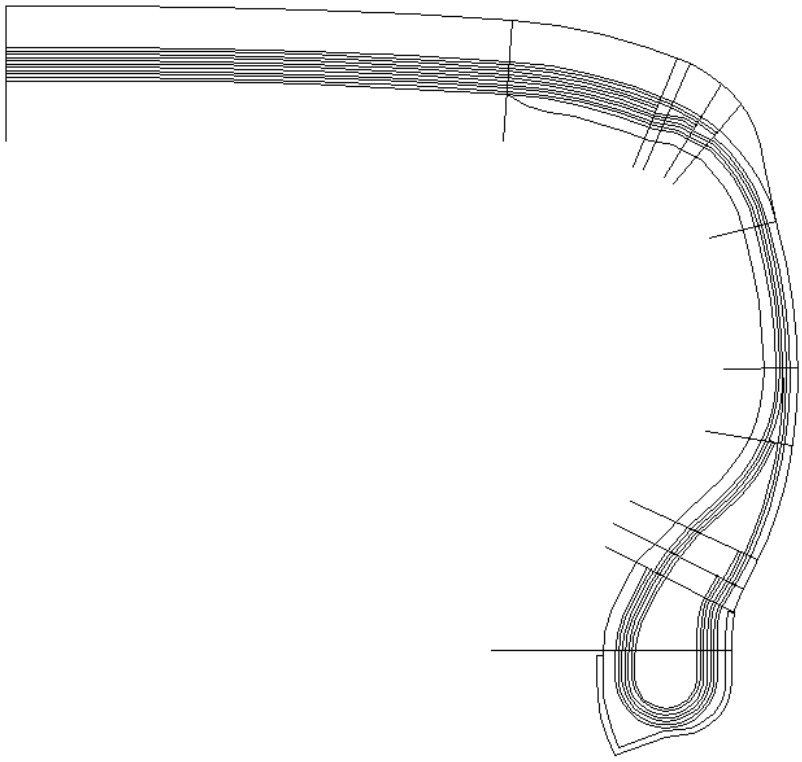

Figure 4.5 Tyre CAD Cross-section Geometry

4.3. RUBBER AND REINFORCEMENT MODELLING

Once the tyre cross-section structure details were obtained, the finite element model of cord-rubber composite is created in ABAQUS. Generally, there exist two methods for modelling cord-rubber composite: laminated shell model and rebar model [62]. In this

study, the rebar layer function in ABAQUS provides the support for modelling cord as rebar element which is embedded in rubber solid element as shown in Figure 4.6.

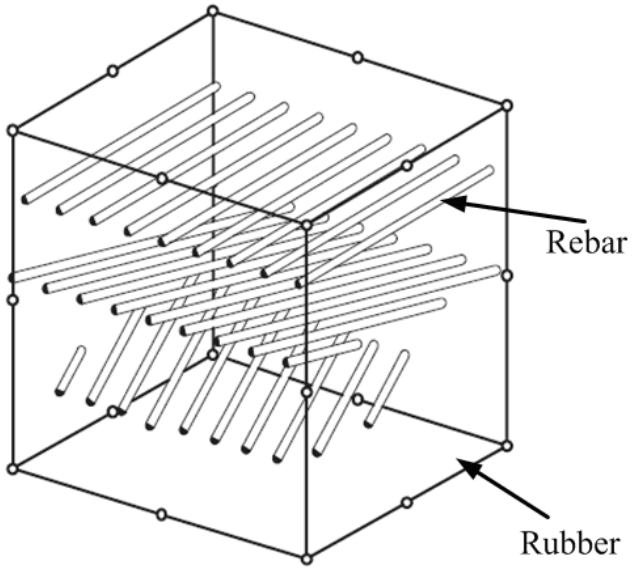

Figure 4.6 Cord-rubber Composite Model by Rebar Element [62]

The rebar layer function in ABAQUS can define the rebar orientation, spacing, thickness, location and material properties which are independent of rubber material properties definition. Material properties of different components obtained from tests were then applied to the model. The modelling procedure introduced in [75] was adopted in this study. A 2D axisymmetric tyre model was developed firstly by importing the 2D cross-section profile into ABAQUS/CAE shown in Figure 4.7 and Figure 4.8. The hybrid axisymmetric continuous element with twist degree of freedom (CGAX4H and CGAX3H) is used to account for the twist feature of the cord along the axisymmetric axis due to anisotropy of fiber reinforcements [56]. Particularly, for the bead region, 2D axisymmetric hybrid element CGAX4H was used with steel property rather than embedding steel wire in rubber, which is effective and efficient. The

reinforcement component was represented by the SFMGAX1 element with 2 nodes, which is embedded in rubber elements in ABAQUS. One layer cap ply with 0 degree orientation (along the circumferential direction), two layers breakers including one layer steel belt with 20 degree orientation and one layer nylon belt with -20 degree orientation, and two layers carcass with 90 degree orientation are modelled by rebar layer and embedded in the corresponding host solid elements. The element set and node set were created for different components for convenient operation in ABAQUS, such as assigning material properties and boundary conditions, and post-processing.

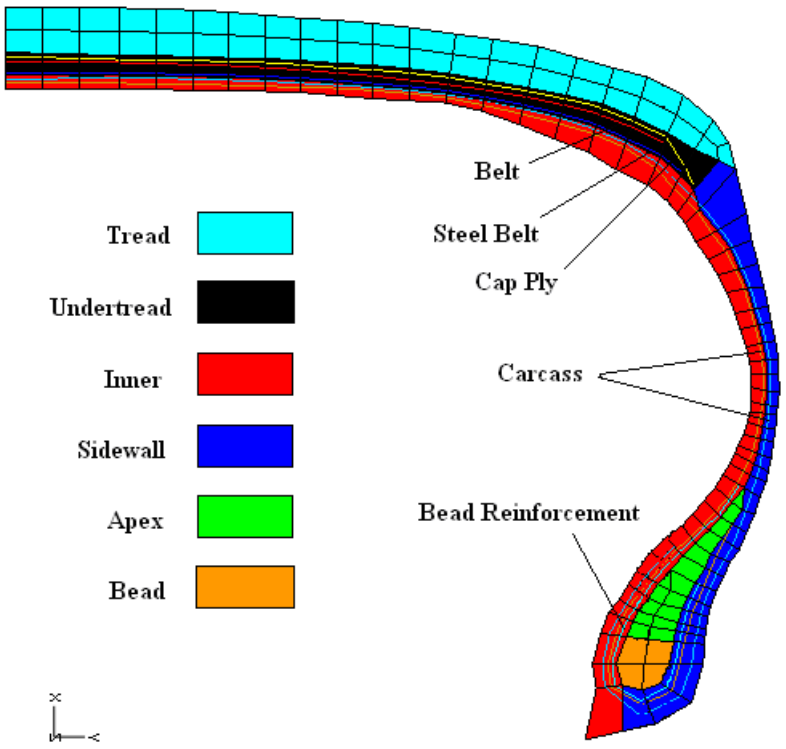

Figure 4.7 Finite Element Model of Tyre Cross-section in ABAQUS (model I)

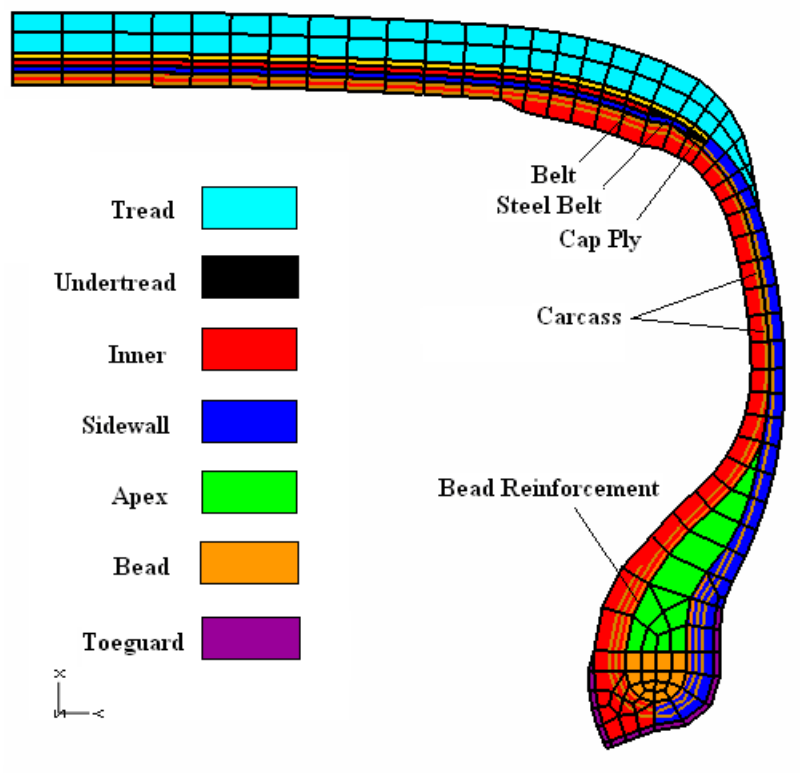

Figure 4.8 Finite Element Model of Tyre Cross-section in ABAQUS (model II)

The 2D axisymmetric model is converted into a 3D finite element tyre model using the symmetric model generation function in ABAQUS. During this process, the 2D axisymmetric elements (CGAX4H and CGAX3H) are transformed into 3D solid elements (C3D8H and C3D6H). The number of circumferential sections can be controlled for different analyses, for example only the contact patch part of the tyre has refined mesh for steady state tyre rolling analysis shown in Figure 4.9. The 2D cross-section is revolved about the symmetric axis generating two $30\times5^{\circ}$ coarse sections and one $40\times1.5^{\circ}$ refined section for the contact patch region. This non-uniform and appropriate mesh not only ensures obtaining accurate prediction but also low cost of computational time which will be discussed in Chapter 5. The structure details such as the cord-rubber composite is still kept after revolving 3D model shown in Figure 4.10.

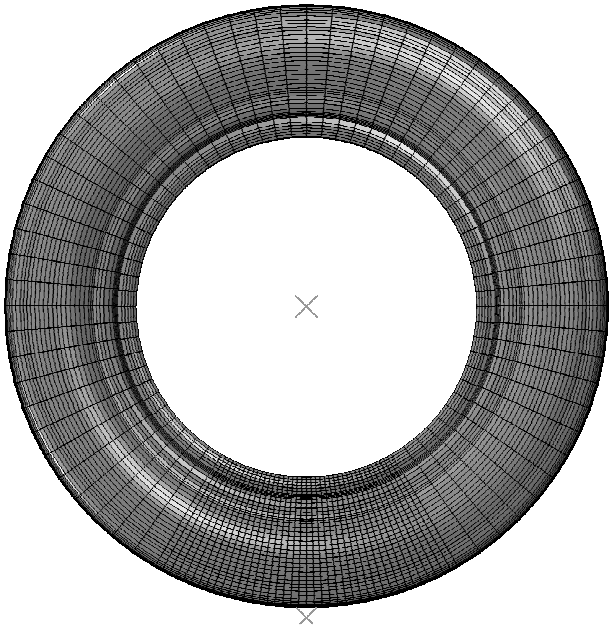

Figure 4.9 Finite Element Tyre Model for Steady State Analysis

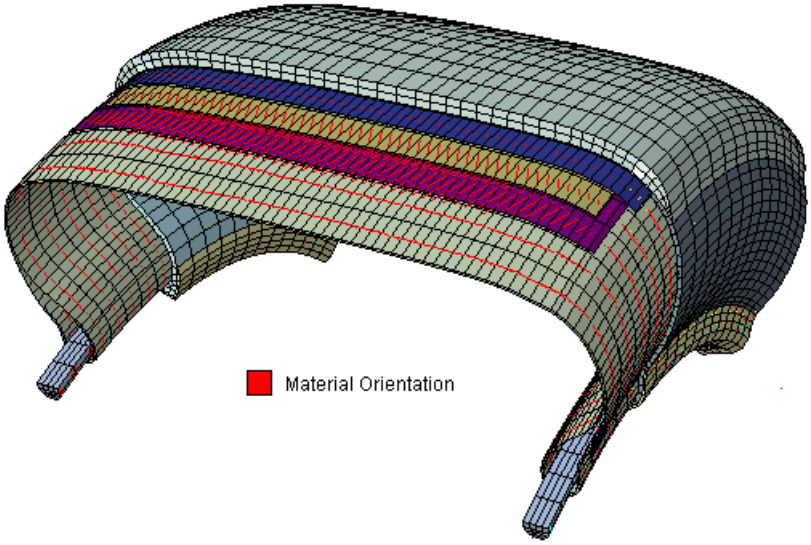

Figure 4.10 Detailed View of 3D Finite Element Tyre Model

4.4. WHEEL AND ROAD MODELLING

Generally, the tyre is mounted on the wheel which transfers force between the tyre and the hub. For tyre dynamics investigation, the wheel has an inevitable influence on tyre behaviour. The tyre/rim contact condition also has a significant effect on tyre durability and fatigue. The knowledge about the normal contact stress and shear stress is valuable for optimal design of tyre bead area and wheel [147, 148].In most of the tyre/rim modelling researches, 2D or 3D symmetric rim profile was used in the tyre/wheel assembly simulation. In [127], two parts of 3D rigid rim (left and right) were moved towards each other until reaching the standard width of the wheel rim. The assembly of the tyre and the wheel is realized virtually and friction coefficient was given as 0.5. A similar method can be found in [149]. However, the real geometry of the wheel is not symmetric and the mass of the wheel can not be omitted for dynamic analysis such as NVH. In this chapter, the 2D tyre models with an analytical rigid wheel and without wheel are shown in Figure 4.11 and Figure 4.12, respectively.

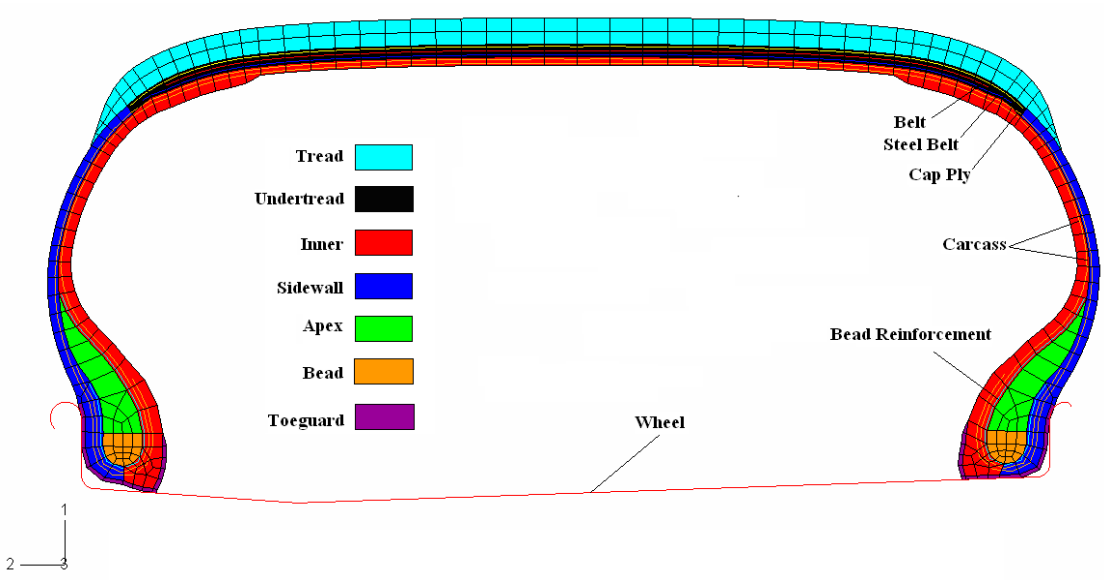

Figure 4.11 2D Finite Element Tyre Model II with Analytical Rigid Wheel

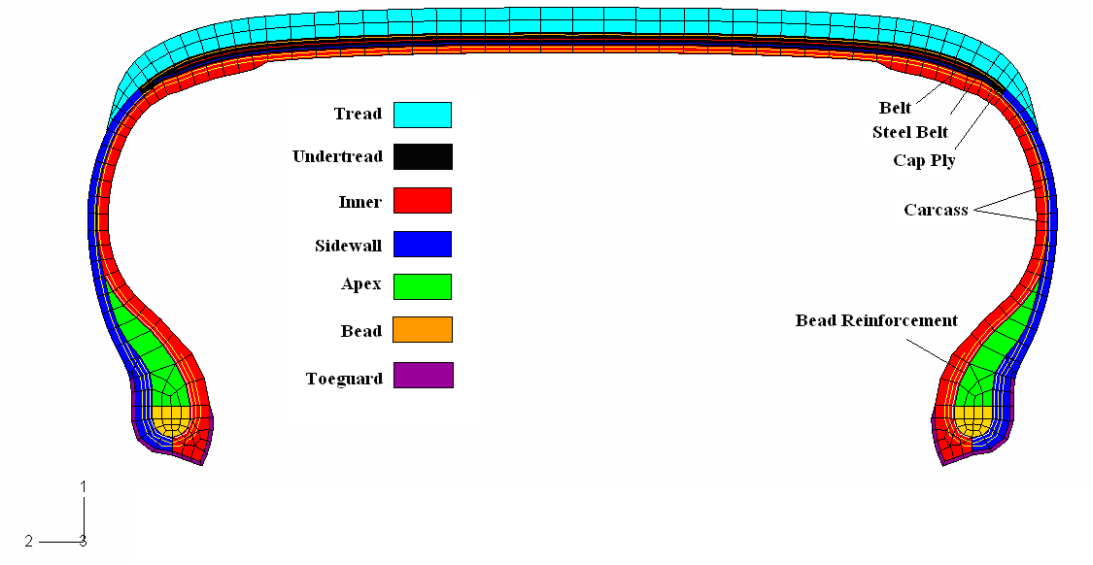

Figure 4.12 2D Finite Element Tyre Model II without Wheel

The rim geometry is non-symmetric as shown in Figure 4.13.

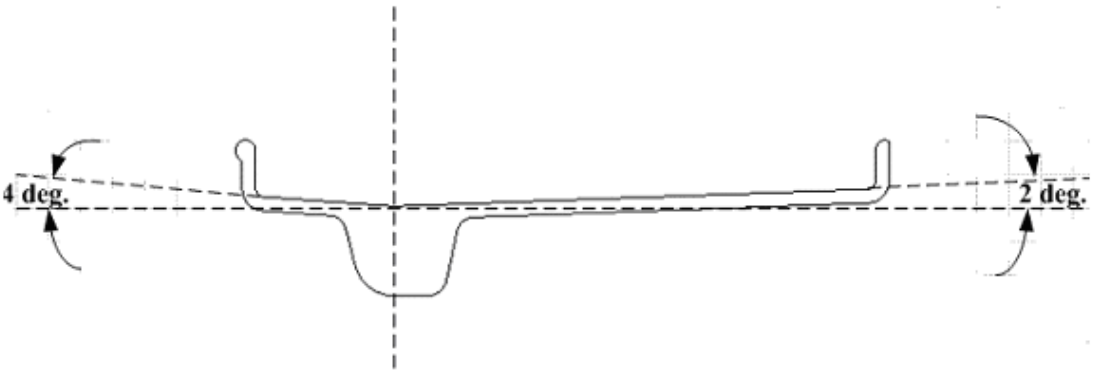

Figure 4.13 Asymmetric Rim Cross-section

It can be found that due to the non-symmetric geometry of the rim the deformation of the tyre in tyre/rim contact region is different on the two sides of the tyre. This difference usually does not induce big difference on tyre global behaviour but it should be considered for local behaviour such as strain around the contact region.

In [71], a modal analysis was carried out for a finite element tyre model assembled with a stiffened steel wheel, a standard aluminium wheel and a standard steel wheel, respectively in order to study the effect of the wheel flexibility on lower frequency modes. It was found that some of the low frequencies from aluminium wheel and steel wheel are lower than that from stiffened steel wheel, which may be caused by the wheel flexibility. However, as mentioned in [11], many published papers demonstrated that the consideration of rigid wheel is appropriate in view of the high stiffness of the wheel relative to the tyre.

In addition, for high frequency tyre dynamic analysis, it is necessary to include the high stiffness property and the inertia of the wheel into the model, such as in tyre/wheel impact simulation. In [150], ABAQUS/Explicit was used to carry out the nonlinear dynamic analysis of wheel impact test, in which a solid wheel was modelled by hexahedral elements and tetrahedral elements. In [151], a finite element tyre/wheel model was used to study the tyre impact under different impact energies. The solid wheel was adopted and the surface to surface with penalty based contact algorithm was utilized for the tyre/rim contact. Both the above two studies show that the predicted results agree well with the experiments.

In this study, three different wheel modelling methods are presented. According to the research requirements, the corresponding and suitable wheel model can be selected. The three wheel models are shown in Figure 4.14.

The first modelling approach ignores the wheel and tyre/rim contact surface is fixed to a reference node, which is suitable for tyre handling analysis such as the steady state analysis [11]. The second modelling approach creates an analytical rigid wheel and the third one considers a total solid wheel model which can be assigned different material properties such as elastic-plastic for tyre/wheel impact analysis. For the first two wheel models, a concentrated mass and rotary inertia need to be included for approximated tyre dynamics analysis.

(a) (b) (c)

Figure 4.14 Wheel Models

As for the road model, many researches take the road as analytical rigid surface or the rigid drum surface since the road stiffness is usually much higher than that of the tyre. Meanwhile, the analytical rigid surface with six degrees of freedom controlled by one reference node is suitable for most of the tyre FEA. However, for studying some special road types and conditions such as soil, sand and water, the rigid road model is useless and it cannot provide any stress and strain results occurring to the road. In this case, the road needs to be modelled as solid with special designed 8-node hexahedral element. This model usually has two layers where the bottom one is much stiffer than the top

one. In [152], the top layer of soil road model is assumed to have elastoplastic mechanical behaviour and the bottom layer is assumed as elastic. In [153], the top layer of water road model is created by Eulerian element and the bottom layer is modelled as rigid body. In order to enable water scattering, a void layer was added to the top of the water layer using Eulerian element. In this thesis, the analytical rigid road model was adopted without considering different road types and road conditions. However, as an example, both the analytical rigid road model and solid road model are presented herein shown in Figure 4.15. The first one is the analytical rigid surface. The second one is the solid model for soil road or hydraulic road.

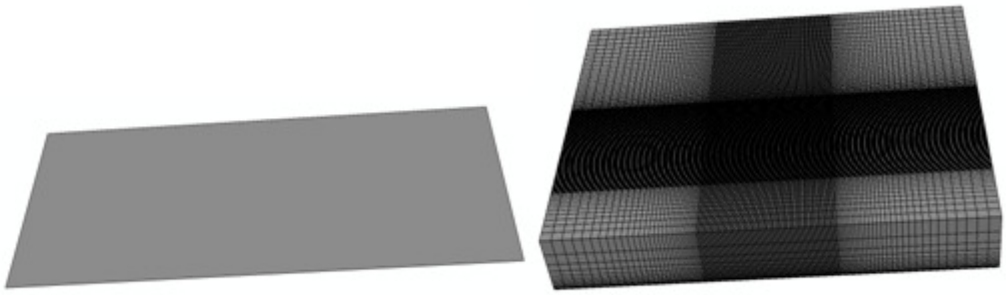

(a) Analytical Rigid Road **(b) Solid Road Model**

Figure 4.15 Road Models

4.5. SUMMARY

In this chapter, a finite element tyre modelling method was developed using ABAQUS. A novel method for deriving tyre cross-section geometry based on image-processing was introduced when no CAD tyre information is available. The image processing technology provides a feasible and practical approach for FE tyre cross-section modelling. This approach can distinguish the different features of the composite

structure including bead, plies, cord-end and tread groove. Considering the structural difference caused by manufacturing errors among individual tyre products, the image-based FE tyre modelling method is reasonable. With the tyre cross-section geometry, a 2D axisymmetric finite element tyre model is created and the cord-rubber composite is modelled by rebar element embedded in the solid matrix. A 3D finite element tyre model is revolved from the 2D model. Three types of approaches, fixed bead region nodes, rigid wheel and solid wheel, were introduced for modelling tyre/wheel assembly. Two types of road model, analytical rigid surface and solid, are used to deal with the tyre/road contact problem. However, in this study only the analytical rigid surface road model was used due to its cost-effectiveness. Based on this method, an integration process for automated generation of FE tyre model could be developed with the assistance of appropriate optical device and image processing algorithm, which can largely reduce the cost and time for FE tyre modelling.

CHAPTER 5

EXPERIMENTAL VALIDATION OF FINITE ELEMENT TYRE MODEL

5.1. INTRODUCTION

The 2D and 3D finite element tyre models have been developed in the chapter 4. It is necessary to validate the finite element tyre models created based on the material properties and geometry information. Only the validated tyre model can be used as a virtual simulation platform to provide reliable predicted data instead of experiment. A finite element tyre model with sufficient mesh density is expected to be used for the validation out of consideration for achieving reasonable solution with acceptable numerical convergence and accuracy. E. O. Bolarinwa [11] described a convergence study of tyre mesh density where he took account of the effect of different mesh densities on tyre maximum displacement, stress at contact interface and total CPU time. Generally, the mesh density of tyre model determines each element's dimension, which influences the accuracy of FEA prediction results. A poor mesh of finite element tyre model may cause larger element aspect ratio than is desirable, which could lead to inaccurate prediction or convergence problem. The aspect ratio is the ratio of the longest to shortest edge of an element in ABAQUS. However, overly refined mesh of tyre model scarifies the efficiency of computational analysis and more time cost is needed. Therefore, it is necessary to find a trade-off solution between tyre mesh density and computational efficiency. For static and steady state analysis, the FE tyre model with non-uniform circumferential mesh density was used as shown in Figure 4.9 in Chapter 4

and a convergence study on tyre mesh density was carried out on the tyre footprint region from a very coarse mesh to a very fine mesh as shown in Figure 5.1.

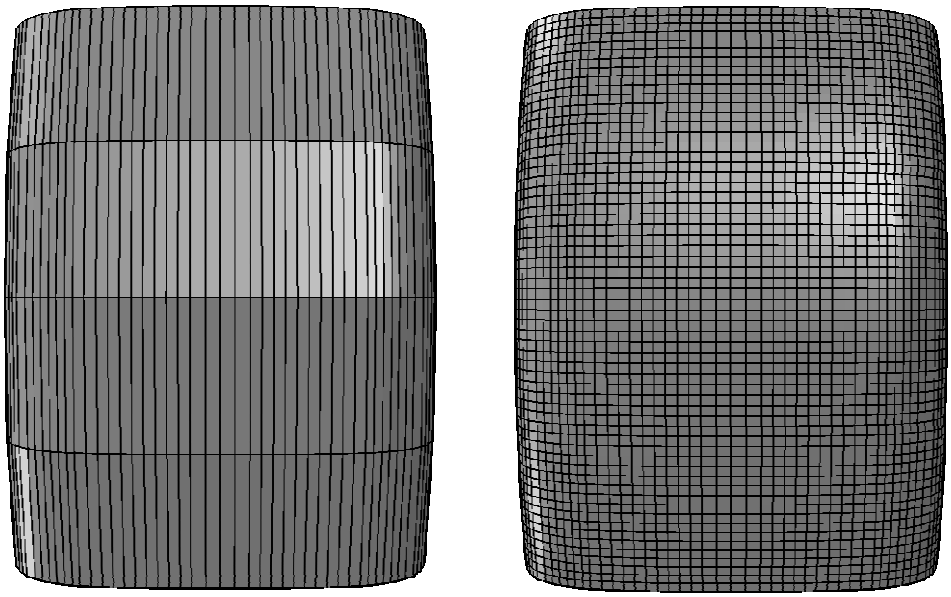

(a) $4\times15^{\circ}$ **Very Coarse Mesh** **(b)** $60\times1^{\circ}$ **Very Fine Mesh**

Figure 5.1 Tyre Mesh Convergence Study

Static footprint analysis was carried out at inflation pressure 80 kPa and preload 1000 N for different mesh densities. The maximum tyre contact patch pressure and the total CPU time required are shown in Figure 5.2.

It is shown that the maximum contact pressure approaches to being stable when the mesh density is higher than 30 sections, while the total CPU time continues to increase with increasing mesh density. An appropriate mesh density was selected based on Figure 5.2 considering the accurate prediction and reasonable CPU time, which would be used for further tyre model validation.

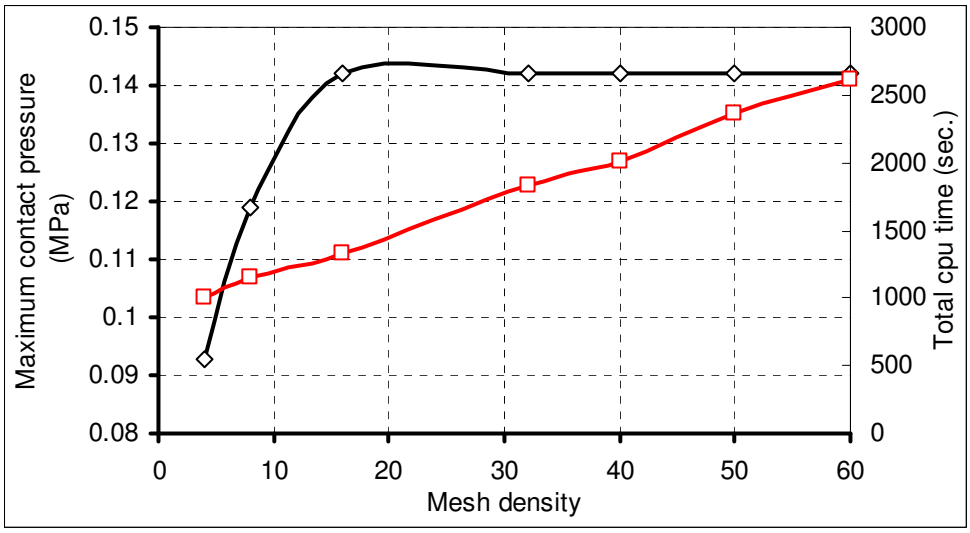

Figure 5.2 Convergence of Contact Pressure for Tyre Mesh Study

Different types of validation methods have been tried before, such as inflated geometry [10, 11], stiffness [154], footprint [10, 155], strain [26] and force [54], etc. In order to support the rest of the study of this thesis, a general-purpose validation was carried out comparing FE results with experiment including inflated geometry, vertical static stiffness, footprint, and sidewall strain. After these validations, it is believed that the finite element tyre model is not only capable of predicting tyre global behaviour but also the local behaviour. All the validation approaches adopted in this chapter are static. The finite element tyre model II is used in this chapter. The validation of finite element tyre model I can be found in Appendix.

5.2. INFLATION VALIDATION

5.2.1 INFLATION EXPERIMENT

As a fundamental validation method, inflated geometry variation can reflect the similarity of different tyre regions such as tread and sidewall between real tyre and finite element tyre model. Due to the axisymmetric nature of tyre geometry, only the displacement on the outside surface of half tyre cross-section was measured and validated. A trial-axial Coordinate Measuring Machine (CMM) shown in Figure 5.3 was used to measure the coordinates of the nodes outside tyre cross-section before and after inflation.

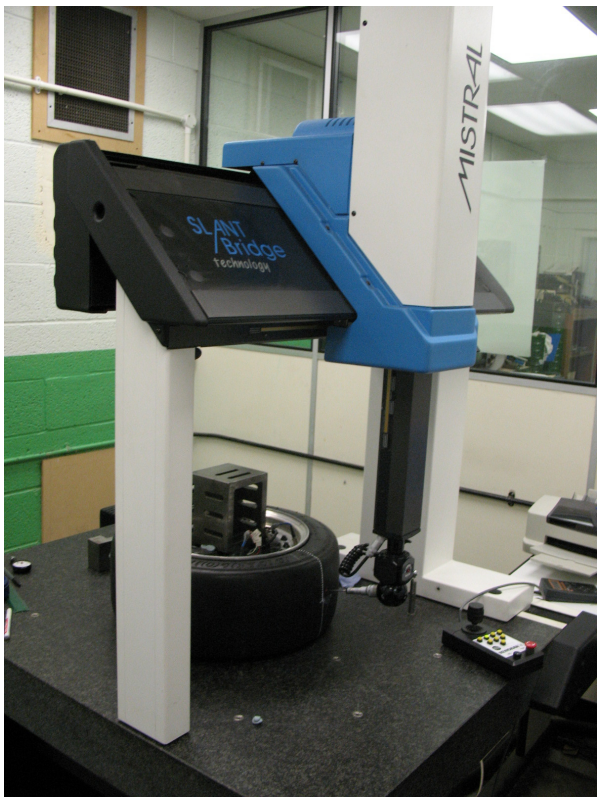

Figure 5.3 Coordinate Measuring Machine

The CMM consists of a movable structure which is capable of measuring a point in space. The record of a point's coordinates from a force sensitive sensor-touch trigger probe is stored in specialized software. It can then be imported into CAD software or saved in a graphics (igs) file for further processing. In this study, the initial status of the tyre mounted on a rim was at cold inflation pressure 0 kPa. Half of the external profile was detected along its cross-section. Then the tyre was inflated and the measurement procedure was repeated at different pressure levels. Because the CMM was operated manually, the nodes obtained have irregular spacing which can not match the nodes in the finite element tyre model. Meanwhile, the external profile of the bead region cannot be measured because of the block of rim.

5.2.2 INFLATION ANALYSIS

The 2D axisymmetric FE tyre model was used to simulate tyre inflation. The axisymmetric finite element model is usually sufficient for studying tyre inflation and mounting [10, 149], mechanical-thermal coupling [156] and burst [53], etc. Results, such as stress and strain distribution, profile changes, contact pressure distribution on the tire-rim interface and temperature effect can be obtained from 2D tyre FEA.

In this study, the tyre-rim assembly was simplified and a rigid body was created between the tyre-rim interface nodes and rim reference node by tie function. Thus all the degrees of freedom (two translational degrees and two rotational degrees) of the tyre-rim interface nodes can be fixed by applying the boundary condition to the rim reference node. The inflation pressure was applied to the inner surface of tyre cross-section as shown in Figure 5.4.

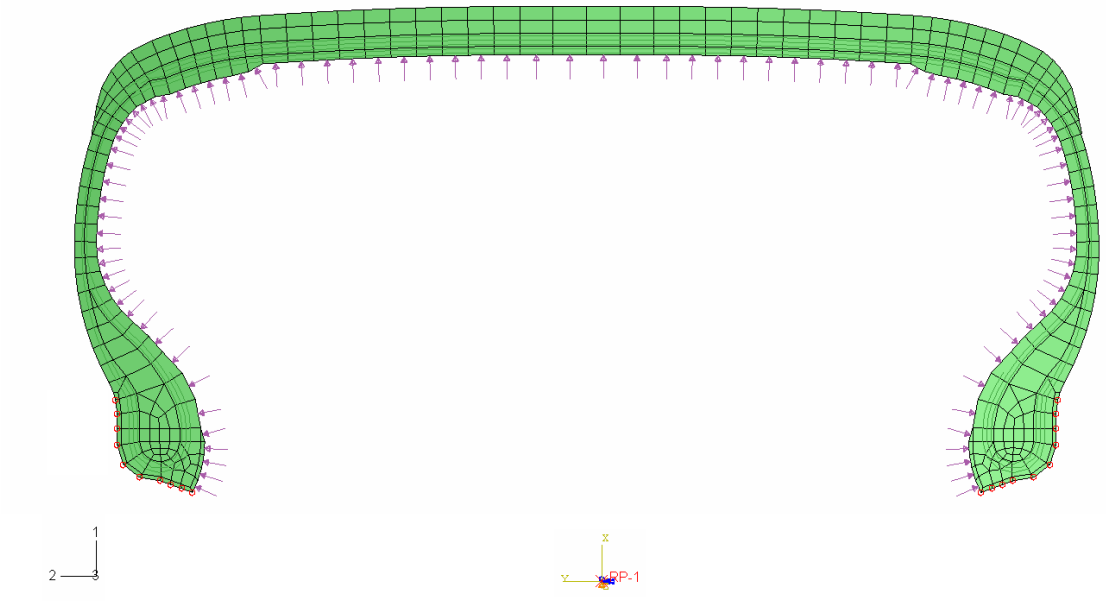

Figure 5.4 Boundary Condition of 2D Axisymmetric Tyre Model II

Although the wheel model was not involved in the 2D FEA, the simplification can still reveal the deformation and stress distribution away from the bead-rim interface region as mentioned in [11].

5.2.3 COMPARISON AND DISCUSSION

For tyre static state, the geometry changes under inflation is a basic validation method used for validating the FE tyre model. The normal inflation pressure considered for the tyre is 80 kPa. The simulation of the inflation process was carried out using ABAQUS/Standard. The tyre profile change in experiment and simulation was plotted in Figure 5.5.

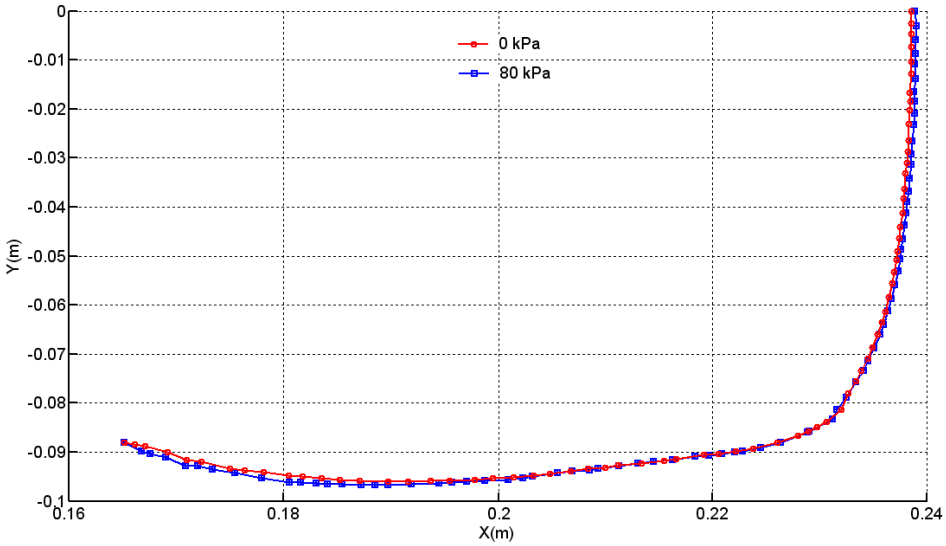

(a) Experiment Measurement

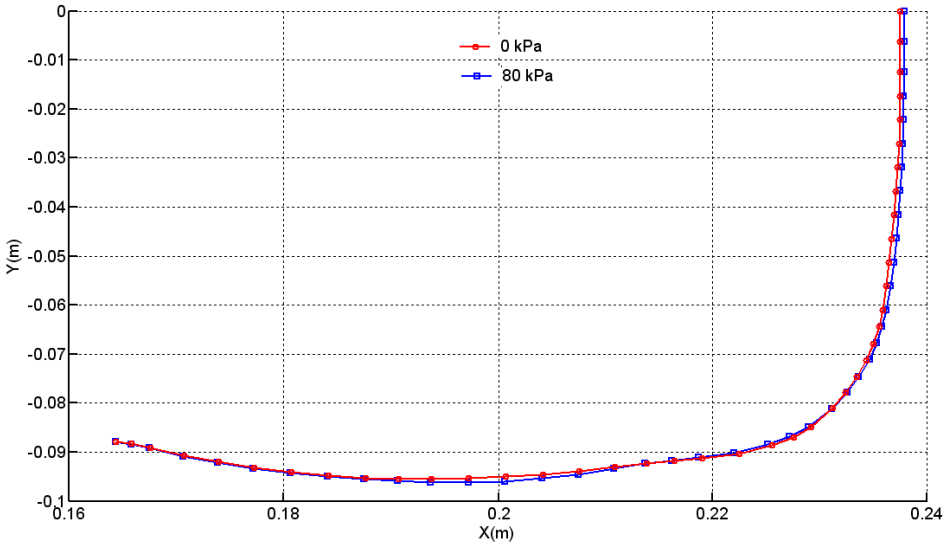

(b) Model Measurement

Figure 5.5 Comparison of External Tyre Profile at 80 kPa Inflation Pressure

The above figures show very small changes in the tyre profile between cold pressure 0 kPa and inflated pressure 80 kPa from both experiment and FE model, which makes it difficult to validate the FE tyre model virtually by comparison of profile position on the

plots. This inconvenience is caused by the small inflation pressure viz. 80 kPa which generates tiny displacement compared with the tyre global size. However, by considering the tyre profile displacement (i.e. change in position), it is possible to give a reasonable comparison between experiment and FEA since the CMM can provide a measurement with 0.01 mm accuracy. Hence, experimental error of up to 5% can be expected in the smallest displacement (0.22 mm at 40 kPa). The tyre inflation pressures 40 kPa, 60 kPa, 80 kPa, 100 kPa and 120 kPa were chosen herein for the investigation of inflated displacement comparison. The displacement of the tyre tread region in the *X* direction is denoted as U1 while the displacement of the tyre sidewall region in the *Y* direction is denoted as U2. The average displacement U1 and the average displacement U2 from the approximately same region between experiment tyre and FE tyre are listed in Table 5.1 and Table 5.2, respectively. It can be seen from the tables that the predicted displacement by finite element tyre model correlates reasonably with the experimental data with the maximum error 13.64%. The displacement increases with the increase of inflation pressure while maximum displacement happens on tyre sidewall.

Table 5.1 Displacement U1 in Tread

Inflation Pressure (kPa)	Experiment (mm)	Finite Element Tyre Model II (mm)	Absolute Difference (%)
0	0.00	0.00	0.00
40	0.22	0.19	13.64
60	0.33	0.29	12.12
80	0.39	0.38	2.56
100	0.52	0.48	7.69
120	0.63	0.58	7.94

Table 5.2 Displacement U2 in Sidewall

Inflation Pressure (kPa)	Experiment (mm)	Finite Element Tyre Model II (mm)	Absolute Difference (%)
0	0.00	0.00	0.00
40	0.59	0.56	5.08
60	0.69	0.70	1.45
80	0.80	0.79	1.25
100	0.90	0.87	3.33
120	0.96	0.92	4.17

5.3. STATIC STIFFNESS VALIDATION

5.3.1 STATIC STIFFNESS EXPERIMENT

Although the 2D axisymmetric tyre model gives a good correlation on tyre inflated geometry, the 3D tyre model still needs to be used for further validation in order to deal with complex situations such as tyre/road contact and tyre rolling. The prevalent parameters for 3D finite element tyre model validation are stiffness and footprint. In this section, the tyre vertical static stiffness which affects vehicle ride performance is adopted to validate the finite element tyre model. A tri-axial electro-hydraulic tyre dynamic rig with a 2.44 meters drum in the University of Birmingham was used to carry out the stiffness experiment. The configuration of the test rig is shown in Figure 5.6. The large diameter drum was used to simulate the road. In order to obtain the tyre vertical stiffness, different levels of displacement were applied to the tyre incrementally and the corresponding vertical loads were measured by a calibrated load cell.

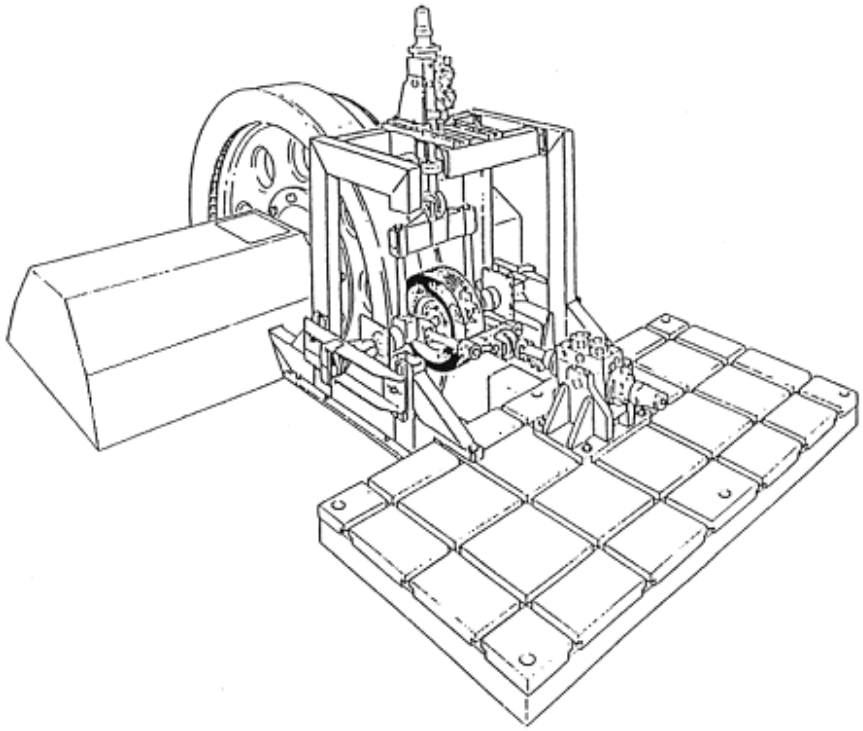

Figure 5.6 Tri-axial Electro-hydraulic Tyre Dynamic Rig

5.3.2 STATIC STIFFNESS ANALYSIS

A similar procedure to the experiment was carried out during the finite element analysis for tyre vertical stiffness. The 2D axisymmetric tyre model was revolved to generate a 3D FE tyre model. An analytical rigid road surface was pushed towards the tyre by a small displacement initially in order to stabilize the simulation. Then the same displacements as those in the experiment were applied to the road reference node to generate increasing tyre deformation on the contact patch. The response forces to these displacements were measured from the tyre rim reference node. The status of the tyre under deformation due to vertical displacement is shown in Figure 5.7.

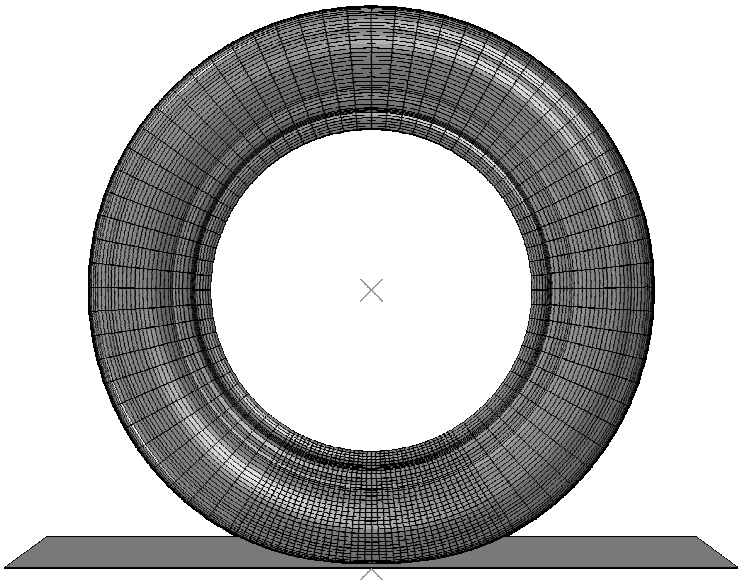

Figure 5.7 Deformed Tyre under Vertical Displacement

5.3.3 COMPARISON AND DISCUSSION

The vertical stiffness test and simulation were carried out under different inflation pressures including 40 kPa, 60 kPa, 80 kPa, 100 kPa and 120 kPa. Table 5.3 shows the force/displacement results obtained at the normal inflation pressure of 80 kPa from measurement and finite element tyre model II. Figure 5.8 to Figure 5.12 show the original plots of tyre vertical load vs. displacement from experiment and FE model for different inflation pressures. It can be found that the vertical load and displacement show an approximately linear relationship, from which it can be considered that the tyre vertical stiffness tests were carried out in the linear range of vertical stiffness as described in Figure 2.1. Although there were discrepancies at some individual points in the original plots such as Figure 5.12, the tyre vertical stiffness was calculated by linear curve fitting the relationship between tyre vertical load and displacement at each

inflation pressure condition. The tyre vertical stiffness viz. the tangent of the linear curve at different inflation pressures was obtained as listed in Table 5.4.

Table 5.3 Displacement /Force Data from Measurement and Model at Inflation Pressure 80 kPa

Displacement (mm)	Measured Force (N)	Finite Element Tyre Model II Displacement (mm)	% Absolute Difference
0	0	0	0
2.54	160	2.398	5.59
5.08	360	4.946	2.64
7.62	590	7.808	2.47
10.16	780	10.107	0.52
12.7	1000	12.62	0.63
15.24	1270	15.672	2.83
17.78	1490	18.124	1.93

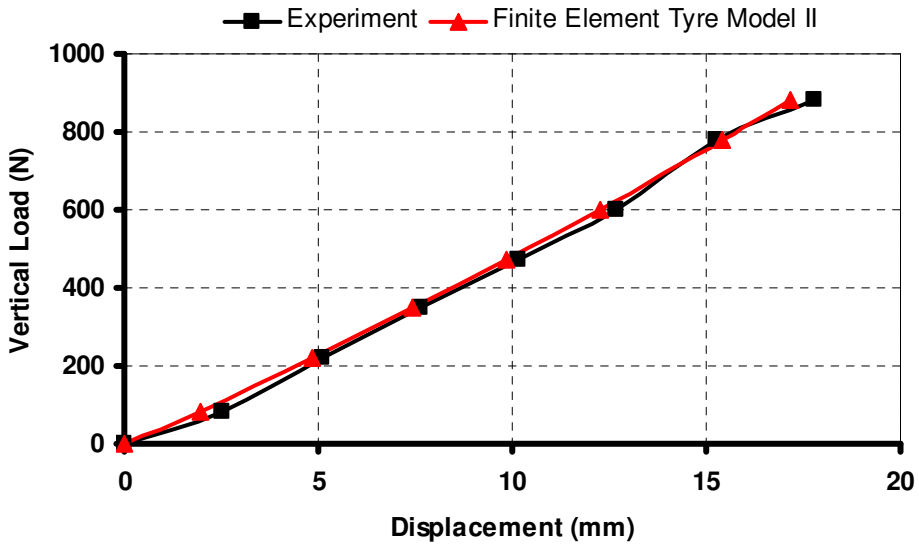

Figure 5.8 Vertical Displacement/Load at 40 kPa Inflation Pressure

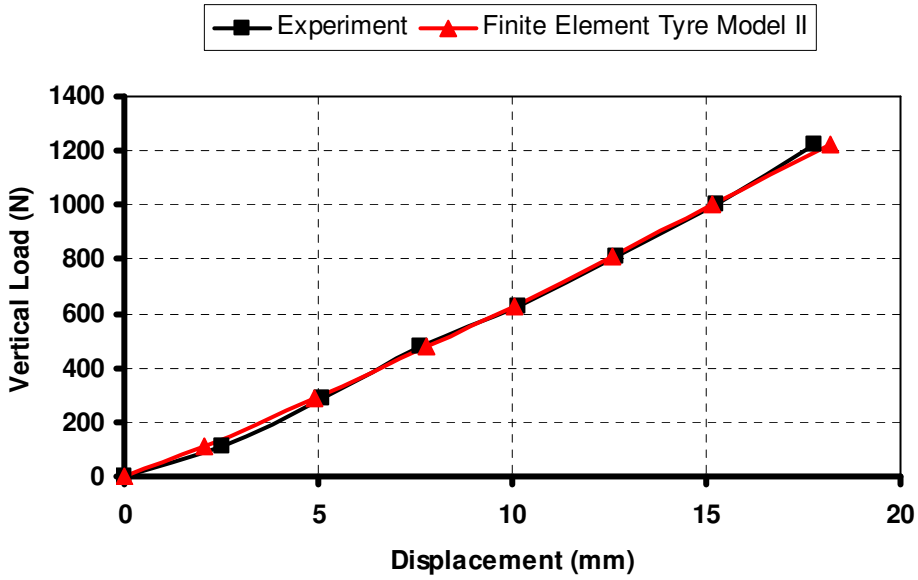

Figure 5.9 Vertical Displacement/Load at 60 kPa Inflation Pressure

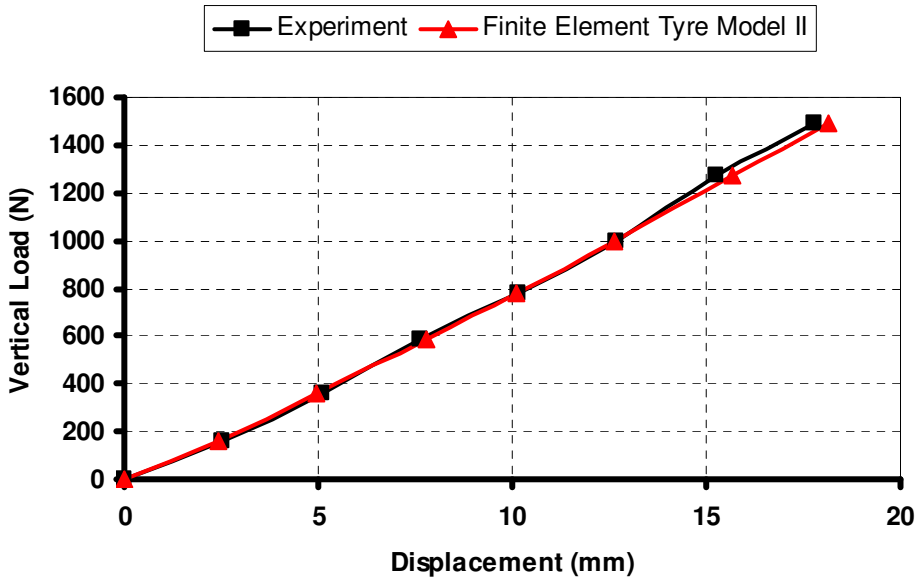

Figure 5.10 Vertical Displacement/Load at 80 kPa Inflation Pressure

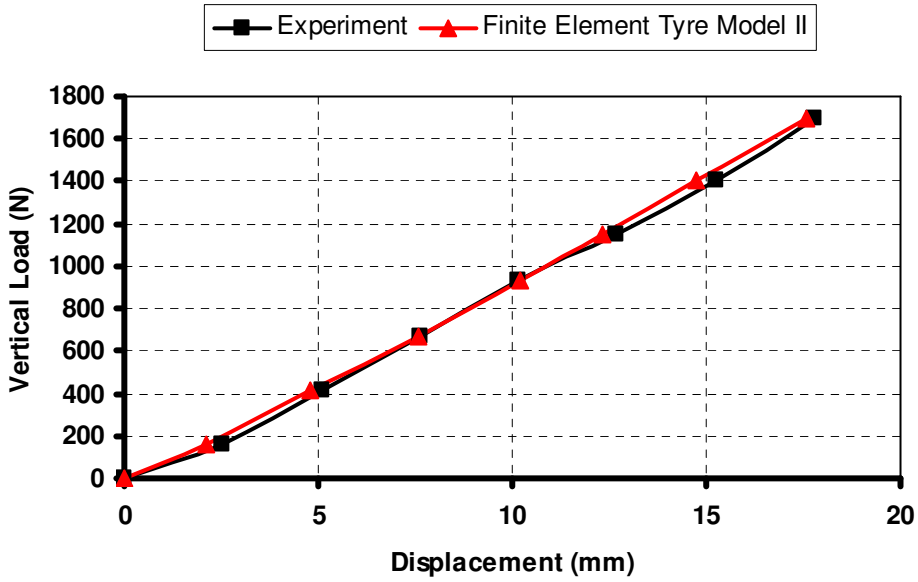

Figure 5.11 Vertical Displacement/Load at 100 kPa Inflation Pressure

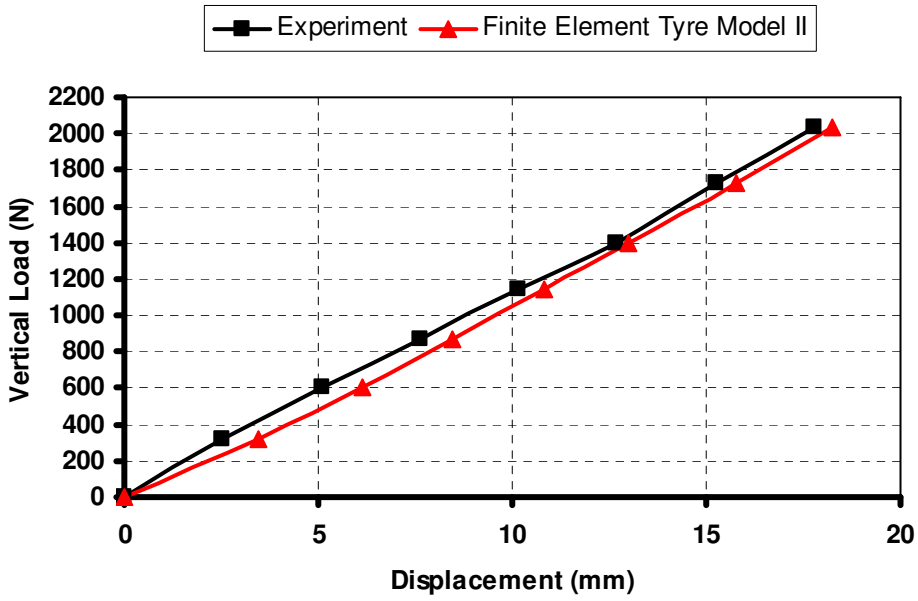

Figure 5.12 Vertical Displacement/Load at 120 kPa Inflation Pressure

Table 5.4 Vertical Stiffness Validation

Inflation Pressure (kPa)	Vertical Stiffness Experiment (N/mm)	Vertical Stiffness Simulation (N/mm)	Absolute Difference (%)
40	51.18	51.44	0.51
60	68.90	67.42	2.15
80	84.79	82.81	2.34
100	96.46	97.25	0.82
120	112.02	112.34	0.29

As a main expression of tyre vertical elastic properties, the tyre vertical static stiffness values listed in Table 5.4 show a satisfying agreement within 5% error between experiment and FE model. The trend that the vertical stiffness value increases with the increasing inflation pressure was also captured properly by the FE tyre model.

5.4. FOOTPRINT VALIDATION

5.4.1 FOOTPRINT EXPERIMENT

The footprint experiment was also carried out using the tri-axial electro-hydraulic tyre dynamic rig. A sheet of white paper was attached to the drum contact surface. Black ink was smeared to the tyre tread surface. Once the tyre makes contact with the drum under load, the tyre contact patch is printed on the white paper. When the target load was reached during the experiment, the load was held for a short term before being removed

in order to achieve a footprint that was as accurate as possible. The experiment configuration can be seen in Figure 5.13.

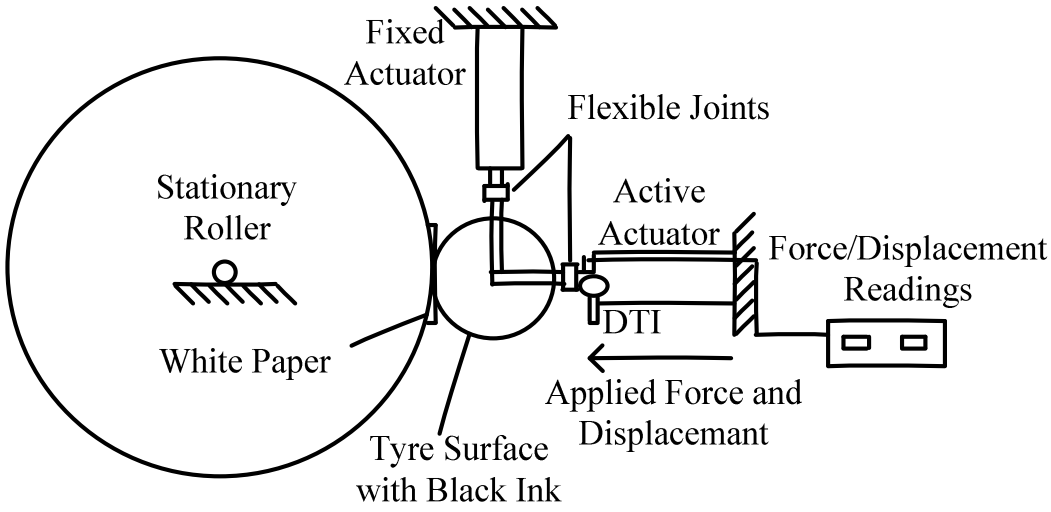

Figure 5.13 Configuration for Footprint Experiment

During the experimental procedure, different loads and inflation pressures have been tried in order to investigate their effect on tyre contact patch area. The footprint white paper was scanned into computer and the contact area was calculated by image processing in CAD software. In this way, it can guarantee the calculation accuracy and efficiency better than physical measurement such as using a planimeter.

5.4.2 FOOTPRINT ANALYSIS

The simulation procedure for footprint is similar to the stiffness analysis. Two cases were simulated in footprint analysis. Firstly, at inflation pressure 80 kPa, the vertical load 250 N, 500 N, 750 N, 1000 N and 1250 N were applied to the road reference node respectively to enable the road make contact with the tyre. Secondly, at vertical load

750N, the inflation pressure 40 kPa, 60 kPa, 80 kPa, 100 kPa and 120 kPa were applied to the tyre inner surface, respectively. Both the inflation pressure effect and vertical load effect on tyre footprint were investigated by these numerical experiments. The contact area is requested in "contact output" in ABAQUS. ABAQUS provides the function "COPEN" to show the closed node region in the contact patch and the function "CPRESS" to show the contact pressure node region. Both of them can reflect the contact patch shape when proper resolution is given for the colour legends of the contour.

5.4.3 COMPARISON AND DISCUSSION

As a major investigated phenomenon, the footprint of the tyre provides significant information on tyre characteristics. Figure 5.14 shows footprint shape comparison between experiment and finite element analysis at normal inflation pressure 80 kPa and normal vertical load 750 N. The variations of tyre footprint area due to the variation of inflation pressure and vertical load were measured for both the experiment and model as shown in Figure 5.15 and Figure 5.16. It can be found that the tyre contact patch areas from experiment are slightly smaller (within 10%) than the corresponding FEA results. This discrepancy is caused by the curvature of the circular drum on which the test was carried out in place of the flat road, which has the effect of reducing the tyre contact patch area. It is evident that the tyre finite element model is capable of predicting the variations of the footprint area due to the changes of inflation pressure and vertical load. The trend of tyre contact area considering the variation of tyre inflation pressure and vertical load are consistent with the findings in [11]. The tyre footprint area increases with the increasing vertical load and the decreasing inflation pressure.

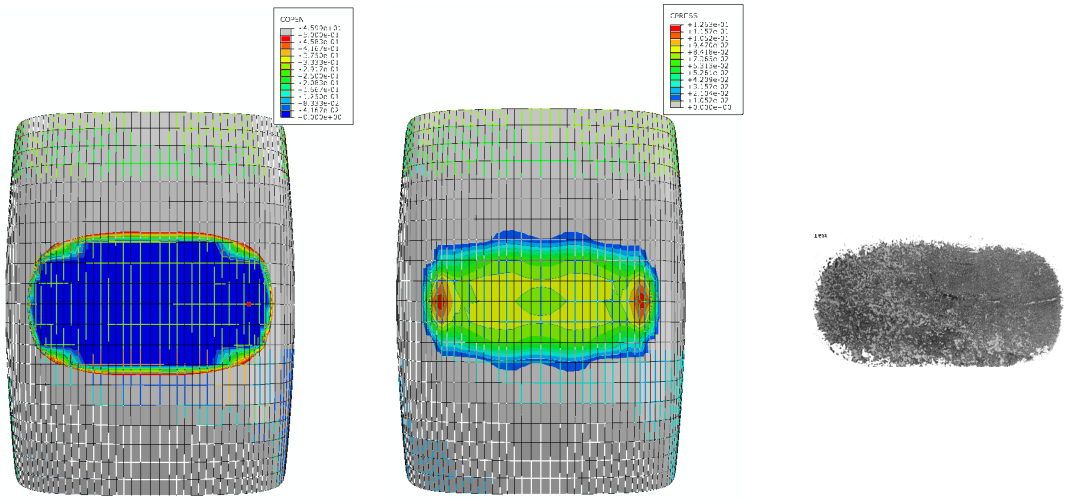

(a) Footprint from "COPEN" **(b) Footprint from "CPRESS"** **(c) Footprint from Test**

Figure 5.14 Footprint Shape Comparison at Inflation Pressure 80 kPa and Vertical Load 750 N

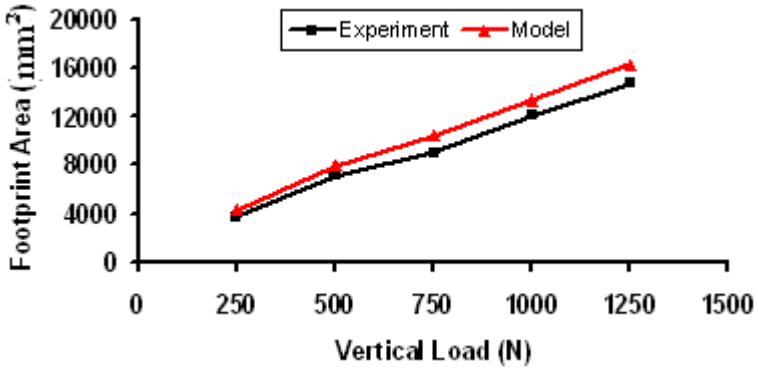

Figure 5.15 Variation of Footprint Area with respect to Vertical Load

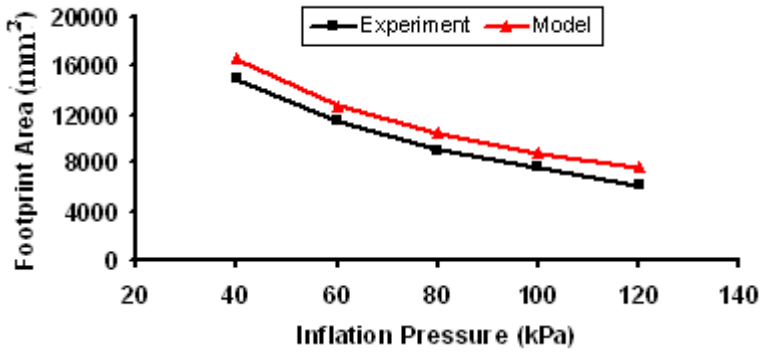

Figure 5.16 Variation of Footprint Area with respect to Inflation Pressure

5.5. SIDEWALL STRAIN VALIDATION

5.5.1 SIDEWALL STRAIN EXPERIMENT

The outer surface strain where the service failure (veneer crack, white sidewall splice crack and torque crack) [20] usually occurs rather than inner surface strain of the tire sidewall is investigated herein to validate the capability of tyre model to predict tyre local characteristics. Preliminary trends of surface strains with respect to inflation pressure, vertical load and circumferential angle from tests carried out on the 175/505 R13 tyre are presented.

The sidewall strain is measured on the mid-sidewall of the slick sport 175/505 R13 tyre using SoMat 2100 Field Computer System. The experiment configuration is shown in Figure 5.17.

Figure 5.17 Configuration of Sidewall Strain Experiment

Three annealed constantan foil strain gages with tough, high-elongation polyimide backing which can measure large deformation up to 20% were bonded to the tyre mid-sidewall with a compatible adhesive after the recommended surface preparation process. The location of strain gauge falls into the range 30 mm to 35 mm approximately from the bead. The first strain gage is located along the meridional direction and the second one is in the circumferential direction. The third one has a 45 degree angle (angular) with respect to the former two as shown in Figure 5.17. A small type of field computer was used as its portable, microprocessor-based data acquisition system and designed for easy data collection in a variety of test environments. Figure 5.18 illustrates the terminology used for static strain test.

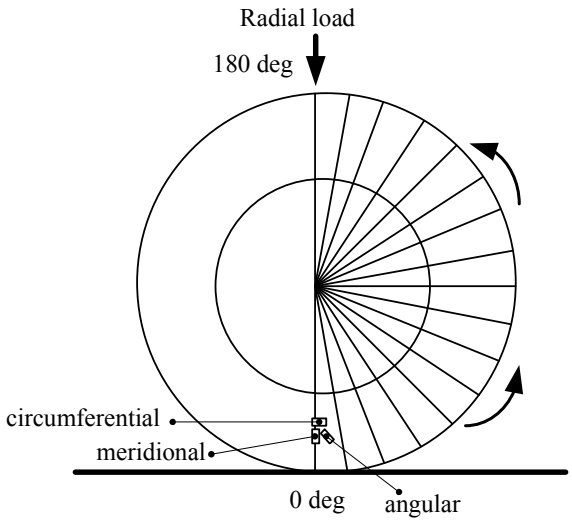

Figure 5.18 Illustration of Terminology for Strain Test

As shown above, the tyre was rotated to make the strain location have different angle with the vertical radius at inflation pressure 80 kPa and vertical load 750 N.

5.5.2 SIDEWALL STRAIN ANALYSIS

For the finite element tyre model, the radial load was applied to the rim reference node. The strain on the node which is approximately located at the same position as that in the test was acquired. A cylindrical coordinate system was used in order to guarantee the simulated strain is the same as the test. A path consisting of the nodes at the same sidewall position was created along the tyre circumferential direction.

5.5.3 COMPARISON AND DISCUSSION

As the shear strain value and the principal strain on the tyre sidewalls are of significant concern to tyre failures [20, 157], the maximum principal strain and the maximum in-plane shear strain are calculated, using the following equations:

$$\begin{aligned} \varepsilon_x &= \varepsilon_0 \\ \varepsilon_{xy} &= \varepsilon_{45} - \frac{\varepsilon_0 + \varepsilon_{90}}{2} \\ \varepsilon_y &= \varepsilon_{90} \end{aligned} \tag{5.1}$$

Maximum principal strain:

$$\varepsilon_{1,2} = \frac{\varepsilon_x + \varepsilon_y}{2} \pm \sqrt{\left(\frac{\varepsilon_x + \varepsilon_y}{2}\right)^2 - \left(\varepsilon_x \varepsilon_y - \varepsilon_{xy}^2\right)} \tag{5.2}$$

Maximum in-plane shear strain:

$$\varepsilon_{x'y'} = \sqrt{\left(\frac{\varepsilon_x + \varepsilon_y}{2}\right)^2 - \left(\varepsilon_x \varepsilon_y - \varepsilon_{xy}^2\right)} \tag{5.3}$$

Where the strains ε_0, ε_{90} and ε_{45} represent the strain in the circumferential, meridional and 45 degree direction, respectively.

The calculated principal strain and maximum in-plane shear strain based on the prediction and test results are compared in Figure 5.19 and Figure 5.20.

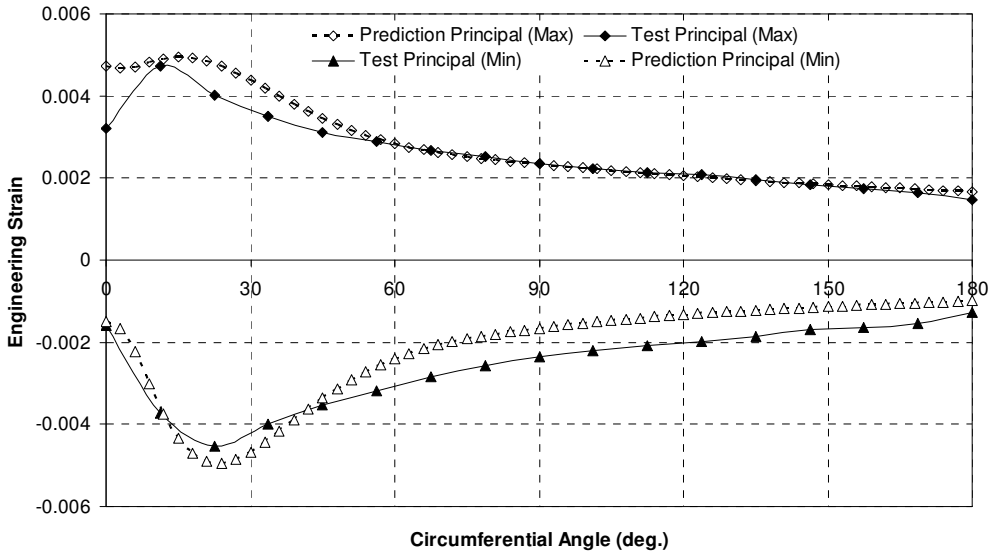

Figure 5.19 Principal Strain under Inflation Pressure and Vertical Load

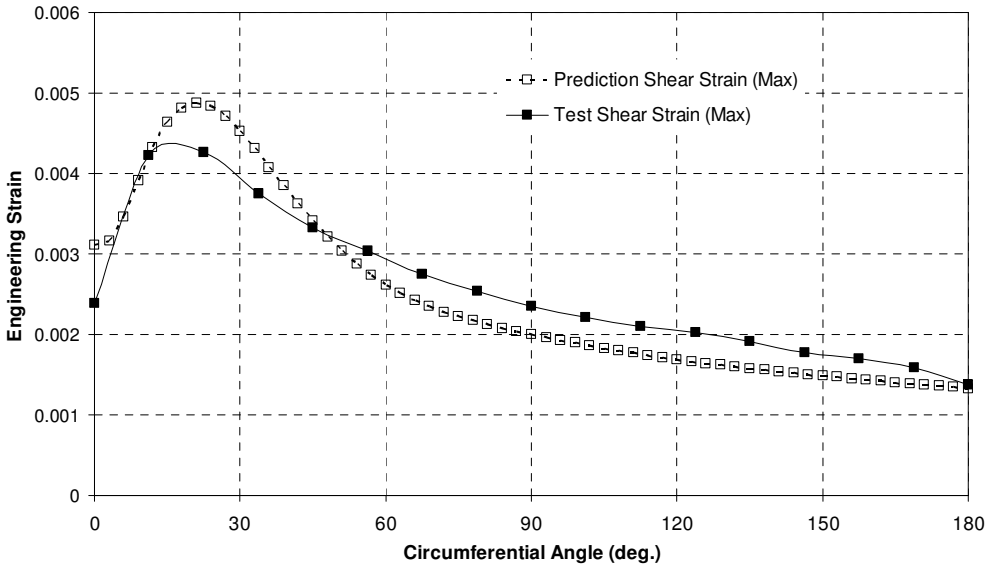

Figure 5.20 Maximum In-Plane Shear Strain under Inflation Pressure and Vertical Load

It can be seen from the results that the principal strains and shear strain peak at approximately 25 degrees. Similar trends have been demonstrated in the reference [20]. This suggests that the deformation of the sidewall near the leading and trailing edges of the tyre contact patch is greater than on the sidewall near the middle of the contact patch.

Prediction of the dynamic strain is the target of this thesis rather than static strain. In Chapter 6, the experiment and model prediction of tyre tread dynamic strain will be discussed. The results presented here show that the FE tyre model provides a reasonable correlation with the experiment.

5.6. DISCUSSION AND SUMMARY

Model validation is a very important and necessary step before the FE model is applied for prediction of tyre static and dynamic behaviour. During the model validation process, errors involved during FE tyre modelling, such as errors caused by the variation of tyre material properties, which could have significant influence on the predicted results from FEA, should be given enough attention. Tyre is a multi-input and multi-output system. Any variation in the value of tyre material properties or structural parameters will affect the tyre response such as force or resonant frequency. Usually, the variation of tyre input variables have larger impact on tyre local response such as local stress rather than global response such as stiffness. For example, increasing the stiffness of tread rubber by 533% leads to an increase smaller than 3.2% of natural frequencies values up to order 10, both in radial and lateral direction according to [73]. A relevant work about

tyre response sensitivity to tyre design parameters based on Design of Experiment method was done by author, which is not contained in this thesis but can be found in Appendix. Generally, the change on tyre reinforcement cords material properties would have a larger impact than the rubber material properties with the same change, because the reinforcement cords make up the support frame for rubber and carry most of the external loads.

In this chapter, both the 2D and 3D tyre model were validated with experimentally measured data. An axisymmetric cross-section 2D model was adopted to simulate the tyre geometry change under different inflation pressures. Corresponding experiment was carried out using CMM. The average displacement of tyre tread and sidewall region was correlated. The 3D tyre model was used for the validation of tyre vertical static stiffness, footprint area and sidewall strain. Although there are some inaccuracies due to factors such as the operational error of the test, the level of correlation between the experiment and FEA was considered satisfactory. These validations, thus lend credence to the method used for acquiring tyre material property and geometry information in this study ensuring that the finite element tyre model gives reasonable tyre performance predictions.

CHAPTER 6

INVESTIGATION OF STRAIN-BASED INTELLIGENT TYRE BY FEA AND EXPERIMENT

6.1. INTRODUCTION

The increasing demand for safety, handling performance, comfort and economy of ground vehicles has highlighted the requirement for advanced, effective and accurate vehicle dynamics control systems.

As the only interface between the vehicle and the road, the tyre is in a very privileged position and possesses vital information which could be useful for the operation of vehicle dynamics control systems. Instead of playing a passive role in the vehicle system, the incorporation of intelligent sensors into the tyre would enable it to play an active role with the capability to provide useful information including tyre/road contact forces, road condition and driving condition to the vehicle dynamics control systems, such as anti-lock brake system (ABS), traction control system (TCS), vehicle stability control system (VSCS) and suspension control system (SCS), etc.

However, some of this tyre information is very difficult to obtain directly, such as the force generated at the tyre/road contact interface. The literature review in Chapter 2 revealed that various sensor technologies have been developed in the past decade

towards the achievement of the functions of an intelligent tyre system [77, 81]. After a serious consideration of the pros and cons of these technologies, a strain-based prototype system was designed and utilized in this study to investigate the relationship between tyre forces and strain characteristics under different working conditions, with the aim of developing a strain-based intelligent tyre which could find application in future vehicle dynamics control systems.

In recent times, a lot of research effort has been devoted to developing strain-based intelligent tyre systems. However most of them have not progressed beyond the initial stage and many critical issues have not been resolved sufficiently to produce a functional system. Such issues include facets of sensor technologies, parameter estimation schemes and algorithm development. The strain-based intelligent tyre is particularly suitable for commercialization because of its low cost and the strain sensor's durability can be enhanced by designing novel flexible strain sensors suitable of being vulcanized into the tyre rubber. Based on the features of tyre strain time history during tyre service, the tyre forces related to the working conditions can be identified, such as the tyre braking force and cornering force. These identified tyre forces may then be utilised for optimising vehicle dynamics control systems or to provide information to the driver on such safety related issues as tyre under-inflation, tread wear, concealed damage, etc. In the future, when the development of the intelligent tyre system has reached an advanced stage, the tyre is expected to be capable of adjusting the tyre/road contact force and friction based on ability to change the tyre/road contact area or material property in order to improve vehicle performance and safety and to reduce fuel consumption.

In this chapter, the characteristics of tyre strain time history are discussed firstly in section 6.2 to demonstrate that it possesses abundant and useful information for estimating tyre forces. Section 6.3 gives a detailed description of the strain-based intelligent tyre prototype system. The experimental procedure of strain measurement is described for tyre steady state straight line rolling and cornering. In section 6.4, the finite element tyre model for simulating tyre steady state rolling is presented. Some guidance notes are introduced for ensuring the stability of the numerical simulation during the finite element analysis of tyre steady state rolling. The corresponding strain data is generated from the finite element tyre model under the same working conditions as the experiment. Finally, in section 6.5, the strain data generated from finite element tyre model is used to establish the estimation model representing the relationship between tyre forces and strain features under free rolling, braking, traction and steering, which largely reduces the number of tests required to provide data for developing the algorithms for estimating the tyre forces.

6.2. CHARACTERISTICS OF TYRE STRAIN

From the literature review about strain-based intelligent tyre systems in Chapter 2, it was found that the strain or deformation measured in most of the relevant researches is from the tyre tread. It is widely admitted that the strain sensor placed in the inner liner of the tread can provide significant, accurate and stable information about the force generated at the tyre/road contact patch [3]. In this study, the strain sensors are also located in the inner liner surface of the tyre tread. Although the determination of the best location for a sensor can be evaluated by the signal-to-noise ratio of the sensor

output, etc. it is also constrained by the range the sensor can measure as well as the available space of the tyre inner liner surface.

The ideal strain time histories acquired from the inner liner surface of the tyre tread along tyre's circumferential direction and axial direction for one revolution during tyre steady state straight line rolling are illustrated in Figure 6.1. The strain rate is defined as the time differential of strain value.

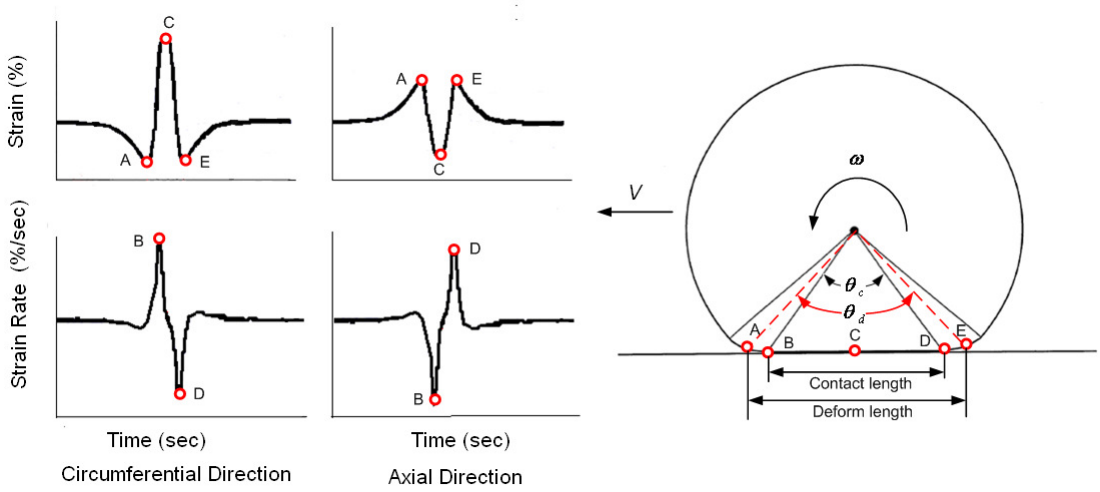

Figure 6.1 Characteristics of Tyre Strain Time History

The tyre strain waveform under steady state straight line rolling shows a nearly symmetric shape with respect to the centre of tyre contact patch, because there is no braking, traction or steering force applied on the tyre. It is evident that the rolling tyre deformation characteristics cause the corresponding variation of strain. The bending deformation occurs around the tyre contact patch area due to the combined effect of vertical load and friction load [8]. For the circumferential strain, tensile strain appears in the contact patch (region between point B and point D) and peaks at the centre of the contact patch, namely point C in Figure 6.1. Compressive strain occurs in the leading

region (left region of point B) and trailing region (right region of point D) outside the tyre contact patch. Therefore, the tread element is under compression before entering the contact patch and after leaving the contact patch, and is stretched within the contact patch during the steady state straight line rolling. According to [8], the contribution from friction load to the generated strain during steady state straight line rolling is modest, which just slightly reduces the variation in the tensile strain. The time derivative waveform of circumferential strain, shown in Figure 6.1 exhibits two peaks. These peaks correspond to the two points with the maximum strain rate at the leading edge and trailing edge of tyre contact patch. The time difference between these two peaks, i.e. points B and D, is the time taken to traverse the contact length between points B and D as shown in Figure 6.1. The tyre deformation characteristics under traction and braking can be found in Figure 2.3 and Figure 2.4 in Chapter 2.

Figure 6.1 shows that the axial strain has a converse trend to the circumferential strain. The relationship between the circumferential strain and axial strain at the same location can be expressed by the equation

$$Poisson\_Ratio = -Axial\_Strain / Circumferential\_Strain$$

Moreover, the axial strain does not only reflect the same features as the circumferential strain but also provides more significant strain information when the tyre is steered. The axial strain distribution in the tyre contact patch when the tyre is steered becomes asymmetric due to the change of contact pressure distribution as well as the shear stress effect which leads to the generation of lateral force and aligning moment. It is one of the main reasons that two axial strain gauges were adopted in this investigation and one to either side of the centreline of the tyre tread to measure the strain distribution during

cornering. The strain data measured from a rolling tyre depends on the tyre working conditions, even the tyre structure parameters. Conversely, the strain data also reflects the variation of these tyre working conditions and could be used to identify them.

In this section, the potential features which may contribute to the estimation of tyre forces are recommended firstly in order to have a better understanding of strain waveform characteristics. Figure 6.1 reveals that the strain far from the contact patch region has a constant value during one revolution of the tyre. The constant strain value is affected by the tyre inflation pressure. Thereby, it is an explicit reflection of the tyre inflation pressure. The tyre/road contact length is reflected by the time difference between point B and D in the strain rate waveform. The time difference between point A and E is related to the deformed length in Figure 6.1. The angles θ_c and θ_d are the rotational angles corresponding to the contact length and deformed length respectively.

These features described above can be used to evaluate the tyre inflation pressure, vertical load, rolling speed and contact patch dimensions, tyre forces, etc. Besides, the amplitude of the strain waveform and the strain shape feature [100] obtained from the tyre under different working conditions also can be helpful for determining tyre forces.

Based on the different points of view of the strain time history, two main features which can be extracted from strain waveform are related to the strain amplitude and the time lag (spatial distribution) [110].

6.3. STRAIN-BASED INTELLIGENT TYRE PROTOTYPE SYSTEM

A strain-based intelligent tyre prototype system has been developed in the Vehicle Dynamics Laboratory in the University of Birmingham. The experimental configuration including the indoor tyre test rig equipped with the strain-based intelligent tyre prototype system is shown in Figure 6.2.

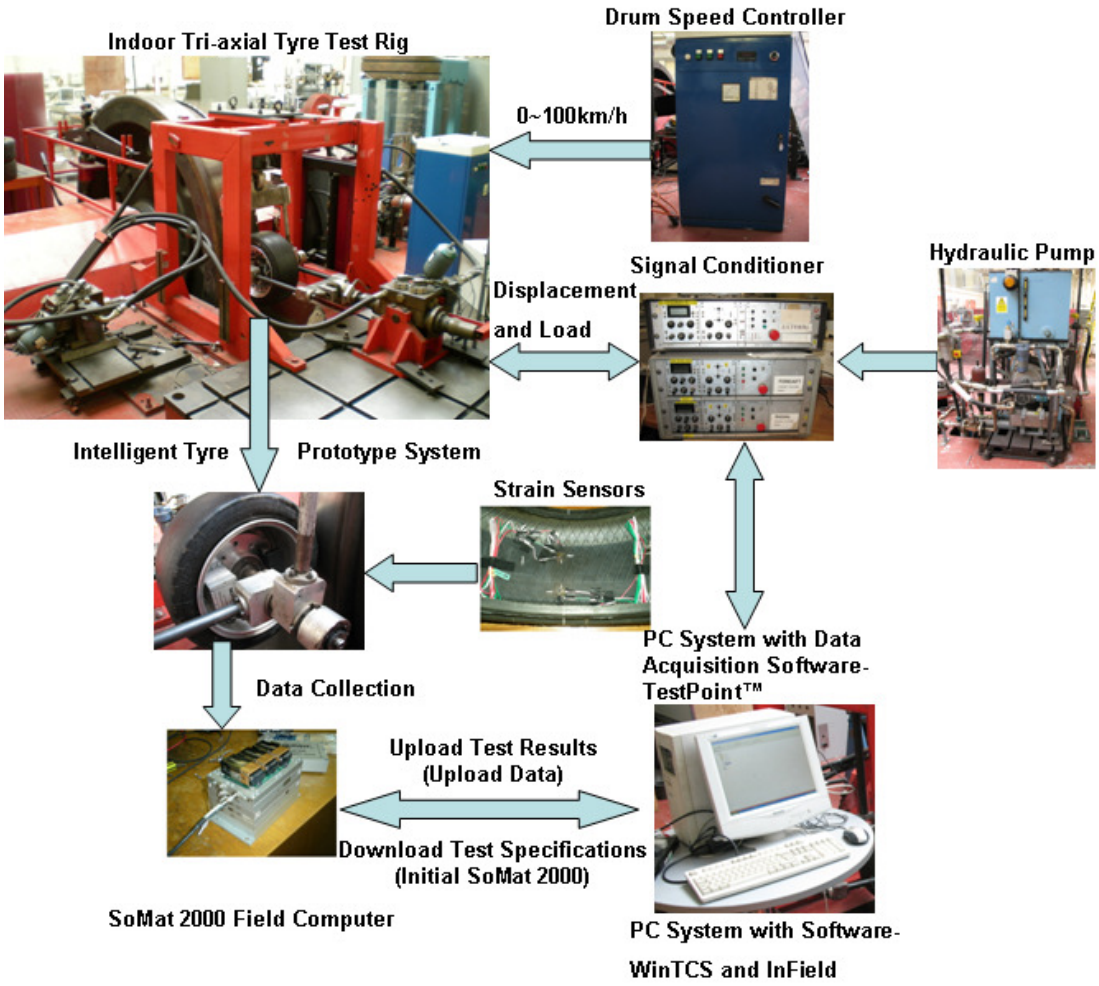

Figure 6.2 Experimental Configuration of Strain-based Intelligent Tyre Test System

In this study, the KYOWA KFEL-2-120-D35L1M2S high-elongation foil strain gauge which can measure up to 15% strain is adopted. These strain gauges are applicable for large strain measurement and destructive testing of metals (steel, stainless steel and aluminium) and plastics (polyethylene and polypropylene). The gauge length is 2 mm with gauge resistance 120 ohm. The tri-axial arrangement of each set of strain gauges on a base (10×10 mm) is shown in Figure 6.3. The strain gauges were attached to the inner liner of the tyre which is so thin that its deformation is dominated by the stiffness of the carcass cords. Therefore it can be considered that there is no local stiffening effect caused by the stiffness of the strain gauge.

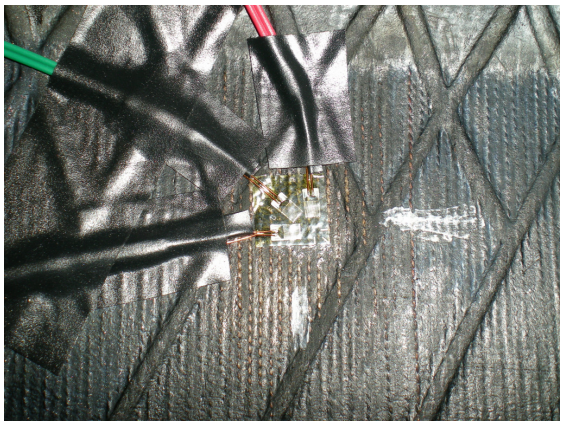

Figure 6.3 Tri-axial Arrangements of Strain Sensors

The two rectangular rosette strain sensors were mounted symmetrically about the tyre tread centre line on the tyre inner liner surface of the tread with the manufacturer recommended adhesive shown as Figure 6.4.

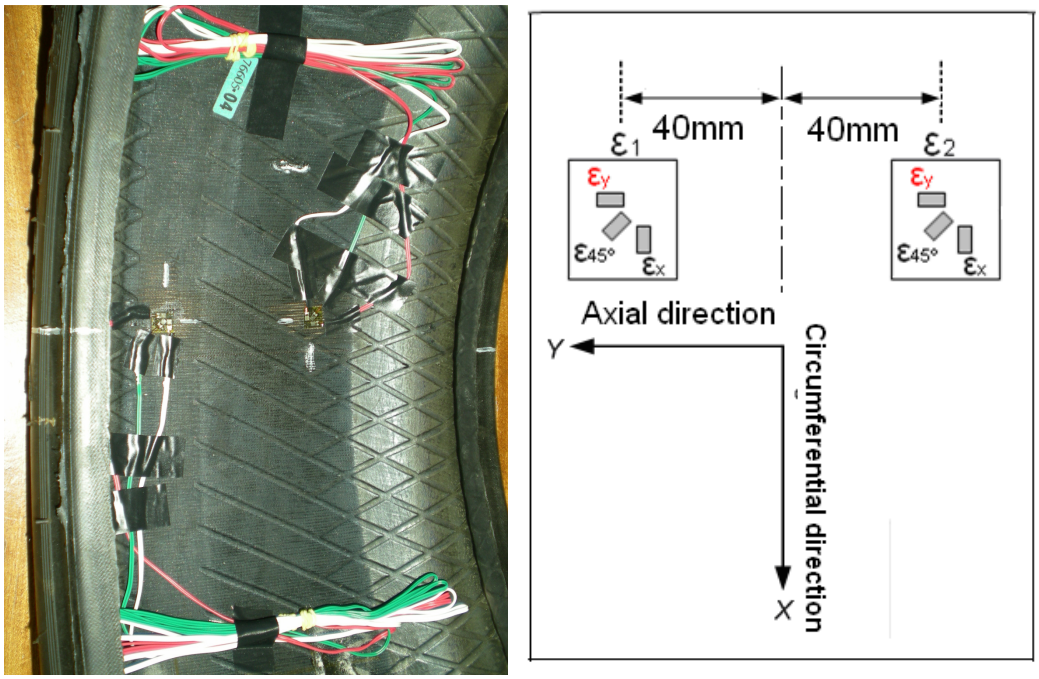

Figure 6.4 Strain Sensor Location Scheme

The design of strain sensors arrangement is expected to not only measure the strain in tyre circumferential, axial and 45 degree directions but also obtain the maximum principal strain and maximum shear strain based on the three strain measurements according to the discussion in section 5 of Chapter 5. However, due to an unexpected problem during the whole installation procedure and initial trial, only the strain sensors with red colour in Figure 6.4 worked properly, which reveals that the reliability and durability of the strain sensor is a significant issue that may arise during the development of strain-based intelligent tyre system in future.

A split wheel including two pieces of rim is adopted in this study in order to avoid interference with the sensor system during tyre wheel assembly procedure as shown in Figure 6.5.

Figure 6.5 Split Wheel

Three new valves were installed on the rim and the lead wires of the strain sensors were packed and routed through the valves to the outside of the tyre as shown in Figure 6.6. Both the inside end and outside end of the valves were sealed to guarantee no air flowing through the clearance in the valves.

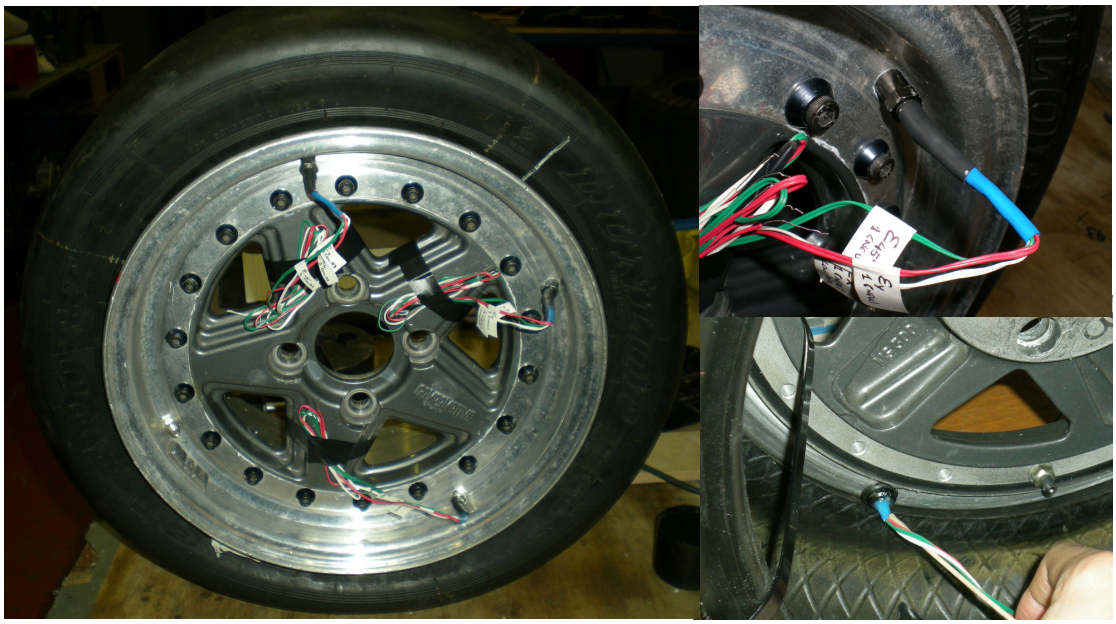

Figure 6.6 Tyre and Wheel Assembly

Then the split wheel was assembled with the tyre and the contact region between the rim and tyre was sealed with adhesive as well. Once the tyre was mounted on the rim, it was inflated to the desired inflation pressure and left for hours in order to check the seal reliability as shown in Figure 6.7.

Figure 6.7 Mounted Tyre and Inflated Tyre

The SoMat 2000 Field Computer was utilized for the test data collection in this study. The SoMat 2000 Field Computer is a portable, microprocessor-based data acquisition system, designed for easy data collection in a variety of test environments. As a module-based device, it has many different function modules. The basic hardware system consists of a Processor module and Power/Communications module as shown in Figure 6.8.

The aluminium case is designed for protection against dust and moisture. The Power/Communication module includes a battery interface which can be linked to three 9 volts batteries, viz. 27 volts in total.

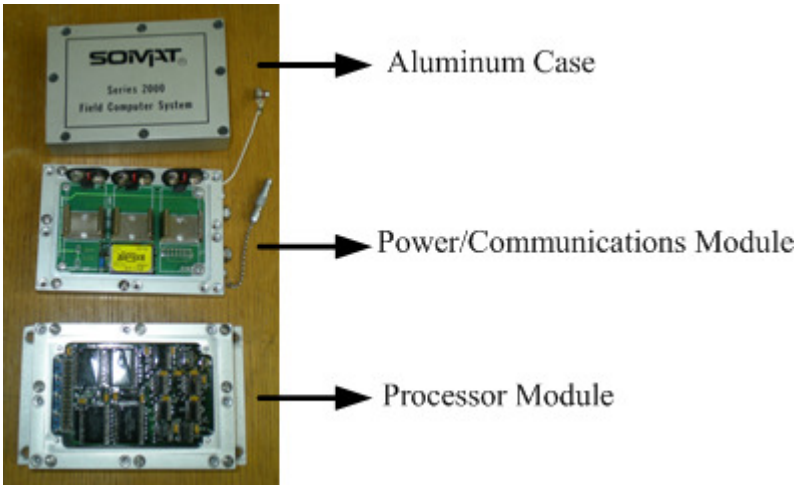

Figure 6.8 Basic Hardware System of SoMat 2000 Field Computer

In this study, three strain gauge modules were selected and added to the system. Each Somat strain gauge module operates as a Wheatstone strain bridge capable of being used in a quarter, half or full bridge configuration. In this study, a quarter bridge configuration was adopted as shown in Figure 6.9.

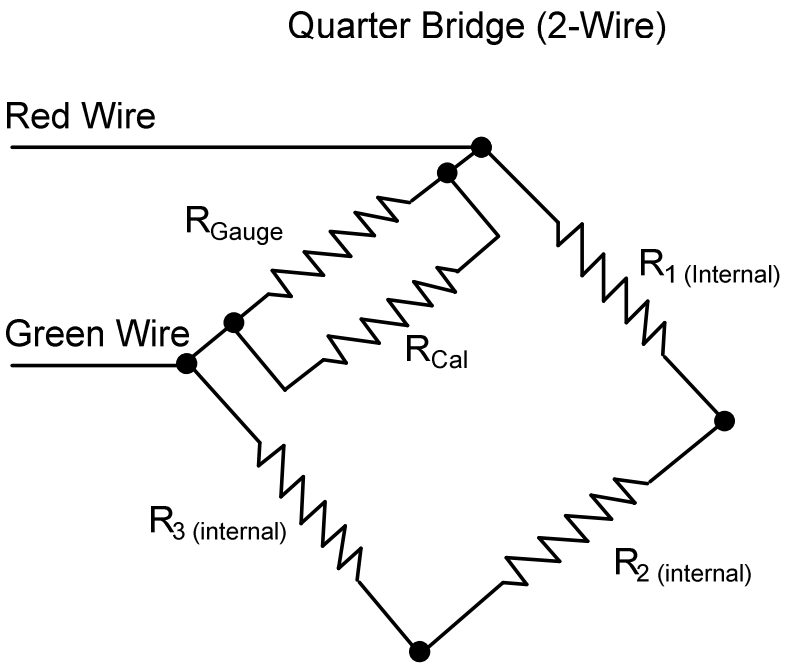

Figure 6.9 Quarter Bridge

The aforementioned batteries were used to provide power supply during the test as shown in Figure 6.10. It should be noted that there is only one channel for each strain gauge module, which means the SoMat 2000 Field Computer system, as configured herein can be used to measure three channels of strain signal simultaneously.

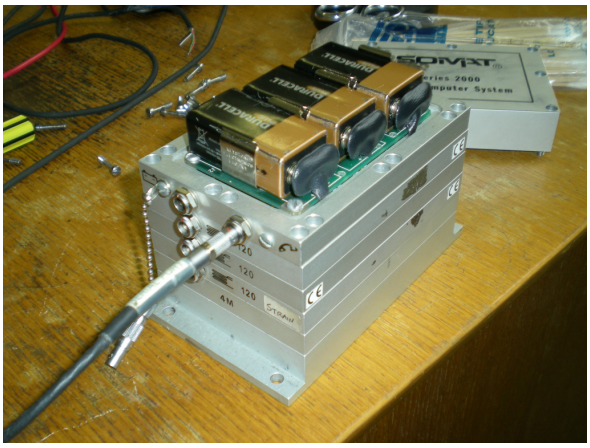

Figure 6.10 SoMat 2000 Field Computer with Strain Gauge Modules and Batteries

The SoMat 2000 Field Computer was driven by Test Control Software for Windows (WinTCS) shown as Figure 6.11. During a test, the data acquisition modules i.e. strain gauge modules were connected to the strain sensors. The user can download the test specification designed using WinTCS from PC to SoMat 2000 Field Computer to initialize and run it.

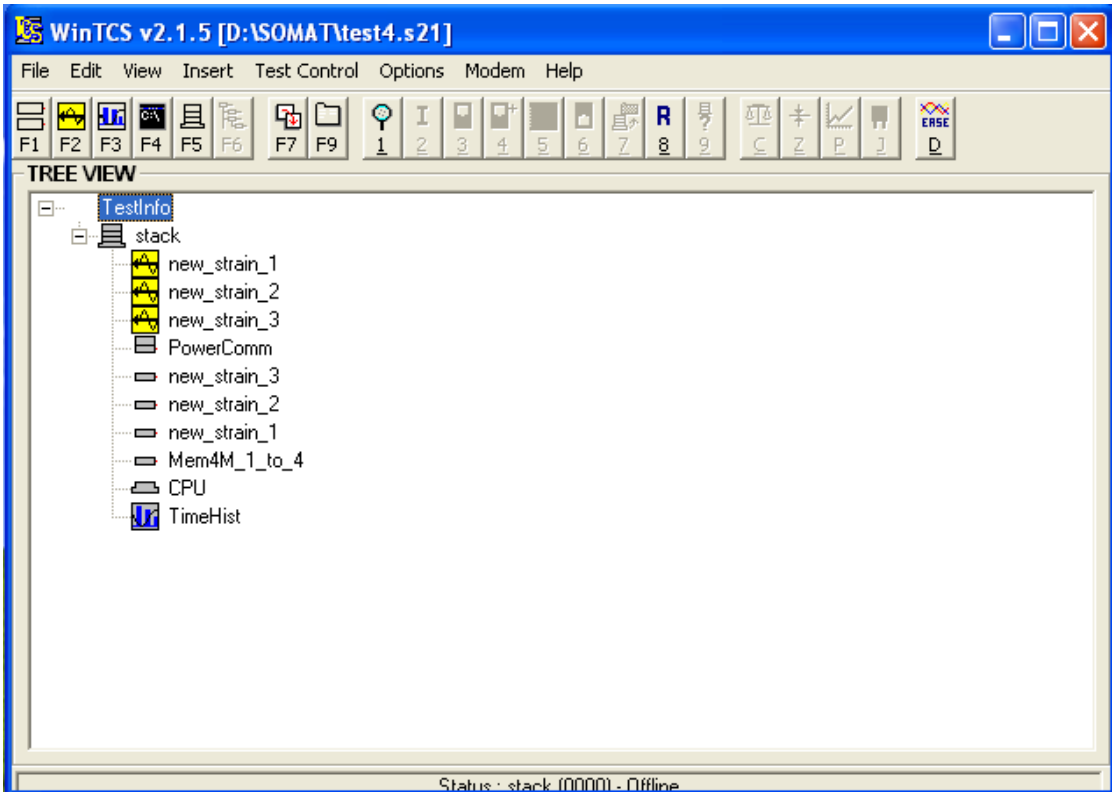

Figure 6.11 Test Control Software for Windows (WinTCS)

Once the WinTCS is set to run the test, the communication cable needs to be removed firstly and then preload and rolling speed are applied to the tyre. The data acquisition modules can generate digital data (data stored and manipulated as bytes of binary digits) by sampling the electrical signals generated by the strain sensors. The microprocessor manipulates and stores these data in the digital memory of the SoMat 2000 Field Computer, where the test data is held until the user uploads the data to a PC. The memory capacity of the SoMat 2000 Field Computer system is 4MB, which limits the time the acquisition process can last as well as the sample rate that can be adopted herein. Once the test is finished, the tyre is stopped from rolling and the load is removed. Then the SoMat 2000 Field Computer and PC are linked with the communication cable to upload the test data and then the memory is emptied.

The SoMat 2000 Field Computer can provide a sampling frequency of between 0.0005 and 5000 Hz, which ensures that the frequency resolution of the strain test data is adequate to capture enough features of the strain waveform per tyre revolution. However, a high sampling frequency increases the demand for memory capacity and decreases the maximum data acquisition time during testing.

In this study, the sampling frequency was set to be 1000 Hz which can record at least 50 data points per tyre revolution at speed 100 km/h. The measurement range of SoMat strain gauge module is from -5000 microstrain to 5000 microstrain, which is suitable for the normal working range of the Formula Student tyre used herein.

The SoMat 2000 Field Computer was attached to the wheel and balanced as shown in Figure 6.12.

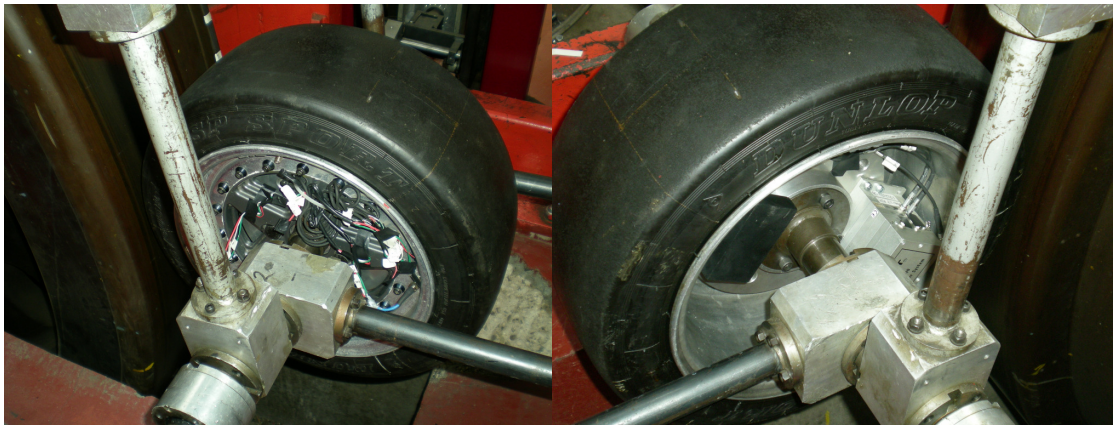

Figure 6.12 Test Configuration of Tyre with SoMat 2000 Field Computer

The test rig configurations for steady state straight line rolling and cornering are displayed in Figure 6.13 (a) and (b), respectively.

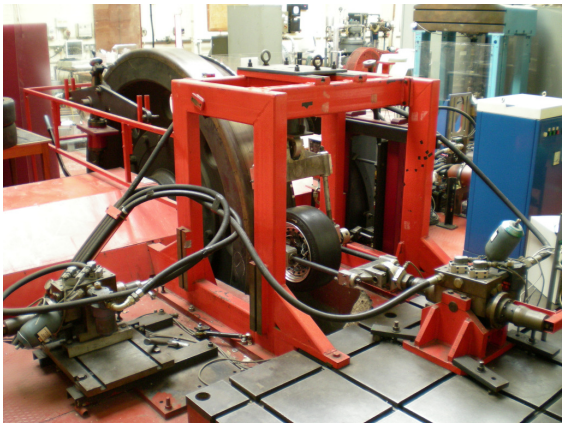

(a) Test rig configuration for straight rolling

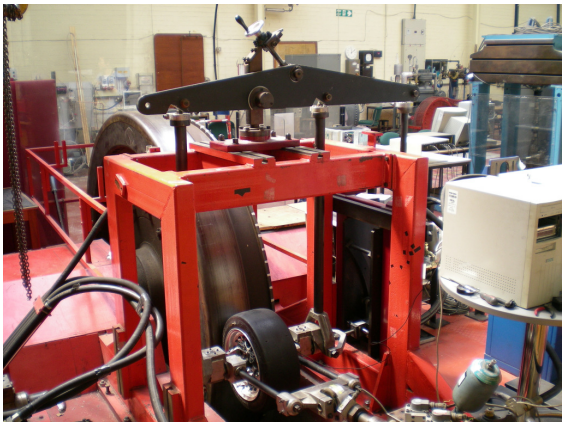

(b) Test rig configuration for cornering rolling

Figure 6.13 Test Rig Configuration

The tri-axial force generated by the tyre can be measured from the test rig using load cells as illustrated in Figure 6.14. The three longitudinal force components can also be utilized to calculate the tyre aligning moment. According to a previous study carried out on this test rig by Emmnanuel Bolarinwa [11], there exists an inconsistence in the measurement of the tyre longitudinal force, which is due to the inadequate resolution of the load cells measuring the longitudinal forces. Therefore only the vertical force and lateral force were measured in this study.

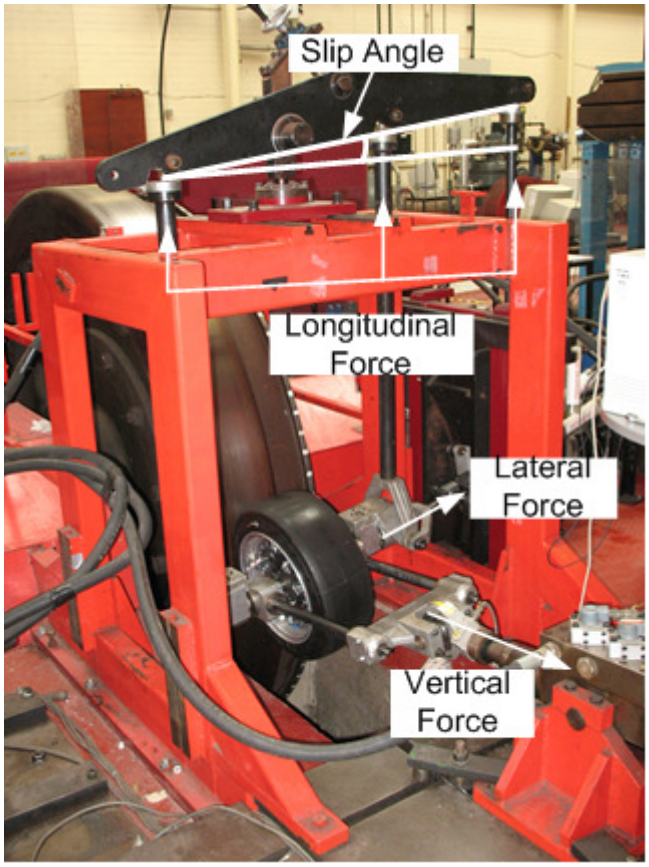

Figure 6.14 Tri-axial Force Measurement Mechanism

The test data were visualized in the software SoMat InField. Figure 6.15 to Figure 6.17 display an example of two channels of data signals (ε_{1y} and ε_{2y}) obtained during a test under 80 kPa inflation pressure, 30 km/h speed, 8 degree slip angle and different vertical loads (500 N, 750 N and 1000 N) in SoMat InField, respectively. It is shown that the magnitude of the axial strain waveform varies due to the change of vertical load.

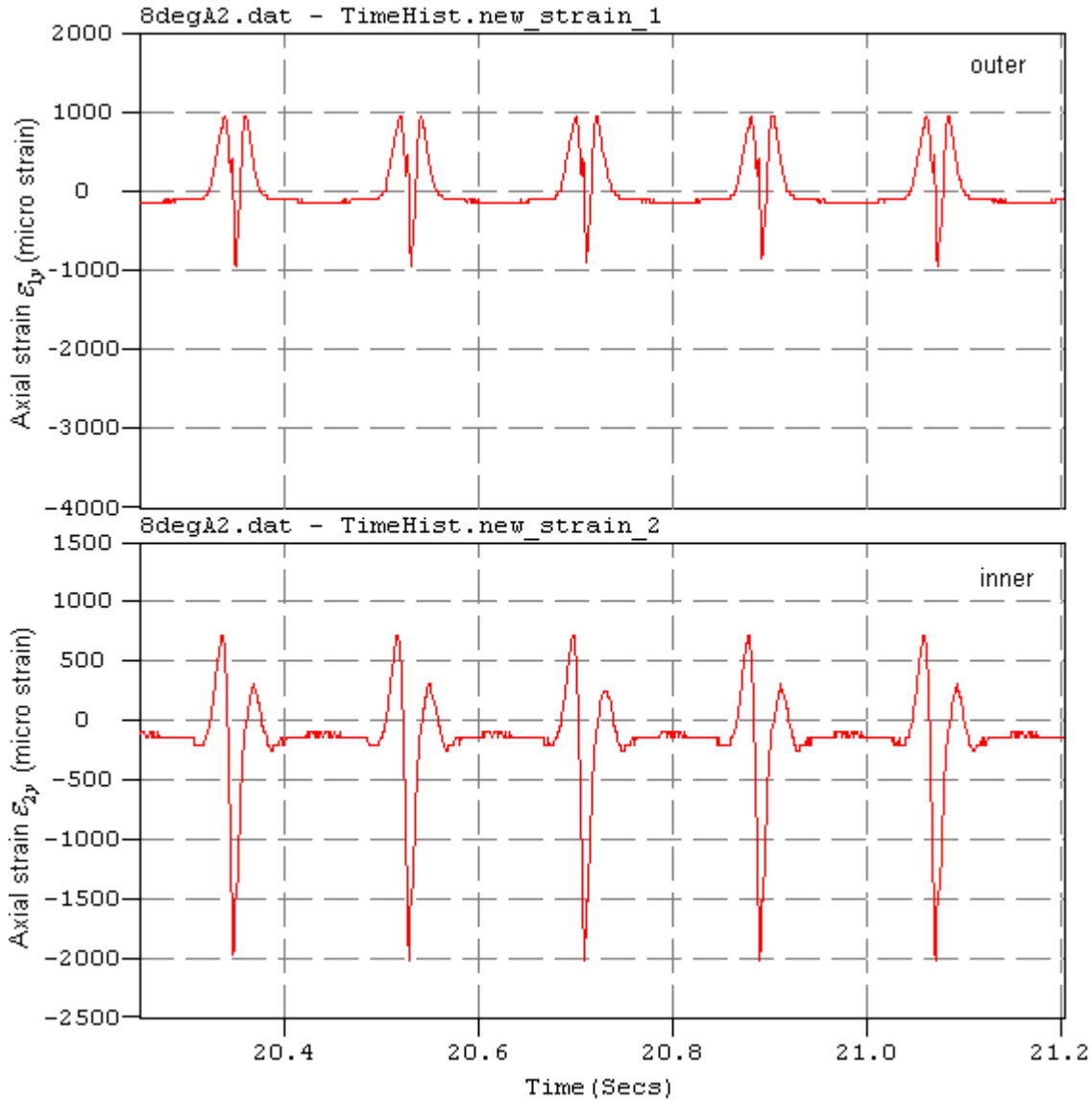

Figure 6.15 Strain Test Data at 80 kPa inflation pressure, 30 km/h speed, 8 degree slip angle and 500 N Vertical Load

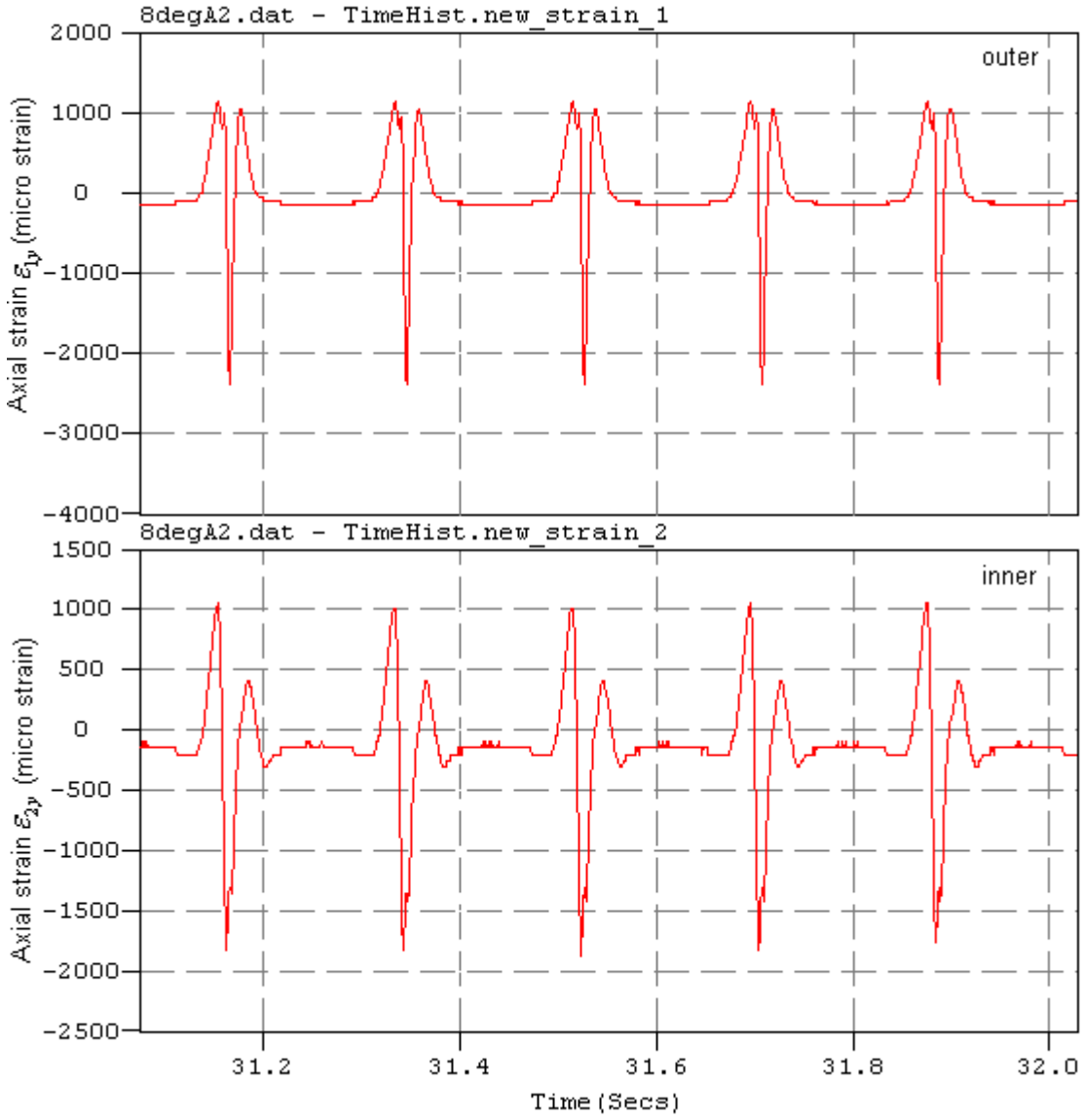

Figure 6.16 Strain Test Data at 80 kPa inflation pressure, 30 km/h speed, 8 degree slip angle and 750N Vertical Load

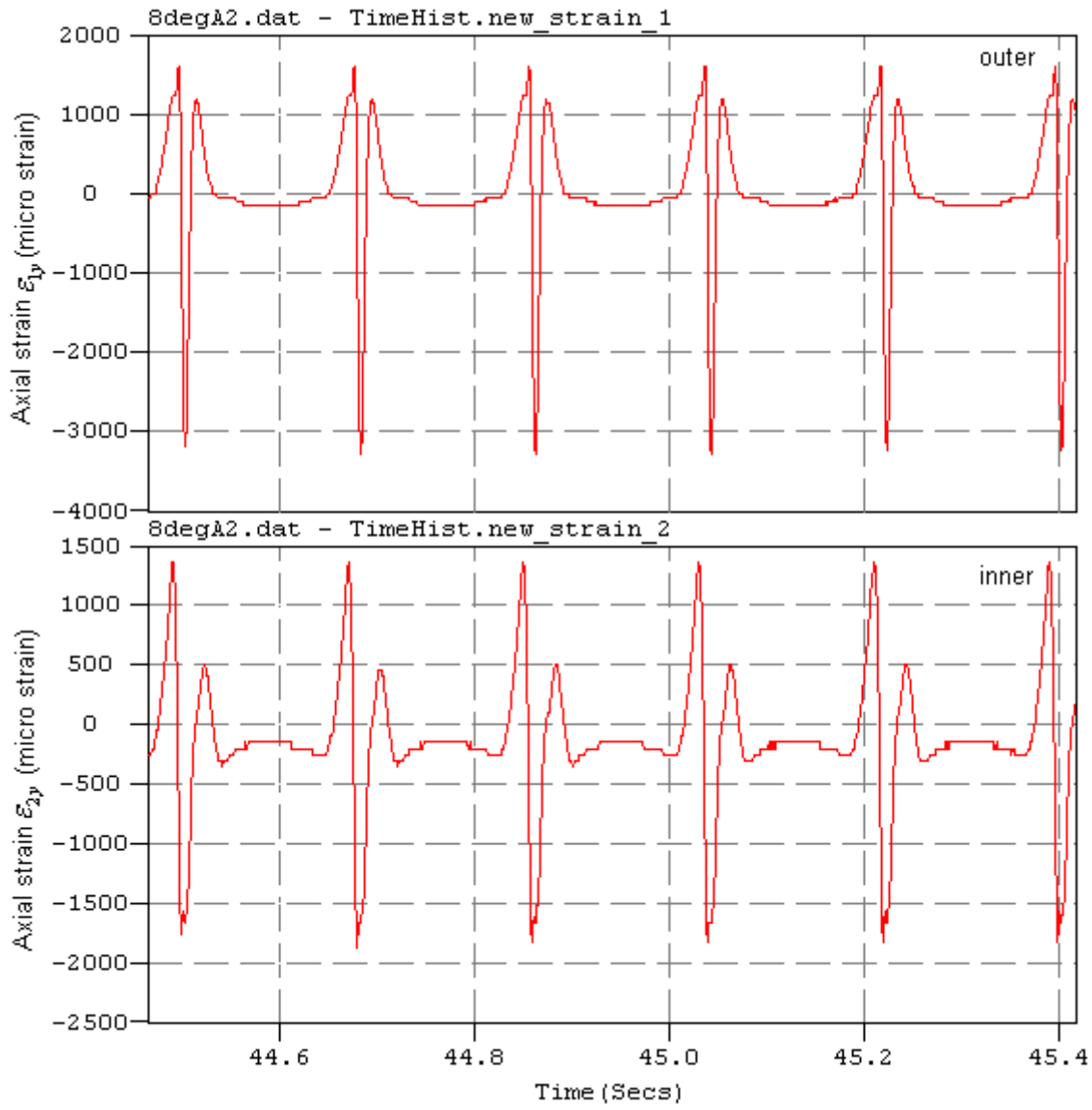

Figure 6.17 Strain Test Data at 80 kPa inflation pressure, 30 km/h speed, 8 degree slip angle and 1000 N Vertical Load

Figure 6.15 to Figure 6.17 show a comparison between the two strain gauge channels. The difference in the maximum compressive axial strain as well as the tensile axial strain peaks between the two channels is caused by the shift in the distribution of tyre contact pressure and shear stress. The "inner" side of tyre is the tyre side towards the corner.

6.4. FINITE ELEMENT ANALYSIS OF TYRE STEADY STATE ROLLING

A finite element tyre model was created to generate numerical simulation data as a replacement for physical tests of the tyre under different working conditions, such as braking/traction, cornering etc. in order to reduce the cost of testing.

In Chapter 5, the fundamental procedure of finite element tyre modelling was introduced. However, in order to achieve a reliable rolling tyre simulation, some guidance notes are still needed for clarification. The basic steps for finite element tyre analysis can be described as follows

1. 2D axisymmetric finite element tyre modelling.
2. 2D rim mounting and inflation analysis.
3. 3D finite element tyre modelling utilizing the ABAQUS function "Symmetric Model Generation".
4. 3D tyre stiffness and footprint analysis.
5. Steady state rolling analysis based on the ABAQUS function of "Steady State Transport" in ABAQUS/Standard Solver.
6. Tyre steady state rolling analysis results was transferred from ABAQUS/Standard to ABAQUS/Explicit to simulate tyre transient rolling analysis.

Material Property: The tyre rubber material property shows nonlinear stress-strain relationship. In Chapter 3, the rubber hyperelastic and viscoelastic material properties were investigated and assigned to the finite element tyre model. It is noted that in some

literatures [126, 158] the linear elastic property was adopted to represent the rubber behaviour approximately. Although this adoption can also provide reasonable prediction of tyre global behaviour such as displacement, it cannot provide precise prediction of local behaviour such as strain. Thus, the usage of nonlinear material property of rubber is essential for accurate tyre local behaviour prediction.

Moreover, in a static or steady state analysis, the "Long Term" parameter in the "Step" module of ABAQUS can be included or excluded depending on whether or not the viscoelastic material response is considered. However, in transient analysis, the viscoelastic effects are not accounted for in the rubber material due to the limitations with the "Import" option.

Mesh: In ABAQUS, a non-uniform discretisation mesh (in the circumferential direction) can be used for the tyre steady state rolling analysis due to the usage of Langrangian/Eulerian formulation. The tyre contact patch region is meshed with a refined mesh density and the remaining region can be meshed in coarser mesh density. For the transient analysis, the reduced-integration solid element was used due to the element type limitation of ABAQUS/Explicit and the whole tyre was meshed with a uniform density. This difference of mesh method is caused by the different solution approach on rotational behaviour between ABAQUS/Standard and ABAQUS/Explicit.

Tyre Rotation: As mentioned in the section 4 of Chapter 4, a rigid body relationship was created between the reference node and the tyre bead region nodes. Not only can

the tyre dynamic response be captured from the reference node but also velocity and torque can be applied to it to drive the tyre rotation.

Two different approaches are provided by ABAQUS for solving the tyre steady state rolling and transient rolling, namely:

A steady state rolling analysis in ABAQUS uses a moving reference frame in which rigid body rotation is described in an Eulerian manner and the deformation is described in a Lagrangian manner. The material is allowed to move through the tyre mesh simulating rolling, while the mesh is kept in constant contact with the road surface without rolling about the axis as shown as Figure 6.18. The finite element mesh describing the tyre in the frame of reference remains stationary. This kinematic description is considered as a mixed Lagrangian/Eulerian formulation.

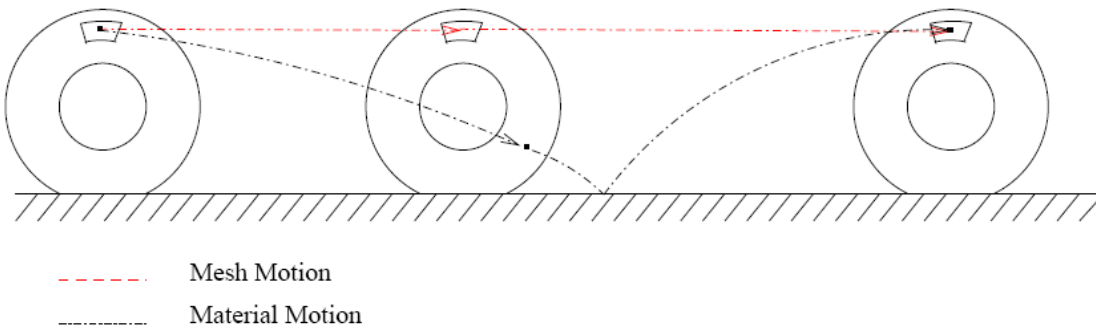

Figure 6.18 Lagrangian/Eulerian Approach for Tyre Steady State Rolling Simulation [159]

In this way, only the mesh in the contact region needs to be refined. Frictional effects, inertia effects and history effects in the material can be accounted for in a *STEADY STATE TRANSPORT analysis. The inertia effect of the rolling tyre gives rise to the

inertia force including centrifugal and Coriolis effects. The inertia effect can be negligible at low and medium speed but may be important for investigating standing wave phenomena and vibration behaviour of the tyre at high speed [126].

The solution obtained from the steady-state transport analysis in ABAQUS/Standard can be used as the initial condition for the tyre transient rolling analysis in ABAQUS/Explicit. Therefore, the time consumption due to the preloading and acceleration using explicit time integration can be avoided [75].

The transient rolling is based on the Lagrangian approach, namely both the material and mesh translate and rotate as the tyre rolling shown as Figure 6.19. The tyre contact patch dynamically changes due to the rotation of the tyre. Thus, the tyre circumferential mesh should be fine and uniform. These repeated dynamic impact caused by the nodes entering the contact region induce an unavoidable high frequency noise. Thus, compared to the steady state rolling, the output plot of transient rolling analysis usually needs to be filtered.

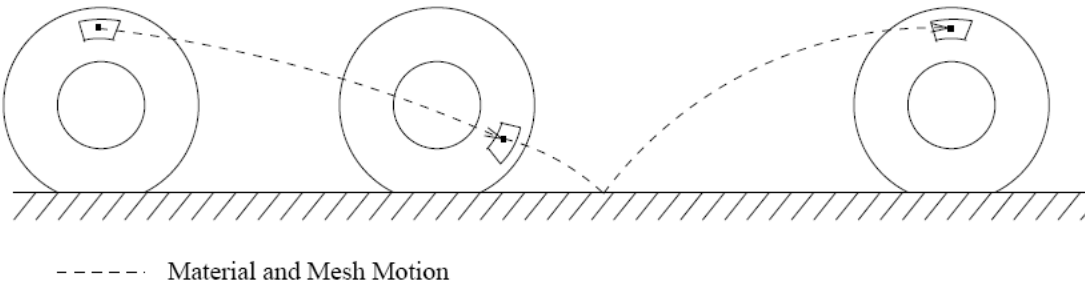

Figure 6.19 Lagrangian Approach for Tyre Transient Rolling Simulation [159]

Contact Friction: Generally, the tyre is modelled as a deformable body, while the road is modelled as a rigid body, the illustration about which can be found in Chapter 4. During the finite element analysis of a tyre, two contact problems need to be considered: tyre/road contact and tyre/rim contact. As mentioned in the section 4 of Chapter 4, the tyre/rim contact has been simplified by approximately fixing the tyre/rim interface at the tyre bead region, which is considered reasonable for steady state tyre analysis [11]. For the tyre/road contact problem, a surface-based solution e.g. master/slave formulation provided in ABAQUS is adopted. The rigid road surface is selected as the master surface while the tyre tread outer surface is the slave surface. The tangential coulomb friction coefficient is assigned to the contact pair with a small elastic slip value of 0.02 as suggested in the ABAQUS user manual in order to account for the relative sliding of contact surfaces.

In the static simulation step, a lower friction coefficient such as between 0 and 0.2 should be chosen to obtain a better convergence. For steady state rolling simulation, the friction coefficient is generally changed between 1.0 and 1.2 for the racing tyre. However, if the classic coulomb friction model cannot meet the requirement of the research, ABAQUS also provides user subroutine FRIC (in ABAQUS/Standard) or VFRIC (in ABAQUS/Explicit) for modelling general friction conditions [160].

Solver: For the steady state rolling analysis in ABAQUS/Standard, the implicit solver was used, while the explicit solver was adopted for tyre transient rolling analysis in ABAQUS/Explicit. The ABAQUS/Standard uses the implicit Hilber-Hughes-Taylor (HHT) operator for the integration of the equations of motion. The HHT method is an

improved algorithm based on the Newmark method, which has the ability to eliminate undesirable high frequency oscillations [161]. The equation for a dynamic problem at time t_{n+1} can be described as

$$M\ddot{X}_{n+1} + (1+\bar{\alpha})KX_{n+1} - \bar{\alpha}KX_n = F_{n+1} \tag{6.1}$$

Where the M and K are the symmetric mass and stiffness matrices. F_{n+1} is the time dependent external force vector. $\bar{\alpha}$ is the numerical damping parameter. If $\bar{\alpha} = 0$, the above equation becomes Newmark method.

The position vector X_{n+1} and velocity vector $\dot{X}_{n+1}$ at time t_{n+1} can be written as

$$X_{n+1} = X_n + \Delta t\dot{X}_n + \Delta t^2(1/2-\beta)\ddot{X}_n + \Delta t^2\beta\ddot{X}_{n+1} \tag{6.2}$$

$$\dot{X}_{n+1} = \dot{X}_n + \Delta t(1-\bar{\gamma})\ddot{X}_n + \Delta t\gamma\ddot{X}_{n+1} \tag{6.3}$$

Where $\Delta t = t_{n+1} - t_n$ is the step-size. The β and $\bar{\gamma}$ are two assumed parameters. In ABAQUS, $\bar{\beta} = 1/4$, $\bar{\gamma} = 1/2$, and the HHT operator is unconditionally stable.

The ABAQUS/Explicit uses the central-difference operator for the integration of the equations of motion. The dynamic equation is described as

$$\ddot{X}_n = M^{-1} \cdot (F_n - I_n) \tag{6.4}$$

where M is the diagonal lumped mass matrix, F is the applied load vector, and I is the internal force vector. The explicit central difference integration rule is

$$\dot{X}_{(n+1/2)} = \dot{X}_{(n-1/2)} + \frac{\Delta t_{(n+1)} + \Delta t_{(n)}}{2}\ddot{X}_{(n)} \tag{6.5}$$

$$\dot{X}_{(n+1)} = \dot{X}_{(n+1/2)} + \frac{1}{2}\Delta t_{(n+1)}\ddot{X}_{(n+1)} \tag{6.6}$$

$$X_{(n+1)} = X_{(n)} + \Delta t_{(n+1)} \dot{X}_{(n+1/2)} \tag{6.7}$$

The subscript n refers to the increment number and $n-1/2$ and $n+1/2$ refer to mid-increment values.

From the above introduction, it can be seen that for implicit integration the operator matrix needs to be inverted and the solution is iteratively calculated using Newton's Method. However, the explicit procedure does not need iterations. Thus each increment is relatively inexpensive in explicit integration compared to implicit integration. However the central-difference operator is conditionally stable and the size of time increment in explicit dynamic analysis is limited. More details can be obtained by referring to [162].

According to these features of the ABAQUS solver, the computational cost for implementing a steady state rolling simulation in ABAQUS/Explicit increases with rolling speed. Whereas the computational cost in ABAQUS/Standard is independent of the magnitude of the tyre rolling speed. Also, the numerical noise generated in the simulation by ABAQUS/Explicit has a detrimental effect on the extraction of strain features such as the derivative strain waveform. Since the predicted results using both ABAQUS/Standard and ABAQUS/Explicit give reasonable correlation with the test data [11, 56], the tyre steady-state rolling analysis was carried out in ABAQUS/Standard herein.

Strain: The correct choice of strain output from finite element tyre analysis is very important for a successful prediction. ABAQUS provides different types of strain output

for nonlinear analysis such as integrated strain measure E, nominal strain measure NE, and logarithmic strain measure LE. By default, the strain output in ABAQUS/Standard is the "integrated" total strain (output variable E) which is composed of the elastic strain EE, the inelastic strain IE, and the thermal strain THE. The strain output in ABAQUS/Explicit is logarithmic strain (output variable LE) as default. Nominal strain (output variable NE) can be requested in both ABAQUS/Standard and ABAQUS/Explicit. However, the "integrated" total strain is not available in ABAQUS/Explicit.

Nominal strain is also called Engineering strain. It is defined as $\varepsilon_{nom} = \frac{L - L_0}{L_0}$. The nominal stress is $\sigma_{nom} = \frac{P}{A_0}$. Where L is the current gauge length, L_0 is the original gauge length. P is the applied force on specimen and A_0 is the original cross section area of specimen.

Logarithmic strain is also called true strain. It is defined as $\varepsilon_{true} = \ln\left(\frac{L}{L_0}\right) = \ln\left(1 + \varepsilon_{nom}\right)$.

The true stress is defined as $\sigma_{true} = \sigma_{nom}\left(1 + \varepsilon_{nom}\right)$.

It should be noted that the strain output from the experiment of strain-based intelligent tyre prototype system and the finite element tyre analysis is the engineering strain.

The data acquisition location is selected to match the corresponding position in the test shown in Figure 6.20.

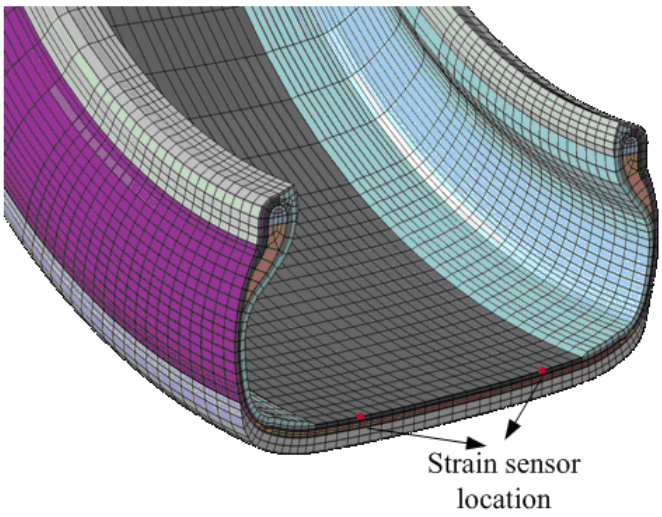

Figure 6.20 Data Acquisition Location in Finite Element Tyre Model

Once the finite element tyre model had been created correctly, the steady state straight line rolling was carried out based on the restart from the static deflection analysis. The steady state transport option is used to obtain the steady state straight line free rolling solutions by capturing the state of zero torque on the wheel between full-braking and full-traction conditions while varying the tyre angular speed at the desired constant road speed. Likewise, the braking and traction forces can be obtained from the above procedure. Then steady state simulation of tyre steering subjected to slip angle and camber angle can be implemented and the tyre dynamic response can be measured during this procedure.

6.5. ESTIMATION OF TYRE FORCE BASED ON TYRE STRAIN INFORMATION

The intelligent tyre concept has developed from the safety issues affecting the vehicle. It is expected that the tyre can provide accurate and synchronized information about the vehicle driving status for optimising its control system. The well known vehicle control systems are the antilock braking systems (ABS), traction control systems (TCS) and electronic stability control system (ESCS). The ABS is a closed-loop device designed to prevent tyre locking and skidding during braking. The TCS can limit the amount of traction force generated at the wheels to prevent loss of traction [163]. The ESCS can detect the loss of steering control, and then trigger the ABS to apply individual brakes to improve the tyre cornering behaviour and minimize the skids. All the operations of ABS, TCS and ESCS needs an electronic control unit (ECU), which compares the signals from each wheel sensor and measures the acceleration or deceleration of individual wheel.

As discussed in Chapter 2, the relationship between braking/traction force and tyre longitudinal slip is nonlinear due to the tyre/road contact mechanical property. Therefore, it is difficult for drivers to apply the optimum amount of brake pedal force to stop the vehicle in the minimum distance. Moreover, it is practically impossible in different road conditions such as wet, muddy or icy road surface since the tyre-road contact friction is varying [163]. The lateral slip of the vehicle tyre is also very important for the vehicle stability control. Due to the grip limitation in the tyre lateral direction, once the lateral force demand during vehicle cornering exceeds the maximum force generated at the tyre/road contact patch, the vehicle would lose control which may

lead to traffic accident. To complicate things further, in real driving situations there may be a combination of braking/traction and steering. Since they have an interactive effect on each other, the ABS and TCS control must be suitable for an extended large slip angle range.

It is obvious that the tyre/road contact forces i.e. braking/traction force and lateral force need to be better controlled near to the optimum to prevent loss of grip and hence loss of vehicle stability. Another important factor which may cause traffic accidents is the under inflation of the tyre, which could lead to the change of tyre force and even the loss of control. The vehicle sub-systems such as the tyre should be in a healthy condition in order to achieve an optimum operation of vehicle control. Therefore, the hazardous tyre and road conditions would be required to be sent to the driver by a drive warning information system.

In order to satisfy the aforementioned demands, the intelligent tyre is under development to improve the vehicle safety and provide accurate vehicle dynamics control. As a potentially important technology, the strain-based intelligent tyre developed in this study is expected to provide accurate information about tyre status to the vehicle control system as well as the driver. The information may include the wheel speed, inflation pressure, tyre forces and road condition, etc.

The roadmap of the methodology for developing the strain-based intelligent tyre in this study is illustrated in Figure 6.21 .

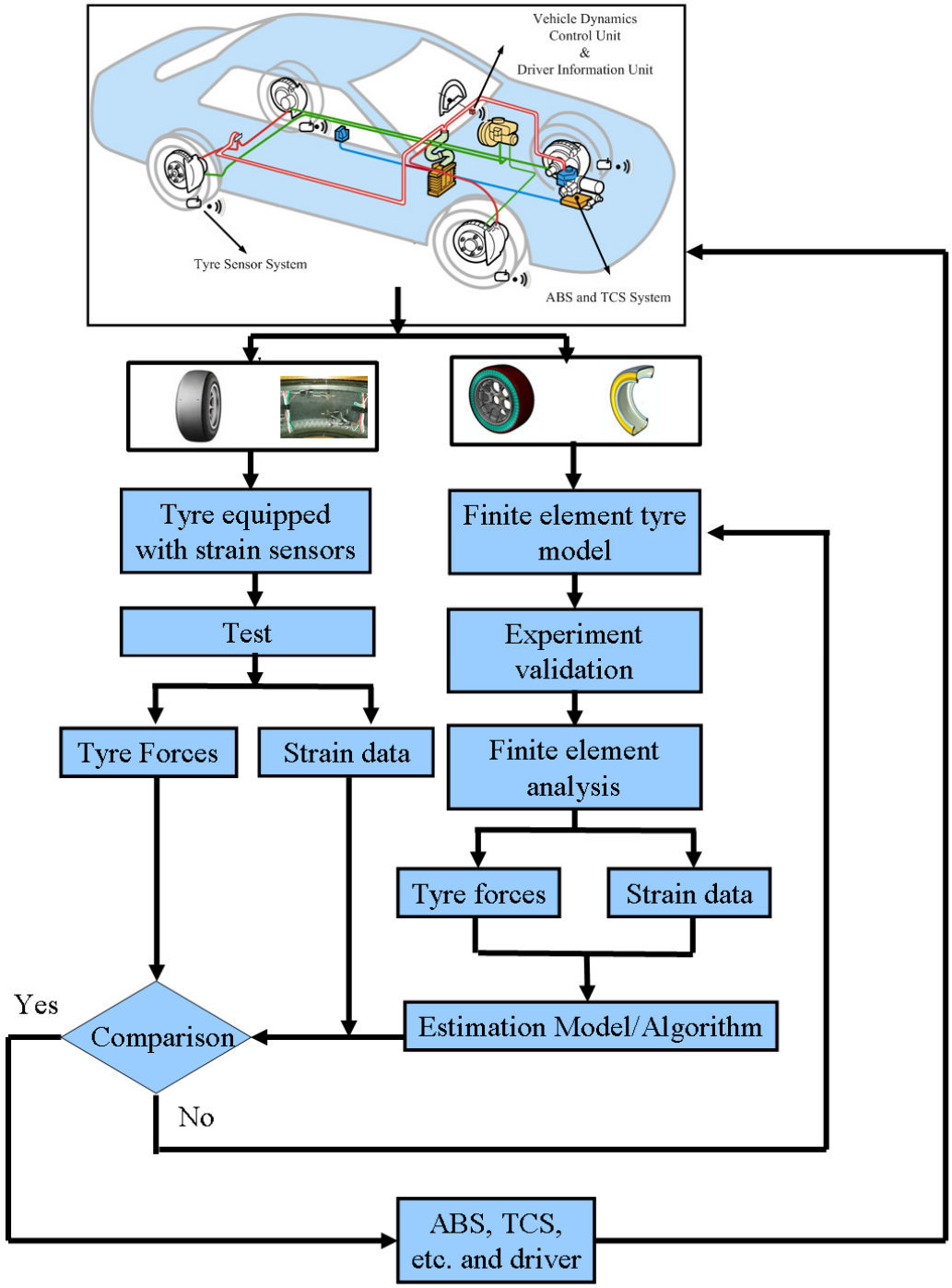

Figure 6.21 Methodology of Developing Strain-based Intelligent Tyre

It can be seen that the estimated relationship between strain data and tyre forces obtained from the validated finite element tyre model is extracted firstly. Then, the test strain data are substituted into the estimation model to obtain the estimated forces which

will be compared with the test forces in order to prove the validity of the estimation model. This method potentially provides an efficient and effective approach for estimating tyre force based on the tyre strain data information for developing the intelligent tyre.

6.5.1 STEADY STATE STRAIGHT LINE ROLLING

Steady state straight line rolling is the fundamental mode of vehicle tyre maneuver. A series of steady state straight line rolling tests were carefully designed and conducted on the indoor tyre test rig considering the range of the tyre's operating parameters as follows:

- Tyre Speed Range: 10 km/h ~ 50 km/h.
- Tyre Inflation Pressure: 80 kPa ~ 140 kPa.
- Tyre Preload: 250 N ~ 1000 N.

The range of tyre inflation pressure and preload covers the tyre normal working conditions. However, the tyre rolling speed range only covers the low speed conditions since it is difficult to capture the tyre strain feature at high speed using the selected sampling frequency.

- **Estimation of tyre angular velocity.**

One of the potential applications of strain-based intelligent tyre system is providing accurate tyre angular velocity measurement instead of using additional sensors, such as speed sensor. During the test, the time period per tyre revolution can be measured from

the strain time history. The tyre angular velocity is then calculated as 2π divided by the time period.

With the same tyre working conditions as the test, a steady state rolling simulation was carried out at tyre pressure 80kPa, preload 750N and velocity 30km/h. In order to find a free rolling speed, the tyre was simulated spinning from full braking to full traction. The tyre was considered to reach the free rolling speed when the traction torque is equal to zero as shown as Figure 6.22.

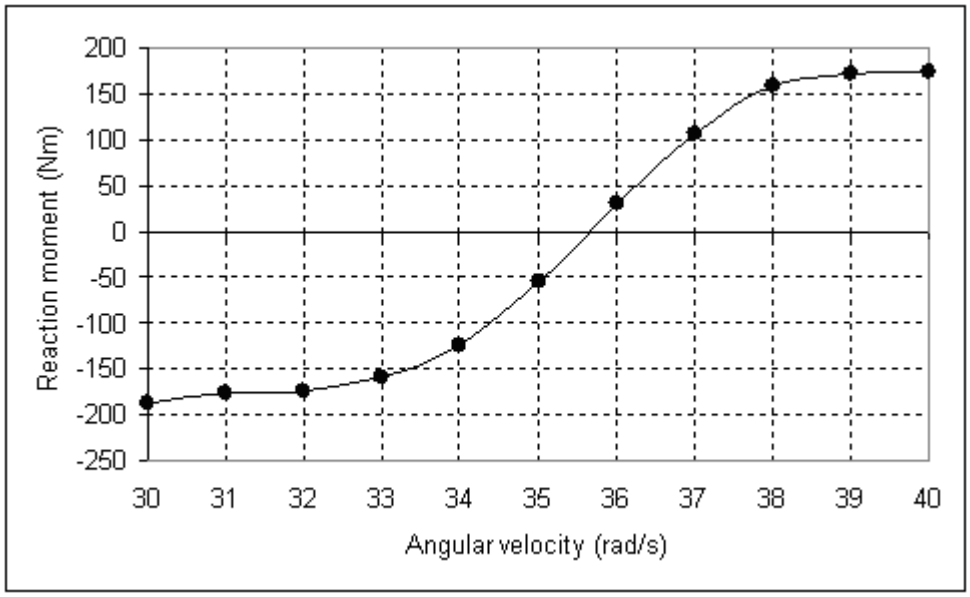

Figure 6.22 Determination of Tyre Free Rolling Speed

The tyre rolling speed obtained from test and simulation is 35.66 rad/s and 35.63 rad/s respectively, which shows a good agreement.

An estimation model for estimating tyre rolling speed is extracted based on the finite element analysis for different tyre travelling velocities as shown in Figure 6.23.

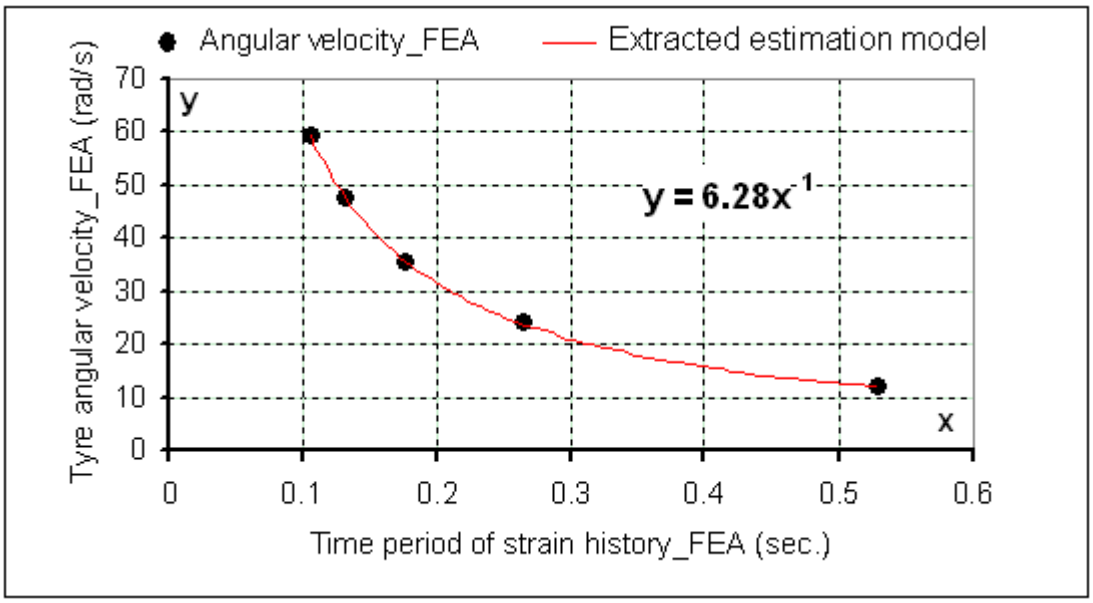

Figure 6.23 Extraction of Tyre Angular Velocity Estimation Model Based on FEA at 750 N Preload and 80 kPa Inflation Pressure

Figure 6.23 displays a nonlinear power relationship between the tyre angular velocity and the time period of strain time history obtained from FEA. By substituting the time period of test strain data into the extracted estimation model, the estimated tyre angular velocity for the test can be obtained as shown in Figure 6.24.

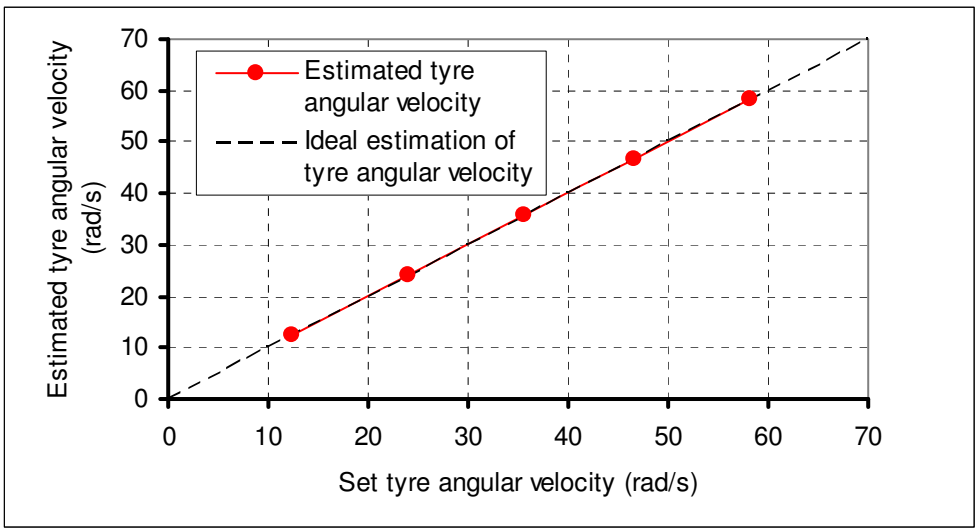

Figure 6.24 Tyre Angular Velocity Estimation at 750 N Preload and 80 kPa Inflation Pressure

The results from the estimation model based on test strain time history period are close to the ideal estimation of tyre angular velocity. The estimated target can be either tyre angular velocity or tyre travelling velocity.

Moreover, it is known that the tyre angular velocity varies due to the change of tyre preload and inflation pressure. In order to validate the robustness of the angular velocity estimation model for the tyre herein, the effect of preload and inflation pressure was investigated as shown in Figure 6.25 and Figure 6.26. The working condition 750N preload, 80kPa inflation pressure and 30km/h speed was considered as the reference point, viz. the bias of angular velocity is zero.

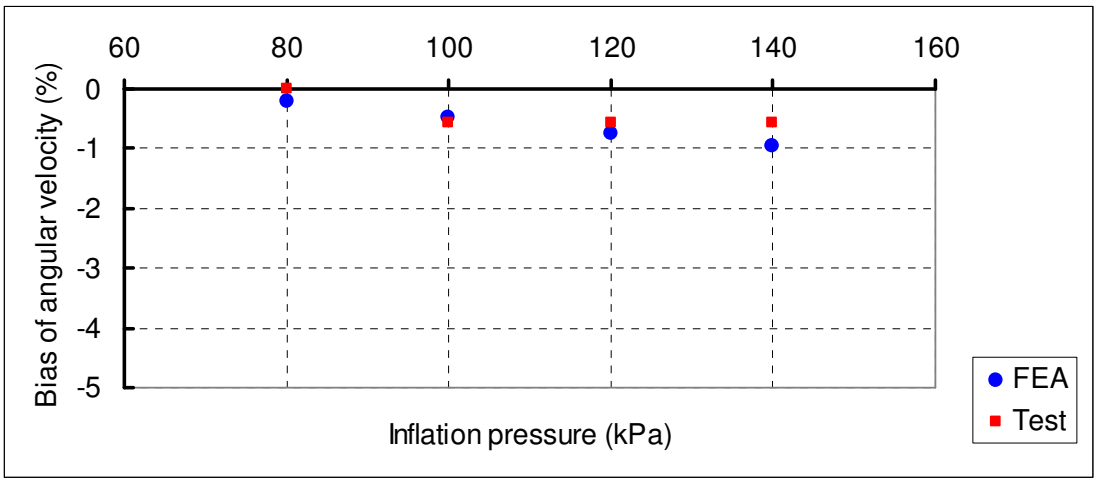

Figure 6.25 Effect of Tyre Inflation Pressure on Angular Velocity at 750 N Preload and 30 km/h Speed

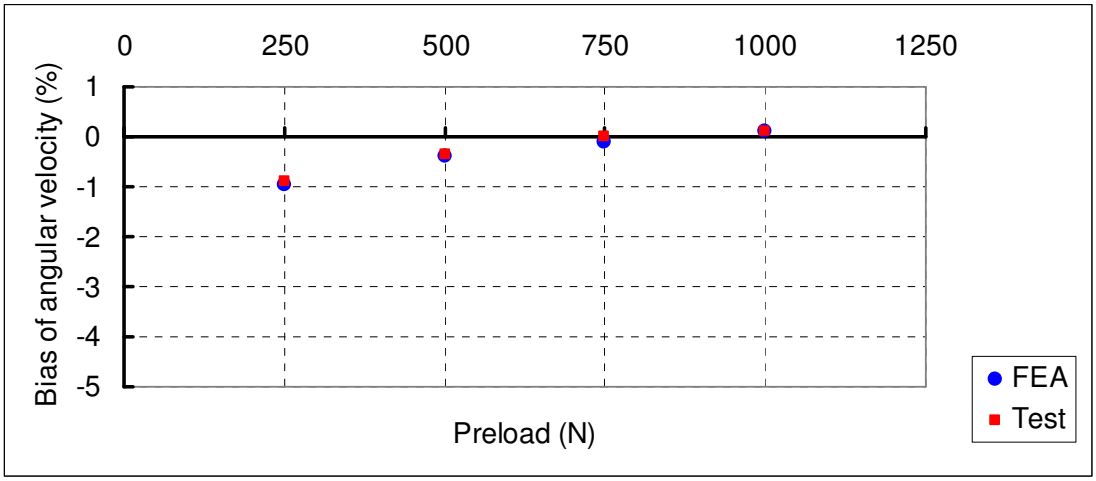

Figure 6.26 Effect of Tyre Preload on Angular Velocity at 80 kPa Inflation Pressure and 30 km/h Speed

It is shown that the tyre angular velocity decreases with the increase of preload and the reduction of inflation pressure. Meanwhile, the range of tyre preload and inflation pressure investigated in this study has a very modest effect (no more than 1%) on the tyre angular velocity. Therefore, the tyre angular velocity estimation model is robust for the tyre normal working conditions range during straight line rolling. The effect of preload and inflation pressure on the tyre angular velocity estimation needs to be evaluated for other tyres and their working conditions to confirm the relationship described above.

- **Estimation of tyre preload and inflation pressure**

The predicted and measured axial strains at normal inflation pressure 80 kPa, preload 750 N and speed 30 km/h are compared in Figure 6.27. In Figure 6.27, the 180 degree position corresponds to the tyre contact patch centre, while the 0 degree and 360 degree correspond to the same position diametrically opposite the tyre contact patch centre. As can be seen, only the region around tyre contact patch experiences large variation of

axial strain, which is about from 120 degree to 240 degree. The maximum tensile strain occurs around 20 degrees to the contact patch centre.

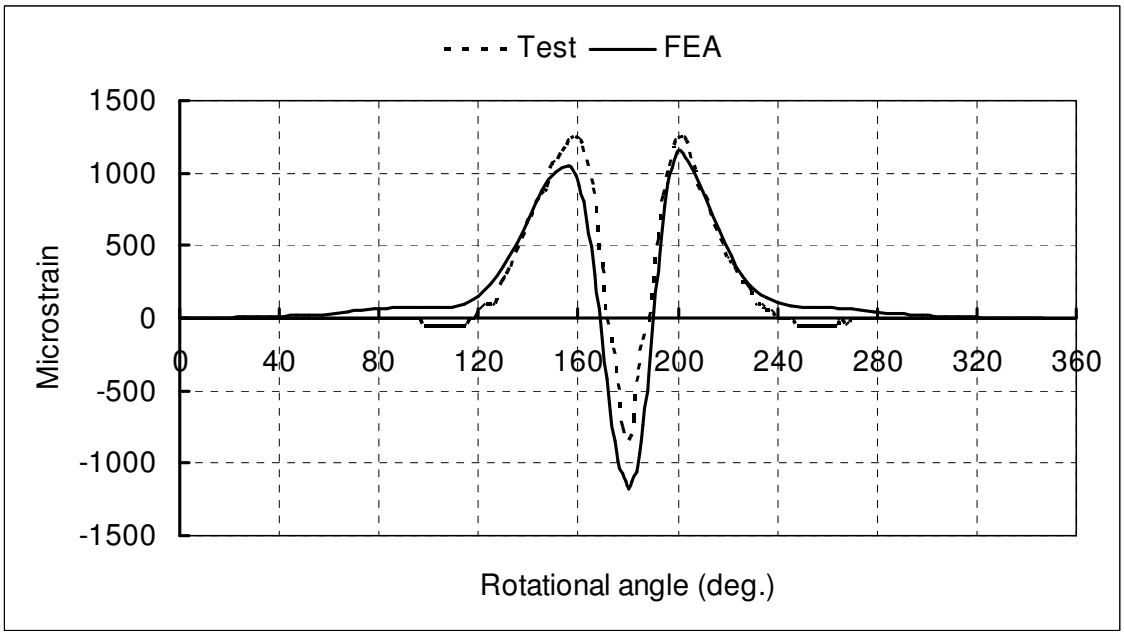

Figure 6.27 Axial Strains Comparison between Test and FEA at 750 N Preload, 80 kPa Inflation Pressure and 30 km/h Speed.

It can be seen from Figure 6.27 that the variation of the tensile and compressive strain around the tyre contact patch region shows similar trends for both finite element analysis and physical test. However, the difference between the maximum compressive strains is apparent, which may be caused by the difference between the finite element tyre model and the real tyre used on the test rig as described in Chapter 4.

Furthermore, the variation of axial strain waveform around the tyre contact patch in the test presents a narrower shape than that in FEA. It is thought to be as a result of the curvature of the drum in the test while the flat road was used in the FEA.

Therefore, the strain provided by finite element tyre model can be considered reasonably close to the test data. The average value of the two tensile strain peaks was adopted herein to construct the relationship with tyre preload and inflation pressure.

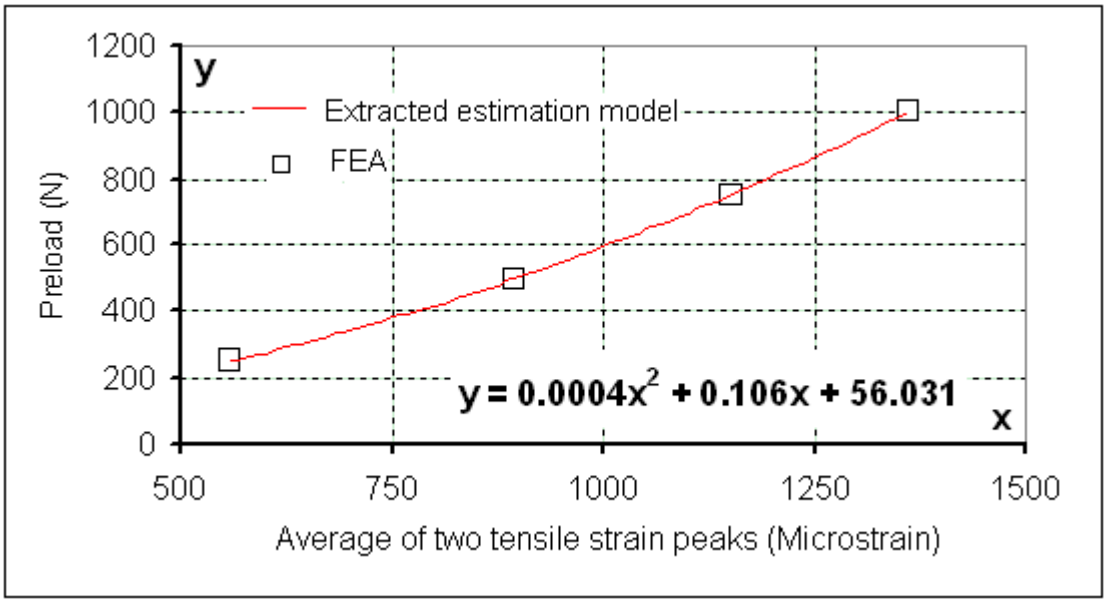

Figure 6.28 Extraction of Tyre Preload Estimation Model based on FEA at 80 kPa Inflation Pressure and 30 km/h Speed

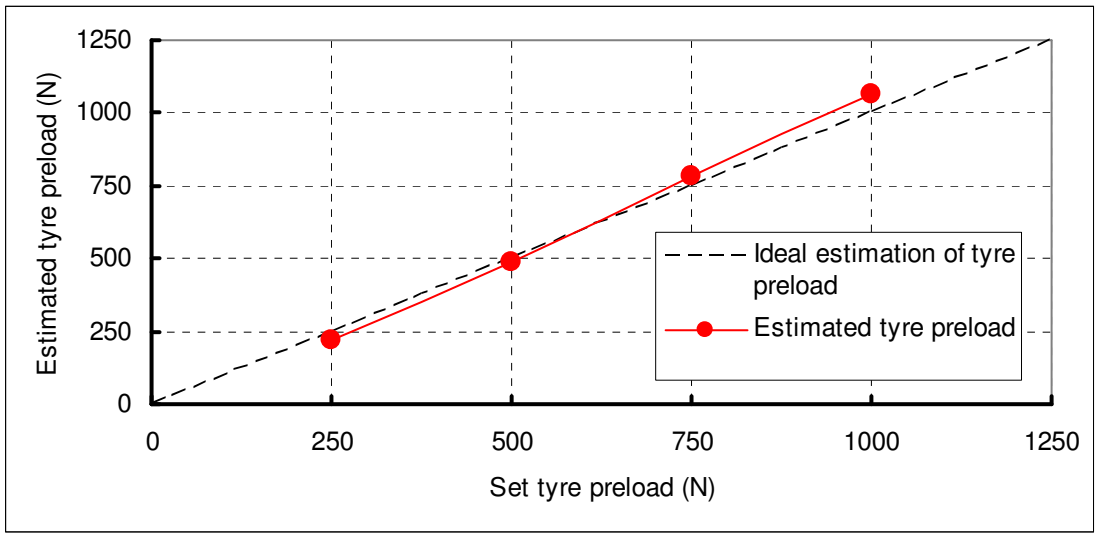

Figure 6.29 Tyre Preload Estimation at 80 kPa Inflation Pressure and 30 km/h Speed

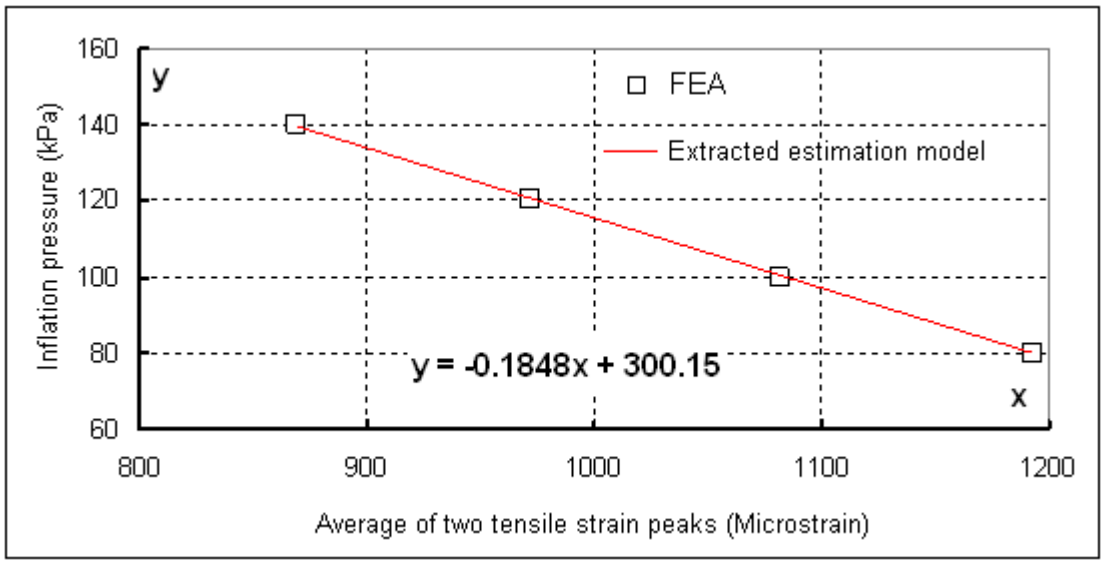

Figure 6.30 Extraction of Tyre Inflation Estimation Model based on FEA at 750 N Preload and 30 km/h Speed

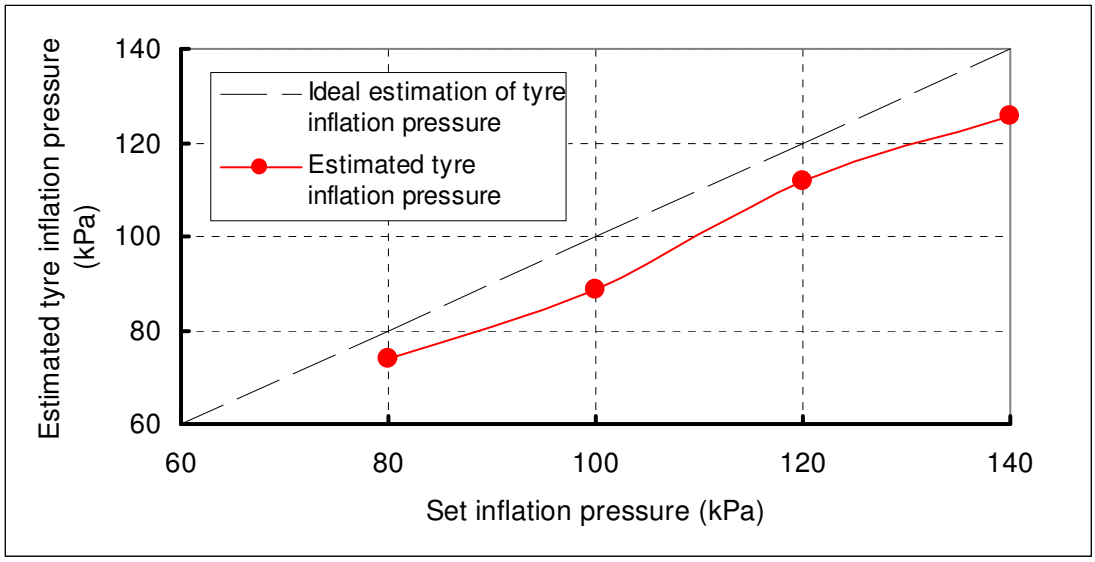

Figure 6.31 Tyre Inflation Pressure Estimation at 750 N Preload and 30 km/h Speed

It can be found from the above figures that the average maximum tensile strain shows an increasing trend with increasing preload and decreasing inflation pressure. The estimation model of tyre preload and inflation pressure gives a reasonable estimation within 10% error with respect to the ideal estimation. Since the tyre preload and

inflation pressure have a combined influence on tyre strain variation, the estimation of tyre preload may require information about the inflation pressure information from tyre TPMS or the other estimation methods.

Furthermore, according to the test results, the velocity variation has a very modest impact on the value of axial strain in comparison with the variation of preload and inflation pressure as shown in Figure 6.32.

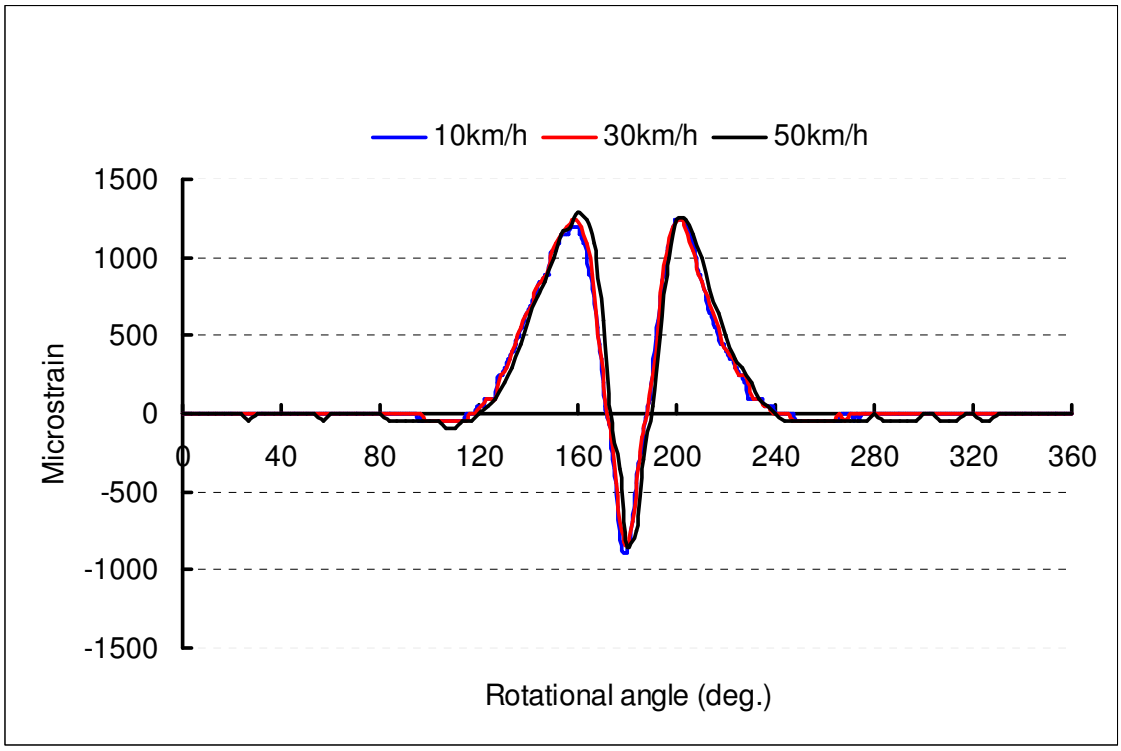

Figure 6.32 Axial Strains under Different Velocities from Test at 750 N Preload and 80 kPa Inflation Pressure

The inertia effects on the strain at these speeds are negligible. However, at higher speeds the inertia effect on the strain may be significant due to its pushing on the tyre tread component against the road. The investigation in the rest of this chapter will only

consider the speed of 30km/h as an example with different preloads and inflation pressures.

6.5.2 BRAKING AND TRACTION

A nonlinear relationship exists between tyre longitudinal slip and tyre longitudinal force during tyre braking/traction. A better estimation of tyre braking and traction behaviour can provide an optimum operation of ABS and TCS in order to achieve the maximum braking/traction force occurring at the peak of the relationship curve. The braking/traction force can be expressed as the friction coefficient multiplied by the tyre preload.

$$F_x = \mu F_z \tag{6.8}$$

Due to the absence of a braking/traction device on the present test rig, the braking/traction test could not be carried out in the lab. However, the finite element tyre model was used to investigate the tyre braking and traction behaviour under straight line rolling to give a predicted insight into the relationship between tyre braking/traction force and axial strain characteristics.

The typical axial strain waveform under 750N preload and 80kPa inflation pressure, caused by different tyre working conditions was predicted from the finite element analysis as shown in Figure 6.33.

The front tensile strain peak ε_f decreases while the rear tensile strain peak ε_r increases when the tyre is braking, and vice versa for tyre traction. The tensile strain peak ratio is

defined as $r_\varepsilon = \varepsilon_f / \varepsilon_r$. This characteristic of axial strain is adopted for the estimation of tyre braking/traction force herein.

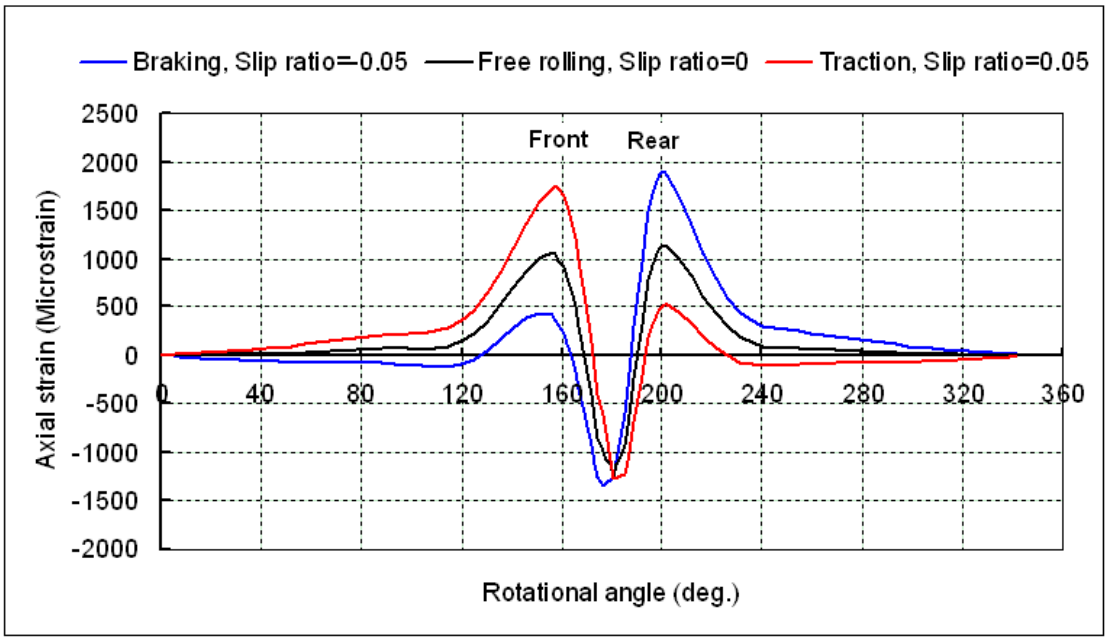

Figure 6.33 Axial Strain Waveform under Tyre Braking, Free rolling and Traction

The predicted braking/traction force with respect to the tyre longitudinal slip ratio was investigated for different tyre preloads at inflation pressure 80kPa as shown in Figure 6.34.

The relationship between tensile strain peak ratio and longitudinal force for different preloads at 80kPa can be extracted and used for the estimation of tyre longitudinal force.

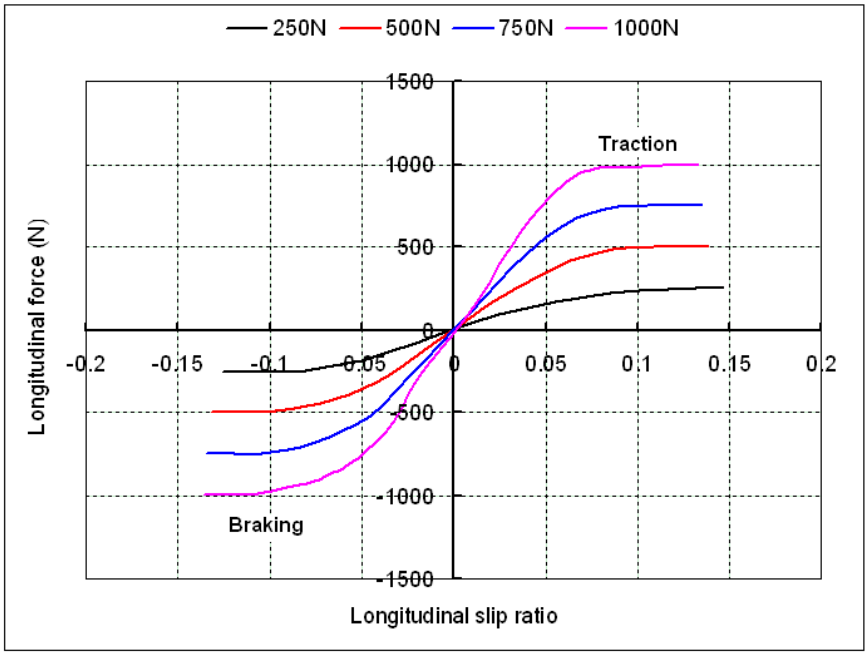

Figure 6.34 Braking/traction Force versus Longitudinal Slip with respect to Different Preloads at Inflation Pressure 80 kPa

Figure 6.35 shows the extracted estimation model for the slip range -0.1~0.1.

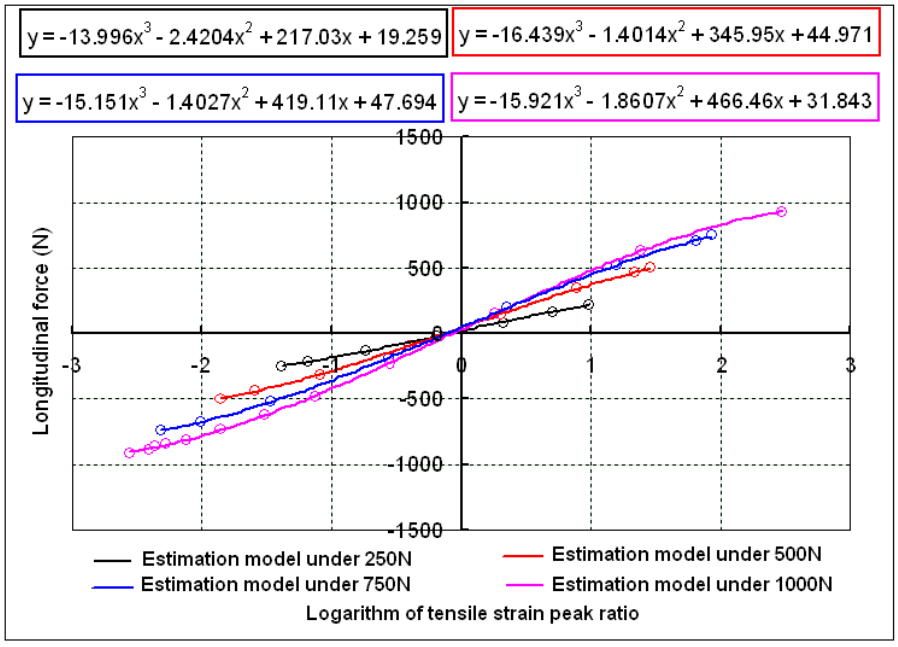

Figure 6.35 Longitudinal Forces versus Tensile Strain Peak Ratio with respect to Different Preloads at Inflation Pressure 80 kPa

The extracted estimation models from different preload conditions were used to estimate the effect of inflation pressure and friction coefficient on tyre longitudinal force and compared with FEA results. The tensile strain peak ratio at 750 N preload, 1.0 friction coefficient and different inflation pressures were substituted into the estimation model and the results are shown in Figure 6.36.

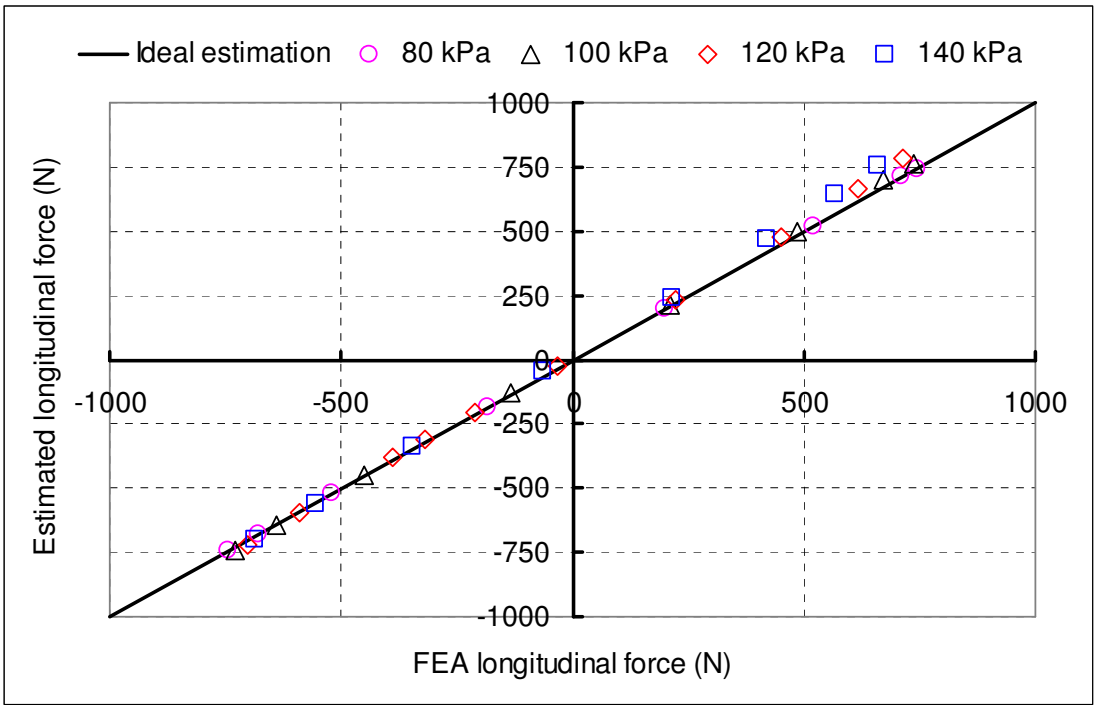

Figure 6.36 Estimated Longitudinal Force versus FEA Longitudinal Force at 750 N Preload, 1.0 Friction Coefficient and Different Inflation Pressures

The tensile strain peak ratio at 750 N preload, 80 kPa inflation pressure and different friction coefficient were substituted into the estimation model and the results are shown in Figure 6.37.

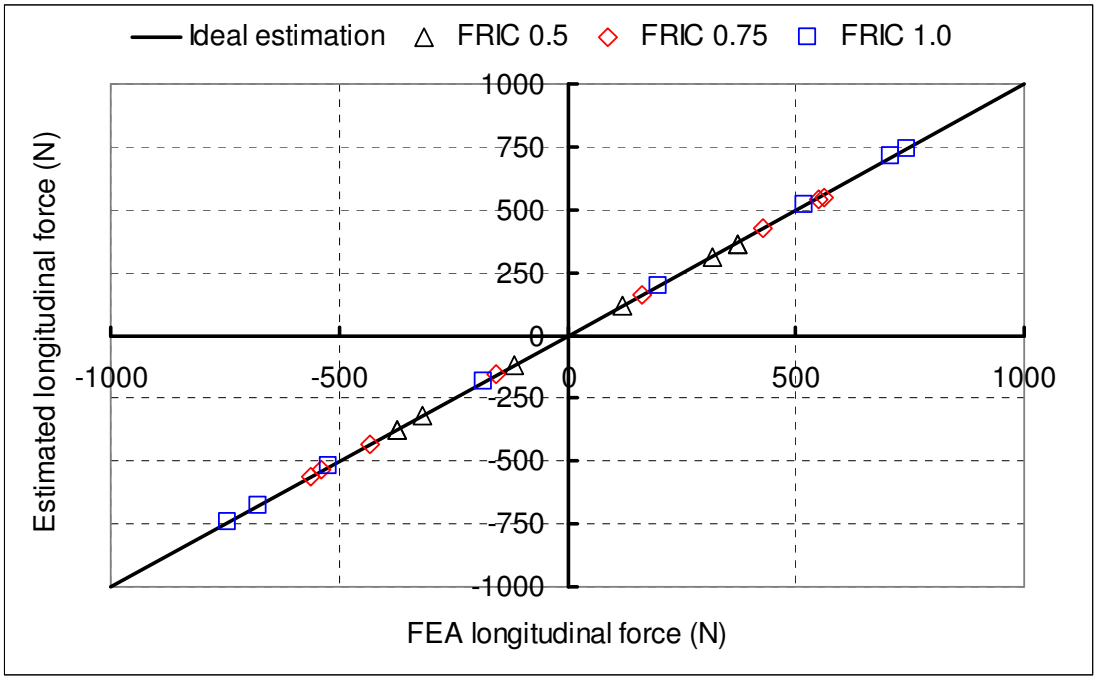

Figure 6.37 Estimated Longitudinal Force versus FEA Longitudinal Force at 80 kPa Inflation Pressure, 750 N Preload and Different Friction Coefficient

It can be seen that the estimation model shows a strong applicability for different inflation pressures and friction coefficients. The estimated results give a reasonable estimation of the longitudinal force compared with the corresponding results from FEA for the inflation pressure range of the tyre used in this study. The maximum error observed on longitudinal force between estimation and FEA is 14.55%, which occurs at 140 kPa, slip ratio 0.115 and 1.0 friction coefficient. However, it was also found that the error on estimating longitudinal force, based on the estimation model, increases with increasing inflation pressure. Therefore, the estimation model needs to be evaluated for larger range of inflation pressure in order to provide accurate estimation.

The above investigation demonstrated that the preload has a dominant effect on extracting tyre longitudinal force estimation model. In addition, there also exist other

methods to extract the estimation model, for example, the estimation model based on the relationship between strain rate difference/ratio and tyre longitudinal force. The estimation method selected here provides for a more efficient real time estimation and is considered a feasible and promising approach for estimating tyre braking/traction force which could serve for the vehicle ABS and TCS system.

6.5.3 TYRE CORNERING BEHAVIOUR

The investigation of tyre cornering behaviour provides the possibility to improve vehicle stability control system based on the estimation of tyre steering force. In this study, a series of tyre cornering tests were carried out on the AEC test rig by applying different slip angles to the tyre to simulate tyre steering as shown in Table 6.1.

Table 6.1 Test Scheme for Steady State Cornering Rolling

Slip Angle α (α=0, 1, 2, 3, 4, 6, 8)			
Pressure=80 kPa		Vertical Load	
V1=10 km/h	500 N	750 N	1000 N
V3=30 km/h	500 N	750 N	1000 N
V5=50 km/h	500 N	750 N	1000 N
Pressure=100 kPa		Vertical Load	
V1=10 km/h	500 N	750 N	1000 N
V3=30 km/h	500 N	750 N	1000 N
V5=50 km/h	500 N	750 N	1000 N
Pressure=120 kPa		Vertical Load	
V1=10 km/h	500 N	750 N	1000 N
V3=30 km/h	500 N	750 N	1000 N
V5=50 km/h	500 N	750 N	1000 N
Pressure=140 kPa		Vertical Load	
V1=10 km/h	500 N	750 N	1000 N
V3=30 km/h	500 N	750 N	1000 N
V5=50 km/h	500 N	750 N	1000 N

The tyre cornering forces generated at 80 kPa inflation pressure, 30 km/h speed and different vertical loads were compared with the corresponding FEA results as shown in Figure 6.38. The cornering behaviour at each slip angle was achieved separately in FEA by applying longitudinal velocity and axial velocity on the tyre to simulate the slip effect where the ratio between the axial velocity and the longitudinal velocity is equal to the tangent of the corresponding slip angle.

As can be seen, the cornering force increases rapidly with increasing slip angle for small slip angles range. With the slip angle increasing, the cornering force reaches a stable level that the friction on the tyre contact patch can sustain. Further increase of slip angle does not produce higher cornering force. The vertical load has a significant effect on the lateral force generated during the tyre cornering process.

It should be noted that during FEA the friction coefficient is chosen after several iterations in order to obtain reasonable comparison since the tyre/drum contact friction coefficient is unknown as shown in Figure 6.39.

It can be seen that the stable level of tyre cornering force predicted by FEA is approximately equal to the value of vertical load multiplied by the friction coefficient. The predicted cornering force with respect to different slip angles shows a global similarity in trend and level with the test results.

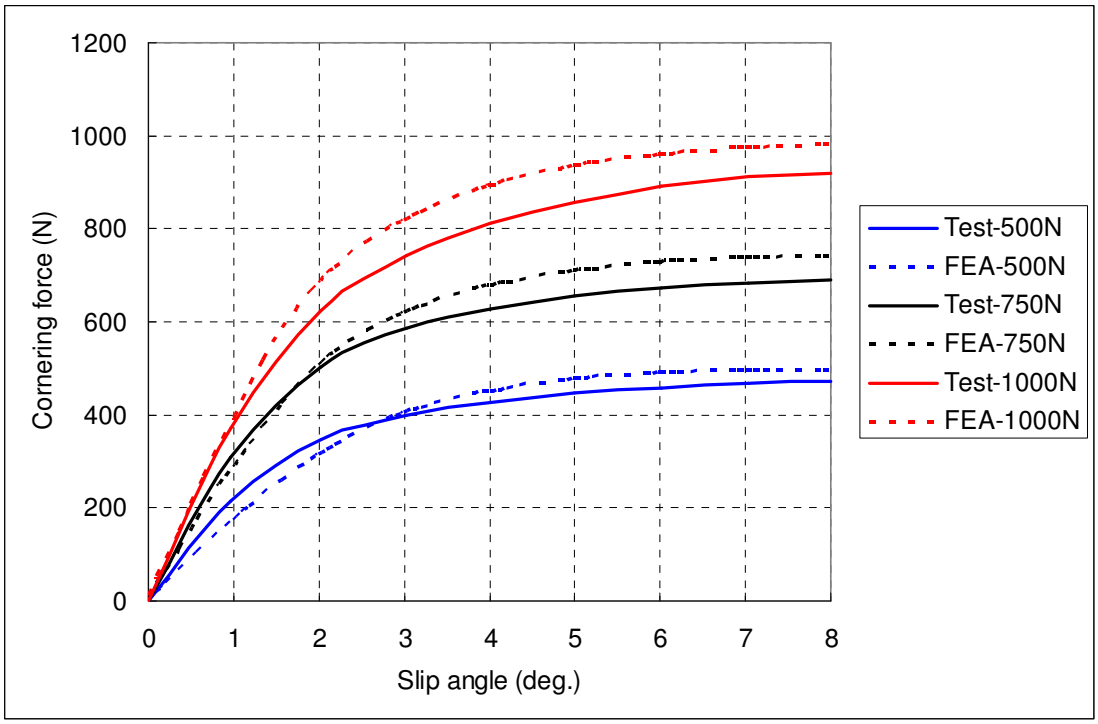

Figure 6.38 Comparison of Cornering Force between Test and FEA at 80 kPa Inflation Pressure, 1.0 Friction Coefficient and 30 km/h Speed.

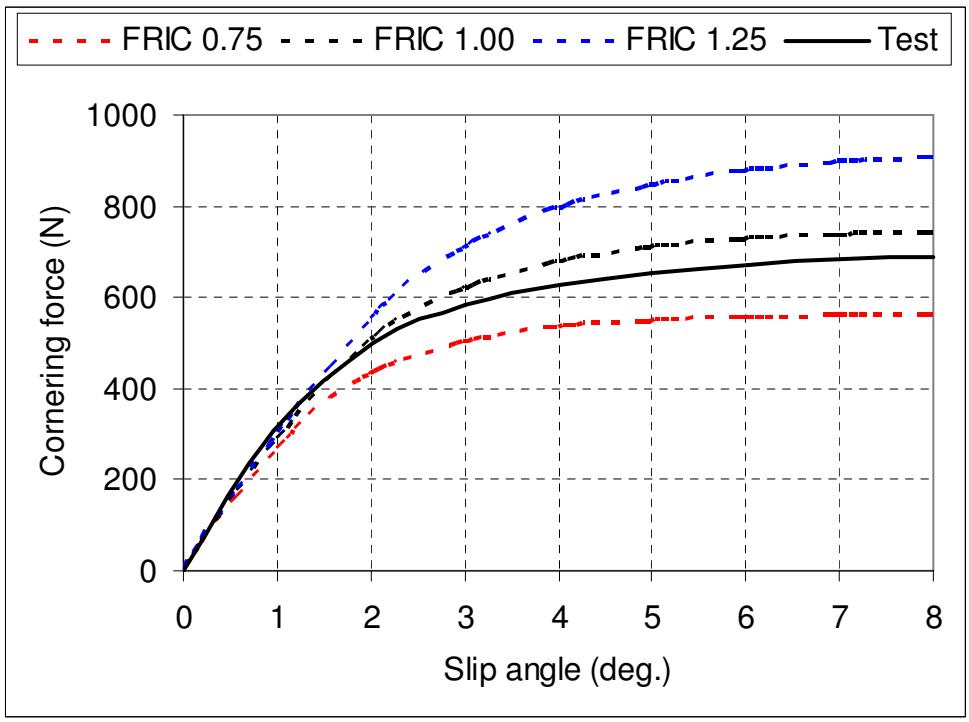

Figure 6.39 Effect of Friction Coefficient on Tyre Cornering Force at 750 N Preload, 80 kPa Inflation Pressure and 30 km/h Speed

Due to the cornering effect, the tyre contact pressure concentration shifts to the outer side of the tyre contact patch region as shown in Figure 6.40 , which leads to the redistribution of related shear stress and the variation of lateral strain across the width of the tyre contact patch including its edge regions. As a result of this, the tensile lateral strain peak on the outer side of the tyre increases and the value on the inner side decreases. These features can be captured by the tensile lateral strain peaks ratio between outer side and inner side.

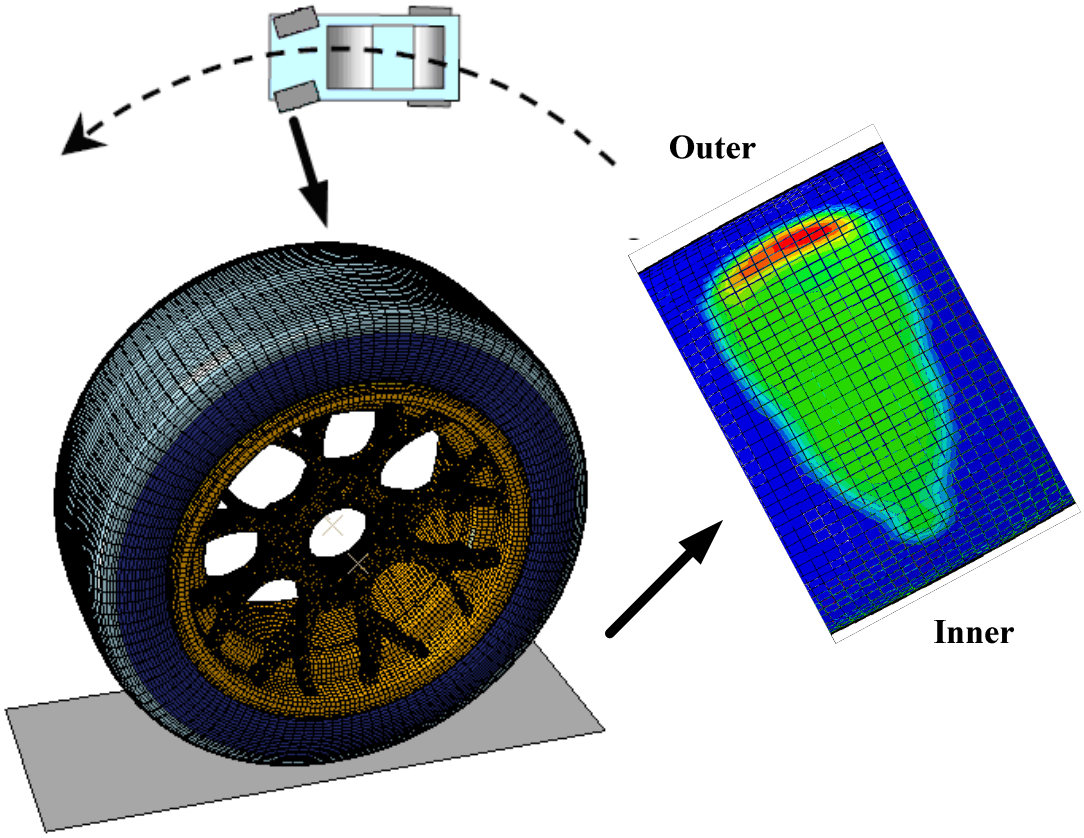

Figure 6.40 Contact Pressure Distributions under Steering with Pure Slip Angle

The tyre cornering force estimation models were established by extracting the relationship between tyre tensile lateral strain ratio and tyre cornering force from FEA as shown in Figure 6.41 .

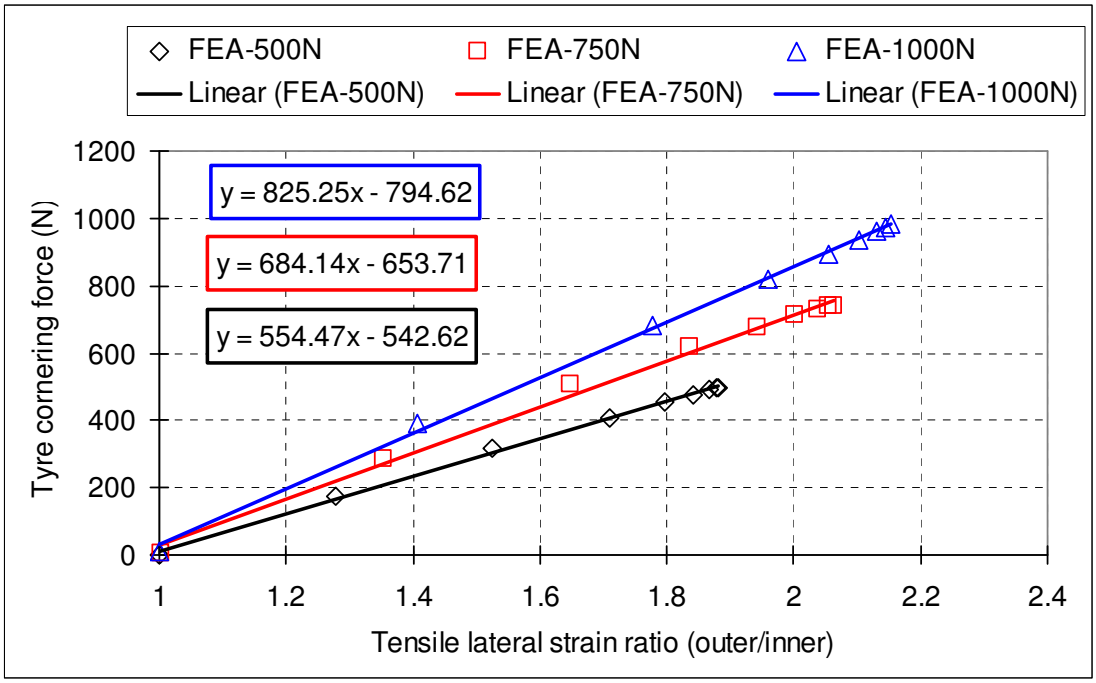

Figure 6.41 Extraction of Tyre Cornering Force Estimation Model based on FEA at 80 kPa Inflation Pressure, 30 km/h Speed and Different Preloads

Then, the tensile lateral strain ratios obtained from tests were substituted into the estimation models to estimate the test cornering forces as shown in Figure 6.42.

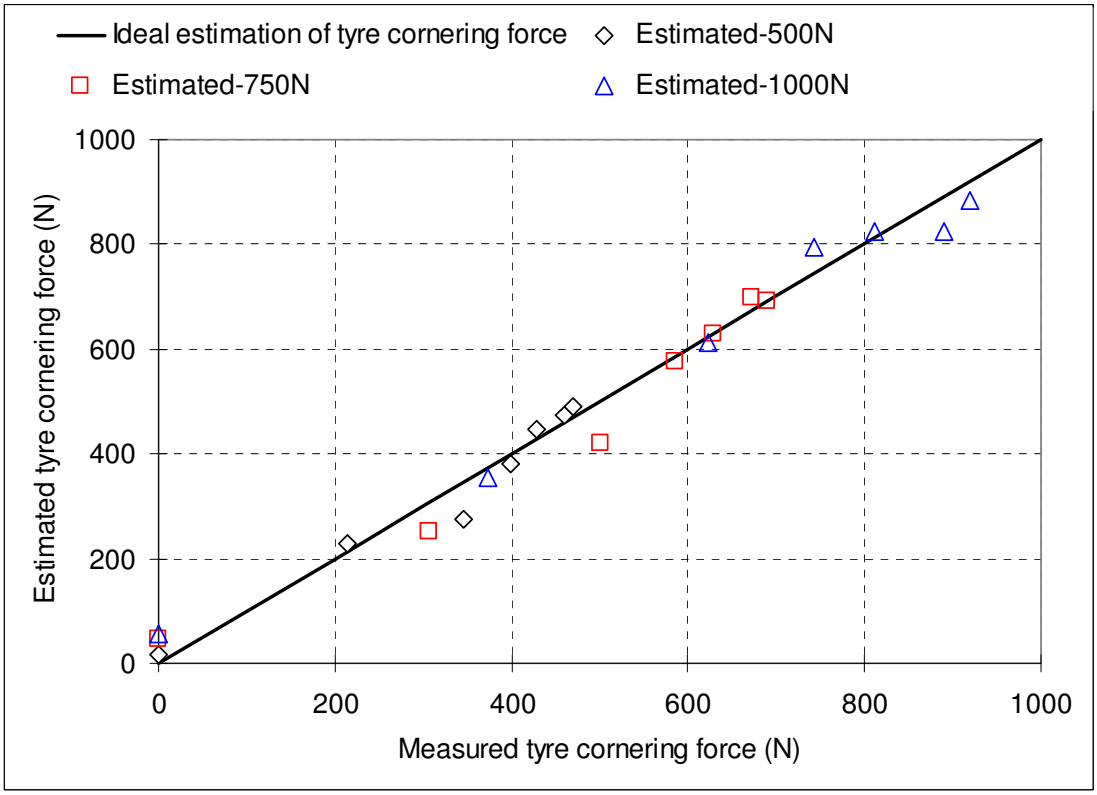

Figure 6.42 Tyre Cornering Force Estimation at 80 kPa Inflation Pressure, 30 km/h Speed and Different Preloads

Figure 6.42 shows a good agreement between the estimated tyre test cornering forces and the ideal estimation of tyre cornering forces.

The results presented in this chapter have shown that Finite Element Analysis is capable of quite accurate prediction of tyre behaviour under both static and dynamic conditions. It is therefore an efficient replacement for physical tyre tests which can be both expensive and time consuming. Moreover the difficulties in measuring tyre strains for different tyre operating conditions have been demonstrated in this study. In light of the large number of tests that would be required for developing a tyre force estimation model, FEA is considered a feasible and suitable choice for developing tyre force estimation model, such as the tyre cornering force estimation model extracted from the

validated finite element tyre model. However, in order to achieve a universal estimation algorithm for estimating tyre cornering force at different tyre preloads, inflation pressures, rolling speeds and slip angles to serve the vehicle dynamics control system in real time, more effort will be required to build upon the preliminary estimation models achieved in this chapter. This will be further discussed in Section 6.6.

Furthermore, as described in Chapter 2, the application of camber to a tyre generates camber thrust at the tyre/road contact patch resulting in lateral force on the tyre. The effect of camber angle on tyre contact patch pressure is shown in Figure 6.43.

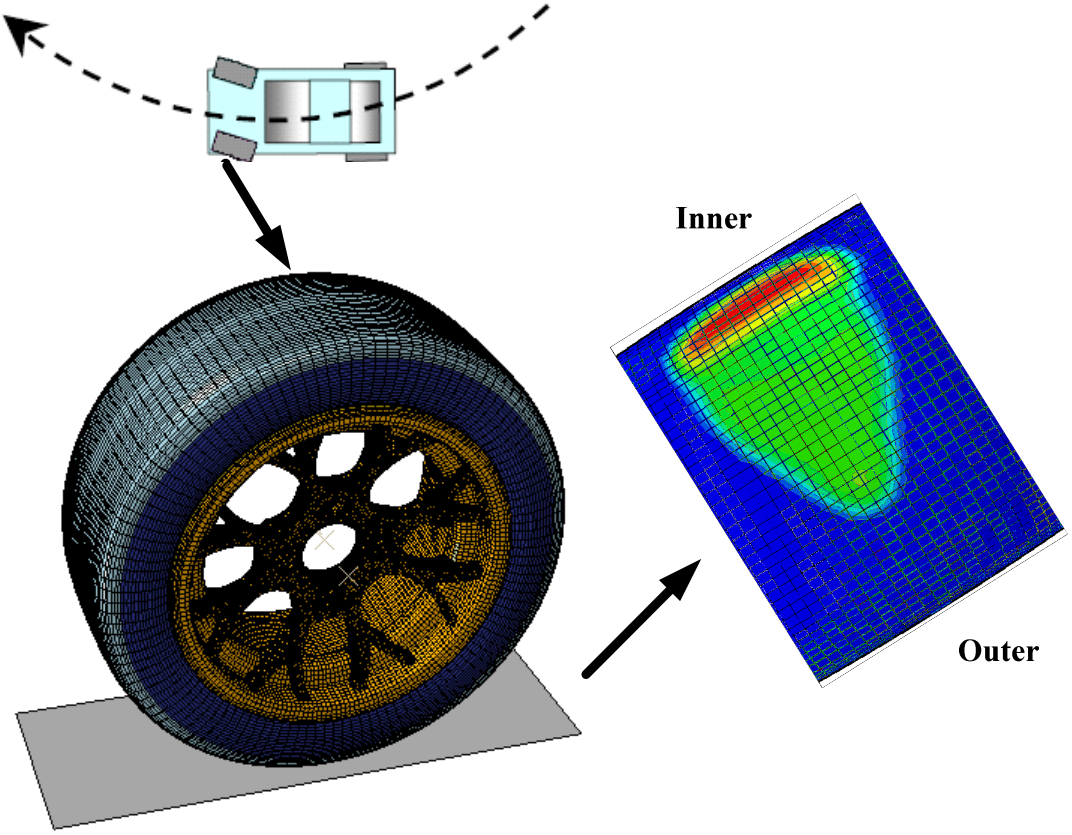

Figure 6.43 Contact Pressure Distributions under Steering with Pure Camber Angle

It can be found from Figure 6.40 and Figure 6.43 that the cornering force is generated under the superimposed effect of slip angle and camber angle during tyre cornering. The finite element tyre model herein can also be used to study the complex tyre behaviour in place of tests to estimate the effect of camber angle on tyre cornering force. The correlation between the tensile lateral strain ratio and tyre cornering force caused by combined slip angle and camber angle is shown in Figure 6.44.

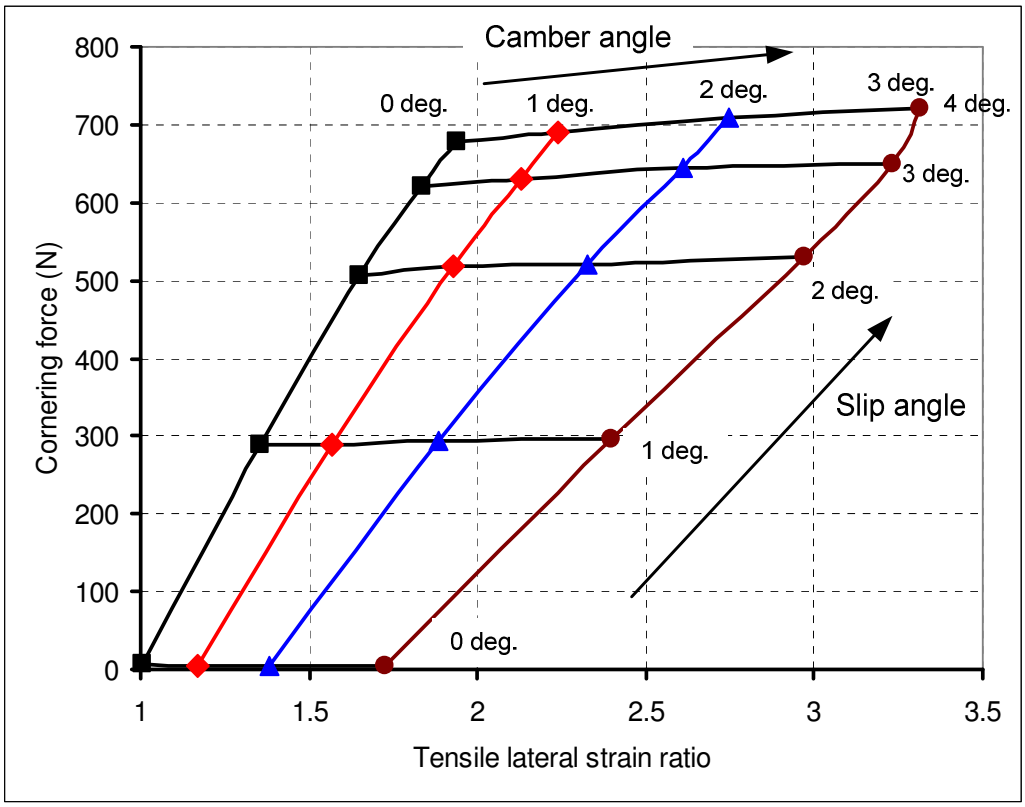

Figure 6.44 Effect of Combined Slip Angle and Camber Angle on Tyre Cornering Force Estimation

It is shown that the involvement of camber angle translates the correlation curve to the larger tensile lateral strain ratio and cornering force with the increase of camber angle. Thus the camber angle effect can be estimated from the mapping relationship.

6.6. DISCUSSION AND SUMMARY

As discussed in the previous section, the execution of physical tests on a tyre can be quite expensive, difficult and time consuming, and the measurement and transmission of strain data presents it own challenges. However, the finite element tyre model provides a reliable and relatively more convenient solution for predicting tyre local and global behaviours. In this study, some features of the strain waveform were captured by finite element tyre model, and were then utilized to estimate tyre operating conditions. However there still exist discrepancies between the strain waveforms from test and FEA results.

The general procedure illustrating the application of tyre force estimation models in the intelligent tyre is shown in Figure 6.45.

As can be seen from Figure 6.45, the currently achieved estimation models in this thesis still require additional inflation pressure information from TPMS and friction coefficient information because the measured strain features result from the combined effects of different tyre parameters which are difficult to decompose. The possible solution to decompose the combined effects is to select special strain sensor location [109] or involve sidewall strain measurement [101]. To some extent, the multi-input method viz. involving measured strain features from both tyre contact patch and tyre sidewall could provide for better reliability and precision of the extracted estimation models. However, in order to estimate the tyre working parameters during real tyre service, the estimation model needs to be based on a time-varying response rather than steady-state response of the tyre. Therefore, a universal estimation model based on time-

varying response is necessary in order to achieve a practical application. The universal estimation model could be obtained based on look-up tables by interpolating the existing formulas which are based on steady-state response. However, considering the complexity of real tyre working conditions as well as the inadequacy of the current formula-based estimation model, an intelligent algorithm based on techniques such as artificial neural network and fuzzy logic may provide the solution to deal with such complicated situations. This is the main task in future work.

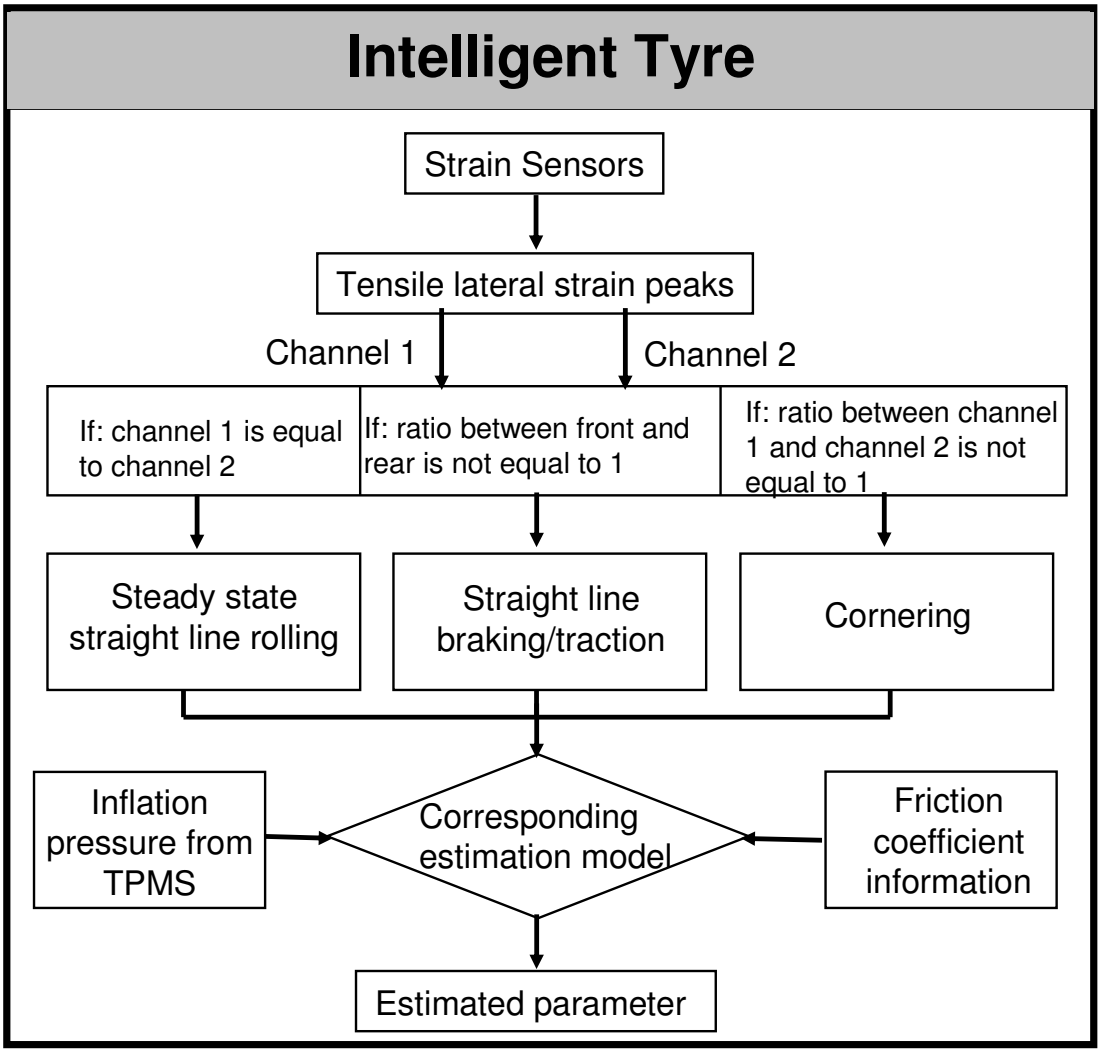

Figure 6.45 General Procedure of the Application of Tyre Force Estimation Models

According to the work of Morinaga, H., et al. [3] and Ryosuke Matsuzaki [164], both the tyre contact patch length and deformation length can also be extracted from the strain time history and used to construct the relationship with tyre preload, inflation pressure and cornering force, which can be considered as an alternative to the method based on the tensile lateral strain studied in this chapter. However, because the contact patch length is calculated from the differential of strain in the time domain, the requirement on the continuity of test strain data is strict. Therefore, there is a need for adequate test strain data, and post processing of these data, such as curve fitting, is necessary in order to get accurate and comparable calculation results. It is unlikely that this can be achieved in real time.

For the strain-based intelligent tyre experiment, although the prototype system described above is suitable for the feasibility study of the intelligent tyre system, the limitation regarding the power supply, communication and sensor are apparent. As a prototype system, the design of the strain-based intelligent tyre system is quite basic and the size of it is large. Three main aspects of the system can be improved in order to achieve an advanced intelligent tyre system for commercialization. These are the sensor technology, the power supply and the communication interface.

The strain sensor utilized in the advanced intelligent tyre system should be capable of measuring large strain generated during different tyre working conditions. The strain sensor attached to the tyre surface or embedded into tyre rubber should not behave as a filter of the signal or stiffen the local surface. For example, Ryosuke Matsuzaki introduced a patch-type strain sensor made from soft material [164]. Multi-sensors

should be supported by the data acquisition system. From the commercial point of view, the strain sensor should be cheap and highly durable, i.e. it should be able to withstand very high static and dynamic stresses.

The large volume, weight and limited battery life of the SoMat 2000 Field Computer system is not suitable for online monitoring of a rolling tyre. The measurement range of SoMat 2000 Field Computer strain gauge module is still small considering the possible large deformation of the tyre. Moreover, the communication interface of the SoMat 2000 Field Computer is not wireless which makes the online monitoring impossible. The cable packing still needs further integration.

In order to overcome these problems, a small size, self-powered, wireless communication and robust strain-based intelligent tyre is under development by the author's colleague in the School of Mechanical Engineering in the University of Birmingham. Initial trials to validate the self-powered design for measuring tyre inflation pressure and temperature have been successfully achieved. The proposed advanced intelligent tyre system working diagram is shown in Figure 6.46.

In the advanced strain-based intelligent tyre system, the flexible strain sensor such as the one mentioned in [164] could be utilized and integrated into the tyre during the tyre vulcanizing process. Three different methods including battery, solar energy harvesting and piezo power generator are available for supplying power to the advanced strain-based intelligent tyre system.

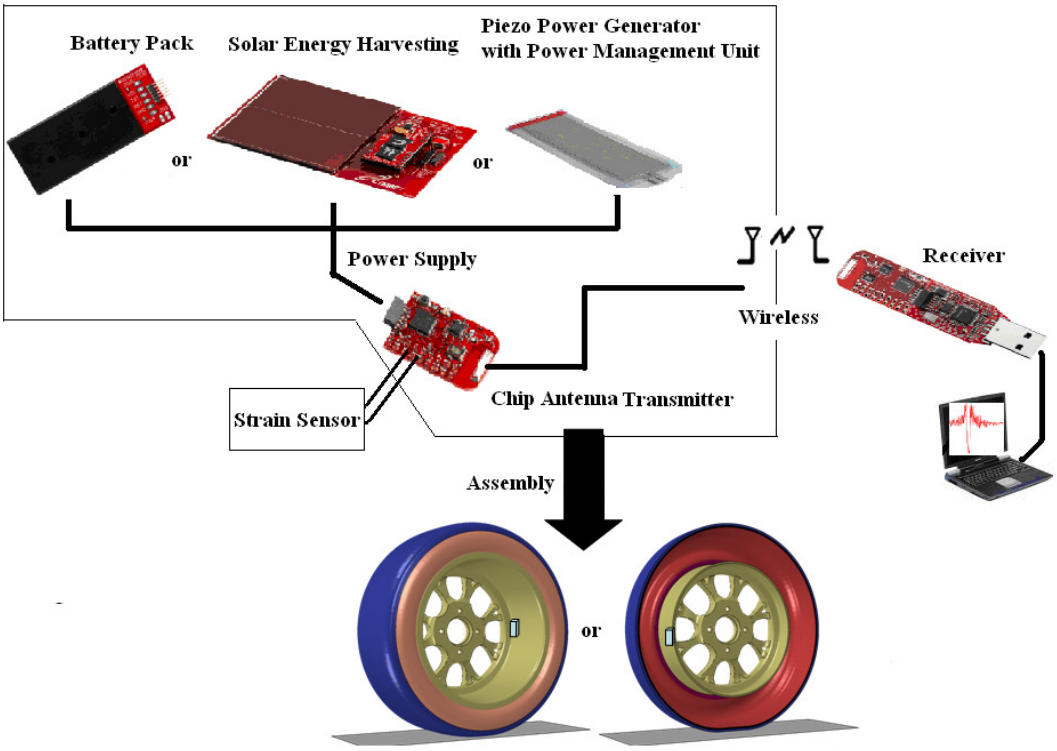

Figure 6.46 Proposed Advanced Strain-based Intelligent Tyre System

The prototype of advanced strain-based intelligent tyre under development adopts a small size piezo power generator which generates power from the deformation of the rolling tyre. Relevant trials have been carried out in the lab to demonstrate that the piezo power generator can produce enough power to supply the whole system. A power manager/regulator is used to stabilize the output of the piezo power generator. A commercial small-sized device was selected for wireless transmitter and receiver, which was demonstrated to be robust enough to protect the signal transmission from the interference of the tyre structure and working environment [165].

As a summary, in this Chapter, the characteristics of tyre strain waveform have been introduced firstly in order to be used for the estimation of tyre working conditions. The

strain-based intelligent tyre prototype was created in the lab with two lateral strain sensors located on the inner liner surface of the tyre tread. A series of tests for tyre steady state straight line rolling and cornering rolling were carried out and the corresponding strain data were collected. In order to obtain a reliable finite element tyre model which is capable of providing computationally efficient and effective prediction of tyre strain and global behaviour, some guidance notes about tyre finite element analysis were presented. The strain data from FEA were compared with test results, and then used to correlate with tyre working conditions such as tyre angular velocity, preload, inflation pressure, braking/traction force and cornering force. As physical testing is a very difficult and expensive way to obtain all the data necessary for developing the algorithms for the relationship between tyre strain and tyre working conditions, tyre FEA provides an accurate prediction and is an appropriate tool to use in place of testing. From both the test and FEA, it has been demonstrated that the extracted features from tyre strain waveform possess great potential for developing intelligent tyre estimation model.

CHAPTER 7

CONCLUSIONS AND FUTURE WORK

With the increasing demand for tyre working condition information for developing accurate vehicle dynamics control system and advanced vehicle active safety system, the comprehensive understanding of tyre behaviour in the tyre contact patch supported by intelligent tyre technology presents a possible solution. The study herein thus proposed an effective and efficient method using finite element tyre model, complemented by experiment, to give an insight into the relationship between tyre strain feature and tyre forces. It is expected that these relationships could be used to estimate tyre behaviour and working parameters and then serve for optimising vehicle dynamics control system and providing tyre warning information for the driver.

7.1. CONCLUSIONS

In this study, a comprehensive overview about the popularity of finite element tyre model and the development of intelligent tyre system was presented. Most of the studies reported in the literature on the development of intelligent tyre technology are mainly focused on experiments which are not time and cost efficient. Only a few of these studies are based on finite element analysis. Considering the potentially huge market of the intelligent tyre in future, a research on the development of intelligent tyre system utilizing a combination of experiments and finite element analysis was proposed in this thesis. After evaluating the pros and cons of different existing and potential intelligent tyre technologies, a strain-based intelligent tyre system was developed to generate the

test results for comparison with the predicted results from finite element tyre model. The finite element tyre model was developed using finite element code ABAQUS considering the advantages it offers over other FE codes on modelling tyre complex material property and geometry.

Three contributions resulting from the research reported in this thesis are listed as follows:

1. An efficient experiment method was developed for obtaining tyre material properties with limited test facilities and without material specimen support from tyre manufacturers.

2. A novel image-based tyre structure modelling method was developed. This enables the tyre structure lay-up to be determined from images of tyre cross-section where tyre structural details are not available from tyre manufacturers.

3. The link between tyre strain features and tyre mechanical properties such as forces were established based on experiment and finite element analysis. Further, tyre force estimation models were developed based on tyre strain measurement which could provide useful information for vehicle chassis control system.

More details about the three contributions are explained as follows.

1. The use of accurate tyre material properties is a major requirement for conducting a successful tyre analysis using the finite element method. Obtaining these material properties however poses a major challenge for tyre modellers and researchers due to

the complex nature of tyre material and associated proprietary protections of constituent material properties by tyre manufactures. In view of this limitation, a simple and effective procedure for generating tyre materials data used in tyre finite element analysis (FEA) was developed during this study and is the subject of a paper published in the SAE International Journal of Materials and Manufacture [166]

2. A fundamental requirement for tyre modelling process is accurate and adequate information about the tyre cross-section, especially the composite structure, before further procedures of FEA can be carried out. Although many papers have been published on the use of FEA to investigate tyre behaviour using 3D tyre model, the procedure for obtaining geometric data of the tyre cross-section is generally not revealed. Furthermore, out of commercial considerations, most tyre manufacturers will not provide the structural details of their tyre products. In order to satisfy the demands of FEA and overcome the barrier of minimal or no supporting information from tyre manufacturers, an image based technique was developed to obtain the geometric data of a tyre cross-section by scanning images of a cut cross-section, which is able to provide an accurate description of the profile of the tyre cross-section and the locations of ply lines and cord-ends [167].

3. Tyre dynamic strain data were obtained from tests on a rolling tyre as well as from FE simulation. The extracted features of strain waveform from both the test and FEA were compared and used to set up relationships with the tyre mechanical properties such as forces in order to provide the estimation model for developing intelligent tyre technology. Furthermore, the finite element tyre model was also used to simulate tyre

braking/traction and the tyre cornering caused by combined slip angle and camber angle. The relationship between the strain features and tyre mechanical parameters revealed the versatile functions and potential of the strain-based intelligent tyre system for optimising vehicle dynamics control system in future.

7.2. FUTURE WORK

Although the study presented in this thesis demonstrated that the finite element tyre model is capable of providing reasonable prediction of tyre behaviour for the development of intelligent tyre technology, there still exist some limitations that need to be overcome such as the disparity between predicted and measured contact patch length. Meanwhile, further improvements for both model and experiment need to be made in order to achieve an accurate estimation of tyre mechanical parameters. Consequently, the future work needs to consider two main aspects: finite element tyre model and experiment.

7.2.1 FE TYRE MODEL FUTURE WORK

It was found that the finite element tyre model developed in this work is deficient on predicting tyre local behaviour such as strain, even though it can give a good agreement in tyre global behaviour. Apart from the difference between tyre model and real tyre, the nonlinear rubber material property model generated from simple tensile test and used in this study cannot simulate these situations properly. This drawback can be overcome by re-modelling the rubber behaviour utilizing compressive and even biaxial test data. Likewise, the viscoelastic material property and hysteresis behaviour of rubber are also

needed to be modelled, which benefits the investigation of tyre dynamic response as well.

With the increase of tyre rolling speed, another issue arises, the increase of tyre temperature which leads to a larger volume of air in tyre, i.e. increasing tyre inflation pressure. This phenomenon has been observed during testing. In order to mimic this situation, the thermal dependent material property needs to be involved and the fluid cavity function in ABAQUS can be used to simulate the variation of tyre inflation pressure due to the change of tyre air volume.

It is known that the tyre contact patch includes an adhesion region and a sliding region for a rolling tyre. In this study, the contact patch property, i.e. the friction model is a simple coulomb friction model which cannot represent the complex behaviour occurring in the contact patch properly. It is suggested that a complex friction model or user subroutine is adopted in future work to get a better simulation of tyre contact behaviour. Moreover, since the road conditions such as water, soil and snow also influence the tyre/road contact behaviour, the special designed road models are needed for these road conditions such as the model introduced in section 4.4 of Chapter 4.

7.2.2 EXPERIMENT FUTURE WORK

Although the AEC tyre test rig is capable of simulating several tyre working conditions and providing reasonable vertical and lateral force measurement, some deficiencies were also observed in the past tests. Some vibrations were detected in the rolling drum which affects the tyre response, especially the local behaviour measurement. A

refurbishment of the AEC tyre test rig is desirable to improve the accuracy of measurement.

Furthermore, during the cornering test, the slip angle was applied by tuning the tyre angle manually and then measured the angle by angle gauge. Once the slip angle was set, the test would be running and the lateral force was recorded. Therefore, the slip angle increment is restricted considering the measurement precision. And the whole test procedure of tyre cornering involves iterative tune and measurement. An automatic operation system which can dynamically tune the tyre slip angle (and camber angle) and record the tyre response automatically is desirable. In this way, the test results can be more consistent and accurate.

Since the braking/traction is a very important tyre behaviour during driving, the addition of a braking/traction device to the test rig would greatly contribute to the measurement and estimation of tyre braking/traction force.

To change the road condition, a number of road surfaces would have to be manufactured and added to the steel drum surface. The harsh road condition would introduce noise into the measured strain waveform data, thus the noise need to be filtered by hardware or software.

Other aspects of the experiment future work are about the intelligent tyre prototype system. As mentioned in Chapter 6, a small-size and advanced self-powered, data acquisition system with wireless transmission is under development in the lab. The

wireless transmitter is capable of sending data signals through the tyre body structure to the receiver meters away. The self-powered system is capable of generating power from the tyre dynamic deformation, obviating the need for batteries and guaranteeing unlimited service life. The requirements of the strain sensor are high durability, adequate sensitivity and measurement range to capture the cyclic deformation of the rolling tyre. A higher data sampling rate can be utilized to ensure better capture of the strain waveform since data volume will no longer be limited by memory. Bi-axial strain measurement on inner liner surface of the tyre tread as well as sidewall would be implemented to identify the relationship between the tyre strain and tyre mechanical parameters systematically. Apart from strain sensors, other sensors such as inflation pressure sensor and temperature sensor can be integrated into the prototype system for better evaluating the system performance.

The last but not the least, a "smart" and robust estimation model (or algorithm) would have to be developed based on the relationship between the tyre strain waveform features and tyre working conditions. Different potential approaches are available including data look-up table, nonlinear regression formulation and intelligent algorithm, etc. Considering the complex and combined effect of tyre working conditions on tyre strain waveform and the impact of road irregularities, an artificial intelligence based algorithm such as fuzzy logic and artificial neural network (ANN) is thought to be a likely choice. Once the above improvements have been achieved using the advanced intelligent tyre prototype system on the indoor tyre test rig, further field tests would have to be implemented on real cars. At present, the advanced intelligent acquisition system is under test with different sensors.

LIST OF REFERENCE

1. Andrzejewski, R., Awrejcewicz, J., *Nonlinear Dynamics of A Wheeled Vehicle*. 2005, New York: Springer.
2. The TREAD Act, http://www.tireindustry.org/pdf/TREAD_Act_Summary.pdf.
3. Morinaga, H., Wakao, Y., Hanatsuka, Y., and Kobayakawa, A., *The Possibility of Intelligent Tire (Technology of Contact Area Information Sensing)*, in *FISITA*. 2006.
4. Morinaga, H., *Sensor-incorporated Tire and Tire Condition Estimating Method*, in *United States Patent*. 2009.
5. Nagaya, G., *Method for Estimating Tire Slip Angle and A Tire with Sensors Mounted Therein*, in *United States Patent*. 2009.
6. *APOLLO Project Report "Final Report Including Technical Implementation Plan (Annex) Deliverable 22/23"*. 2005.
7. Matsuzaki, R., Todoroki, A., *Intelligent Tires Based on Measurement of Tire Deformation.* Journal of Solid Mechanics and Materials Engineering, 2008. **2**(2): p. 269-280.
8. Ryosuke, M., Naoki, H., Akira, T., and Yoshihiro, M., *Analysis of Applied Load Estimation Using Strain for Intelligent Tires.* Journal of Solid Mechanics and Materials Engineering, 2010. **4**(10).
9. Krithivasan, V., Green, R., Jackson, R., and Choe, S.-Y., *Development of Measurement Algorithms of Tire States by Tire Deformations Study*. 2011, Auburn University.
10. Burke, A.M., *Finite Element Simulation and Experimental Analysis of Stationary and Roatating Tyre Behaviour*, in *Mechanical Engineering*. 1998, University of Birmingham: Birmingham.
11. Bolarinwa, E.O., *Investigation of the Dynamic Characteristics of Radial Tyre using the Finite Element Method*, in *Mechanical Engineering*. 2004, University of Birmingham: Birmingham, UK.
12. Pacejka, H.B., *Tyre and Vehicle Dynamics*. 2nd ed. ed. 2006, Oxford: Elsevier.
13. Zegelaar, P.W.A., *The Dynamic Response of Tyres to Brake Torque Variations and Road Unevennesses*. 1998, Delft University of Technology: Delft. p. 315 p.

14. Hall, W., *Finite Element Modelling and Simulation for a 'Smart' Tyre*, in *School of Engineering*. 2003, University of Warwick: Warwick.
15. Thieme, H.v.E., Dijks, A.J., *Measurement of Tire Properties*, in *Mechanics of Pneumatic Tires*, Clark, S.K., Editor. 1981, U.S. Department of Transportation. National Highway Traffic Safty Administration. p. 541-720.
16. Ridha, R.A., Clark, S.K., *Tire Stress and Deformation*, in *Mechanics of Pneumatic Tires*, Clark, S.K., Editor. 1981, U.S. Department of Transportation. National Highway Traffic Safty Administration. p. 475-540.
17. Ramji, K., Goel, V.K., and Saran, V.H., *Stiffness Properties of Small-sized Pneumatic Tyres.* Proceedings of the Institution of Mechanical Engineers Part D: Journal of Automobile Engineering, 2001. **216**: p. 107-114.
18. Loeb, J.S., Guenther, D.A., Chen, H.-H.F., and Ellis, J.R., *Lateral Stiffness, Cornering Stiffness and Relaxation Length of the Pneumatic Tire.* SAE International, 1990. **900129**.
19. Ellis, J.R., *Vehicle Handling Dynamics*. 1994, London: Mechanical Engineering Publications Limited.
20. Chow, C.L., Woo, C.W., *The Effect of Inflation Pressure and Vehicle Loading on the Sidewall of A Radial Tire.* Experimental Mechanics, 1980. **20**(5): p. 379-385.
21. Sokolov, S.L., *Calculation of the Stress-Strain State of Pneumatic Tires by the Finite Element Method.* Journal of Machinery Manufacture and Reliability, 2007. **36**(1): p. 45-49.
22. Wang, T.M., Daniel, I.M., and Huang, K., *Stress Analysis of Tire Sections.* Tire Science and Technology, TSTCA, 1996. **24**(4): p. 349-366.
23. Biderman, V.L., Drozhzhin, P.K., Pugin, V.A., and Shchaveleva, V.F., *Experimental Investigation of Deformations in Elements of Pneumatic Tires.* Transactions Tire Research Institute, 1957. **3**: p. 5-15.
24. Biderman, V.L., Pugin, V.A., *Wire Strain Gauge for Measurements of Large Deformation (Ruassian)* Zavodskaya Laboratoriya, 1958. **24**(7).
25. Woolley, R.P., Hurry, J.A., *High Range Strain Gage*. 1956: U.S. 2739212.

26. Moser, R., Lightner, J.G., *Using Three-dimensional Digital Imaging Correlation Techniques to Validate Tire Finite-Element Model.* Experimental Techniques, 2007. **31**(4): p. 29-36.
27. Jazar, R.N., *Vehicle Dynamics: Theory and Application*. 2008, New York: Springer.
28. Gillespie, T.D., *Fundamentals of Vehicle Dynamics*. 1992, Warrendale: Society of Automotive Engineers, Inc.
29. Pacejka, H.B., Sharp, R.S., *Shear Force Development by Pneumatic Tyres in Steady State Conditions: A Review of Modelling Aspects.* Vehicle System Dynamics, 1991. **20**(3&4): p. 121-175.
30. Wong, J.Y., *Theory of Ground Vehicles*. 2001: Wiley and Sons.
31. Milliken, W.F., Milliken, D.L., *Race Car Vehicle Dynamics*. 1995, Warrendale: Society of Automotive Engineers, Inc.
32. Muller, S., Uchanski, M., and Hedrick, K., *Estimation of the Maximum Tire-Road Friction Coefficient.* Journal of Dynamic Systems, Measurement, and Control, 2003. **125**: p. 607-617.
33. Narby, E., *Modeling and Estimation of Dynamic Tire Properties*, in *Department of Electrical Engineering*. 2006, Linkopings Universitet: Linkoping.
34. Tighe, S., Li, N., Falls, L.C., and Haas, R., *Incorporating Road Safety into Pavement Management.* Journal of the Transportation Research Boad, 2007. **1699/2000**: p. 1-10.
35. Eichhorn, U., Roth, J., *Prediction and Monitoring of Tyre/Road Friction*, in *XXIV FISITA Congress*. 1992: London. p. 67-74.
36. Breuer, B., Eichhorn, U., and Roth, J. *Measurement of Tyre/Road Friction Ahead of the Car and Inside the Tyre*. in *International Symposium on Advanced Vehicle Control*. 1992.
37. Ivanov, V., Shyrokau, B., and Siakhovich, V., *Road Identification for Its Integrated Systems of Automotive Active Safety.* Transport, 2005. **XX**(2): p. 55-61.
38. Sandberg, U., Ejsmont, J.A., *Tyre/Road Noise Reference Book*. 2002, Kisa, Sweden: Informex.

39. Umeno, T., *Estimation of Tire-Road Friction by Tire Rotational Vibration Model.* R&D Review of Toyota CRDL, 2002. **37**(3).
40. Gustafsson, F., *Monitoring Tire-Road Friction Using The Wheel Slip*, in *IEEE Control Systems Magazine*. 1998. p. pp42-49.
41. Liu, C.-S., Peng, H., *Road Friction Coefficient Estimation For Vehicle Path Prediction.* Vehicle System Dynamics, 1996. **25**(1): p. 413--425.
42. Pasterkamp, W.R., Pacejka, H.B., *The Tyre as a Sensor to Estimate Friction.* Vehicle System Dynamics, 1997. **27**: p. 409-422.
43. Yamazaki, S., Furukawa, O., and Suzuki, T., *Study on Real Time Estimation of Tire to Road Friction.* Vehicle System Dynamics Supplement, 1997. **27**: p. 225-233.
44. Matusko, J., Petrovic, I., and Peric, N., *Neural Network Based Tire/Road Friction Force Estimation.* Engineering Application of Artificial Intelligence, 2008. **21**(3): p. 442-456.
45. Erdogan, G., Hong, S., Borrelli, F., and Hedrick, K., *Tire Sensors for the Measurement of Slip Angle and Fricition Coefficient and Their Use in Stability Control Systems*, in *SAE 2011 World Congress & Exhibition*. 2011, SAE International: Detroit, MI, USA.
46. Lugner, P., Pacejka, H., and Ploche, M., *Recent Advances in Tyre Models and Testing Procedures.* Vehicle System Dynamics, 2005. **43**(6-7): p. 413-436.
47. Captain, K.M., Boghani, A.B., and Wormley, D.N., *Analytical Tire Models for Dynamic Vehicle Simulation.* Vehicle System Dynamics, 1979. **8**(1979): p. 1-12.
48. Pacejka, H.B., Baker, E., *The Magic Formula Tyre Model.* Vehicle System Dynamics, 1992. **21**(1): p. 1-18.
49. Pacejka, H.B., Besselink, I.J.M., *Magic Formula Tyre Model with Transient Properties.* Vehicle System Dynamics, 1997. **27**(1): p. 234-249.
50. Burke, A.M., Olatunbosun, O.A., *New Technologies in Tyre Modal Analysis using MSC/NASTRAN.* International Journal of Vehicle Design, 1997. **18**(2): p. 203-212.
51. Burke, A.M., Olatunbosun, O.A., *Static Tyre/Road Interaction Modelling* Meccanica, 1997. **32**(5): p. 473-479.

52. Olatunbosun, O.A., Burke, A.M., *Finite Element Modelling of Rotating Tires in the Time Domain*, in *The Nineteenth Annual Conference of the Tire Society*. 2000: Akron, Ohio.
53. Bolarinwa, E.O., Olatunbosun, O.A., *Finite Element Simulation of the Tyre Burst Test.* Proceedings of the Institution of Mechanical Engineers Part D: Journal of Automobile Engineering, 2004. **218**: p. 1251-1258.
54. Olatunbosun, O.A., Bolarinwa, E.O., *FE Simulation of the Effect of Tire Design Parameters on Lateral Forces and Moments.* Tire Science and Technology, TSTCA, 2004. **32**(3): p. 146-163.
55. Bolarinwa, E.O., Olatunbosun, O.A., and Burnett, M., *A Study of Tyre Cornering Behaviour using a Finite Element Model*, in *Computational Mechanics, WCCM VI in conjunction with APCOM'04*. 2004: Beijing, China.
56. Kabe, K., Koishi, M., *Tire Cornering Simulation using Finite Element Analysis.* Journal of Applied Polymer Science, 2000. **78**: p. 1566-1572.
57. Ghoreishy, M.H.R., *A Numerical Study on the Non-linear Finite Element Analysis of a Tyre under Axisymmetric Loading.* Iranian Polymer Journal, 2002. **11**(5): p. 325-332.
58. Ghoreishy, M.H.R., Malekzadeh, M., and Rahimi, H., *A Parametric Study on the Steady State Rolling Behaviour of a Steel-belted Radial Tyre.* Iranian Polymer Journal, 2007. **16**(8): p. 539-548.
59. Ghoreishy, M.H.R., *Finite Element Analysis of the Steel-belted Radial Tyre with Tread Pattern under Contact Load.* Iranian Polymer Journal, 2006. **15**(8): p. 667-674.
60. Ghoreishy, M.H.R., *Finite Element Analysis of Steady Rolling Tyre with Slip Angle: Effect of Belt Angle.* Plastics, Rubber and Composites, 2006. **35**(2): p. 83-90.
61. Ghoreishy, M.H.R., *Steady State Rolling Analysis of a Radial Tyre: Comparison with Experimental Results.* Proceedings of the Institution of Mechanical Engineers Part D: Journal of Automobile Engineering, 2006. **220**: p. 713-721.
62. Guan, Y., Zhao, G., and Cheng, G., *Influence of Belt Cord Angle on Radial Tire under Different Rolling States.* Journal of Reinforced Plastics and Composites, 2006. **25**(10): p. 1059-1077.

63. Ojala, J.K., *Using ABAQUS in Tire Development Process*, in *ABAQUS Users' Conference*. 2005. p. 1-10.

64. Ghosh, P., et al., *Optimization of Tyre Design Parameters Through Finite Element Analysis and Correlation with Performance.* SAE International, 2007. **SAE Paper No. 2007-26-043**.

65. Abe, A., Kamegawa, T., and Nakajima, Y., *Optimum Young's Modulus Distribution in Tire Design.* Tire Science and Technology, TSTCA, 1996. **24**(3): p. 204-219.

66. Abe, A., Kamegawa, T., and Nakajima, Y., *Optimization of Construction of Tire Reinforcement by Genetic Algorithm.* Optimization and Engineering, 2004. **5**: p. 77-92.

67. Cho, J.R., Jeong, H.S., and Yoo, W.-S., *Multi-objective Optimization of Tire Carcass Contours using a Systematic Aspiration-level Adjustment Procedure.* Computational Mechanics, 2002. **29**: p. 498-509.

68. Cho, J.R., Kim, K.W., and Jeong, H.S., *Numerical Investigation of Tire Standing Wave using 3-D Patterned Tire Model.* Journal of Sound and Vibration, 2007. **2007**(4-5): p. 795-807.

69. Zhang, Y., Palmer, T., and Farahani, A., *A Finite Element Tire Model and Vibration Analysis: A New Approach.* Tire Science and Technology, TSTCA, 1998. **26**(3): p. 149-172.

70. Shiraishi, M., Yoshinaga, H., Iwasaki, N., and Hayashi, K., *Making FEM Tire Model and Applying It for Durability Simulation*, in *6th International LS-Dyna Users Conference*. 2000: Detroid.

71. Wheeler, R.L., Dorfi, H.R., and Keum, B.B., *Vibration Modes of Raidal Tires: Measurement, Prediction, and Categorization Under Different Boundary and Operating Conditions.* SAE International, 2005. **2005-01-2523**.

72. Negrus, E., Anghelache, G., and Stanescu, A., *Finite Element Analysis and Experimental Analysis of Natural Frequencies and Mode Shapes for A Non-rotating Tyre.* Vehicle System Dynamics Supplement, 1997. **27**: p. 4.

73. Anghelache, G., Moisescu, R., *Analysis of Rubber Elastic Behaviour and Its Influence On Modal Properties.* MATERIALE PLASTICE, 2008. **45**: p. 6.

74. Bolarinwa, E.O., Olatunbosun, O.A., *Development of an Integrated CAD/FE Tire Design System.* Tire Technology International, 2005: p. 10-13.
75. *An Integrated Approach for Transient Rolling of Tires*, in *Abaqus Technology Brief*. April 2007, SIMULIA.
76. Yamanishi, T., Matsuda, K., *Integrated Tire Analysis and Simulation*, in *2nd MSC Worldwide Automotive Conference*. 2000.
77. Li, L., Wang, F.-Y., *Advanced Motion Control and Sensing for Intelligent Vehicles*. 2007, New York: Springer.
78. Zhuang, J., *Modern Vehicle Tyre Technology*. 2001: Press of Beijing University of Technology.
79. Schrullkamp, T., Goertz, H., and Husemann, T. *Development of An Intelligent Tire-Experiences from the APOLLO Project*. in *Intelligent Tire Technology Conference*. 2005. Frankfurt am Main, Germany.
80. Goertz, H., Husemann, T. *The Mechatronic Tyre for Online Determination of Tyre Contact Patch Forces*. in *The 31st FISITA World Automotive Congress*. 2006. Yokohama, Japan.
81. APOLLO Project Report "Intelligent Tyre Systems - State of the Art and Potential Technologies Deliverable D7",
82. Eaton, W.P., Smith, J.H., *Micromachined Pressure Sensors: Review and Recent Developments.* Smart Electronics and Mems - Smart Structures and Materials 1997, 1997. **3046**: p. 30-41.
83. Thomas, B., *The Sidewall Torsion Sensor System.* Darmstädter Reifenkolloquium, 1998: p. 8.
84. Stelzer, A., et al., *Wireless SAW Sensors for Surface and Subsurface Sensing Applications.* Subsurface and Surface Sensing Technologies and Applications Iii, 2001. **4491**: p. 358-366.
85. Reindl, L.M., Pohl, A., Scholl, G., and Weigel, R., *SAW-Based Radio Sensor Systems.* IEEE Sensors Journal, 2001. **1**(1).
86. Pohl, A., Ostermayer, G., Reindl, L., and Seifert, F. *Wireless Measurement of Tyre Pressure Using Passive SAW Sensors*. in *Proceedings Sensor 97*. 1997.
87. Cyllik, A., Strothjohann, T., and Scholl, G., *The Intelligent Tire-Applications of the Tread Sensor*, in *VDI BERICHTE*. 2001.

88. Mbgori, V., Magori, V.R., and Seitz, N., *On-Line Determination of Tyre Deformation, a Novel Sensor Principle*, in *IEEE Ultrasonics Symposium* 1998.
89. APOLLO, www.vtt.fi/apollo.
90. FRICTION, http://friction.vtt.fi/.
91. Tuononen, A., *Optical Position Detection to Measure Tyre Carcass Deflections and Implementation for Vehicle State Estimation*, in *Department of Engineering Design and Production*. 2009, Helsinki University of Technology: Helsinki.
92. Tuononen, A.J., *Optical Position Detection to Measure Tyre Carcass Deflections.* Vehicle System Dynamics, 2008. **46**.
93. Tuononen, A.J., *On-board Estimation of Dynamic Tyre Forces from Optically Measured Tyre Carcass Deflections.* International Journal of Heavy Vehicle Systems, 2009. **16**: p. 362-378.
94. Tuononen, A.J., *Vehicle Lateral State Estimation based on Measured Tyre Forces.* Sensors, 2009. **9**.
95. Tuononen, A., Hartikainen, L., *Optical Position Detection Sensor to Measure Tyre Carcass Deflections in Aquaplaning.* International Journal of Vehicle Systems Modelling and Testing, 2008. **3**: p. 189-197.
96. Tuononen, A.J., Matilainen, M.J., *Real-time Estimation of Aquaplaning with An Optical Tyre Sensor.* Proceedings of the Institution of Mechanical Engineers, Part D: Journal of Automobile Engineering, 2009. **223**: p. 1263-1272.
97. Caretta, R., *Method and System for Monitoring the Deformations of A Tyre in Motion*. 2003: United States.
98. Takashi, T., Atsuhiko, T., *Apparatus and Method for Inspecting A Sidewall of A Tyre*. 1989: European Patent Office.
99. Yi, J., *A Piezo-Sensor-Based "Smart Tire" System for Mobile Robots and Vehicles* IEEE/ASME Transactions on Mechatronics, 2008. **13**: p. 95-103.
100. Erdogan, G., Alexander, L., and Rajamani, R., *A Novel Wireless Piezoelectric Tire Sensor for the Estimation of Slip Angle.* Measurement Science and Technology, 2010. **21**: p. 1-10.
101. Erdogan, G., *New Sensors and Estimation Systems for the Measurement of Tire-Road Friction Coefficient and Tire Slip Variables*. 2009, The University of Minnesota.

102. Cullen, J.D., Arvanitis, N., Lucas, J., and Al-Shamma'a, A.I., *In-field Trials of A Tyre Pressure Monitoring System based on Segmented Capacitance Rings.* Measurement, 2002. **32**: p. 181–192.

103. Todoroki, A., Miyatani, S., and Shimamura, Y., *Wireless Strain Monitoring using Electrical Capacitance Change of Tire: Part I-with Oscillating Circuit.* Smart Materials and Structures, 2003. **12**: p. 403-409.

104. Todoroki, A., Miyatani, S., and Shimamura, Y., *Wireless Strain Monitoring using Electrical Capacitance Change of Tyre:Part II-Passive.* Smart Materials and Structures, 2003. **12**: p. 410–416.

105. Matsuzaki, R., Todoroki, A., *Passive Wireless Strain Monitoring of Tyres using Capacitance and Tuning Frequency Changes.* Smart Materials and Structures, 2005. **14**: p. 561–568.

106. Matsuzaki, R., Todoroki, A., *Passive Wireless Strain Monitoring of Actual Tyre using Capacitance-Resistance Change and Multiple Spectral Features.* Sensors and Actuators A, 2006. **126**: p. 277–286.

107. Sergio, M., et al., *On A Road Tire Deformation Measurement System using A Capacitive-Resistive Sensor.* Smart Materials and Structures, 2006. **15**: p. 1700–1706.

108. Matsuzaki, R., Todoroki, A., *Wireless Flexible Capacitive Sensor based on Ultra-flexible Epoxy Resin for Strain Measurement of Automobile Tires.* Sensors and Actuators A, 2007. **140**: p. 32–42.

109. Miyoshi, A., Tsurita, T., and Kunii, M., *System and Method for Determining Tyre Force*, in *Patent Application Publication*. 2005: United States.

110. Braghin, F., et al., *Measurement of Contact Forces and Patch Features by Means of Accelerometers Fixed Inside the Tire to Improve Future Car Active Control.* Vehicle System Dynamics, 2006. **44,Supplement**: p. 3-13.

111. Bachmann, V., Fach, M., and Breuer, B., *Future Car-Tires as Provider of Information for Vehicle Systems to Enhance Primary Safety*, in *SAE Future Transportation Technology Conference & Exposition*. 1998: Costa Mesa, CA. p. 1-7.

112. Pohl, A., Steindl, R., and Reindl, L., *The "Intelligent Tire" Utilizing Passive SAW Sensors-Measurement of Tire Friction.* IEEE Transactions on Instrumentation and Measurement, 1999. **48**(6): p. 1041-1046.
113. Matsuzaki, R., Keating, T., Todoroki, A., and Hiraoka, N., *Rubber-based Strain Sensor Fabricated using Photolithography for Intelligent Tires.* Sensors and Actuators A, 2008. **148**: p. 1-9.
114. Matsuzaki, R., Todoroki, A., *Wireless Monitoring of Automobile Tires for Intelligent Tires.* Sensors, 2008. **8**: p. 8123-8138.
115. Miyoshi, A., *Pneumatic Tyre with Specially Arranged Strain Sensors*, in *United States Patent*. 2009: United States
116. Mishra, A., et al., *Embedded Wireless Sensors for Aircraft/Automobile Tire Structural Health Monitoring*, in *IEEE SECON*. 2006: Reston, VA,.
117. Ohori, M., et al. *Fundamental Study of Smart Tire System*. in *2006 IEEE Intelligent Transportation Systems Conference*. 2006. Toronto, Canada,.
118. Hall, W., Mottram, J.T., and Jones, R.P., *Finite Element Simulation of A Rolling Automobile Tyre to Understand Its Transient Macroscopic Behaviour.* Proceedings of the Institution of Mechanical Engineers Part D: Journal of Automobile Engineering, 2004. **218**: p. 1393-1408.
119. Walter, J.D., *Cord Reinforced Rubber*, in *Mechanics of Pneumatic Tires*, Clark, S.K., Editor. 1981, U.S. Department of Transportation. National Highway Traffic Safty Administration. p. 123-202.
120. Tyres, http://www.formulastudent.de/academy/pats-corner/advice-details/article/tyres/.
121. Lin, Y.-J., Hwang, S.-J., *Temperature Prediction of Rolling Tires by Computer Simulation.* Mathematics and Computers in Simulation, 2004. **67**(2004): p. 235-249.
122. Ghosh, P., Saha, A., Bohara, P.C., and Mukhopadhyay, R., *Material Property Characterization for Finite Element Analysis of Tires.* Rubber World, 2006.
123. Smith, L.P., *The Language of Rubber: An Introduction to the Specification and Testing of Elastomers*. 1993: Butterworth-Heinemann.
124. Helnwein, P., Liu, C.H., Meschke, G., and Mang, H.A., *A New 3-D Finite Element Model for Cord-reinforced Rubber Composites-Application to Analysis*

of Automobile Tires. Finite Element in Analysis and Design, 1993. **14**(1993): p. 1-16.

125. Kao, B.G., Muthukrishnan, M., *Tire Transient Analysis with an Explicit Finite Element Program.* Tire Science and Technology, TSTCA, 1997. **25**(4): p. 230-244.
126. Tonuk, E., Unlusoy, Y.S., *Prediction of Automobile Tire Cornering Force Characteristics by Finite Element Modeling and Analysis.* Computers and Structures, 2001. **79**(2001): p. 1219-1232.
127. Guan, Y., Zhao, G., and Cheng, G., *FEA and Testing Studies on Static Camber Performance of the Radial Tire.* Journal of Reinforced Plastics and Composites, 2007. **26**(18): p. 1921-1936.
128. Pelc, J., *Static Three-dimensional Modelling of Pneumatic Tyres using the Technique of Element Overlaying.* Proceedings of the Institution of Mechanical Engineers Part D: Journal of Automobile Engineering, 2002. **216**(9): p. 709-716.
129. Pelc, J., *Towards Realistic Simulation of Deformations and Stresses in Pneumatic Tyres.* Applied Mathematical Modelling, 2007. **31**(2007): p. 530-540.
130. Kim, W.-D., Kim, W.-S., Woo, C.-S., and Lee, H.-J., *Some Considerations on Mechanical Testing Methods of Rubbery Materials using Nonlinear Finite Element Analysis.* Polymer International, 2004. **53**: p. 850-856.
131. *Nonlinear Finite Element Analysis of Elastomers*, in *Technical Paper*. 2000, MSC.Software Corporation.
132. Time Domain Viscoelasticity, ABAQUS Analysis User's Manual Version, Dassault System.
133. Peel, L.D., Jensen, D.W., *Nonlinear Modeling of Fiber-Reinforced Elastomers.*
134. Fleming, Livingston, eds. *Tire Reinforcement and Tire Performance*.
135. Chen, P., et al. *Inspection of Tyre Tread Defects using Image Processing and Pattern Recognition Techniques*. in *Vision, Sensors, and Control for Automated Manufacturing Systems*. 1993. Boston, MA, USA: The International Society for Optical Engineering.
136. Chao, Z., Yin-hang, C., *Modified Threshold Algorithm for Feature Extraction of Tyre Surface Wear.* Journal of Beijing JiaoTong University, 2007. **31**(2).

137. Slabeyciu, J., Kostial, P., Cuth, V., and Bokuvka, O., *Vibrational Modes of Tyres-FEM Modelling and Experimental Investigation*, in *18th Danubia-Adria-Symposium on Experimental Methods in Solid Mechanics*. 2001: Austria.

138. Timothy, S., John, T., and Konstantin, G., *Full-field Dynamic Displacement and Strain Measurement using Pulsed and High-speed 3D Image Correlation Photogrammetry: Part I.* Experimental Techniques, 2004. **27**(3): p. 47-50.

139. Baruchel, J., ed. *X-ray Tomography in Material Science* 2000, Hermes Science: Paris.

140. Dunsmuir, J.H., et al. *Microtomography of Elastomers for Tire Manufacture* in *Developments in X-Ray Tomography II*. 1999: The International Society for Optical Engineering.

141. Drobina, R., Machnio, M.S., *Application of the Image Analysis Technique for Textile Identification.* AUTEX Research Journal, 2006. **6**(1): p. 40-48.

142. Voisin, S., Page, D., Koschan, A., and Abidi, M. *Reconstructing 3D CAD Models for Simulation Using Imaging-Based Reverse Engineering*. in *Proceedings of SPIE Modeling and Simulation for Military Applications*. 2006. Orlando, FL.

143. Danielson, K.T., Noort, A.K., and Greens, J.S., *Computational Strategies for Tire Modeling and Analysis.* Computers & Structures, 1996. **61**(4): p. 673-693.

144. Jaroslav, M., *Finite Element Analysis and Simulations in Biomedicine: a Bibliography (1985-1999).* Engineering Computations, 2000. **17**(7).

145. Sarkar, S.N., Komoroski, R.A., *NMR Imaging of Morphology, Defects, and Composition of Tire Composites and Model Elastomer Blends.* Macromolecules, 1992. **25**(5): p. 1420-1426.

146. Simpleware, http://www.simpleware.com/.

147. Jeusette, J.P., Theves, M., *Finite Element Analysis of Tire/Rim Interface Forces Under Braking and Cornering Loads.* Tire Science and Technology, TSTCA, 1992. **20**(2): p. 83-105.

148. Pelle, R.G., *FEM Simulation of the Tire/Rim Seating Process.* Tire Science and Technology, TSTCA, 1994. **22**(2): p. 76-98.

149. Korunovic, N., Trajanovic, M., and Stojkovic, M., *FEA of Tyres Subjected to Static Loading.* Journal of the Serbian Society for Computational Mechanics, 2007. **1**(1): p. 87-98.

150. Chang, C.-L., Yang, S.-H., *Simulation of Wheel Impact Test using Finite Element Method.* Engineering Failure Analysis, 2009.

151. Neves, R.R.V., Micheli, G.B., and Alves, M., *An Experimental and Numerical Investigation on Tyre Impact.* International Journal of Impact Engineering, 2009.

152. Xia, K., *Finite Element Modeling of Tire/Terrain Interaction: Application to Predicting Soil Compaction and Tire Mobility.* Journal of Terramechanics, 2010.

153. Okano, T., Koishi, M., *Hydroplaning Simulation using MSC.Dytran*, in *The 2nd MSC Worldwide Automotive Conference* 2000.

154. Gruber, P., Sharp, R.S., and Crocombe, A.D., *Friction and camber influences on the static stiffness properties of a racing tyre.* Proceedings of the Institution of Mechanical Engineers Part D: Journal of Automobile Engineering, 2008. **222**: p. 1965-1976.

155. Park, S.-J., et al. *Comparison of Tire Contact Pressure between Physical Experiment and Computer Simulation*. in *Proceedings of ACMD06*. 2006.

156. Allen, J.M., Cuitino, A.M., and Sernas, V., *Numerical Investigation of the Deformation Characteristics and Heat Generation in Pneumatic Aircraft Tires, Part II. Thermal Modeling.* Finite Elements in Analysis and Design, 1996. **23**: p. 265-290.

157. Janssen, M.L., Walter, J.D., *Rubber Strain Measurements in Bias, Belted-Bias and Radial Ply Tires.* Journal of Industrial Textiles, 1971. **1**(2): p. 102-117.

158. Hu, Y.K., Abeels, P.F.J., *Agricultural Tire Deformation in the 2D Case by Finite Element Methods.* Journal of Terramechanics, 1994. **31**(6): p. 18.

159. Herron, J.R., *Application of ALE Contact to Composite Shell Finite Element Model for Pneumatic Tires*. 2005, The University of Toledo.

160. Steen, R.v.d., *Tyre/road Friction modeling Literature Survey*. 2007, Eindhoven University of Technology: Eindhoven.

161. Hussein, B., Negrut, D., and Shabana, A.A., *Implicit and Explicit Integration in the Solution of the Absolute Nodal Coordinate Differential/algebraic Equations.* Nonlinear Dynamics, 2008. **54**: p. 14.

162. *Implicit Dynamic Analysis & Explicit Dynamic Analysis*, in *ABAQUS Theory Manual*.

163. Austin, L., Morrey, D., *Recent Advances in Antilock Braking Systems and Traction Control Systems.* Proceedings of the Institution of Mechanical Engineers Part D: Journal of Automobile Engineering, 2000. **214**(6): p. 14.

164. Matsuzaki, R., *A Study on Intelligent Tires based on Measurement of Tire Deformation*. 2007, Tokyo Institude of Technology: Tokyo.

165. http://elcodis.com/datasheet.php?c=1752578&c_name=EZ430-RF2500-SEH&doc=187625.

166. Yang, X., Olatunbosun, O.A., and Bolarinwa, E.O., *Materials Testing for Finite Element Tire Model.* SAE International Journal of Materials and Manufacture, 2010. **3**(1): p. 211-220.

167. Yang, X., Olatunbosun, O.A., and Bolarinwa, E.O., *Generation of Tyre Cross-sectional Geometry for FE Tyre Model Using Image Processing Techniques.* International Journal of Engineering Simulation, 2009. **10**(1).

APPENDIX: PUBLICATION

JOURNAL

1. X. Yang, O.A. Olatunbosun, E.O. Bolarinwa, "Generation of Tyre Cross-sectional Geometry for FE Tyre Model Using Image Processing Techniques," International Journal of Engineering Simulation. Vol.10, No.1, 2009.

2. X. Yang, O.A. Olatunbosun, E.O. Bolarinwa, "Materials Testing for Finite Element Tire Model." SAE Int. J. Mater. Manuf. 3(1): 211-220, 2010.

3. X. Yang, O.A.Olatunbosun, "Optimization of Reinforcement Turn-up Effect on Tyre Durability and Operating Characteristics for Racing Tyre Design." Materials & Design (June 2011) doi:10.1016/j.matdes.2011.06.014.

CONFERENCE

1. X. Yang, O.A. Olatunbosun, "Optimization of Reinforcement Turn-up Effect on Tire Durability and Operating Characteristics for Racing Tire Design using Finite Element Analysis," Presented at 28th Annual Conference on Tire Science and Technology, Akron, Ohio, USA, 2009.

2. Olatunbosun, Oluremi, Yang, Xiaoguang, Behroozi, Mohammad, Garcia Pozuelo, Daniel. "Development of An AI-Based Model to Determine Vehicle Tire Design Configuration." FISITA 2010. F2010-C-213.

3. X. Yang. "Finite Element Tyre Modelling and Simulation." Presented at Birmingham Environment for Academic Research (BEAR) Postgraduate Conference, June 2010.